Development of targeted nanoparticles for the treatment of Pulmonary Hypertension

A thesis submitted in fulfilment of the requirements for the degree of

Doctor of Philosophy

By

Scheilly Liu Tsilova

UCL School of Pharmacy

Research Departments of Pharmaceutics and Pharmacology

University College London

29-39 Brunswick Square, London, WC1N 1AX

January 2025

Declaration of Authorship

I, Scheilly Liu Tsilova, confirm that the work presented in this thesis is my own. Where information has been derived from other sources, I confirm that this has been indicated in the thesis.

Acknowledgement

Every PhD student thinks about what they want to write in their acknowledgement for a good amount of time, especially during challenging times or leading up to the end of their PhD. I had always said that mine would be pages long because of the many people who left a mark during this PhD, so thank you to all these great people for contributing to this achievement.

First and most importantly, I would like to thank my supervisory team! Especially my legend of a supervisor, Dr Maryam Parhizkar, who was the first to see my potential as a PhD candidate. Her support got me through this incredible and challenging journey and made me into the doctoral candidate I am today. I could write pages and pages about how she influenced my growth, but really I can only thank her for pushing me to be the best version of myself, believing in my capabilities, and always caring about my work and well-being. Thank you, Maryam, for your time, from checking calculations and manuscripts to dealing with my teary outbursts of frustration. Thank you for the care, the laughs, the tough love, and ultimately, for being a loyal and supportive supervisor (and for trusting me with the lab). You do not get enough praise for what you do and genuinely deserve.

I would also like to thank my other primary supervisor, Professor Rebecca Lever, for giving me the privilege of being your PhD student and, especially, for all the invaluable supervision on the cell work and the PhD in general. But more importantly, I would also like to thank you for always making time to see me and for being encouraging and reassuring about my work. Your words of positivity have always uplifted me, and I have always left our meetings feeling good about my work and myself. Thank you for always being available and for continuously checking on my well-being.

Finally, I would like to thank my clinical supervisor, Dr Benjamin Schreiber, who introduced me to this project in December 2018 and for his unwavering advocation for pulmonary hypertension research. Thank you for always helping me take a step back and look at the big picture of my project but, most importantly, to be a reminder of the

unmet need we are trying to address. Your enthusiasm and curiosity for my research consistently fuelled my sense of purpose within this project.

I would also like to thank the amazing colleagues and friends I made during those 4 years. I first want to thank the senior members of the lab when I first started. Thank you, Dr Shorooq Abukhamees for taking the time to help me with calculations without judgment. Dr Zoe Rahim, thank you for helping me get started with my cell work and for your patience and belly laughs. Thank you, Amal, for being nurturing and always making me feel like everything would eventually be okay. Thank you, Dr Hamta Majd, for always reassuring me and inspiring me to work as hard as you did. Dr Yinan Liu, thank you for sharing this challenging adventure with me, from setting up the lab in 402 to writing up our thesis together. Rama, thank you for your friendship and for helping me with the BCA assay work. Han and Yuki, thank you for your kindness and comfort and for being such a ray of sunshine during the gloomy period of this PhD. Thank you, Fanjin for all the scientific insights and discussions we shared. And, of course, Amenah, Mazna, Luca, Widyan, XinYi, Jichao, Beshair, thank you all for making this PhD journey as exciting and memorable as it was! I would also like to say a big thank you to the technical team at the School of Pharmacy, especially Satinder Sembi. Thank you for always taking the time to help and hear everyone's (especially the PhDs') concerns.

I also want to thank my close friends for their strong support. Thank you, Yun, Noelle, Rachel, and Lynn, for the emotional and mental support and the laughs about becoming adults. Thank you, Edith and Eden, for listening to my rant about my project, helping me grow and giving me the unconditional love and support I needed during my write-up.

Unconventionally, I also want to thank and acknowledge my therapist, Wendy Woodcock, who has tremendously helped me navigate these last 3 years mentally and emotionally. For every moment of doubt and defeat, she gave me the tools and the strength to change my narrative to hopeful and proud. She has been central to my personal development and my journey to self-acceptance and self-love during my PhD. Thank you for the invaluable mental support.

I wouldn’t be here without the help of my entire family back in Madagascar. Thank you all for continuously supporting me emotionally and financially since I moved to the UK 10 years ago and encouraging me to pursue my PhD. Especially my mother, Tsilova Urlika Chan. Thank you for being my role model and inspiration for your resilience and hard work ethic. Thank you for raising me to be a strong and brave woman and showing me you can do anything you set your mind while still being humble and caring towards others. Thank you for investing in me; I would not have reached this point without you. Merci Maman.

I want to thank my other half, Jean Martin Gabriel Daniel, who has been with me for as long as I have done this PhD. I also want to express my deep appreciation and gratitude to Mary Jane Daniel, his mother, for her kindness and warmth, for welcoming me into her family when mine was out of reach and for nurturing me (mostly with food) throughout this PhD.

Martin, words are not enough to express my gratitude for your unconditional love and dedication over the last 4 years. Thank you for being my home, my anchor and my sun throughout these years. Thank you for taking on so much when I started writing up, for never complaining, for never failing to make me laugh and for always making me tea. You have inspired me through your own discipline and resilience to push through and believe in myself. Thank you for loving me so hard and genuinely; it made it easier for me to love and believe in myself.

Finally, I want to acknowledge myself for doing the work and research, working on my confidence and knowledge, and for completing this thesis. I want to recognise how difficult this all was, but no matter how challenging it was or how close I was to admitting defeat, I picked myself up countless times and did not let my anxiety and depression win.

Dedication

This thesis is dedicated to

Women in **S**cience, **T**echnology, **E**ngineering, and **M**athematics.

Past, present, and future – Women who inspire change, overcome obstacles and redefine the limits of achievement.

And to

My Mother, as my first woman in STEM inspiration.

Tsilova Urlika Chan

Whose countless sacrifices have made this achievement possible.

Finally, to

My younger self,

For all she endured to get where I am.

Thank you for never giving up.

Abstract

Pulmonary arterial hypertension (PAH) is an ultimately fatal condition that arises due to over-proliferation and apoptosis resistance of pulmonary artery cells. Current treatments only alleviate symptoms and do not resolve cellular dysfunction. Imatinib, a tyrosine kinase inhibitor, was studied for PAH but abandoned in Phase 3 trials due to its lack of safety and efficacy following systemic delivery. Many drug delivery systems, including nanoparticles (NPs), were researched to address the problems of free drug administration, but the encapsulation methods used were inefficient, costly, and involved complex, multi-step processes, leading to issues such as toxicity, polydispersity, and low encapsulation efficiency. Additionally, when administered in vivo, NPs primarily relied on the leaky vasculature for delivery, lacking specific targeting.

This work aimed to improve imatinib delivery by encapsulating it in poly(lactic-co-glycolic acid) (PLGA) NPs, produced by electrospray (ES), a more efficient one-step process that avoids surfactants, high temperatures, and significant waste. The NPs were functionalised with an antibody to target relevant cells for improved drug delivery. The NPs were optimised for size, shape, composition, and morphology, and characterised for drug encapsulation efficiency and release profile in vitro and tested on various cell lines. The NPs were functionalised by conjugating a model antibody via carbodiimide chemistry.

ES enabled the production of PLGA NPs with controlled size and hydrophobicity, allowing for high encapsulation efficiency and controlled drug release. Imatinib-loaded NPs reduced cell viability in lung cancer cells, had effects similar to free drug on endothelial cells, and had enhanced antiproliferative effects on arterial smooth muscle cells, in both the absence and presence of mitogen stimulation. Two antibody conjugation methods were identified, and a standard protein assay proved unreliable for quantification due to interferences.

This work developed efficient, targeted PLGA nanoparticles further to develop targeted pulmonary drug delivery strategies for PAH.

Impact statement

Pulmonary arterial hypertension (PAH) remains uncured after decades of research, and current treatments are ineffective in resolving the condition. Novel therapies show potential in addressing vascular dysfunctions, but their efficacy, safety, stability, and bioavailability are limited when systemically administered. This work proposes targeted polymeric nanoparticles (NPs) as a drug delivery system for imatinib, a promising drug repurposed from cancer treatment. The targeted NPs were developed to selectively deliver imatinib to affected cells, addressing their dysfunction while preserving the safety of healthy cells, and showing significant clinical, academic, and industrial impact.

Clinical Impact

This novel treatment has considerable clinical potential for PAH, offering therapeutic benefit and improving patient comfort. Targeted imatinib-loaded NPs can be directly delivered to affected cells, reducing systemic delivery and toxicity while enabling higher drug doses. This enhances the treatment's effectiveness, reducing the frequency of administration and contributing to patient comfort and compliance. This approach marks a significant step in PAH treatment research. Additionally, imatinib's effectiveness extends beyond PAH; it is an effective anti-cancer drug for gastrointestinal tumours and other blood disorders. Therefore, these NPs can be repurposed for cancer treatments by changing the type of ligand conjugated to the NPs.

Industrial Impact

Nanoparticles have gained attention for enhanced drug delivery, offering improved bioavailability, reduced side effects, and controlled drug release. The industrial implications of this work lie in the electrospray technique used to produce the targeted nanoparticles. This method is flexible, producing NPs of various sizes and characteristics by manipulating the parameters. The nanoparticles are versatile, capable of carrying various materials and payloads, which supports a wide range of

applications. This flexibility can help researchers encapsulate different agents while maintaining control over the final product. Furthermore, the continuous nature of the electrospraying technique facilitates upscaling production for commercial and industrial applications.

Academic Impact

PLGA was chosen for its high control over drug release and surface functionalisation capabilities using carbodiimide chemistry. This work explored various methods to confirm success, offering a better understanding of expected results following conjugation. It highlights the limitations of each quantification method, saving future researchers time and resources by avoiding unreliable techniques. These findings provide critical scrutiny of published work on carbodiimide functionalisation. Since bevacizumab was used as a model antibody, other antibodies or proteins with amine groups can also functionalise PLGA NPs for different targets. The antibody conjugation optimisation can offer a platform for researchers to improve nanoparticle functionalisation.

Moreover, testing drug-loaded NPs on vascular cells demonstrates the importance of optimising methods for reliable results. Investigating imatinib's effect on endothelial and smooth muscle cells revealed how cell culture conditions can influence apparent drug efficacy. For instance, testing smooth muscle cell growth provided insights into treatment timing, medium composition, and cell confluence. This information could aid researchers seeking to investigate the effects of drug treatment on cell behaviours in vitro, and offers tested hypotheses for improved experiments. Optimising the timing of cell growth, drug action, and drug release from particles provides insights into the challenges of testing drug delivery approaches on a biological system.

UCL Research Paper Declaration Form

For a research manuscript that has already been published (if not yet published, please skip to section 2):

(a) What is the title of the manuscript?

Polymeric nanoparticles produced by electrohydrodynamic atomisation for the passive delivery of imatinib

(b) Please include a link to or doi for the work:

https://doi.org/10.1016/j.ejpb.2024.114412

(c) Where was the work published?

European Journal of Pharmaceutics and Biopharmaceutics

(d) Who published the work?

Scheilly Liu Tsilova, Benjamin Emmanuel Schreiber, Rebecca Lever, Maryam Parhizkar

(e) When was the work published?

September 2024

(f) List the manuscript's authors in the order they appear on the publication:

Scheilly Liu Tsilova, Benjamin Emmanuel Schreiber, Rebecca Lever, Maryam Parhizkar

(g) Was the work peer reviewed?

Yes

(h) Have you retained the copyright?

Yes

(i) Was an earlier form of the manuscript uploaded to a preprint server (e.g. medRxiv)? If 'Yes', please give a link or doi If 'No', please seek permission from the relevant publisher and check the box next to the below statement:

No

☒ I acknowledge permission of the publisher named under 1d to include in this thesis portions of the publication named as included in 1c.

For multi-authored work, please give a statement of contribution covering all authors (if single-author, please skip to section 4):

Scheilly L. Tsilova: Writing – original draft, Validation, Methodology, Investigation, Formal analysis, Data curation, Conceptualization. **Benjamin E. Schreiber:** Writing – review & editing, Supervision, Investigation, Conceptualization. **Rebecca Lever:** Writing – review & editing, Validation, Supervision, Methodology, Investigation,

Conceptualization. **Maryam Parhizkar:** Writing – review & editing, Supervision, Resources, Project administration, Investigation, Conceptualization.

In which chapter(s) of your thesis can this material be found?

Chapter 3 Optimisation via electrospraying, physical-chemical characterisation and in-vitro efficacy of imatinib-loaded PLGA NPs

e-Signatures confirming that the information above is accurate (this form should be co-signed by the supervisor/ senior author unless this is not appropriate, e.g. if the paper was a single-author work):

Candidate:

Scheilly Tsilova

Date: 4th December 2024

Supervisor/Senior Author signature (where appropriate):

Dr Maryam Parhizkar

Date: 21st January 2025

Table of Contents

Declaration of Authorship **2**

Acknowledgement **3**

Dedication **6**

Abstract **7**

Impact statement **8**

Clinical Impact 8

Industrial Impact 8

Academic Impact 9

UCL Research Paper Declaration Form **10**

Table of Contents **12**

List of Figures **15**

List of Tables **21**

List of Equations **22**

List of Abbreviations and acronyms **23**

Communications **29**

Poster presentations 29

Oral presentation 30

Journal article publication 30

Chapter 1. Introduction and literature review ***31***

1.1. General introduction **32**

1.2. Pulmonary hypertension **34**

1.2.1. Introduction to PH 34

1.2.2. Symptoms and diagnosis 36

1.2.3. Pathology and pathogenesis 37

1.2.4. Pulmonary hypertension treatments 39

1.2.5. Potential new treatments 44

1.2.6. Imatinib and the PDGF pathway 51

1.3. Drug delivery systems (DDS) **55**

1.3.1. Nanoparticles as DDS 55

1.3.2. Poly Lactic-co-Glycolic Acid (PLGA) 57
1.3.3. Active targeted PLGA NPs 58

1.4. PLGA-based DDS for PAH 68

1.4.1. Encapsulating Imatinib in micro-nanoparticles 74

1.5. Electrohydrodynamic atomisation or electrospray (ES) 79

1.5.1. Electrosprayed particles as DDS 79
1.5.2. Parameters affecting the particles 81

1.6. Thesis aims and rationale 86

1.6.1. Thesis overview 87

Chapter 2. Materials and Methodology 89

2.1. Materials 90

2.1.1. Electrospraying Materials 90
2.1.2. Cell studies materials 93
2.1.3. Antibody Conjugation Materials 95

2.2. Methods 98

2.2.1. Production of micro and nanoparticles via electrospraying 98
2.2.2. Physical-chemical characterisation of the polymeric particles 98
2.2.3. Testing the nanoparticles on cells 100
2.2.4. Antibody conjugation to polymeric particles 104

Chapter 3. Optimisation via electrospraying, physical-chemical characterisation and in-vitro efficacy of imatinib-loaded PLGA NPs 109

3.1. Introduction 110

3.2. Methodology 112

3.2.1. Imatinib-loaded nanoparticles and rhodamine-B loaded nanoparticles (RhD-B NPs) production and characterisation 112
3.2.2. Cell studies 116

3.3. Results and discussion 118

3.3.1. Impact of choice of solvent on the generated particles 118
3.3.2. Imatinib-loaded particles characterisation 122
3.3.3. Effect of the imatinib-loaded NPs (F6 and F8) and RhD-B NPs (F9) on A549 cells. 134

3.4. Conclusion 141

Chapter 4. The Effect of the electrosprayed NPs on vascular cells 142

4.1. Introduction 143

4.2. Methodology 144

4.2.1. Measurement of HUVEC viability 144

4.2.2. Measurement of HPASMC viability 144

4.2.3. Measurement of mitogen-stimulated HPASMC viability 145

4.3. Results and Discussion 150

4.3.1. Effect of imatinib-loaded NPs on human umbilical vein endothelial cells (HUVECs) 150

4.3.2. Effect of imatinib-loaded NPs on pulmonary artery smooth muscle cells (HPASMCs) 154

4.3.3. Effect of imatinib-loaded NPs on pulmonary artery smooth muscle cells (HPASMCs) following stimulation via mitogen (PDGF-BB) 159

4.4. Conclusion 169

Chapter 5. Quantifying antibody conjugation to PLGA nanoparticles via carbodiimide conjugation 170

5.1. Introduction 171

5.2. Methodology 174

5.2.1. Carbodiimide conjugation of bevacizumab to PLGA NPs 174

5.2.2. Bicinchoninic acid assay (BCA) reliability test 176

5.2.3. Further methods to quantify antibody conjugation 176

5.2.4. Bevacizumab Sandwich ELISA Kit 178

5.3. Results and Discussion 179

5.3.1. Optimisation of the conjugation protocol 179

5.3.2. Physicochemical characterisation 183

5.3.3. Quantifying antibody conjugation 193

5.4. Conclusion 202

Chapter 6. Conclusions and Future work 203

6.1. Conclusion 204

6.2. Future work 207

6.2.1. Project-specific future work 207

6.2.2. Broad future work 209

References 213

List of Figures

Figure 1.1. WHO Classification of Pulmonary Hypertension [27]. Diagram created using XMind. 35

Figure 1.2. Diagram of a typical pulmonary artery vascular structure compared with a PH-affected vasculature [35]. Image created using BioRender. 38

Figure 1.3. Imatinib's mechanism of action. Image created using BioRender. 52

Figure 1.4. Diagram of the electrospray (EHDA) set-up. Diagram created using BioRender. 80

Figure 1.5. EHD experimental parameters affecting the size and shape of nanoparticles. Created using BioRender [218,222,232]. 85

Figure 2.1. PLGA chemical structure, drawn using ChirysDraw. 90

Figure 2.2. Imatinib chemical structure, adapted from [255]. 91

Figure 2.3. Rhodamine-B chemical structure, adapted from [258]. 91

Figure 2.4. EDC chemical structure, drawn using ChirysDraw [264] 95

Figure 2.5. NHS chemical structure, drawn using ChirysDraw [266] 96

Figure 2.6. MES chemical structure, adapted from [269]. 96

Figure 2.7. Diagram of the conjugated NPs bound to the secondary antibody. Primary antibodies are conjugated to PLGA NPs via their variable region using the NH_2 terminal group. Secondary antibodies' variable region is bound to the primary's constant region. Diagram drawn using Biorender and adapted from [270]. 97

Figure 2.8. MTT assay to evaluate cell viability following treatment of cells. Modified template from Biorender. 102

Figure 2.9. Carbodiimide conjugation of an antibody to a carboxylic group terminated polymer. Image created using ChirysDraw and Biorender and adapted from [162]. .. 104

Figure 2.10. The bicinchoninic acid assay (BCA assay). Image created using Biorender. 105

Figure 2.11. Bevacizumab ELISA Sandwich kit process. Image created using Biorender. 107

Figure 2.12. Simplified schematic of the flow cytometry [289]. Image created using Biorender. 108

Figure 3.1. Scanning electron microscopy (SEM) images of electrosprayed particles with their respective size distribution using four solvents: acetone, dimethylacetamide, dichloromethane, and tetrahydrofuran. Data are expressed as the mean +/- s.e. mean of 3 independent experiments carried out in triplicates. 121

Figure 3.2. Scanning electron microscopy (SEM) images of all formulations of NPs with their respective size distribution and PDI. Data are expressed as the mean +/- s.e. mean of 3 independent experiments carried out in triplicates. 124

Figure 3.3. A. Zeta potential of pure imatinib, blank (F1 and F3) and imatinib-loaded PLGA NPs with PLGA ratio 50:50 (F2) and 75:25 (F4). Data are expressed as the mean +/- s.e. mean of 3 independent experiments, each carried out in triplicates (*P < 0.05, **P < 0.01, ***P < 0.001; data analysed by one-way ANOVA followed by Tukey's post hoc test.) and B. Corresponding FTIR spectrum with pure PLGA spectrum (50:50 and 75:25). Red circles showing the Imatinib specific amine group in the drug encapsulated PLGA nanoparticles..... 127

Figure 3.4. A. Respective encapsulation efficiency of imatinib in F2, F4, F6, F8 IMA-NPs. B. Imatinib cumulative percentage release from F2, F4, F6 and F8 IMA-NPs and pure imatinib after being suspended in PBS over seven days. Data are expressed as the mean +/- s.e. mean of 3 independent experiments (*P < 0.05, **P < 0.01, ***P < 0.001; encapsulation efficiency data analysed by Kruskal-Wallis test). 129

Figure 3.5. A. MTT assay results and B. Live/Dead cells ratio, both conducted 72 hours after treatment with imatinib-loaded NPs and free imatinib. Data are expressed as the mean +/- s.e. mean of 3 independent experiments (*P < 0.05, **P < 0.01, ***P < 0.001; data analysed by one-way ANOVA followed by Tukey's post hoc test). 135

Figure 3.6. Live/Dead Assay on A549 cells 72 hours after treatment with medium (untreated), F5 NPs (blank), and F6 NPs (imatinib-loaded), both at 1mg/ml and a range of imatinib concentrations (50, 100, 150μM). Live cells were stained green with Calcein AM, and dead cells were stained red with BOBO™-3 Iodide. 136

Figure 3.7. A. The uptake assay result was obtained 24 hours after treating A549 cells with rhodamine-B-loaded NPs. Data are expressed as the mean +/- s.e. mean of 3 independent experiments, each carried out in duplicate (*P < 0.05, **P < 0.01, ***P < 0.001; data analysed by one-way ANOVA followed by Tukey's post hoc test.) B. Corresponding EVOS fluorescence images demonstrating the uptake of RhD-B pointed out by red arrows..... 138

Figure 4.1. Summary of the methods used to test cell viability of HUVECs. The dotted squares mark each optimisation; important changes are highlighted in red. 147

Figure 4.2. Summary of the methods used to test cell viability of HPASMCs. The dotted squares mark each optimisation; important changes are highlighted in red. 148

Figure 4.3. Summary of the methods used to test cell viability of PDGF-stimulated HPASMCs. The dotted squares mark each optimisation; important changes are highlighted in red. 149

Figure 4.4. HUVEC viability, as a percentage of untreated control, was investigated via MTT assay 72 hours after treatment with blank and 1mg/mL imatinib-loaded NPs and free imatinib A. with less than 100% confluence B. with 100% cell confluence. Data are expressed as the mean +/- s.e. mean of 3 independent experiments, carried out in duplicates (*P < 0.05, **P < 0.01, ***P < 0.001; data analysed by one-way ANOVA followed by Dunnett's post hoc test). 152

Figure 4.5. Effect of A. low and B. high imatinib concentration and cell confluency on HPASMC viability 72hrs after treatment. Data are expressed as the mean of a single experiment +/- s.d. of 8 measurements. 155

Figure 4.6. Time course of HPASMC viability, as a percentage of untreated control, when treated with a range of imatinib concentrations. Data are expressed as the mean

of a single experiment +/- s.d. of 8 measurements (*P < 0.05, **P < 0.01, ***P < 0.001; data analysed by two-way ANOVA followed by Dunett's post hoc test). 157

Figure 4.7. Time course of HPASMC viability as a percentage of untreated control, when treated with blank and imatinib-loaded NPs and free imatinib. Data are expressed as the mean +/- s.e. mean of 4 independent experiments (*P < 0.05, **P < 0.01, ***P < 0.001; data analysed by two-way ANOVA followed by Dunett's post hoc test). 158

Figure 4.8. Untreated HPASMC viability, as a percentage of untreated control, was measured via MTT assay A. 24 hours and B. 48 hours following stimulation using the mitogen PDGF. Optimisation 0 and 1 marked the introduction of the mitogen, the same way for the untreated cells; Optimisation 2 seeded the cells and treated/stimulated them simultaneously, and Optimisation 3 used a low serum medium during the stimulation/treatment stage. Data are expressed as the mean of a single experiment +/- s.d. of 8 measurements (*P < 0.05, **P < 0.01, ***P < 0.001; data analysed by two-way ANOVA followed by Sidak's post hoc test). 161

Figure 4.9. HPASMC viability, as a percentage of untreated control, was measured after treatment with imatinib-loaded NPs and free 150μM imatinib, with and without PDGF stimulation, via MTT assay A. 24 hours and B. 48 hours after treatment. Data are expressed as the mean of a single experiment +/- s.d. of 8 measurements (*P < 0.05, **P < 0.01, ***P < 0.001; data analysed by two-way ANOVA followed by Sidak's post hoc test). 163

Figure 4.10. HPASMC viability, as a percentage of untreated control, was measured after treatment with blank, imatinib-loaded NPs and free 176μM imatinib, with and without PDGF stimulation, via MTT assay A. 24 hours and B. 48 hours after treatment. Data are expressed as the mean of a single experiment +/- s.d. of 8 measurements (*P < 0.05, **P < 0.01, ***P < 0.001; data analysed by two-way ANOVA followed by Sidak's post hoc test). 164

Figure 4.11. HPASMC viability, as a percentage of untreated control, was measured after seeding and treatment at the same time with blank, imatinib-loaded NPs and free

20μM imatinib, with and without PDGF stimulation, via MTT assay A. 24 hours and B. 48 hours after treatment. Data are expressed as the mean of a single experiment +/- s.d. of 8 measurements (*P < 0.05, **P < 0.01, ***P < 0.001; data analysed by one-way ANOVA followed by Sidak's post hoc test). 165

Figure 4.12. HPASMC viability, as a percentage of untreated control, was measured after treatment in low-serum media with blank, imatinib-loaded NPs and free 20μM imatinib, with and without PDGF stimulation, via MTT assay A. 24 hours and B. 48 hours after treatment. Data are expressed as the mean of a single experiment +/- s.d. of 8 measurements (*P < 0.05, **P < 0.01, ***P < 0.001; data analysed by two-way ANOVA followed by Sidak's post hoc test). 167

Figure 5.1. Nanoparticle production via electrospraying and antibody conjugation through carbodiimide chemistry to PLGA NPs (Bev-PLGA NPs (Cd)) and through antibody adsorption to PLGA NPs (Bev-PLGA NPs (Ads)). Image created using ChirysDraw and Biorender and adapted from [162]. 173

Figure 5.2. Schematic of the secondary antibody experiment. 177

Figure 5.3. Bevacizumab standards in a four-parameter logistic (4PL) regression curve. 178

Figure 5.4. A. Zeta potential of unreacted NPs (PLGA NPs) activated NPs (NHS-PLGA NPs) and conjugated NPs (Bev-PLGA NPs). Data are expressed as mean +/- s.e. mean of 3 independent experiments (*P < 0.05, **P < 0.01, ***P < 0.001; data analysed by one-way ANOVA followed by Tukey post hoc test). B. FTIR spectrum confirming the activation of the PLGA NPs and showing conjugation spectra as antibody concentration increases. 184

Figure 5.5. ^{1}H-NMR spectra of pure PLGA, acid-terminated PLGA and the electrosprayed acid-terminated PLGA NPs (PLGA NPs) in $CDCl_3$, B. ^{1}H-NMR spectra of lyophilised NHS-PLGA NPs in duplicates with electrosprayed acid-terminated PLGA NPs as a negative control for activation in $CDCl_3$. 188

Figure 5.6. ^{1}H-NMR spectra of lyophilised Bev-PLGA NPs with a range of antibody concentrations (1μL, 2μL, 4μL) in $CDCl_3$, along with lyophilised NHS-PLGA NPs and

electrosprayed acid-terminated PLGA NPs as negative controls for conjugation in $CDCl_3$. 190

Figure 5.7. Flow cytometry analysis of A. Activated PLGA NPs (NHS-PLGA NPs),B. conjugated PLGA NPs (Bev-PLGA NPs) and C. their overlap following incubation with secondary antibody Alex Fluor 488..... 192

Figure 5.8. Optical density (O.D.) results from the BCA assay of the increasing concentration of A. EDC (R^2=0.99), B. NHS (R^2=0.98), C. PLGA NPs (R^2=0.99), D. the resulting conjugated PLGA NPs (Bev-PLGA NPs), the activated (NHS-PLGA NPs) and unreacted NPs (PLGA NPs). Data expressed as mean +/- s.e. mean of 3 independent (*P < 0.05, **P < 0.01, ***P < 0.001, ****P < 0.0001 ; data analysed by one-way ANOVA followed by Dunnett post hoc test), dotted lines represent the 95% confidence interval bands. 194

Figure 5.9. Measured bevacizumab concentration of activated (NHS-PLGA NPs). conjugated NPs (Bev-PLGA NPs (Cd) and adsorbed (Ads)) following carbodiimide conjugation and adsorption, respectively. Data expressed as mean +/- s.e. mean of 3 independent experiments (*P < 0.05, **P < 0.01, ***P < 0.001, ****P < 0.0001; data analysed by one-way ANOVA followed by Tukey post hoc test), ... 198

List of Tables

Table 1.1. Currently approved therapy for the management of pulmonary hypertension. 43

Table 1.2. Potential novel treatments for PAH 50

Table 1.3. Examples of various agents conjugated to PLGA particles using carbodiimide chemistry with the method of detection used. 64

Table 1.4. Drugs encapsulated in PLGA M/NPs for the treatment of PAH. 73

Table 1.5. Various drug delivery systems encapsulating imatinib with their different method of fabrication. 76

Table 1.6. Relevant differences between emulsion techniques and electrospray. ... 78

Table 1.7. Solvents relevant characteristics for the electrospraying of PLGA particles. Data was recovered from their respective material safety data sheets [246–249]. 83

Table 2.1. Common solvents used to prepare PLGA particles NPs. 92

Table 3.1. Nanoparticles (NPs) production parameters. 113

Table 3.2. Release kinetics models of imatinib-loaded NPs. 131

Table 5.1. Reagents used to prepare each samples with their respective moles. PLGA NPs moles were calculated based on the PLGA mass found in 5mg of NPs. (PLGA concentration is 2%wt, 5mg of NPs is produced using approximately 1.2mL polymeric solution which is equivalent to 24mg of PLGA). 175

Table 5.2. Carbodiimide conjugation protocol optimisation. 182

List of Equations

Equation 2.1. Beer-Lambert's law, where A is the absorbance or optical density, ε is the molar absorption coefficient, c is the sample concentration, and l is the path length (cm) [278]. 100

Equation 2.2. Cell viability equation using MTT assay, where OD = optical density/ absorbance. 102

Equation 2.3. Percentage of live cells, seen as cell viability, using the Live/Dead Assay 103

Equation 3.1. Encapsulation Efficiency equation. 115

Equation 3.2. Theoretical Drug Loading equation. 115

Equation 3.3. Actual Drug Loading equation. Measured drug mass was determined by measuring the absorbance of dissolved particles at λ_{max} and obtaining the concentration through the calibration curve. 115

Equation 3.4. The Korsmeyer-Peppas model 130

Equation 5.1. Four parameter (4PL) logistic regression model, where OD = optical density, Conc = antibody concentration, a = minimum value, b = Hill's curve slope, c = concentration at an inflexion point, and d = maximum value. 178

List of Abbreviations and acronyms

^{1}H-NMR	Proton nuclear magnetic resonance
5-LO	5-lipoxygenase
5HT	5-hydroxytryptamine
6MWT	6-minute walk test
A549	Lung carcinoma epithelial cells
anti-ACE	Anti-Angiotensin-converting enzyme
ACE	Acetone
ADL	Actual drug loading
AGE	Advanced glycation end products
API	Active Pharmaceutical Ingredient
ATP	Adenosine triphosphate
BCA	Bicinchoninic acid
BCRA1	Breast cancer gene 1
Bev	Bevacizumab
bFGF	Basic fibroblast growth factor
BMPR2	Bone Morphogenetic Protein Receptor 2
CCBs	Calcium channel blocker
CDCl3	Deuterated chloroform
cGMP	Cyclic guanosine monophosphate
CML	Chronic myelogenous leukaemia
COPD	Chronic obstructive pulmonary disease

CTEPH	Chronic thromboembolic pulmonary hypertension
DCM	Dichloromethane
DDS	Drug Delivery System
DLS	Dynamic light scattering
DMAc	Dimethylacetamide
DMEM	Dulbecco's Modified Eagle Medium
DMSO	Dimethyl sulfoxide
DNA	Deoxyribonucleic acid
DTPA	Diethylenetriaminepentaacetic acid
EA	Ethyl Acetate
EDC	1-ethyl-3-(3-dimethyl aminopropyl) carbodiimide hydrochloride
EE	Encapsulation efficiency
EGFR	Endothelial growth factor receptor
EHDA	Electrohydrodynamic atomisation
ELISA	Enzyme-linked immunosorbent assay
Em	Emission
ERAs	Endothelin receptor antagonist
ES	Electrospray
ET-1	Endothelin-1
ETA	Endothelin receptor A
ETB	Endothelin receptor B
FBS	Fetal Bovine Serum
Ex	Excitation

FDA	Food and Drug Administration
FTIR	Fourier transformed infrared
GA	Glycolic acid
GMP	Good Manufacturing Practices
HBSS	Hanks' Balanced Salt solution
HDAC	Histone deacetylase
HDAC6	Cytoplasmic histone Deacetylase
HER2	Human epidermal growth factor receptor 2
HIV	Human immunodeficiency virus
HMBC	Heteronuclear Multiple Bond Correlation
HPASMCs	Human arterial smooth muscle cells
HME	Hot-melt extrusion
HRP	Horseradish peroxidase
HSQC	Heteronuclear Single Quantum Coherence
HUVECs	Human Umbilical Vein Endothelial Cells
IC50	Half-maximal inhibitory concentration
IL-6	Interleukin 6
IMA-NPs	Imatinib-loaded NPs
IP	prostaglandin I_2
JNK	Jun N-terminal kinase
LA	Lactic acid
LTs	Leukotrienes
M/NPs	Micro/nanoparticles

MCT	Monocrotaline
MES	2-(N-morpholino) ethane sulfonic acid
mi-RNA	micro-RNA
MTT	3-(4,5-dimethylthiazol-2-yl)-2,5-diphenyltetrazolium bromide
nHAp	Nano-Hydroxyapatite
NHS	N-hydroxy succinimide
NPs	Nanoparticles
OD	Optical Density
PAECs	Pulmonary endothelial cells
PAGE	Poly-acrylamide gel electrophoresis
PAH	Pulmonary arterial hypertension
PAP	Pulmonary arterial pressure
PARP	Poly(ADP-ribose) polymerase
PAs	Prostacyclin analogues
PASMCs	Pulmonary arterial smooth muscle cells
PBCA	Polybutylcyanoacrylate
PBS	Phosphate Buffered Saline
PDE-5	Phosphodiesterase type 5
PDGF	Platelet-derived growth factor
PDGFR	Platelet-derived growth factor receptor
PDI	Polydispersity index
PEI	Polyethyleneimine
PGA	Poly-glycolic acid

PH	Pulmonary hypertension
PLA	Poly-lactic acid
PLGA	Poly(lactic-co-glycolic acid)
PSMA	Prostate-specific membrane antigen
PVR	Pulmonary vascular resistance
R2	R squared
RAGE	receptor for advanced glycation end
RHC	Right heart catheterisation
RhD-B	Rhodamine-B
RNA	Ribonucleic acid
ROCK	Rho-associated protein kinase
RT	Room temperature
RV	Right ventricle
SEM	Scanning Electron Microscopy
SESD	Spontaneous emulsification solvent diffusion
TDL	Theoretical drug loading
TEM	Transmission Electron Microscopy
TGF-(β)	Transforming growth factor beta
THF	Tetrahydrofuran
TMB	3,3',5,5'-Tetramethylbenzidine
TNBS	2,4,6-trinitro-benzenesul-phonic acid
TTE	Transthoracic echocardiogram
TUNNEL	Terminal deoxynucleotidyl transferase dUTP Nick End Labelling

UV-Vis	Ultraviolet-visible
VEGF	Vascular endothelial growth factor
WHO	World Health Organisation

Communications

Poster presentations

- “Development of micro/nanoparticles for targeted drug delivery in the treatment of pulmonary arterial hypertension” *Scheilly Tsilova; Dr Maryam Parhizkar; Dr Rebecca Lever; Dr Benjamin Schreiber* - **Poster presentation** at the 13th World Meeting on Pharmaceutics, Biopharmaceutics and Pharmaceutical Technology in Rotterdam 28th -31st March 2022.
- “Development of micro/nanoparticles for targeted drug delivery in the treatment of pulmonary arterial hypertension” *Scheilly Tsilova; Dr Maryam Parhizkar; Dr Rebecca Lever; Dr Benjamin Schreiber* - **Poster presentation** at the 5th Meeting of the UCL Cross-Disciplinary Network on Soft Materials on 20th June 2022.
- “Encapsulation of Imatinib in Polymeric Nanoparticles towards Treatment of Pulmonary Hypertension” *Scheilly Tsilova; Dr Maryam Parhizkar; Dr Rebecca Lever; Dr Benjamin Schreiber* - **Poster presentation** at the BioMedEng 22 Conference at UCL Engineering and UCL Medical Sciences under the umbrella of our UCL Institute of Healthcare Engineering on 8-9th September 2022
- “Development of micro/nanoparticles for targeted drug delivery in the treatment of pulmonary arterial hypertension” *Scheilly Tsilova; Dr Maryam Parhizkar; Dr Rebecca Lever; Dr Benjamin Schreiber* - **Poster presentation** at the JPAG Pharmaceutical Analysis Research Awards & Careers Symposium 2nd November 2022
- “Development of micro/nanoparticles for targeted drug delivery in the treatment of pulmonary arterial hypertension” *Scheilly Tsilova; Dr Maryam Parhizkar; Dr Rebecca Lever; Dr Benjamin Schreiber* - **Poster presentation** at the 6th Meeting of the UCL Cross-Disciplinary Network on Soft Materials 7th July 2023
- “Development of micro/nanoparticles for targeted drug delivery in the treatment of pulmonary arterial hypertension” *Scheilly Tsilova; Dr Maryam Parhizkar; Dr Rebecca Lever; Dr Benjamin Schreiber* - **Poster presentation** at the Controlled Release Society Annual Meeting and Exposition 24-28th July 2023

Oral presentation

- “Development of targeted nanoparticles for the treatment of pulmonary arterial hypertension” *Scheilly Tsilova; Dr Maryam Parhizkar; Dr Rebecca Lever; Dr Benjamin Schreiber* - **Oral presentation** at the UCL School of Pharmacy PhD Research Day 17th April 2024
- “Development of targeted nanoparticles for the treatment of pulmonary arterial hypertension” *Scheilly Tsilova; Dr Maryam Parhizkar; Dr Rebecca Lever; Dr Benjamin Schreiber* - **Oral presentation** at 3 Minute Thesis Competition in the Faculty of Life Sciences 14th May 2024 (Public vote winner)

Journal article publication

- **Tsilova, S. L.,** Hassoun A. R., Schreiber, B. E., Lever, R., & Parhizkar, M. Methods to Quantify Antibody Conjugation To Electrosprayed PLGA Nanoparticles Via Carbodiimide Chemistry. *(under review)*
- **Tsilova, S. L.,** Schreiber, B. E., Lever, R., & Parhizkar, M. (2024). Polymeric nanoparticles produced by electrohydrodynamic atomisation for the passive delivery of imatinib. *European Journal of Pharmaceutics and Biopharmaceutics*, *202*,114412. https://doi.org/10.1016/J.EJPB.2024.114412
- Parhizkar, M., Wang, F., Elbadawi, M., **Tsilova, S. L.,** Gaisford, S., & Basit, A. (2022). Machine Learning Predicts Electrospray Particle Size. *SSRN Electronic Journal*. https://doi.org/10.2139/SSRN.4017219
- Wang, F., Elbadawi, M., **Tsilova, S. L.,** Gaisford, S., Basit, A. W., & Parhizkar, M. (2022). Machine learning to empower electrohydrodynamic processing. *Materials Science and Engineering*, *132*, 112553. https://doi.org/10.1016/j.msec.2021.112553

Chapter 1. Introduction and literature review

1.1. General introduction

Pulmonary arterial hypertension (PAH) is a progressive and ultimately fatal condition defined by high pulmonary arterial blood pressure due to pulmonary artery cell over-proliferation and apoptosis resistance (endothelial and smooth muscle cells). The current treatments only alleviate symptoms and have low bioavailability and half-life but mainly do not resolve the cell dysfunction [1]. Novel therapies have been developed to address those issues on a cellular level. Imatinib is a chemotherapeutic small molecule acting as a tyrosine kinase inhibitor. It was considered a revolutionary treatment for chronic myeloid leukaemia by inhibiting the molecular drivers of the disease (BCR-ABL tyrosine kinase) and was therefore approved by the Food and Drug Administration (FDA) and marketed by Novartis for this indication in 2001 [2]. Imatinib has been researched for its potential to treat PAH and for its effectiveness at inhibiting smooth muscle cell over-proliferation by inhibiting a family of tyrosine kinase receptors, which includes the platelet-derived growth factor receptors (PDGFR) and c-KIT. However, the efficacy of the oral route of administration and, ultimately, the resulting oral bioavailability highly depends on the physical-chemical properties of the drug, such as aqueous solubility, permeability and stability, drug metabolism and the target site [3].

Therefore, an alternative delivery system was considered to achieve optimal bioavailability and efficacy. Targeted drug delivery provides active delivery of therapeutics to the affected cells, improving bioavailability, reducing drug distribution to other organs and tissues, and minimising systemic toxic effects [4]. Several studies investigating this mode of drug delivery have looked at poly(lactic-co-glycolic acid) (PLGA), an FDA-approved biodegradable polymer. Polymeric drug delivery systems show improved storage stability, more sustained and controlled delivery of their compounds, and the ability to be functionalised [5]. Imatinib has previously been encapsulated to address vascular smooth muscle proliferation in pulmonary arterial hypertension; however, the studies used costly and time-consuming multi-step processes that can lead to increased risk of errors, unwanted interaction with the drug, polydisperse and large particles, and low encapsulation efficiency [6–11].

Electrohydrodynamic atomisation or electrospray (ES) is a one-step technique that fabricates nano-systems [12]. The manufacturing is simple and inexpensive, with mild preparation conditions, and allows great flexibility in the type of materials used and control over the resulting products and their characteristics [13,14].

Ensuring accurate drug delivery to the relevant diseased cells increases the effectiveness of the treatment [15]. Imatinib acts on the intracellular ATP-binding site of the tyrosine kinase receptors, mainly the PDGFRs; therefore, imatinib needs to be internalised [16]. This internalisation depends on the size, shape (in passive targeting) or surface chemistry (in active targeting) of the nanoparticles. Both targeting strategies can allow the internalisation of the NPs. Still, active targeting is more influential in dictating the intracellular trafficking and the intracellular destination of the NPs, affecting the overall therapeutic outcome [17]. This targeted delivery can be achieved by conjugating antibodies to the drug delivery system, which will then deliver the drug specifically to the pulmonary artery cells [18]. The antibody-conjugated NPs will be delivered to the cells exposing the corresponding antigen instead of being systemically delivered and relying on the enhanced permeability and retention (EPR) effect [19]. This work necessitates producing and optimising electrosprayed imatinib-loaded nanoparticles, testing their efficacy on cell lines, including PAH-relevant cells, and generating antibody-conjugated NPs to enhance their delivery.

The following literature review will first focus on the pulmonary hypertension, its pathogenesis, the current approved treatments and novel treatments researched. The latter will introduce imatinib and the need to introduce drug delivery systems for its delivery. PLGA-based nanoparticles as targeted drug delivery systems are then explored, with a further examination on the electrospray technique as the method of fabrication.

1.2. Pulmonary hypertension

1.2.1. Introduction to PH

Pulmonary Hypertension (PH) is a pathophysiological state defined as a high mean pulmonary arterial pressure of ≥ 25mm Hg at rest or ≥30mm Hg with exercise [20]. PH is not uncommon, as it affects around 1% of the global population and has a high prevalence for those over 65 years old (10%) [21]. PH is linked to a large group of diseases, including congenital heart diseases, connective tissue diseases, liver disease (cirrhosis) and chronic lung diseases such as emphysema [22]. Therefore, diagnostic classification of the condition is crucial for its treatment and prognosis, as some form of therapy that is effective in one classification of PH may yield different results in another. A standard classification was created in 1998 and updated by the World Health Organization (WHO) in 2013, as displayed in Figure 1.1 [23]. Pulmonary arterial hypertension (PAH) is the first category of PH, which can be idiopathic, heritable (mutation in bone morphogenetic protein receptor type II (BMPR2) gene in 80% of cases), drug/toxin-induced, or associated with connective tissue disease, human immunodeficiency virus (HIV), congenital heart disease, or schistosomiasis [24,25]. PH due to left heart disease, the most common form of PH, forms the second group. The third group of PH results from chronic lung diseases and/or hypoxia, including chronic obstructive pulmonary disease (COPD). The fourth group of PH is caused by chronic thromboembolic pulmonary hypertension (CTEPH) and other pulmonary artery obstructions. The fifth category results from unclear and/or multifactorial mechanisms. PAH, the first group of PH, will be investigated further in this thesis [21,25,26].

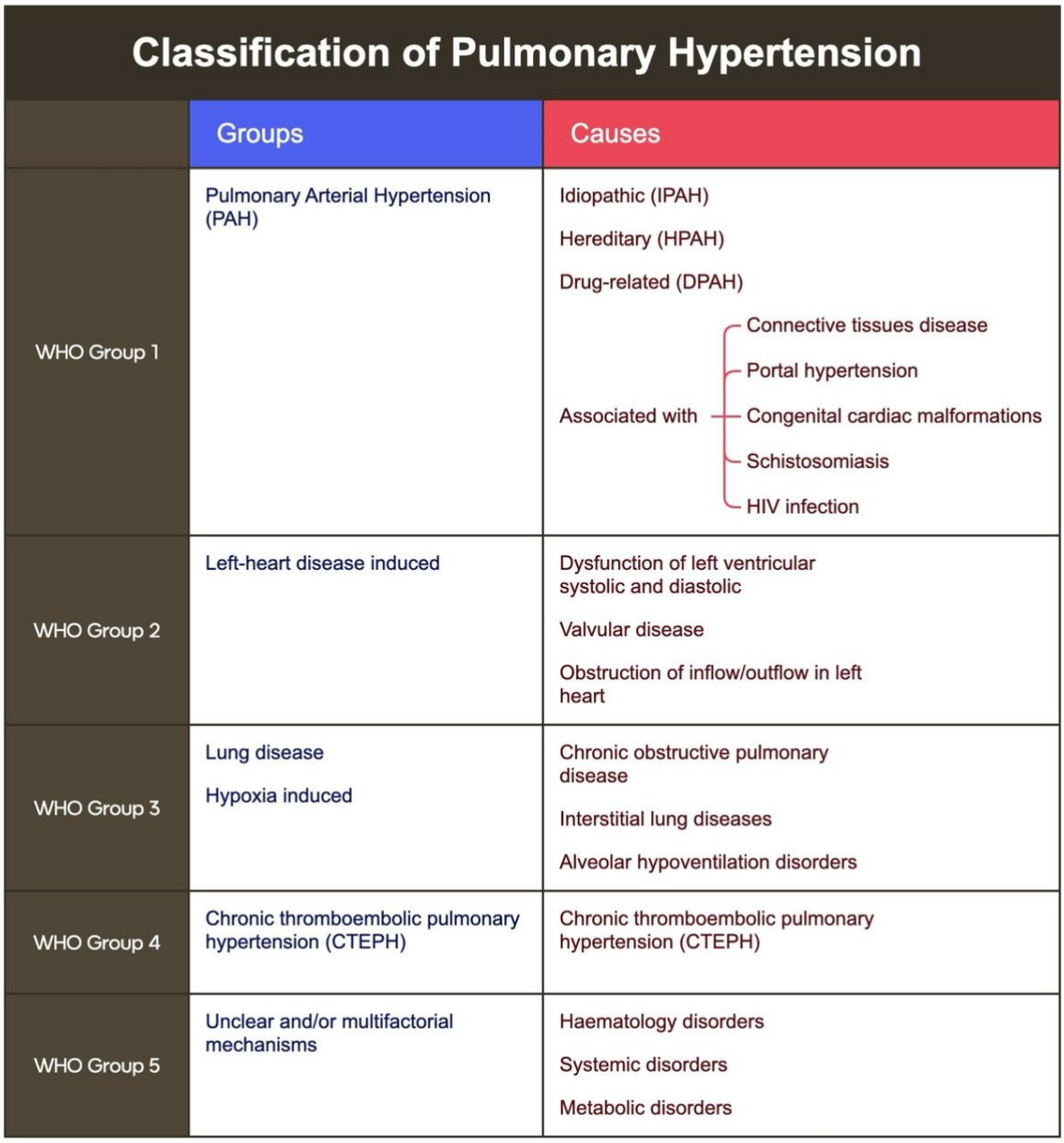

Figure 1.1. WHO Classification of Pulmonary Hypertension [27]. Diagram created using XMind.

1.2.2. Symptoms and diagnosis

General PH symptoms include dyspnoea, fatigue, angina, or syncope, which are non-specific. This means that despite increasing awareness of PAH, there is still a significant delay between the onset of symptoms and the diagnosis of PAH [28]. The diagnosis of PAH starts with consideration of clinical symptoms, with further tests undertaken to investigate the diagnosis if PH is suspected. Exercise capacity tests such as the 6-minute walking test (6MWT) and cardiopulmonary exercise testing (CPET) are performed to provide prognostic information [27]. CPET evaluates integrative exercise responses involving the pulmonary or cardiovascular system, such as gas exchange, ventilatory efficiency and cardiac function during exercise [29]. The 6MWT assesses the patient's aerobic capacity activity by measuring the distance they can walk in 6 minutes, which evaluates the responses of all the systems, mainly pulmonary and cardiovascular, involved during exercise. The test also measures the response to treatments in PAH patients and is often used as a primary endpoint in clinical trials for PAH [30]. Preliminary diagnostic tools for PAH include transthoracic electrocardiogram (TTE), chest radiograph, or echocardiography. TTE can demonstrate right ventricular hypertrophy and right atrial dilation, supporting evidence of PH. However, it does not have adequate sensitivity and specificity to diagnose PAH [31,32]. More invasive diagnostic tools, such as right heart catheterisation (RHC), are used to confirm the diagnosis. Right heart catheterisation assesses PH severity and diagnoses PAH by a hemodynamic procedure that allows direct measurements of the mean pulmonary arterial pressure (PAP), calculation of the pulmonary vascular resistance (PVR), and the performance of vasoreactivity testing at rest [31,33]. Immunology and blood tests can also help detect biomarkers to facilitate the diagnosis and monitoring of the condition. For instance, elevated uric acid levels are associated with higher mortality [34] Brain natriuretic peptides have also been used to indicate mortality risk, as their elevation has been associated with right ventricular overload [32]. High-sensitivity troponin, a myocyte necrosis biomarker, is primarily detectable in patients with PH and can also have predictive value due to its positive correlation with the increase in mortality [23].

1.2.3. Pathology and pathogenesis

As demonstrated in Figure 1.2, the pulmonary artery comprises endothelial cells in the tunica intima, smooth muscle cells in the tunica media, and fibroblast cells in the tunica externa (also known as tunica adventitia) [35]. PAH has been characterised by an abnormal remodelling of the pulmonary arteries, narrowing the blood vessels, which increases vascular resistance. The three types of cells composing the pulmonary artery all contribute to this remodelling. In PAH, the pulmonary artery endothelial cells (PAECs) sustain an injury, cell proliferation, invasion by myofibroblast-like cells and intimal fibrosis, which leads to a thickening of the tunica intima as shown in Figure 1.2.. The enhanced matrix deposition and proliferation cause obstruction of the vascular lumen and the formation of plexiform lesions [36]. These lesions comprise intimal thickening at branching points and, along with cell proliferation, they form a collagen-rich matrix that blocks the vessel. Further, vascular remodelling is induced by apoptosis resistance and sustained cell proliferation of the pulmonary artery smooth muscle cells (PASMCs) in the tunica media, further narrowing the vessels (Figure 1.2). The inflammation caused by PAH also causes the infiltration of inflammatory and immune cells in the tunica externa, leading to the immune cells and the fibroblast cells to activate, which all also contribute to the remodelling of the adventitia and, subsequently, the media and intima [37]. These vascular changes cause vasoconstriction and thrombosis, thus raising the pulmonary arterial pressure (PAP) and ultimately increasing the pulmonary vascular resistance (PVR) [38]. The resulting increased resistance in the pulmonary vasculature means the heart generates higher pressures to maintain cardiac output, which can lead to progressive right ventricular dysfunction. Ultimately, right ventricular (RV) failure develops: the primary cause of death from PAH [39,40].

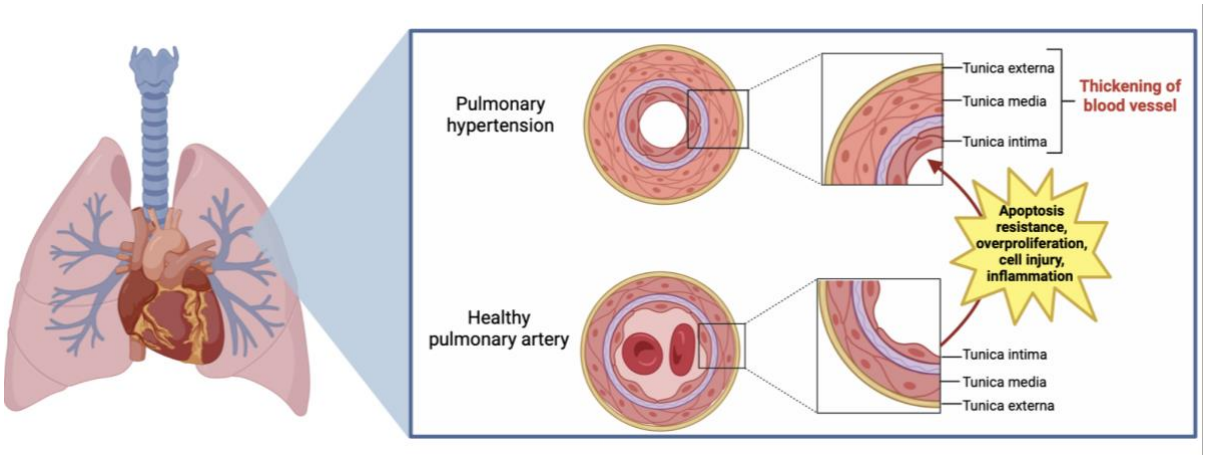

Figure 1.2. Diagram of a typical pulmonary artery vascular structure compared with a PH-affected vasculature [35]. Image created using BioRender.

1.2.4. Pulmonary hypertension treatments

1.2.4.1. Currently approved treatments

Multiple pathways have been investigated to target in managing the condition, and many have addressed the vasodilation/vasoconstriction imbalance [25]. One of the mechanisms involved in vasoconstriction is the increased opening of voltage-gated calcium channels in the PASMCs, which results in elevated cytosolic calcium levels, inducing PASMC contraction and proliferation [41]. This justifies using calcium channel blockers (CCBs) to vasodilate the pulmonary arteries and these drugs were the first to gain acceptance to manage PH [42]. Treatments were also developed that target three other pathways involved in the vascular changes in PAH: the prostacyclin, the nitric oxide, and the endothelin pathway [43,44]. Table 1.1 summarises the currently approved therapy used clinically to manage the condition and its limitations.

Prostacyclin pathway

In PAH, there is an imbalance between prostacyclin, a potent vasodilator and platelet aggregation inhibitor, and thromboxane, a potent vasoconstrictor and smooth muscle mitogen, where prostacyclin levels are reduced, and thromboxane levels are increased [45]. Treatments targeting this pathway were investigated to promote vasodilation by increasing activity of prostacyclin. As shown in Table 1.1, synthetic prostacyclin analogues (PAs) and prostacyclin receptor agonists, such as beraprost and selexipag, were developed to address the imbalance [46]. However, both treatments need frequent dosing because of their short half-life.

Endothelin pathway

Another potent vasoconstrictor is endothelial-1 (ET-1), which is produced by vascular endothelial cells and can act as a mitogen to stimulate smooth muscle cell proliferation in pulmonary arteries [47]. An abundance of endothelin-1 was found in endothelial cells in remodelled vessels, indicating the possibility that ET-1 may contribute to the creation and maintenance of the remodelling [48]. ET-1 binds to endothelin receptor type A (ETA) and B (ETB) to exert its effect, and the dual activation of these receptors mediates the proliferation and vasoconstriction [47]. Therefore, treatments targeting the

ET-1 pathway aim to block its downstream effect [49]. Table 1.1 displays a few treatments targeting this pathway either by inhibiting the activation of the ET-1 receptors (ETA and ETB) using bosentan, for instance, or by inhibiting ETA alone to only activate ETB by using ambrisentan [49]. Severe cases of hepatotoxicity have however been reported following the administration of endothelin receptor antagonists [50].

Nitric oxide pathway

Nitric oxide, on the other hand, is a potent vasodilator and inhibitor of smooth-muscle cell proliferation. The levels of nitric oxide synthase enzymes are decreased in the pulmonary vascular tissue of PAH patients [51]. Nitric oxide works by activating guanylate cyclase, which increases cyclic guanosine monophosphate (cGMP), leading to vasodilation. This effect is short-lived as phosphodiesterase degrades cGMP rapidly [52]. Treatments that target the nitric oxide pathway work by either promoting the effect of cGMP, leading to vasodilation, or inhibiting phosphodiesterase enzyme activity to prolong cGMP half-life [53]. Several treatments were introduced for PAH depending on its severity based on the expected 1-year mortality [54]. Additional supportive therapy includes oxygen, exercise, diuretics, and anticoagulant therapy.

Current therapies stimulate vasodilation or inhibit vasoconstriction by targeting the three pathways mentioned with examples of the drugs currently used clinically. Some current treatments, such as intravenous or inhaled PAs, are limited in their administration or short half-lives, respectively. These reduce their effectiveness, and patients' comfort and compliance, whilst increasing the frequency or duration of side effects [55]. Other treatments, such as endothelin receptor antagonist (ERAs), are limited in their safety profile, as seen in the limitation column of the table. All the treatments displayed above (Table 1.1) can ultimately cause vasodilation, even though they have different mechanisms of action. Therefore, their combination has been the primary therapy used clinically for PAH. The rationale behind combining therapy is simultaneously targeting two or three pathogenic pathways for a synergistic effect [56]. Two types of combination therapy are currently used: initial upfront combination therapy, where the treatments are administered together, and sequential combination

therapy, proposing adding another treatment to a background or initial therapy [57]. Overall, combination therapy improves the management of the condition by further increasing systemic vasodilation. However, it still does not address the underlying cell dysfunction, as it only provides further symptomatic relief. Despite current therapies, the prognosis remains a few years. Therefore, the search for more efficient treatments remains essential [58].

Outcomes	Pathways	Targets	Treatment	Examples of drugs	Limitations	Study
Vasodilatation stimulation	Prostacyclin	prostaglandin I_2 (IP) receptors	Synthetic prostacyclin analogues (PAs)	Epoprostenol, Treprostinil, beraprost and iloprost	Continuous intravenous or subcutaneous infusion and short half-life require frequent dosing.	31,59,60
			Prostacyclin receptor agonist	Selexipag		61
	Nitric Oxide	Soluble guanylate cyclase	Soluble guanylate cyclase stimulator	Riociguat	Oral administration and short half-life require frequent administration.	62,63

Vasoconstriction inhibition	Endothelin-1 (ET-1)	Endothelin receptors (ETA and ETB)	Endothelin receptors antagonist (ERA)	Bosentan and macitentan	Increase of hepatic aminotransferase and abnormal hepatic function. Higher incidence of peripheral oedema.	64–66
			Selective ETA Antagonist	Ambrisentan		67
	Nitric oxide	Phosphodiesterase type 5 (PDE-5)	PDE-5 inhibitors	Sildenafil and tadalafil	Oral route of administration shows lack of pulmonary selectivity and drug tolerance leading to dose increase.	68,69

Table 1.1. Currently approved therapy for the management of pulmonary hypertension.

1.2.5. Potential new treatments

Like cancer, PAH is a multifactorial condition involving multiple pathways, which is why combination therapy is the method of treatment currently used clinically. Additional pathways were therefore investigated to find further targets to address the dysfunction of relevant cells, such as growth factor inhibitors or metabolic modulators [70]. The vascular remodelling the pulmonary arteries undergo in the development of PAH displays similarities to cancer cell behaviour: hyperproliferation, apoptotic resistance, survival of PASMCs and modification of biochemical-metabolic pathways [71]. The cancer-like characteristics of PAH pathogenesis uncover the therapeutic potential of chemotherapy and other anti-cancer treatments to address the condition.

Inhibitors of growth factor kinase receptors, such as imatinib, sorafenib, and fasudil, have been investigated as a potential therapeutic route to stop cell proliferation [72–75]. Approaches inhibiting the activation of other receptor types to inhibit cell proliferation were also looked at, such as inhibiting the activation of the receptor for advanced glycation end (RAGE) pathway using aptamers [76,77]. The RAGE pathway has been found to contribute to the development of the condition via increased inflammation and proliferation of smooth muscle cells [78]. Aptamers are single-stranded oligonucleotides designed to fold into specific structures that bind to proteins. In this context, they bind and inhibit the activation of AGE receptors [79].

DNA-targeted therapies such as olaparib or doxorubicin were investigated to inhibit DNA repair or replication [80,81]. Histone deacetylase (HDAC) inhibitors were studied, and it was found that HDAC6 was upregulated in PAH patients and could be targeted and inhibited by tubastatin A, which decreases the pro-survival mechanism that HDAC6 was responsible for [82]. Epigenetic modifications have also been investigated, and multiple targets emerged from the research.

The BMPR2 loss-of-function mutation in PAH can be inhibited by indirectly reactivating it, using tacrolimus to inhibit BMPR2 repression [83]. Recent research showed that microRNAs (mi-RNA) are dysregulated in PAH, which causes the proliferation of pulmonary endothelial cells (PAECs) and the proliferation and migration of PASMCs

and fibroblasts [84]. Therefore, the encapsulation and delivery of mi-RNA, such as miR-204, can address this dysregulation [85].

Inflammation has also been found to play a significant role in the pathogenesis of the condition [86]. Bardoxolone methyl has been studied to activate the Nfr2 transcription factor, suppressing the pro-inflammatory transcription factor NF-κB effect [87]. The overexpression of pro-inflammatory cytokines like interleukin-6 (IL-6) has also been recorded in PAH. Therefore, a humanised anti-IL-6 receptor antibody, tocilizumab, was repurposed for PAH after being approved to treat various types of arthritis [88]. Another treatment to reduce the condition's inflammatory progression is RF-22c, a competitive inhibitor of the 5-lipoxygenase enzyme responsible for synthesising inflammatory leukotriene mediators [89].

Another uncustomary approach also examined metabolic modulator pathways, to target and activate mitochondrial-mediated apoptosis by inhibiting pyruvate dehydrogenase kinase [90]. Various treatments have also been developed to promote vasodilation of the pulmonary arteries using vasoactive mediators.

These potential new treatments have been summarised in Table 1.2 which displays the treatment investigated, the pathway and molecule it targets, and its mechanism of action.

Target category	Targets	Treatment	Mechanism of action	Stage of research	References
Growth factors kinase receptors	PDGF	Imatinib	Platelet-derived growth factor (PDGF) receptor α and β tyrosine kinase inhibition. reducing of PASMC hyperplasia	Phase III	[72]
	Raf-1, VEGF-R2, and PDGFR-β	Sorafenib	Inhibition of multiple tyrosine receptor kinases known to activate the downstream signalling pathway contributing to PAEC and PASMC hyperplasia	Phase Ib	[73]
	Rho A/ROCK	Fasudil	Vasodilator and potent Rho-kinase inhibitor to increase the expression of apoptotic markers and reduce the expression of growth factors and cell proliferation markers.	Pre-clinical and animal models Phase II	[74,75]
DNA damage	BRCA1 and PARP	Olaparib	Inhibits oral (poly(ADP-ribose) polymerases) PARP-1, a DNA repair enzyme.	Early phase 1	[80]

	Topoisomerase II activity	Doxorubicin	Topoisomerase II activity inhibition, preventing DNA replication in proliferation	One patient tested	[81]
	HDAC6 (Cytoplasmic histone Deacetylase)	Tubastatin A	Pharmacological inhibition of HDAC6 which regulates multiple pro-survival mechanisms.	Pre-clinical and animal models	[82]
Epigenetic modification	micro-RNA (mi-RNA)	Encapsulated miR-204	Its encapsulation and targeted release would prevent metabolic dysfunction and cell proliferation caused by its downregulation	Pre-clinical and animal models	[84,85]
	BMPR2	Tacrolimus/FK506	Dual mechanism: Calcineurin inhibitor and binds BMP signalling repressor FKBP12 to activate the BMP-mediated signalling.	Pre-clinical and animal models	[91]
Inflammation	Nrf2 and NFkB	Bardoxolone methyl	Induction of Nrf2 and suppression of NF-κB to reduce endothelial cell injury and inhibit blood vessel hyperplasia.	Phase II	[87]

	RAGE pathway	RAGE aptamer (AS-1),	The interaction between AGE and its receptor results in Reactive Oxygen Species and cytokines production and stimulates proliferation.	Pre-clinical and animal models	[76,77]
	Enzyme 5-lipoxygenase (5-LO) synthesizing leukotrienes (LTs)	RF-22c	Selective competitive inhibitor of 5-LO to reduce synthesis of leukotrienes, inflammation mediators.	Pre-clinical and animal models	[89]
	Interleukin-6 IL-6	Tocilizumab	Excessive immune stimulation by IL-6 is responsible for lymphoproliferative disorders associated with PAH. IL-6 receptor antagonist blocking inflammation and autoimmunity of IL-6 signalling.	Phase II	[88,92]
Metabolic modulators	Glucose oxidation	Dichloroacetate, Ranolazine	Inhibition of pyruvate dehydrogenase kinase to stop the suppression of mitochondrial	Open label study	[90,93–95]

			glucose oxidation and therefore activate mitochondria-dependent apoptosis	Phase I	
Vasoactive mediators	5-Hydroxytryptamine Transporter (5HT)	Terguride	5HT-receptor antagonists to block vasoconstriction and pro-proliferative factor caused by serotonin action on 5HT receptors in pulmonary vascular cells.	Pre-clinical and animal models	[96]
		Tryptophan hydroxylase 1 (TPH1)	Selective inhibition of tryptophan hydroxylase 1 (TPH1), the enzyme responsible for 5-HT biosynthesis, responsible for vasoconstriction	Pre-clinical and animal models	[97]
	Thromboxane A2	Terbogrel	Thromboxane synthetase inhibitor and thromboxane receptor antagonist blocking Thromboxane A2, a vasoconstrictor, platelet aggregate and a smooth muscle mitogen	Phase II	[98,99]

	Adrenomedullin	Adrenomedullin	Vasodilator peptide isolated from human pheochromocytoma with a powerful hypotensive effect.	Pre-clinical and animal models	[100]
	Apelin pathway	Apelin GPCR APJ and its ligand Apelin	Apelin are protective against PAH and play a role in the maintenance of pulmonary vascular homeostasis.	Pre-clinical	[101]
	3-hydroxy-3-methylglutaryl coenzyme A reductase (HMG-CoA reductase)	Pitastatin	Inhibition of HMG-CoA reductase increase production of endothelial nitric oxide by upregulating its synthase enzyme and hence improving endothelial injury and promote vasodilation.	Animal models	[102]

Table 1.2. Potential novel treatments for PAH

1.2.6. Imatinib and the PDGF pathway

Protein kinases comprise one of the most extensively studied drug targets due to their downstream signalling effect on cell over-proliferation, where their over-expression has been linked to oncogenesis [103]. Imatinib is a chemotherapeutic small molecule acting as a tyrosine kinase inhibitor and was considered a revolutionary treatment for chronic myeloid leukaemia for its ability to convert the fatal cancer into a manageable condition [2]. It was approved by the FDA and marketed by Novartis for this indication in 2001 [2].

Imatinib's mechanism of action was found to be relevant in several types of cancer for its inhibition of protein kinases, mainly ABL, BCR-ABL, PDGFRA, and c-KIT, as shown in Figure 1.3 [21]. Their activation and downstream signalling pathways contribute to cell growth, proliferation, and survival [104]. Imatinib exerts a direct antiproliferative and pro-apoptotic effect inside the cells by competing with adenosine triphosphate (ATP) for its binding site at the tyrosine kinase domain. Studies have reported contradictory evidence on whether imatinib's uptake depends on organic cation influx transporters [105,106], therefore the cellular uptake mechanism of imatinib remains unclear. It has, however, been found that the drug can be effluxed by ATP-dependent transporters such as P-glycoprotein[107,108].

Imatinib has also been prescribed for diseases including gastrointestinal stromal tumours and dermatofibrosarcoma protuberans and has been researched for its potential to treat other types of cancer [109].

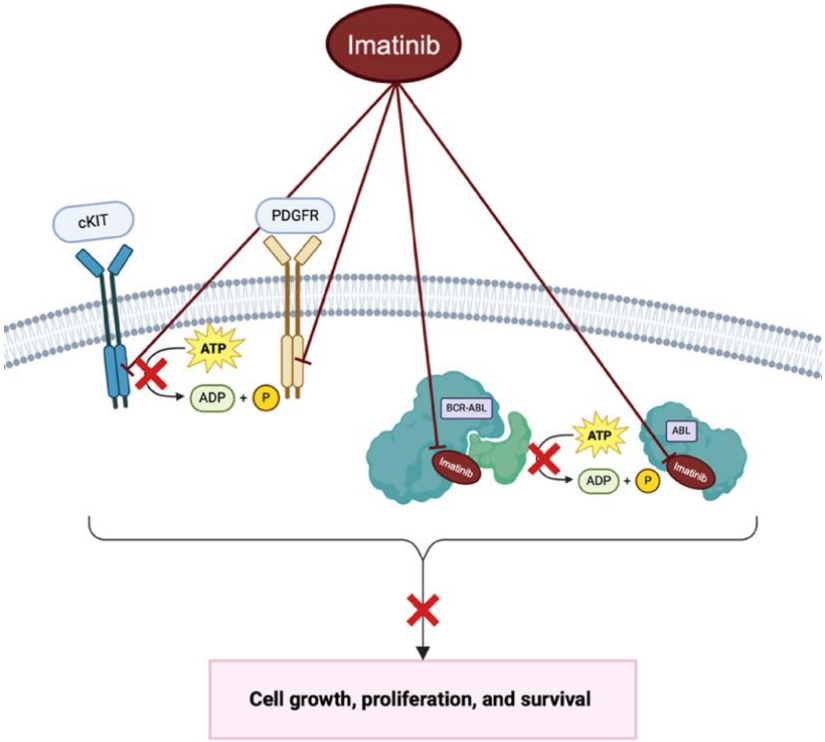

Figure 1.3. Imatinib's mechanism of action. Image created using BioRender.

Imatinib has been investigated for more than a decade for the treatment of severe PAH. Recent studies have found that peptide growth factors such as platelet-derived growth factor (PDGF) play a role in the abnormal remodelling of pulmonary resistance vessels and, therefore, in the progression of pulmonary vascular resistance (PVR) in PAH [110]. Increased expression of PDGF receptor mRNA was found in the pulmonary arteries of patients with severe PAH [110]. The activation of receptor tyrosine kinases elicits this effect, so tyrosine kinase inhibitors were investigated to halt the PVR progression [16]. Imatinib's mechanism of action was relevant in pulmonary hypertension for its pro-apoptotic effects on smooth muscle cells [111]. Indeed, the drug acts on the PDGF signalling pathway, which is implicated in the pathogenesis of PAH. PDGF dimers bind to PDGF-α and PDGF-β receptors to elicit the downstream response of abnormal proliferation, hypertrophy, smooth muscle cell and fibroblast migration [112].

Paracrine signalling pathways from pulmonary endothelial cells (PAECs) contribute to pathogenesis by increasing the release of vasoconstrictors and decreasing the release

of vasodilators acting on the pulmonary smooth muscle cells (PASMCs) [113]. It was found that the hypoxia-induced activation of PDGF receptors on PAECs led to the expression of Tph-1 and subsequent release of serotonin (5-HT), a vasoconstrictor from the endothelial cells [114]. The PAECs have also been found to release growth factors such as PDGF, transforming growth factor-β (TGF-β) or vascular endothelial growth factor (VEGF) during their dysfunction in PAH. This mediates the proliferation and activation of PASMCs, fibroblast cells and PAECs in PAH [115]. Indeed, Wu et al. (2020) also reported an increased release of PDGFs from PAECs in PAH patients, which led to the upregulation of the PDGF receptors in PASMCs. Abnormal hyperpermeable endothelial barrier is induced by lung injury and inflammatory stimulation of the endothelial barrier, which was reported in PAH [116]. Imatinib was also found to reduce the vascular leakage through the suppression of the Abl kinases [117]. Therefore, imatinib can indirectly affect PAECs to reduce vasoconstriction, PASMC proliferation, and migration but can also contribute directly to the resolution of PAH by addressing the leaky vasculature and the inflammation [118–120].

Multiple studies have evaluated imatinib's long-term efficacy and safety. Freyhaus et al. (2011) reviewed the limitations of the current therapies for PAH and outlined the role of PDGF receptors in PAH progression and how imatinib can be regarded as a potential treatment [121]. Ghofrani et al. (2005) examined the effect of imatinib on a single 61-year-old PAH patient over three months in combination with the current therapies, including prostacyclin analogues, endothelin receptor antagonists and PDE-5 inhibitors. The treatment completely reversed the lung vascular remodelling and right-sided heart hypertrophy [122].

Another study was undertaken five years later by Ghofrani et al. (2010), where 59 patients were enrolled in a 24-week randomised, double-blind, placebo-controlled pilot study, which led to a significant decrease in PVR and increased cardiac output in the treatment group. Serious adverse effects, however, occurred in 39% of the imatinib-receiving group [123]. Another Phase III study by Hoeper et al. (2013) enrolled 202 patients over 24 weeks again, and the results were consistent in the imatinib-receiving group with a significant decrease in PVR. However, serious adverse events occurred as well, with 44% reported in the treatment group [124,125]. Frost et al. (2015) extended

that study for a long-term study of the efficacy and safety of imatinib over 204 weeks. Still, it was terminated early, as nearly 94% of patients discontinued the extension study, with 31.3% of them discontinued due to adverse events where serious ones were frequent [126,127]. Therefore, imatinib's clinical potential is limited by its safety profile, and short half-life (~18 h) when administered orally [126]. Thus, an alternative delivery system must be considered for optimal bioavailability and efficacy.

1.3. Drug delivery systems (DDS)

1.3.1. Nanoparticles as DDS

When administered systemically, certain therapies have a low therapeutic effect resulting from ineffective drug delivery. This raises safety and efficacy concerns as patients need a higher dosage to attain an effective drug concentration. Targeted drug delivery provides localised delivery of therapeutics to the affected cells [128]. This increases the drug concentration and retention time at a specific location, which minimises systemic toxic effects and allows for higher-dose drug delivery to achieve greater efficacy with fewer safety issues [4]. Drug delivery systems (DDS) have therefore long been investigated for therapeutics, diagnostics, and preventative applications to achieve this targeted drug delivery, controlled drug release and intracellular delivery [129,130]. These systems also allow for the encapsulation of drugs with poor solubility when administered.

The use of therapies which were previously deemed unsafe or ineffective can be re-evaluated for the treatment of PAH using the targeted drug delivery approach [131]. It was reported that systemic diseases, such as PAH, can be effectively treated by delivering treatments via the pulmonary vasculature using the intravenous route to avoid first-pass metabolism. As mentioned above, both endothelial and smooth muscle cells play a vital role in PAH pathogenesis. Therefore, developing cell-targeted drug delivery would benefit the disease on a cellular level [132].

Lung-targeted drug delivery systems involve drug carriers such as micro or nanoparticles (M/NPs), increasing the drug concentration and efficacy within the target zone by controlling drug release and prolonging the time of action [4]. The drug delivery can be either passively or actively targeted. Passive targeting is based on the drug carrier's length of stay in the blood and its accumulation in target sites, and the DDS size will often determine their biological fate. Passive targeting is mediated by the enhanced permeability and retention (EPR) effect by tailoring drug carrier size, porosity, or shape [128]. The EPR effect depends on the increased vascular permeability caused by inflamed or tumour tissues to enable the retention and accumulation of

inflammatory cells, macromolecules like nutrients or non-targeted drugs at the disease site, leading to the passive diffusion of their load to affected tissues [133]. Active targeting is based on the binding of specific ligands or targeting agents to the surface of drug carriers such as antibodies, glycoproteins, polysaccharides, or glycolipids to recognise and bind to target sites such as pathological cells in brain, liver or tumour cells [134–137].

Nanoparticles (NPs) can be generated using a variety of materials, which, depending on the application, can be customised to have different sizes, shapes, morphology, and physical-chemical properties, such as their release profile [138]. Carbon-based NPs, for instance, have gained attention due to their electrical and heat conductivity and mechanical properties and have been researched for drug and gene delivery, theragnostic application and tissue engineering [139]. Metals such as gold, silver, copper, and zinc can bring optical, electrical, thermal, magnetic, and biological properties to the NPs [140]. Lipid-based, micelles, and polymeric NPs, have been further investigated for their drug delivery capacity as they are biodegradable and non-toxic, and their encapsulation methods can be tailored to their cargo [141]. They can differ in their release profile, encapsulation efficiency and electromagnetic radiation sensitivity [142].

Drug delivery systems carry the drug either by physically entrapping it within the system using nanoparticles for instance, or through chemical modifications to bind it to the system using polymer-drug conjugates [143]. This thesis investigated polymeric NPs further as they demonstrated their stability, safety, and ability to establish a controlled release of their load and protect the drug from the environment through entrapment[144]. More importantly, they have demonstrated the ability for surface functionalisation [142], which was sought after for the development of a targeted drug delivery system in this thesis.

1.3.2. Poly Lactic-co-Glycolic Acid (PLGA)

Poly(lactic-co-glycolic acid) (PLGA) is an FDA-approved biodegradable co-polymer and has been used for more than two decades for multiple applications, including drug delivery systems such as micro and nanoparticles [145]. PLGA is a copolymer composed of monomeric units of lactic acid (LA) and glycolic acid (GA) that are connected by ester linkages [15].

The ratio between lactic and glycolic acid in PLGA (x:y) can be changed for specific applications. For instance, PLGA 50:50 contains an equal amount of lactic acid and glycolic acid. PLGA 75:25 has a ratio of 75:25 lactic: glycolic acid, making the polymer less hydrophilic due to the increased lactic acid ratio [5,146].

The encapsulated drug can be released from a polymeric NP in three phases. The drug release starts with the initial burst release, following the NPs' introduction to the release medium, and drugs embedded on the surface of the NPs are released in a burst as PLGA hydrolysis begins at the surface [147]. The drug then diffuses out through the pores and cracks of the NPs in the second phase. The acidic by-products (glycolic and lactic acid) causes a reduction in pH which leads to further hydrolysis and degradation [148]. This leads to the third phase of the release, where the PLGA matrix erodes as the molecular weight of PLGA decreases to a point where the fragments becomes water-soluble and then fully degrades homogenously [148].

PLGA's physical-chemical properties, such as molecular weight, lactide and glycolic ratio, can affect the release of the encapsulated content by influencing the degradation rate. For example, the more hydrophobic-rich lactic acid PLGA would have a slower degradation as it absorbs less water [5,149]. Choosing the correct type of PLGA remains essential, as the suitable physical-chemical properties will provide a tailored formulation and a highly controllable release profile [19]. PLGA flexibility allows for encapsulating a wide range of molecules, including proteins, antibiotics, peptides, vaccines, cytotoxic and chemotherapeutics agents, and hydrophilic and hydrophobic drugs [149].

1.3.3. Active targeted PLGA NPs

PLGA-based DDS are themselves effective for a controlled and sustained drug release and can passively and actively target the site of action. Indeed, the chemical structure of PLGA, specifically its carboxyl end groups, allows the DDS's surfaces to be modified and functionalised to improve the DDS targeting and allow for an active targeted delivery [144]. Active targeting is more relevant in dictating the intracellular trafficking and the intracellular destination of the NPs to affect the overall therapeutic outcome [150]. Therefore, improving the targeting efficiency is essential to achieve a localised effect on the relevant and specific cells [15].

Active targeting can be achieved by conjugating or decorating cell target ligands, such as antibodies or peptides, on the surface of the particles to encourage the interaction between the PLGA-based DDS and cells [15]. Antibody-conjugated NPs, for instance, would be more likely to be rapidly internalised by the corresponding antigen-presenting cells [150]. A study by Dominguez et al. (2019) investigated trastuzumab, an anti-human epidermal growth factor receptor 2 (HER2) monoclonal antibody, to decorate cisplatin-loaded PLGA NPs and target ovarian cells overexpressing HER2 to improve its chemotherapy [151]. In another study by Patel et al. (2018), another chemotherapeutic, docetaxel, was encapsulated into PLGA NPs to bypass its primary toxicity of lowering white blood cells. The drug-loaded NPs were also functionalised using cetuximab to target epidermal growth factor receptors (EGFRs) for treating lung carcinoma [152]. Another polymer can also functionalise PLGA to enhance its delivery properties. For instance, Khan et al. (2016) created PEG-PLGA conjugates to improve the stability of the anticancer drug bendamustine delivery [153]. Tuyen Dao et al. (2014) used the same conjugate to prolong the circulation time of the antioxidant curcumin. [154]. Aptamers or peptides can also be used to target specific receptors, such as the YSA peptide targeting Ephrin type-A receptor 2 in injured lungs or A10 2'-fluoropyrimidine ribonucleic acid aptamer targeting an antigen on the surface of prostate cancer cells [155,156].

1.3.3.1. Antibody conjugation via carbodiimide chemistry

Several strategies have been used to conjugate agents to polymeric nanoparticles: adsorption (physical absorption, ionic bonding) or covalent bonding (carbodiimide, click and maleimide chemistry) [157]. Maleimide chemistry uses the less abundant sulfhydryl groups of antibodies to form a thioester link with the reactive ester of PLGA [18]. However, a lack of selectivity has been reported due to its unwanted interaction with protein serum, which led to off-target delivery [158]. Click chemistry, on the other hand, is a much more precise method of conjugating as it involves the fast reaction of two functional groups, azide and alkyne, catalysed by copper, that can only react with each other [159]. However, since those groups are not commonly found, they have to be introduced, adding complexity and further optimisation before the reaction occurs [160].

The easiest and most commonly used method is carbodiimide conjugation, which links a carboxylic group to an amine group by creating an amide bond. Indeed, it uses the antibody's primary amines ($-NH_2$) to generate an amide bond with the reactive ester of the PLGA without any chemical modification [161]. The carbodiimide chemistry can be used for a variety of applications, as carboxylic and amine groups are commonly found [162]. The method section 2.2.4 explains the conjugation chemistry in more detail.

The carbodiimide chemistry has been used to conjugate agents such as antibodies or peptides to PLGA particles for various applications and targets [15]. Monoclonal antibodies were mainly used to achieve an active targeted delivery approach [18]. On top of the studies mentioned above, Table 1.3 shows a more comprehensive list of agents conjugated to PLGA particles such as antibodies, peptides, small molecules, and aptamers using the carbodiimide chemistry.

For instance, the anti-human epidermal growth factor receptor 2 (HER2) monoclonal antibody was used by Chen et al. (2008) to deliver PLGA NPs carrying a toxin to solid tumours in breast cancer tissues to enhance its cytotoxic effect [163]. Another epidermal growth factor receptor (EGFR) type was targeted by two antibodies, panitumumab and cetuximab. Panitumumab allowed the targeted delivery of temozolomide, a chemotherapy agent, to EGFR-overexpressing glioblastoma cells [164]. Bevacizumab was also used in a study by Liu et al. (2019) to deliver PLGA NPs loaded with

dexamethasone, a corticosteroid, to target choroidal neovascularisation [165]. Various antibodies were also conjugated to PLGA NPs to target macrophages, such as anti-CD206 and anti-CD64, for targeted immunotherapy in tumour development or rheumatoid arthritis, respectively [166,167]

Conjugates	Target	Method of detection	Reference
A10 2’-fluoropyrimidine ribonucleic acid aptamers	Prostate-specific membrane antigen (PSMA) on the surface of prostate cancer cells	10% TBE–urea poly- acrylamide gel electrophoresis (PAGE)	[155]
YSA peptide	Ephrin type-A receptor 2 (EphA2), in injured lungs	Cellular uptake of NPs	[156]
Bevacizumab	Vascular endothelial growth factor (VEGF)	Bicinchoninic acid assay (BCA)	[165]
Hyaluronic acid	CD44 receptors on the surface of cancer cells	Zeta potential, Size, transmission electron microscopy (TEM)	[168]
Anti-CD133 monoclonal antibody	Cell surface marker CD133 in colorectal cancer	Zeta potential, Size, TEM and cellular uptake	[169]

Human serum albumin	Special albumin receptors on tumour cell membranes	Fourier transform infrared (FTIR), Proton nuclear magnetic resonance (^{1}H-NMR), size and zeta potential	[170]
Herceptin	Human epidermal growth factor receptor 2 (HER2) on the breast cancer cellular membrane	Enzyme-linked immunosorbent assay (ELISA) test and Secondary antibody (Flow cytometry)	[171]
Anti-Fas human monoclonal antibody	Fas is a type 1 membrane protein on plasma membrane of various cancer cells	Bicinchoninic acid assay (BCA)	[172]
Anti-CD64 monoclonal antibody	CD64 is a macrophage-specific cell surface receptor for rheumatoid arthritis	Bradford Assay	[167]
cLABL peptide	Intercellular cell-adhesion molecule-1 (ICAM-1) at inflammatory sites	2,4,6-trinitro-benzenesul- phonic acid (TNBS) colorimetric assay	[173]
Monoclonal antibody	Soluble membrane proteins of breast cancer cells	Bradford assay and secondary antibody (Flow cytometry)	[174]

Trastuzumab (anti-HER2 monoclonal antibody)	Human epidermal growth factor receptor 2 (HER2) for ovarian cancer	Fluorescein conjugation and quantification via ultraviolet-visible (UV-Vis) spectroscopy	[151]
Panitumumab (anti-EGFR antibody)	Epidermal growth factor receptor (EGFR) in glioblastoma cells	Bicinchoninic acid assay (BCA)	[164]
Anti-HER2 monoclonal antibody	Human epidermal growth factor receptor 2 (HER2) on solid tumour cells	Bicinchoninic acid assay (BCA) and Fluorescein conjugation (flow cytometry)	[163]
Polyethylene glycol (PEG)	n/a	FTIR and Proton nuclear magnetic resonance (^{1}H-NMR)	[153]
Anti-CD205 monoclonal antibody	C-type lectin receptor (CD205) on dendritic cells for inflammatory conditions	Bicinchoninic acid assay (BCA) and FTIR	[175]
Anti-CD206 monoclonal antibody	M2 macrophages for tumour immunotherapy	Secondary antibody (Flow cytometry and fluorescence microscopy)	[166]

Wheat germ agglutinin/lectin	Membrane-bound carbohydrates to facilitate receptor-mediated endocytosis into cancer cells	Bicinchoninic acid assay (BCA)	[176]
Cetuximab/anti-EGFR monoclonal antibody	Epidermal growth factor receptor (EGFR) on lung carcinoma cells	Bradford Assay	[152]
Anti- HER-2 antibody	Human Epithelial Receptor-2 (HER2)	Bicinchoninic acid assay (BCA)	[177]
Doxorubicin	Co-delivery of doxorubicin and berberine	FTIR and Proton nuclear magnetic resonance (^{1}H-NMR)	[178]

Table 1.3. Examples of various agents conjugated to PLGA particles using carbodiimide chemistry with the method of detection used.

1.3.3.2. Method for confirming and quantifying conjugation

Various methods have been used to confirm and quantify antibody conjugation to PLGA NPs. For instance, the bicinchoninic acid assay (BCA) was established as a common, easy and inexpensive method to measure the total protein concentration in a sample [179]. Liu et al. (2019) conjugated bevacizumab to PLGA NPs to deliver dexamethasone, a corticosteroid, to target choroidal neovascularisation [165]. They indirectly measured the binding efficiency of bevacizumab to PLGA NPs by measuring unbound antibodies using the BCA assay [165]. McCarron et al. (2008) also used the BCA assay to quantify antibody conjugation before undertaking in-vitro work using the conjugated PLGA NPs to target cancer cells and actively deliver the anti-cancer drug camptothecin [172]. Similarly, Banstola et al. (2020) conjugated panitumumab to target epidermal growth factor receptors (EGFR) and deliver temozolomide to glioblastoma cells. Similarly, they used the BCA assay to confirm the conjugation before undertaking in-vitro studies [164]. Chen et al. (2008) conjugated anti-human epidermal growth factor receptor 2 (HER2) antibodies to target those receptors on solid tumour cells and used the BCA assay as one of the methods used to confirm the conjugation [163].

Another method used was Fourier-transformed infrared spectroscopy (FTIR), a spectroscopy technique that provides information about functional groups present in the sample [163,180]. The technique recognises unique vibrations emitting from covalent bonds within functional groups following their interaction with infrared light [181]. For instance, the technique was used in the study by Manoochehri et al. (2013) to characterise the molecular structure of PLGA NPs following conjugation to human serum albumin [170]. They recognised the presence of the human serum albumin's amide bond in the conjugated NPs spectrum [170]. Another study by Khan et al. (2016) conjugated PEG to PLGA and used FTIR to confirm conjugation through the characteristic functional groups of PEG found in the conjugated NPs [153]. A study by Jahan et al. (2015) also confirmed the structural changes following the conjugation of CD205, a monoclonal antibody, to PLGA NPs using FTIR by showing the amide functional group [175].

Another spectroscopy method used is the proton nuclear magnetic resonance (^{1}H-NMR), which determines the structure of organic molecules by analysing the magnetic properties of protons in the molecule, enabling the identification of molecular structure and functional groups such as the amide functional group [182]. Manoochehri et al. (2013) used ^{1}H-NMR to confirm the conjugation of human serum albumin to PLGA NPs by recognising its characteristics peak in the ^{1}H-NMR spectrum of the conjugated NPs [170]. The same observation was seen in a study by Khan et al. (2016) displaying PEG's characteristic peak in the PLGA-PEG NPs [153]. Another study by Khan et al. (2019) conjugated doxorubicin to PLGA NPs, but conjugation was confirmed by recognising the amide bond in the ^{1}H-NMR spectrum. Structural changes, especially at the surface, are expected when decorating the surface of the PLGA NPs using antibodies.

The NPs' electric charges can be measured on their surface, and any structural changes to the surface of the NPs can lead to changes in their electric charges. The zeta potential has been used to measure those electric charges after applying an electrical field to the NPs. The electric charges on the NPs' surface enable them to move towards the attracting electrode, which then translates to the zeta potential signal (25). A change in the zeta potential following conjugation could help derive information regarding the structural state of the NP's surface and, therefore, imply the success of the conjugation. This method was used to establish further the success of the conjugation of human serum albumin in Manoochehri et al. (2013) and another study by Moura et al. (2014), conjugating the anti-CD64 monoclonal antibody to PLGA NPs.

Fluorescence techniques such as flow cytometry and secondary antibodies were used to indirectly prove the successful conjugation [183]. The secondary antibody's variable region binds to the primary antibody's constant region [184] and emits fluorescence when excited, which can be measured. Multiple studies used the secondary antibody to measure conjugation efficiency. Zhong et al. (2020) and Zhou et al. (2020) conjugated trastuzumab and anti-CD206, respectively, to PLGA NPs to measure the binding efficiency through flow cytometry [166,171]. Kocbek et al. (2007) and Chen et al. (2008)

conjugated monoclonal antibodies against antigen-presenting breast cancer cells to PLGA NPs and showed the conjugation through flow cytometry histogram [163,174].

The Enzyme-Linked Immunosorbent Assay (ELISA) has been considered the gold standard in clinical, pharmaceutical and biomedical laboratories for measuring molecule-specific concentrations [185]. Although ELISA is not commonly used to confirm or quantify antibody conjugation, as the technique is labour-intensive and expensive, its high sensitivity and specificity compensate for those disadvantages [186]. In their study, Zhong et al. (2020) used ELISA to measure antibody activity [171]. The technique was used to compare methods of conjugation, such as in Greene et al. (2017) [187] and Vashist (2012) [188].

Although those methods have been repeatedly used in previous studies, there has been inconsistency in the results obtained to confirm and quantify antibody conjugation. Therefore, there is a gap in the literature for a gold-standard method for quantifying antibody conjugation to PLGA NPs via carbodiimide chemistry.

1.4. PLGA-based DDS for PAH

Limitations for current treatments have already been established to include short half-lives, low bioavailability and adverse systemic effects [39]. To address those limitations, encapsulating the treatments in drug delivery systems, specifically PLGA particles, has been investigated [70]. Indeed, the encapsulation of prostacyclin analogues, endothelin-receptor antagonists such as bosentan, and PDE-5 inhibitors such as sildenafil and tadalafil [189–193] as well as the synthetic hydrogen sulphide donor from Zhang et al. (2021) [194], in PLGA M/NPs prolongs their circulation time, consequently extending their bioavailability and half-life, resulting in reduced dosing frequency and reduced side effects by avoiding systemic delivery as shown in the rationale column in Table 1.4 [70].

The encapsulation in these studies also aimed at reducing side effects and improving the solubility of the API. For instance, various drugs, such as tadalafil [195], curcumin [196] and a fatty oil of *Descurainia Sophia* [197] , were encapsulated mainly to address their poor solubility, increase their drug loading and reduce their side effects. In some cases, the encapsulation enabled the simultaneous delivery of multiple treatments for synergic effects, such as verteporfin and CB-839 [198] or sildenafil and rosiglitazone [199].

The treatments were encapsulated in a wide range of PLGA particle sizes depending on their route of administration, since inhalation and intratracheal administration, for instance, require the particle size to be less than 5µm for efficient deposition in the lungs [200]. Although the encapsulation of these approved treatments could extend the symptomatic relief and, in some cases, the survival of patients [189], the drugs themselves do not resolve the excessive growth and dysfunction of the pulmonary artery endothelial and smooth muscle cells in the long term [71], and cannot reverse the remodelling carried out by the condition [201].

As established above in Table 1.2, many other potential drugs were investigated, and a few were encapsulated for the added benefit of PLGA-based drug delivery systems, as shown in Table 1.4. As observed, a large variety of treatments were investigated to address PAH, but imatinib remained the sole therapy capable of reversing the

remodelling with sufficient clinical efficiency to reach Phase III of clinical trials. The serious adverse effects seen in the trials can potentially be addressed using PLGA NPs.

Encapsulated agent	Rationale for encapsulation	Particle size	Stage of study	Reference
	Approved treatments			
Prostaglandin E_1	For inhalation administration for reduced dosing frequency	1-5μm	Animal models	189,202,203
ONO-1301MS, novel sustained-release PAs	Single injection for sustained release for increased bioavailability	21-71μm	Animal models	
Prostacyclin analogues	Intratracheal administration due to PA's short half-life and serious life-threatening complications from the central venous catheter	20-100nm	Animal models	
Sildenafil and rosiglitazone	Inhaled administration of both treatment for synergic effect and rosiglitazone is a peroxisome proliferator receptor-a-agonist, a reduction of its activity has been associated with PAH.	5μm	Animal models	199,204

Bosentan	Intratracheal administration for better bioavailability and half-life and to reduce the side effect of high level of liver enzymes	312-1350nm	In-vivo pulmonary absorption study	[190]
Sildenafil citrate or Sildenafil	Inhaled formulation improves bioavailability in the lungs. The encapsulation reduces side effects and increase drug load for better scalable process.	2-5μm	In-vivo lung deposition study	[191–193]
		2-9μm	Animal models	
		6-13μm	In vitro aerosolization study	
Tadalafil	Inhaled administration. Low aqueous solubility and its systemic delivery results in unwanted side effects.	35-302nm	In vitro aerosolization study	[205]
Novel treatments				

Fatty oil of Descurainia Sophia	Inhibits PLC/IP3R/Ca2+ signalling pathway to reduce abnormal proliferation of PASMCs. The oil has poor stability and low solubility.	323.87 ± 4.81nm	Animal models	[197]
S-aspirin (ACS14), a novel synthetic hydrogen sulphide donor	Inhaled administration to mimic the slow and continuous generation of hydrogen sulphide.	4.4 ± 0.4μm	Animal models	[194]
CRISPR plasmid DNA (CRISPR–Cas9/guide RNA plasmid DNA)	Endothelial cells-targeted knockdown of Nos3 to inhibit PAH remodelling by the elevated nitrative stress and restore caveolin-1 expression	80-250nm	Animal models	[206]
Verteporfin and CB-839 simultaneously	Synergic effect on two pathways, Verteporfin inhibits a transcription factor and CB-839 inhibits an enzyme. Both inhibitions decreased the hyperproliferative phenotypes of PAH	1-5nm	Animal models	[198]

Curcumin	Curcumin has poor biopharmaceutics properties although has been found to possibly have an effect on PH's oxidative pathways.	237 ± 6nm	Animal models	[196]
Pitastatin	Currently approved dosage is not enough to exert constructive effects. Encapsulation allows for a higher dosage for better clinical implications without raising side effects.	196 ± 29nm	Animal models	[102]
Imatinib	Serious adverse effects were reported in Phase III when systemically administered so encapsulation can address systemic toxicity.	20-100nm	Animal models	[10]

Table 1.4. Drugs encapsulated in PLGA M/NPs for the treatment of PAH.

1.4.1. Encapsulating Imatinib in micro-nanoparticles

Imatinib has been investigated in DDS extensively to address its toxicity, low bioavailability and half-life, for various conditions. Lipid nanoparticles have been studied to encapsulate imatinib in solid-lipid nanoparticles [207] or lipid nanocapsules [208]. Imatinib has mainly been investigated in a PLGA-based drug delivery system, as shown in Table 1.5.

For instance, Benny et al. (2009) developed imatinib-loaded PLGA microspheres to treat glioblastoma. They injected microspheres intracranially into a glioblastoma mouse model, which led to a 79% decrease in tumour volume 14 days after the injection [6]. Another study on resistant glioma cell lines by Khan et al. (2016) looked at introducing imatinib-loaded PLGA nanocarriers to overcome imatinib resistance in glioma, resulting from the overexpression of P-glycoprotein efflux transporters discharging imatinib from leukemic cells [108]. The study showed a better uptake of the NPs and a decrease in the half-maximal inhibitory concentration (IC_{50}) in three different cell lines compared to free drug administration [209]. Imatinib-loaded PLGA microspheres were also studied for the treatment of a further type of brain tumour, craniopharyngioma, where a rat corneal angiogenesis assay was utilised, and the imatinib-loaded microspheres were found to reduce neovascularisation significantly [9].

Imatinib has also been encapsulated to address conditions other than cancer, such as the vascular smooth muscle proliferation seen in both atherosclerosis and, of course, pulmonary arterial hypertension. Esfandyari-Manesh et al. (2020) showed a controlled release of imatinib from peptide-functionalised PLGA NPs developed for the targeted treatment of atherosclerotic regions [7]. Nakamura et al. (2015) demonstrated significant inhibition of smooth muscle cell proliferation 24 hours after administrating the loaded NPs intratracheally on a rat model of pulmonary hypertension [10].

DDS material	Method of fabrication	Application	Reference
Chitosan-based polymer	Ionic gelation technique	Colorectal cancer	[210]
PLGA	Modified double emulsion solvent extraction method	Glioblastoma	[6]
PLGA	Modified emulsion/solvent evaporation technique	Atherosclerosis	[7]
Liposomes	Thin film hydration method	Alzheimer's disease	[211]
PLGA	Emulsion solvent evaporation method	Breast cancer	[8]
Silver	"Green synthesis"	Breast cancer	[212]
PLGA	Modified double emulsion/solvent evaporation technique	Craniopharyngioma	[9]
Polybutylcyanoacrylate (PBCA)	Mini-emulsion polymerization method	Chronic myeloid leukaemia	[213]
Cremophor®	Double water-in-oil–water (w/o/w) nano emulsions	n/a	[214]

PLGA	Coaxial electrospray	Cervical cancer	[215]
Nanohydroxyapatite (nHAp) (bio ceramics)	Co-precipitation	Cancer (general)	[216]
PLGA	Emulsion solvent diffusion method	Pulmonary hypertension	[10]
PLGA	Double emulsion method	n/a	[11]
Solid-lipid (Precirol® ATO 5)	Hot homogenization method	n/a	[207]
N-oleoyl-D-galactosamine	Solvent diffusion technique	Oral delivery	[217]

Table 1.5. Various drug delivery systems encapsulating imatinib with their different method of fabrication.

1.4.1.1. Method of imatinib-loaded NP production

Many methods have been investigated for the fabrication of polymeric nanoparticles. As shown in Table 1.5, the most common method to produce imatinib-loaded PLGA particles is the single or double emulsion evaporation method. These methods have been favoured as they have been fairly researched as the process is relatively simple and do not require specific equipment. These methods also yield batches of particles making it scalable and can be easily suspended in aqueous solution. However, these methods can be time-consuming multi-step processes and procedures requiring additional optimisation, which can lead to increased risks of errors and increased unwanted interaction with the drug[5,218]. These methods also involve high temperatures, surfactants and harsh organic solvents and require the additional step of washing the NPs to remove the surfactant and excess organic solvents, which can be toxic if not washed properly [219]. The nanoparticles are also collected in an aqueous suspension form, significantly reducing their storage stability due to PLGA hydrolysis [5]. The subsequent freeze-drying extends the production time, and pores can be formed from the process, leading to premature drug release and reducing drug loading [220].

The following section will introduce the technique utilised in this study to produce the PLGA particles, electrohydrodynamic atomisation or electrospray (ES), and Table 1.6 compares emulsion techniques and electrospray.

ES does not require the use of surfactants or high temperatures like emulsion techniques. Its one-step process also makes it continuous, avoiding generating significant waste during the multiple production steps [221]. The emulsion methods also lead to extensive experimental load during optimisation in order to produce monodisperse particles of a certain size with a high encapsulation. A new batch of particles have to be produced after each optimisation which is time-consuming [221]. The electrospraying technique allows for quick optimisation due to the precise control of the parameters [218].

Emulsion techniques	Electrospray
Batch method of fabrication	Continuous method of fabrication
Do not require specific equipment	Requires additional equipment that can be costly
High yield	Yield dependent on flow rate
Use of high temperature for solvent extraction	No use of high temperature
Use of surfactant	No use of surfactant
Multiple steps and equipment process	One-step process
High experimental load for optimisation	Lower experimental load for optimisation
Higher amount of waste	Low to no waste
Particles suspension freeze-dried to collect dry	Particles collected dry
Particles easily suspended in aqueous solution	Particles difficult to suspend in aqueous solution

Table 1.6. Relevant differences between emulsion techniques and electrospray.

1.5. Electrohydrodynamic atomisation or electrospray (ES)

1.5.1. Electrosprayed particles as DDS

Electrohydrodynamic atomisation (EHDA) or electrospray (ES) is a one-step technique for fabricating polymer-based delivery systems, nano/microparticles and nano/microfibers. A diagram of the EHDA setup can be found in Figure 1.4. In addition to the benefits of DDS, such as localised delivery, improved solubility and bioavailability, reduced side effects, and controlled sustained drug release, the technique provides additional benefits. The manufacturing is simple and inexpensive with mild preparation conditions, such as the absence of emulsifiers or exposure to organic solvents and high temperature [13,222], which can benefit sensitive biomolecules [223]. The technique's simplicity and versatility provide high reproducibility and scalability, showing high industrial application potential. The large surface area to volume ratio and the large porosity of the particles improve both their sensitivity and capacity [224,225]. Various molecules such as proteins, peptides, enzymes, DNA, RNA, living cells and other hydrophobic and hydrophilic agents can be successfully encapsulated in this single-step process [222].

Production of PLGA NPs using electrospraying has shown its potential in many studies for reducing severe side effects and localised drug delivery. For instance, metronidazole was encapsulated using ES due to its carcinogenicity concerns [226]. A study by Parhizkar et al. (2016) electrosprayed PLGA nanoparticles encapsulating the anti-cancer drug cisplatin for a controlled dosage and release [227]. Studies by Xie et al. (2006) and Chatterjee et al. (2020) electrosprayed paclitaxel and methotrexate NPs, respectively, looking to minimise systemic exposure and ensure a high concentration reaching the brain for malignant glioma [228] or drug-resistant metastatic breast cancer cells [229] respectively. ES has also been used to address solubility and bioavailability issues of certain therapies. For instance, Zhang et al. (2018) electrosprayed PLGA particles loaded with progesterone, a hydrophobic drug, to address its low aqueous solubility, inconsistent bioavailability and high first-pass metabolism from being usually

administered orally [230]. In another study by Kibler et al. (2020), PLGA microparticles carrying IQ-1S, a c-Jun NH2-terminal kinase (JNK) inhibitor, were electrosprayed to improve its poor solubility and address inflammatory conditions. Since IQ-1S tends to crystallise and has poor solubility in organic solvents, electrospraying enabled its encapsulation into PLGA microparticles [231].

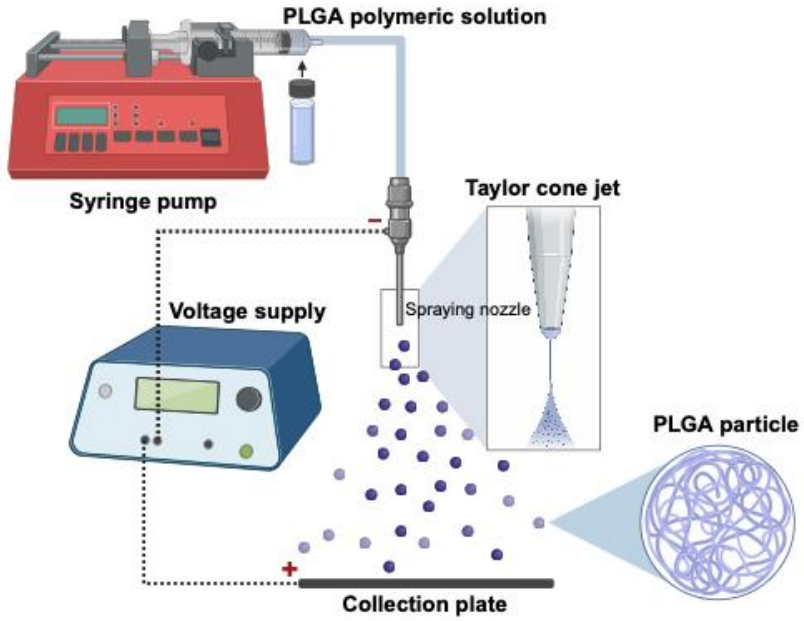

Figure 1.4. Diagram of the electrospray (EHDA) set-up. Diagram created using BioRender.

1.5.2. Parameters affecting the particles

The versatility of electrospraying enables the formation of particles of specific size, morphology, shape, porosity, and composition [232]. Flexibility over the particle's formulation is possible through the tailoring of the multiple processing variables. The process optimisation is highly complex: each parameter plays an equally important role and interdependently influences the particle characteristics [222]. The formation of particles relies on atomising a liquid under an electrical field. Polymer solution droplets are ejected from a nozzle under a specific flow rate. When a droplet is formed, two forces are applied to prevent the droplet from falling: cohesive and adhesive forces [233]. Adhesion forces are intermolecular forces that bind a substance or solution to a surface or, in this case, the nozzle. Cohesive forces are intermolecular forces that bind similar molecules responsible for the solution to stay in bulk and prevent their separation [234]. A voltage is applied at the nozzle to create an electrical field to break the droplet's surface tension. The accumulation of charges causes a protrusion and distorts the droplet at the nozzle into a conical shape known as the Taylor cone. When increasing and reaching the critical voltage, the maximum charge the droplets can carry is reached [235]. The applied voltage creates an electrostatic force called the Coulomb force that competes with the droplet's cohesive forces. Coulomb force of repulsion between the highly charged droplets then breaks the shape of droplets, leading to Coulomb fission, where the surface tension is overcome and subsequent smaller and self-dispersed particles [223,236]. Then, the positive charges within the droplet migrate towards the negatively charged collection plate [237]. While migrating, the solvent evaporates, generating particles on the collection plate. Tailoring these interdependent variables is, therefore, crucial to the generation of desired particles. Figure 1.5 shows how each type of parameter can be tailored to achieve particles of a specific size and shape.

1.5.2.1. Solution parameters

Any parameter affecting the characteristics of the polymer solution is considered when designing a formulation. Increasing the polymer concentration increases viscosity and surface tension as they are closely related [238]. Surface tension measures forces acting at the boundary between liquid and air. Viscosity is related to the polymer molecular weight and the polymer concentration in the solution [238]. A highly viscous solution can generate more elongated particles bridging on fibres, and low viscosity generates more spherical particles, as shown in Figure 1.5. A higher viscosity and surface tension require a higher voltage to overcome the surface tension and break it to form a Taylor cone jet [232]. Figure 1.5 also shows how the solvent evaporation rate can affect the particle size as it is related to the speed of solidification of the particles. If the solvent does not evaporate fast enough, the residual solvent can remain in the collected particles, making them wet and leading to irregular particles [232]. The solvent needs to evaporate fast enough to allow the breakdown of the droplets. If a solvent is too volatile, the electrospraying process can be unstable, and the solvent can evaporate before fission, leading to large, porous, polydisperse particles [232]. High solvent conductivity can favour Coulomb's fission, leading to elongated and small particles and, therefore, high dispersity in the size of the particles [222]. Table 1.7 shows common solvents used for electrospraying and their respective relevant characteristics. For example, Dichloromethane (DCM) [226,239] has the highest evaporation rate, with Tetrahydrofuran (THF) [240,241] and Acetone (ACE) [242,243] close behind. DCM and THF have similar conductivity, and all three solvents have similar viscosity and surface tension. Dimethylacetamide (DMAc) [230,243–245], on the other hand, has the lowest evaporation rate and the highest conductivity, surface tension and viscosity. DMAc and Acetone are the solvents used in this work.

Solvents	Evaporation rate (reference liquid is butyl acetate = 1)	Electrical conductivity (S/m)	Viscosity (mPa·s at 20°C)	Surface tension (dyn/cm at 20°C)
DCM [226,239]	27.5	2–2.5x10^{-9}	0.437	28.20
ACE [242,243]	11.6	2x10^{-5}	0.32	24
DMAc [230,243–245]	0.17	0.5	1.02	32.43
THF [240,241]	8	1.5x10^{-16}	0.456	26.4

Table 1.7. Solvents relevant characteristics for the electrospraying of PLGA particles. Data was recovered from their respective material safety data sheets [246–249].

1.5.2.2. Processing parameters

Once the solvent parameters are set, processing parameters must complement the former to develop particles of the desired size, shape, and morphology. The speed at which the solution is dispensed, or flow rate, is crucial to the size distribution of the particles, i.e., size and polydispersity. Indeed, Figure 1.5 shows that a high flow rate leads to large NPs. When a solution is dispensed rapidly, the solvent has insufficient time to evaporate before reaching the collecting plate, leading to larger and irregular particles [250]. In contrast, A low flow rate can help generate small homogenous nanoparticles. The distance between the tip of the nozzle and the collecting ground impacts the speed of solvent evaporation; a greater distance will give the solvent more time to evaporate before reaching the collecting ground [232].

Optimising the voltage remains essential, as solvents do not evaporate fast enough with a short collecting distance, and fission only occurs early when the voltage is low. A low voltage can also lead to large, irregularly shaped particles. High voltage allows

for the critical voltage limit to be reached quicker and for fission to happen earlier, leading to small and monodispersed particles [251]. However, as displayed in Figure 1.5, when the voltage is too high, the strong electric field can lead to more stretching of the NPs, making them more elongated, emphasising the importance of optimising the voltage [252].

1.5.2.3. Environmental Parameters

A higher temperature speeds up the drying and solidification of the particles. It also increases the solution conductivity and reduces viscosity, leading to a smaller and spherical particle size. High humidity also impacts the solvent evaporation and turns the particles' morphology from solid to porous [222,232]

Although multiple data are generated through individual research to predict particle characteristics, only some are conducted to automate this process. Machine learning, a subset of artificial intelligence, was found to address the optimisation challenge by simulating the EHDA process and consequently automating its workflow. Our work in Wang et al. (2022) demonstrates how ES benefits from machine learning as it can accelerate its optimisation process, for example by using a literature database and experimental validation to predict the particle diameter [253].

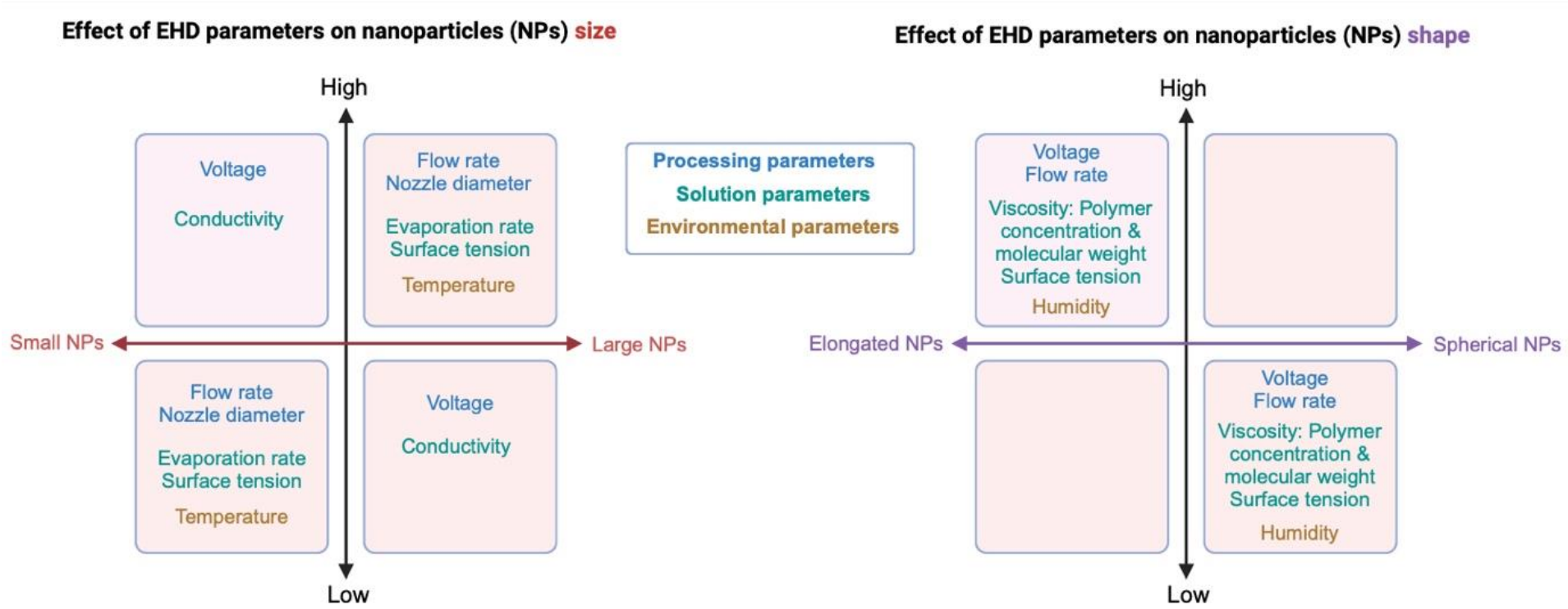

Figure 1.5. EHD experimental parameters affecting the size and shape of nanoparticles. Created using BioRender [218,222,232].

1.6. Thesis aims and rationale

Due to its multifactorial pathology, chemotherapy agents like imatinib are being repurposed to treat pulmonary arterial hypertension. Imatinib has shown tremendous potential for reversing the remodelling and right heart hypertrophy experienced by PAH patients. However, due to its lack of safety when administered systemically, the drug did not advance beyond Phase III of clinical trials for PAH.

Drug delivery systems such as nanoparticles have been established for their potential to carry effective treatments that would have been discontinued due to poor solubility, bioavailability, and safety. Many studies have examined the encapsulation of imatinib in nanoparticles using various methods. However, electrospraying enables the generation of spherical and nanosized particles carrying a high drug load to ensure reproducibility, simplicity, and control over the manufacturing process.

The use of PLGA as the NPs' material allows for a more controlled release of the drug and for the opportunity to actively target the NPs by decorating their surface with relevant antibodies. Because of imatinib's toxicity and efficacy, targeting the delivery system to specific affected cells is essential to reach imatinib's full potential. It has been established previously that the intracellular delivery of imatinib is required for the drug to exert its anti-proliferative effect and to avoid resistance to imatinib in cells.

Therefore, ensuring a targeted delivery to the relevant cells, such as pulmonary arterial endothelial and/or smooth muscle cells, is essential. Conjugating the relevant antibodies to the NPs ensures that they dock onto corresponding antigen-presenting cells and are internalised more effectively and rapidly. This work aims to develop a treatment for pulmonary hypertension by actively delivering electrosprayed imatinib-loaded nanoparticles to pulmonary endothelial and smooth muscle cells. The nanoparticles will address the toxicity that prevented imatinib from being approved previously and ensure the NPs are precisely delivered to the relevant cells, enabled by the appropriate antibodies decorating their surface. This thesis will address these aims as outlined in the overview below.

1.6.1. Thesis overview

Chapter 2 – Methodology

This chapter outlines the polymer, solvents, and drugs used to fabricate the NPs, the different cell lines tested, and the reagents involved in conjugating the antibody to the NPs. It then explains how the particles were produced and characterised. It displays how the effect of the imatinib-loaded NPs on cells was measured and how it was established that the NPs were internalised by cells. The methods of conjugation of the antibody to the NPs are explained, and the methods to detect its successful conjugation are also outlined here.

Chapter 3 – Production and optimisation via electrospraying, physical-chemical characterisation and in-vitro efficacy of imatinib-loaded PLGA NPs

This chapter investigates the impact of electrospraying parameters on the size and morphology of the particles produced. It outlines the physical-chemical characterisation of the imatinib-loaded particles. It also investigates the effect of using different types of PLGA and how the NP characteristics can affect imatinib's subsequent release. It confirms the expected antiproliferative effect of imatinib, carried by the PLGA NPs, on a cancer cell line and confirms their uptake into cells.

Chapter 4 – The effect of imatinib-loaded NPs on vascular cells

This chapter demonstrates the effect of the drug-loaded NPs on endothelial cells and pulmonary arterial smooth muscle cells. It shows that imatinib's known impact on endothelial and smooth muscle cell viability can be replicated and even enhanced using the imatinib-loaded NPs. High control over the release of imatinib to the cells is also demonstrated in this chapter. This chapter addresses the effect of imatinib on pulmonary artery smooth muscle cell viability when stimulated with the growth factor PDGF, which is known for participating in the pathogenesis of PAH.

Chapter 5 – The antibody conjugation to electrosprayed PLGA NPs via carbodiimide chemistry

This chapter describes the optimisation of protocols in conjugating the model antibody bevacizumab to electrosprayed PLGA NPs via carbodiimide chemistry and the various methods used to confirm and quantify the conjugation. It also demonstrates the validity of the techniques used. Finally, the chapter investigates the adsorption method as an alternative way of attaching antibodies.

Chapter 6 – Conclusion and Future Work

This chapter summarises the findings of this work and provides a conclusion to the overall project work. It also discusses any future work suggestions for each aspect of the project. A full list of references can also be found here.

Chapter 2. Materials and Methodology

2.1. Materials

2.1.1. Electrospraying Materials

2.1.1.1. PLGA

PLGA, or poly(lactic-co-glycolic) acid, is a biodegradable copolymer composed of polylactic acid (PLA) and polyglycolic acid (PGA), as shown in Figure 2.1[5]. The polymers PURASORB® PDLG 5002, 7502 and 5002A represent PLGA 50:50, 75:25 and 50:50 acid terminated, respectively, purchased from Corbion. All polymers have an intrinsic viscosity (IV) of 0.2 dL/g, and a molecular weight at 17 000 g/mol (246). PLGA is attractive because of its safety, stability, and biocompatibility profile as a biodegradable material and the high control over the PLGA release profile [5]. PLGA's carboxyl end groups allow the functionalisation of the surface of the PLGA-based delivery system [15]. In this study, PLGA 50:50 and 75:25 were investigated to produce imatinib-loaded NPs, and the acid-terminated version of PLGA 50:50 was used to fabricate the NPs for antibody conjugation.

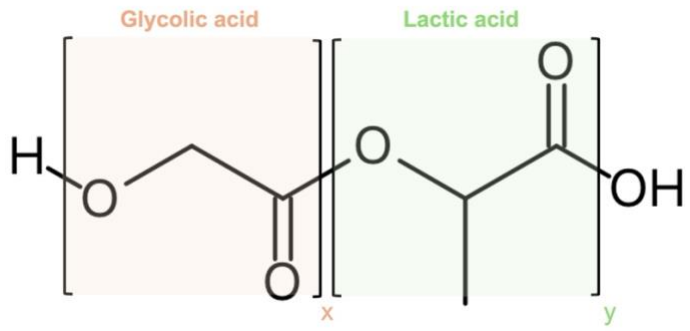

Figure 2.1. PLGA chemical structure, drawn using ChirysDraw.

2.1.1.2. Imatinib

Imatinib ($C_{29}H_{31}N_7O$, 493.6g/mol) is an FDA-approved tyrosine kinase inhibitor for treating chronic myelogenous leukaemia [255]. It is a white powder, usually orally administered [256]. Its salt version, imatinib mesylate, was developed to improve its solubility; however, since imatinib was encapsulated in this work, its non-salt version was used here [257]. It has shown potential for treating pulmonary hypertension and was

taken to phase 3 clinical trials for this indication, before being discontinued due to lack of safety, and was chosen for this study as its encapsulation could address the issues related to its toxicity [125]. The drug was acquired by Cambridge Bioscience, and its chemical structure is shown in Figure 2.2.

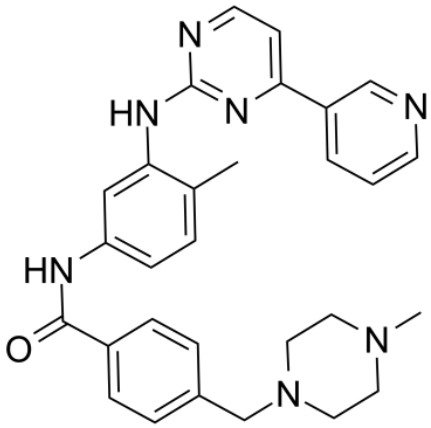

Figure 2.2. Imatinib chemical structure, adapted from [255].

2.1.1.3. Rhodamine-B

Rhodamine-B ($C_{28}H_{31}ClN_2O_3$, 479.01g/mol), also named 9-(2-carboxyphenyl)-3,6-bis(diethylamino)-10λ⁴-xanthen-10-ylium chloride is a fluorescent dye. The green powder becomes brightly pink when dissolved. The dye is hydrophilic and has been used as a model dye to visualise and quantify the cellular uptake of the particles. The excitation and emission wavelengths of Rhodamine-B are 543nm and 569nm, respectively. Rhodamine-B was purchased from Sigma-Aldrich/Merck, and its chemical structure is shown in Figure 2.3.

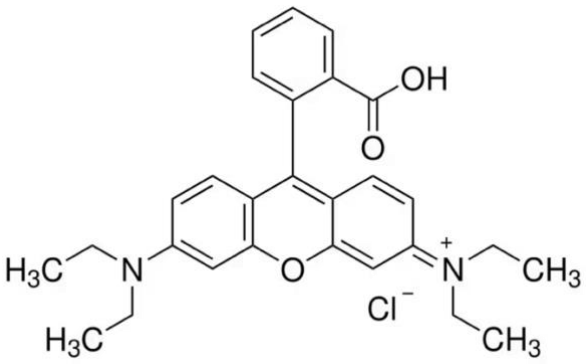

Figure 2.3. Rhodamine-B chemical structure, adapted from [258].

2.1.1.4. Solvents

Table 2.1 shows the solvents used to produce micro/nanoparticles via electrospraying. DCM, EA, and THF were purchased from Sigma-Aldrich, and DMAc was purchased from Fisher Chemicals.

Solvent category	Solvent	Chemical formula
Chlorinated solvents	Dichloromethane (DCM)	CH_2Cl_2
Ketones	Acetone (ACE)	C_3H_6O
	Dimethylacetamide (DMAc)	C_4H_9NO
Esters	Ethyl acetate (EA)	$C_4H_8O_2$
Ethers	Tetrahydrofuran (THF)	C_4H_8O

Table 2.1. Common solvents used to prepare PLGA particles NPs.

2.1.1.5. Additional materials

BioDesign Cellulose Dialysis Tubing Strips, 14000 MWCO, were purchased from ThermoFisher Scientific and phosphate-buffered saline (PBS) tablets were purchased from MP Biomedicals, Inc. They were both used for the drug release experiments in Chapter 3.

2.1.2. Cell studies materials

This study tested three cell types: a lung adenocarcinoma cell line (A549), primary Human Umbilical Vein Endothelial Cells (HUVECs), and primary Human Pulmonary Arterial Smooth Muscle Cells (HPASMCs). For cell viability/proliferation assays, CellTiter 96 ® Non-Radioactive Cell Proliferation Assay Kit (MTT) was purchased from Promega and a 3-(4,5-dimethylthiazol-2-yl)-2,5-diphenyltetrazolium bromide (MTT) solution (0.5%w/v) was then made by dissolving MTT salt purchased from Sigma-Aldrich/Merck in phosphate-buffered saline (PBS). Dimethyl sulfoxide (DMSO), a polar aprotic solvent, was purchased from Sigma-Aldrich and used as a cryoprotectant to cryopreserve cells and to dissolve formazan in MTT assays.

2.1.2.1. A549

A549 cells are human lung cancer cell line, more specifically alveolar basal epithelial cells growing in a monolayer. Their squamous nature helps the diffusion of water and electrolytes across the alveoli [259]. A549 cells were purchased from PromoCell and grown in Dulbecco's Modified Eagle Medium (DMEM), supplemented with 10% fetal bovine serum and 1% penicillin-streptomycin. Media, supplements, and Phosphate-buffered saline (PBS) were purchased from ThermoFisher. Trypsin-EDTA 1X (0.25% trypsin/2.21mM EDTA in HBSS) was used to passage this cell line and was purchased from Cambridge Bioscience.

2.1.2.2. Primary Human Umbilical Vein Endothelial Cells (HUVECs)

HUVECs are isolated from umbilical cords and cultured to study general endothelial function including and have a characteristic “cobblestone” morphology [260]. The HUVECs were purchased from PromoCell and grown using an endothelial cell growth medium supplemented with a proprietary mixture purchased from PromoCell. Hanks’ Balanced Salt solution (HBSS) was purchased from Sigma-Aldrich. Trypsin-EDTA X1, 0.2g EDTA, was used to passage these cells and was purchased from Merck Life Sciences.

2.1.2.3. Human Pulmonary Artery Smooth Muscle Cells (HPASMC)

HPASMCs are nonstriated muscular cells isolated from human pulmonary arteries. They are localised in the arterial media layer in the middle of the artery wall [261]. The cells and a complete smooth muscle cell medium with growth factor supplement were purchased from Cell Biologics. 0.05% Trypsin, 0.53nM EDTA 1X, was used to passage these cells and was purchased from Corning, and phosphate-buffered saline (PBS) was purchased from ThermoFisher. The low-serum media used was Dulbecco's modified eagle medium (DMEM), supplemented with 1% fetal bovine serum and 1% penicillin-streptomycin, they were all purchased from Thermo Fisher.

2.1.2.4. Platelet-derived growth factor-BB (PDGF-BB)

PDGF-BB is a potent mitogen from the PDGF family composed of two homodimers (PDGF-B). The mitogen controls the growth of connective tissues and smooth muscle cells by binding to the PDGF receptors, which belong to the class III receptor tyrosine kinases [262]. The PDGF-BB protein was purchased from Sigma-Aldrich.

2.1.3. Antibody Conjugation Materials

2.1.3.1. Bevacizumab

Bevacizumab (Bev) is a humanised IgG anti-VEGF-A monoclonal antibody. It is currently FDA-approved for treating several types of cancer by binding to VEGF-A and preventing it from binding to its receptor [263]. The antibody is usually administered intravenously and in combination with other chemotherapy agents. It was purchased from Cambridge Bioscience and supplied by MedChem Express.

2.1.3.2. EDC

EDC (1-ethyl-3-(3-dimethyl aminopropyl) carbodiimide hydrochloride) ($C_8H_{17}N_3HCl$, 191.7g/mol) is a crosslinker used to couple carboxylic groups to primary amines by forming amide bonds when the carboxylic groups interact with EDC in a mildly acidic environment (pH 4.7-6) and creates an active and unstable intermediate ready to react with primary amines [264,265]. EDC was purchased from Thermo Fisher Scientific, and its chemical structure is shown in Figure 2.4.

Figure 2.4. EDC chemical structure, drawn using ChirysDraw [264]

2.1.3.3. NHS

NHS (N-hydroxy succinimide) ($C_4H_5NO_3$, 115.09g/mol) is a reagent responsible for controlling and modifying crosslinking reactions using EDC. Adding NHS to the coupling reaction improves the coupling efficiency, increases its yield and provides stability of the activated carboxylates for conjugation with primary amines [266,267]. NHS was purchased from Thermo Fisher Scientific, and its chemical structure is shown in Figure 2.5.

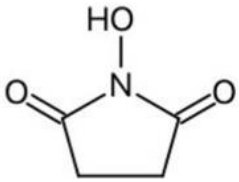

Figure 2.5. NHS chemical structure, drawn using ChirysDraw [266].

2.1.3.4. MES

MES (2-(N-morpholino) ethane sulfonic acid) ($C_6H_{13}NO_4S$, 195.24g/mol) is a zwitterionic buffer, which means its acid or base is a dipolar ion [268]. MES buffers work efficiently in acidic environments (pH 5.5-6.7). This buffer stabilises a reaction's pH by accepting or donating protons, essential in reactions sensitive to pH fluctuations [269]. MES was purchased from Santa Cruz Biotechnology, and its chemical structure is shown in Figure 2.6.

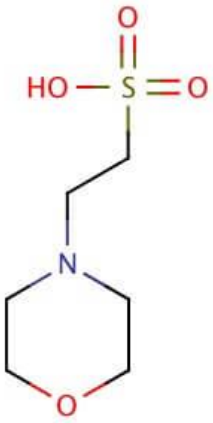

Figure 2.6. MES chemical structure, adapted from [269].

2.1.3.5. Alexa Fluor 488-conjugated secondary antibody

Alexa Fluor488 is a green, fluorescent dye excited by 488nm laser line, conjugated to a secondary antibody, such that fluorescence outputs can be used to detect binding of primary antibodies [184]. This secondary antibody was used to detect bevacizumab covalently bound to the PLGA NPs to confirm its conjugation. The secondary antibody must be specific to the antibody species and the isotype of the primary antibody. Since bevacizumab is humanised, Alexa Fluor 488 goat anti-human IgG (H+L) was purchased from Invitrogen by ThermoFisher Scientific. The secondary antibody has

both its heavy and light chains (H+L), and its variable region or light chain binds to the primary antibody (Bevacizumab) constant region [184] as shown in Figure 2.7.

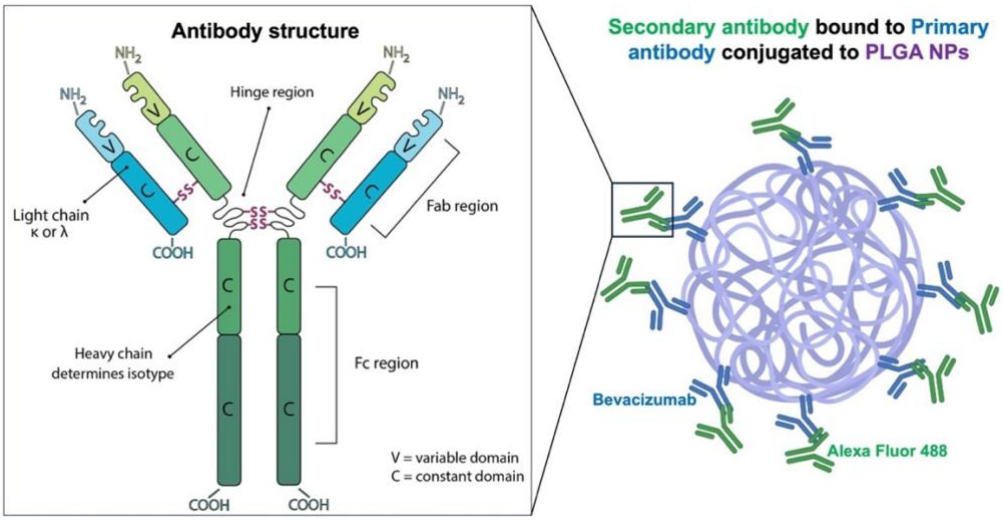

Figure 2.7. Diagram of the conjugated NPs bound to the secondary antibody. Primary antibodies are conjugated to PLGA NPs via their variable region using the NH_2 terminal group. Secondary antibodies' variable region is bound to the primary's constant region. Diagram drawn using Biorender and adapted from [270].

2.1.3.6. Additional materials

Deuterated chloroform ($CDCl_3$) was purchased from Sigma-Aldrich and was the solvents of choice for the Proton Nuclear Magnetic Resonance (^{1}H-NMR) experiments. Vivaspin 6 Centrifugal Concentrators 300000 MWCO PES were used to filtrate the excess reactants resulted from the antibody conjugation through carbodiimide chemistry and were purchased from Sartorius.

2.2. Methods

This section provides a general description of the methods used in the thesis, and a more detailed description of the methodology is given in each of the relevant chapters.

2.2.1. Production of micro and nanoparticles via electrospraying

Droplets of polymer solution are dispensed from a stainless-steel 22G, ID: 0.41 mm and OD: 0.72 mm, nozzle under a flow rate created by a syringe pump. A voltage power supply creates an electrical field at the nozzle to break the droplet's surface tension. Once the surface tension is overcome, the droplets migrate, and the specific solvent chosen evaporates towards the negatively charged collection plate placed 20cm from the needle. The electrospraying technique has been optimised to create a range of particles in Chapter 3. The technique was subsequently used throughout the study to produce the particles tested in Chapters 4 and 5.

2.2.2. Physical-chemical characterisation of the polymeric particles

2.2.2.1. Scanning electron microscopy (SEM)

Scanning electron microscopy is an imaging technique which uses electron beams on a sample to obtain a magnified image of the sample. Once the electrons hit the samples, they bounce back, and the detectors detect the high and low-energy electrons that interact with the atoms of the samples, delivering information about the sample surface topography [271,272]. The electrosprayed particles were collected on a microscope slide, then cut and attached to aluminium SEM stubs using a double-sided carbon sticker (TAAB Laboratories, UK). To acquire high-resolution images, the sample was made conductive by being coated with a conductive material. The samples were gold-coated using a Quorum Q150T Sputter Coater (Quorum Technologies Ltd, UK). The SEM column remained under vacuum to prevent contaminants from interfering with the electron beams and affecting the image resolution [273]. The Thermo Scientific Phenom Pro G6 Desktop SEM was used to obtain the SEM images. It has a resolution of ≤ 6 nm, with an acceleration voltage of 15 kV and a magnification of 350 000x. The image processing software ImageJ (NIH, USA)

was used to determine the particle size distribution using the measuring functions on three separate images. The SEM was used in Chapters 3 and 5 to analyse the size and morphology of the particles produced.

2.2.2.2. Zeta potential

The zeta potential provides information about the surface charge of the nanoparticles by applying an electrical field to the NPs. The slipping plane is a boundary where ions and the particle form a stable entity. When the electrical field is applied, the particles move towards the oppositely charged electrode, which also moves the ions within the slipping plane towards the electrode. The movement of ions around the NPs provides a signal interpreted as the zeta potential [274]. The nanoparticles were suspended in deionised water and transferred to a plastic cuvette with built-in electrodes (DTS1070). The Zetasizer Ultra from Malvern Panalytical measured the zeta potential, which is used in Chapters 3 and 5 to obtain information about the surface charge of the particles after drug encapsulation or antibody conjugation.

2.2.2.3. Fourier transform infrared spectroscopy (FTIR)

FTIR is a method that detects molecular vibrational energy after exposing a sample to infrared light in the mid-IR region of 4000 to 400cm^{-1}. The transmitted radiation is measured while the sample absorbs the rest, producing distinct spectral bands [275]. When the absorption occurs, the sample jumps to an excited vibrational state; its chemical bonds can stretch or bend when excited. The vibration frequencies of the bonds between the atoms in the material create absorption peaks identifying its chemical fingerprint, such as functional groups [276].

A PerkinElmer Spectrum 100 FT-IR was used to obtain the FTIR spectra for Chapters 3 and 5, which show the FTIR spectrum of PLGA particles after drug encapsulation or antibody conjugation. The samples were dispersed on the crystal light path and compressed to obtain respective spectra and were then recorded in the wavelength region of 4000 to 650cm^{-1}. A background scan was performed, followed by a sample scan. Both scans consisted of 8 scan times, and each sample was run in triplicates to confirm the spectra.

2.2.2.4. Ultraviolet-visible (UV-Vis) spectroscopy

Ultraviolet and visible spectroscopy records the absorption of UV-Vis electromagnetic radiation by a substance in the region of 200 to 800nm. A UV-visible spectrophotometer measures how much light a sample absorbs at different wavelengths in the UV or visible range. It plots the wavelengths of absorbed light against absorbance (or optical density), following the Beer-Lambert law [277]. Beer's law, as shown in Equation 2.1, states that the absorption of the light by the sample is proportional to the number of absorbing molecules in the sample, allowing the technique to be used to find a sample's concentration [278].

$$A = \varepsilon c l$$

Equation 2.1. Beer-Lambert's law, where A is the absorbance or optical density, ε is the molar absorption coefficient, c is the sample concentration, and l is the path length (cm) [278].

The path length is the length of the cuvette used to hold a sample, usually 1cm. The wavelength at which the sample reaches the maximum absorption is denoted as λ_{max}. Therefore, a UV-Vis spectrophotometer (Cary Series UV-Vis Spectrophotometer, Agilent Technology) was used to find the λ_{max} of the materials used and to measure the absorbance of samples subsequently. The technique was used to measure the drug encapsulation and drug release from the NPs in Chapter 3.

2.2.3. Testing the nanoparticles on cells

2.2.3.1. Cell sub-culturing/passaging

To bring up frozen cells, they were thawed, resuspended in warm medium, and placed in a 75cm^2 flask; the medium was changed 24 hours later. The medium was subsequently changed every other day after washing adherent cells we with PBS for the A549 and HPASMC cells and HBSS for HUVECs.

When the cells reached 60-70% confluence, they were sub-cultured by rinsing the flask thrice with PBS or HBSS to remove medium and separated from the culture flask using trypsinisation [279]. 2mL of trypsin was added to the washed cell layer and was incubated at 37ºC for 3 minutes. 8mL of fresh warmed medium was added to the flask

to inactivate the trypsin, and the resulting cell suspension was centrifuged at 1060 rpm for 5 minutes to collect the cells. The supernatant was discarded, and the cell pellet was resuspended in 2mL of medium. The suspension was added to a solution of Trypan Blue in a ratio of 1:1 to count the cells via Luna II Automated Cell Counter automatically. The cells were either seeded in plates or passaged into a new T75 flask or cryopreserved using 10% DMSO in culture medium as a cryoprotectant. The cells were frozen slowly by reducing the temperature at approximately 1ºC per minute using a controlled rate cryo-freezing container overnight and moved to liquid nitrogen the next day.

This passaging protocol has been used for the in vitro testing of the imatinib-loaded NPs in Chapter 3 for A549 cells and Chapter 4 for HUVECs and HPASMCs.

2.2.3.2. Fluorescence microscopy

Fluorescence microscopy relies on fluorescent dyes (fluorophores), which are molecules that absorb light at one wavelength (excitation) and emit it at a longer wavelength (emission) [280]. Since most molecules are not naturally fluorescent, fluorophores label the target molecules. This technique usually uses epifluorescence, in which the fluorescence excitation light illuminates the sample with the same objective of detecting the emission from the sample. EVOS fluorescence microscope was used to visualise cells for the LIVE/DEAD assay and the uptake studies described in Chapter 3.

2.2.3.3. Cell viability measurement via MTT assay

The MTT assay measures cell viability based on the cells' ability to convert the soluble tetrazolium salt MTT (3-(4,5-dimethylthiazol-2-yl)-2,5-diphenyltetrazolium bromide) into an insoluble formazan precipitate. Tetrazolium salts receive electrons from oxidoreductase, dehydrogenase enzymes, and electron donors [281]. The salts are reduced at ubiquinone and cytochrome b and c sites in the mitochondrial electron transport chain. This reaction changes the yellow salts into blue formazan crystals, which can be dissolved in an organic solvent, such as DMSO, after 4 hours and quantified using UV-Vis spectrophotometry plate reader (SpectraMax) at 570nm [282].

The MTT assay, therefore, measures cell viability using its mitochondrial activity. MTT assays were performed after the treatment of the cells with blank PLGA NPs, imatinib-loaded NPs, and imatinib alone, as displayed in Figure 2.8. Cell viability was calculated using Equation 2.2.

$$Cell\ viability\ (\%) = \frac{OD^{sample} - OD^{background}}{OD^{control}} \times 100$$

Equation 2.2. Cell viability equation using MTT assay, where OD = optical density/ absorbance.

CellTiter 96 ® Non-Radioactive Cell Proliferation Assay Kit (MTT) was used for the MTT assay tests on the A549 cell lines described in Chapter 3. MTT solution (0.5%w/v) made with PBS was used for the MTT assay tests on the HUVECs and HPASMCs described in Chapter 4.

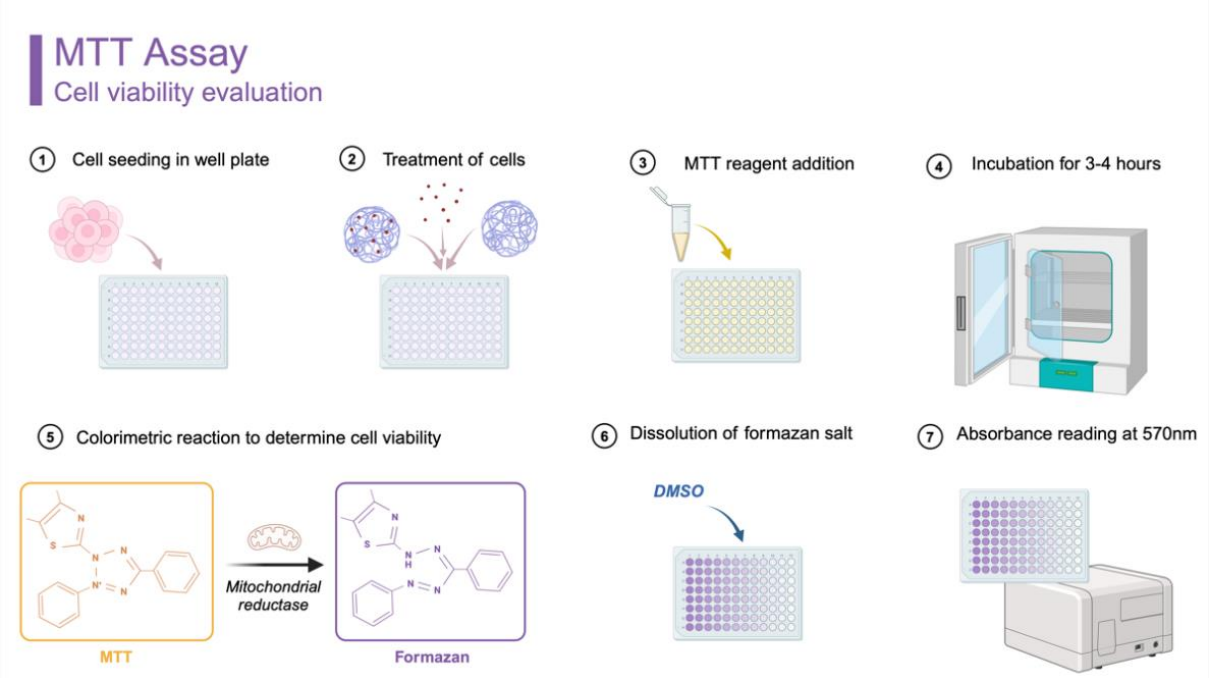

Figure 2.8. MTT assay to evaluate cell viability following treatment of cells. Modified template from Biorender.

2.2.3.4. LIVE/DEAD Assay

The LIVE/DEAD™ Cell Imaging Kit (488/570) is a two-colour fluorescence cell viability assay. It contains Calcein AM, a cell-permeant dye that stains live cells green, and BOBO-3 iodide, which stains dead cells red. Calcein AM can cross the cell membrane and be converted into Calcein, the anionic fluorescent form, by intracellular esterase [283]. Calcein is retained in live cells and fluoresces green when excited at 488nm (emission/excitation 488/515nm). On the other hand, BOBO-3 iodine, a dimeric cyanine nucleic acid stain, can only enter cells via a damaged cell membrane and binds to nucleic acids to emit its red fluorescence at 570nm (emission (Em)/excitation (Ex) 570/602nm). The fluorescence signal was measured on a fluorescence microplate reader (SpectraMax), and fluorescence microscopy was used to visualise the live and dead cell fluorescence signals following the treatment of cells. The LIVE/DEAD assay kit was purchased from ThermoFisher. The cell viability was calculated using Equation 2.3. This assay measured the percentage of live A549 cells in Chapter 3 following their treatment with the produced NPs.

$$Percentage\ of\ live\ cells\ (\%) = \frac{Fluorescence\ of\ live\ cells}{Fluorescence\ of\ live + dead\ cells} \times 100$$

Equation 2.3. Percentage of live cells, seen as cell viability, using the Live/Dead Assay

2.2.4. Antibody conjugation to polymeric particles

2.2.4.1. Carbodiimide conjugation

Carbodiimide conjugation is the most widely used technique for linking carboxylic acids to primary amines through amide bond formation, typically using NHS and EDC. EDC activates the carboxylic acid group in this reaction, forming an unstable O-acylisourea intermediate [162]. This intermediate reverts to the carboxylic group if it does not interact with an amine. Therefore, when the NHS is added, its primary amino group causes a nucleophilic attack, which improves the coupling efficiency and replaces this intermediate to produce a reactive ester, the "activated" PLGA or NHS-PLGA and urea as a by-product. When the primary amine on the antibody is added, it replaces the NHS ester, forming an amide bond with the carboxylic acid and the generation of NHS as a by-product [18,162,284].

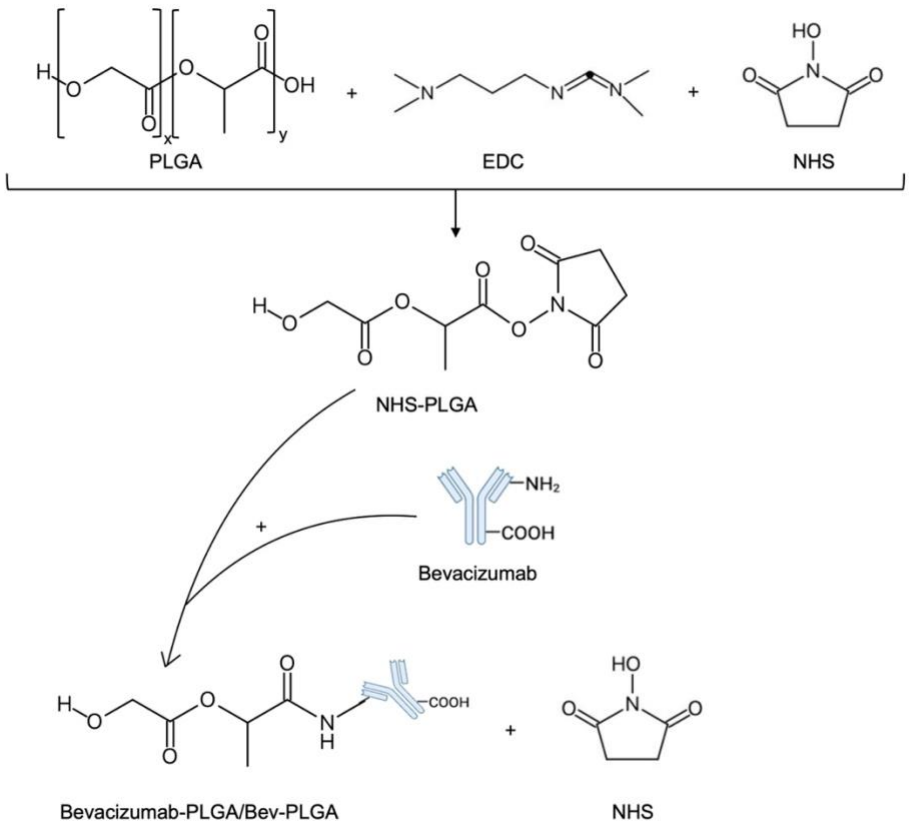

Figure 2.9. Carbodiimide conjugation of an antibody to a carboxylic group terminated polymer. Image created using ChirysDraw and Biorender and adapted from [162].

2.2.4.2. *Characterising conjugation*

The bicinchoninic acid assay (BCA Assay)

The BCA assay is a colorimetric assay that measures protein concentration in a sample based on a chemical reaction that causes a change of colour. Peptide bonds and certain amino acids such as cysteine, tryptophan, and tyrosine enable the reduction of cupric ions (Cu^{2+}) to cuprous ions (Cu^{+}) in an alkaline medium, also known as the biuret reaction. The resulting cuprous ions then react with the sodium of two bicinchoninic acids to generate a purple complex [285]. The Pierce BCA Protein Assay kit was used in the study to measure protein concentration, as displayed in Figure 2.10. A working reagent was created by adding a carbonate buffer containing BCA (reagent A) and a cupric sulphate solution (reagent B) in a 50:1 ratio. 200µL of the working reagent was added to 25µL of the tested sample. The mixture was left to incubate for 30 minutes at 37ºC for the reaction to occur. After the purple Cu^{+}+BCA was formed, the absorbance was measured at 562nm [286]. The corresponding protein concentration was then found using a calibration curve created by using albumin standards. The kit was obtained from Thermo Scientific (Waltham, MA).

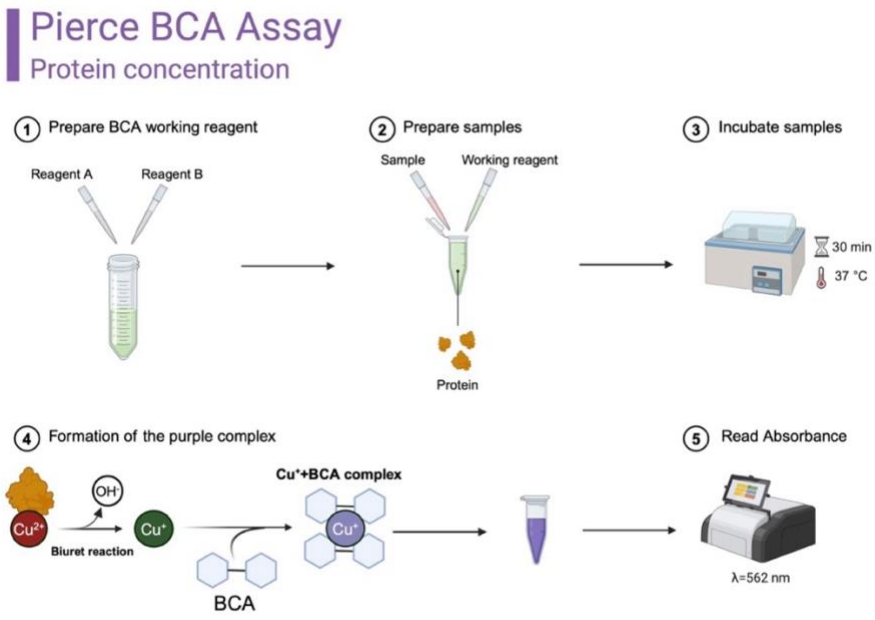

Figure 2.10. The bicinchoninic acid assay (BCA assay). Image created using Biorender.

Proton Nuclear Magnetic Resonance (^{1}H-NMR)

Proton Nuclear Magnetic Resonance (^{1}H-NMR) spectroscopy is a technique for determining the structure of organic molecules by analysing the magnetic properties of hydrogen atoms (protons) in the molecule. In ^{1}H-NMR, a sample is placed in a magnetic field and exposed to radiofrequency radiation, which causes protons to resonate at frequencies that depend on their chemical environment. It provides information about the number and types of protons, their environments, and their connection within the molecule, enabling the identification of molecular structures and functional groups [287]. The samples were analysed using ^{1}H-NMR through a Bruker Avance Neo 400 MHz NMR spectrometer using Deuterated chloroform ($CDCl_3$) as the deuterated solvent. This technique was used to confirm the success of the conjugation in Chapter 5 by inferring its chemical structure and functional group following conjugation.

Bevacizumab Sandwich ELISA Kit

In the standard ELISA procedure, a sample containing the antigen of interest is added to a solid-phase antibody and allowed to bind. After washing, an enzyme-labelled antibody is introduced, forming a “sandwich complex”. ELISA can also quantify specific antibodies in a sample by binding the antigen, rather than the antibody, to the solid phase, with a second enzyme-labelled antibody targeting the analyte antibody. Unbound antibodies are washed away, and an enzyme substrate is added; the reaction leads to a colour change proportional in intensity to the antigen or antibody concentration in the sample [288].

The ELISA kit in this study used the latter to measure the concentration of bevacizumab. The Bevacizumab Sandwich ELISA Kit process has been summarised in Figure 2.11 and was purchased from GenScript. Anti-idiotypic monoclonal antibody-coated 96-well plates from the kit were used to capture and detect Bevacizumab. Following conjugation, the particles were diluted 1:50, and 100µL was added to each well and incubated for an hour at room temperature (RT). Each sample’s concentration was also measured in duplicate. After incubation, the wells were washed four times with the wash solution provided. 100µL Biotin Anti-Bevacizumab Antibody was added

to each well to detect the antibody, incubated for 30 minutes at RT, and then washed again four times. 100µL of the enzyme conjugate, streptavidin-horseradish peroxidase (HRP), was added to each well, incubated for 10 minutes and rewashed four times. 100µL of the substrate for the enzyme, TMB (3,3',5,5'-Tetramethylbenzidine), was then added to react with the HRP enzyme for 15 minutes in the dark at RT. Finally, 50µL of the stop solution was added to halt the substrate-enzyme reaction, and the optical density (OD) was measured on a UV-Vis Spectrophotometer plate reader (SpectraMax) at a wavelength of 450nm.

The samples' bevacizumab concentration was determined using the OD measured, and the concentration was calculated from a calibration curve created using bevacizumab standards. The bevacizumab ELISA kit was used to measure bevacizumab concentration following conjugation in Chapter 5.

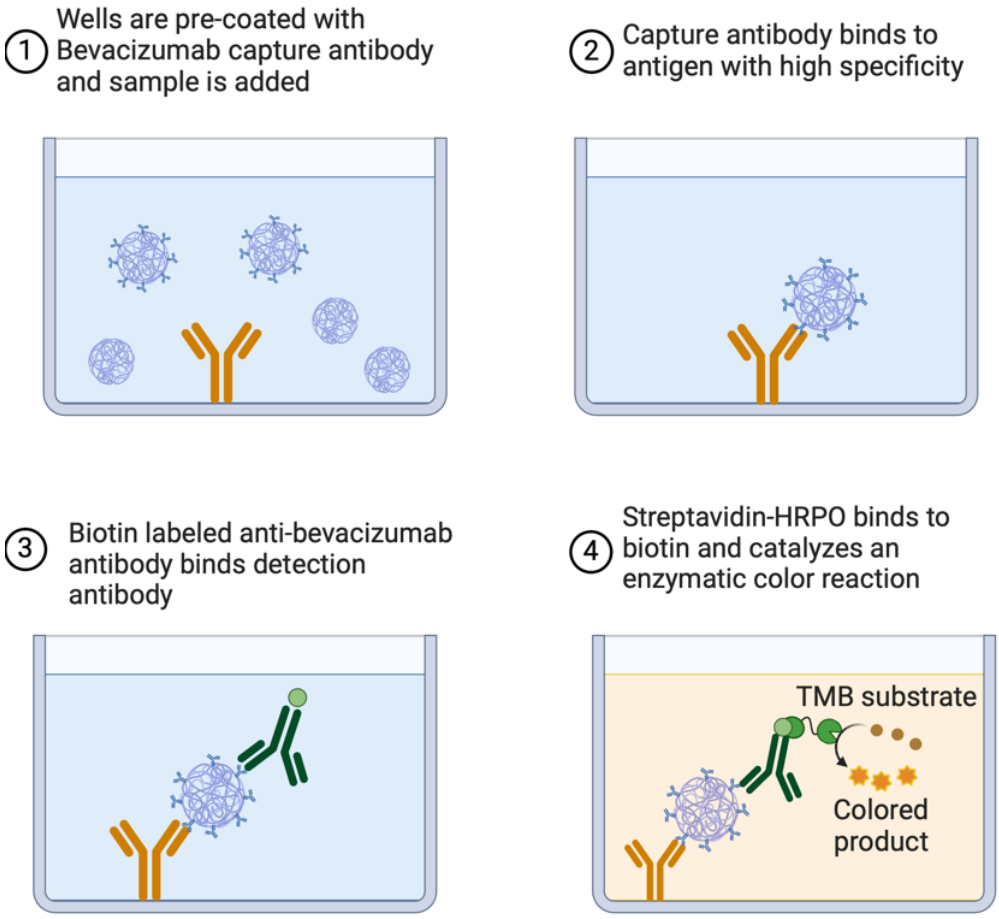

Figure 2.11. Bevacizumab ELISA Sandwich kit process. Image created using Biorender.

Flow cytometry using Alexa Fluor 488-conjugated secondary antibody.

Flow cytometry is a technique whereby single cells or particles traverse single or multiple lasers while suspended. Each particle is analysed based on how it scatters the light emitted from the laser. The visible light scatter is measured in the forward and side scatter, providing information about the size and internal complexity of the cells or particles, respectively, as shown in Figure 2.12. The colour filter lets fluorescent light at a specific wavelength range pass through and be read. By exposure to different lasers at different wavelengths, various fluorophores can be detected. The flow cytometry data can be shown in a dot plot or a histogram, depending on the application [289]. A secondary antibody was used to bind to bevacizumab to confirm antibody conjugation further. The resulting complex was analysed using flow cytometry (Attune Flow Cytometry, Thermo Fisher Scientific) to measure fluorescence emitting from the NPs. Alexa Fluor 488-conjugated goat anti-human IgG (H+L) was used as the secondary antibody as Alexa Fluor 488 can be specifically excited by the 488nm laser and detected by the BL-1 Alex Fluor 488 channel (Ex: 488nm; Em:500-560nm). This secondary antibody and flow cytometry technique were used in experiments described in Chapter 5.

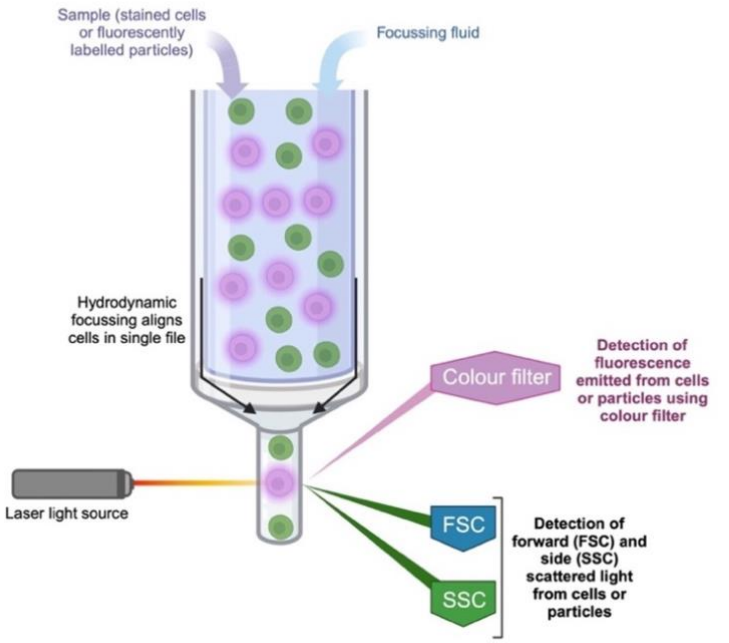

Figure 2.12. Simplified schematic of the flow cytometry [289]. Image created using Biorender.

Chapter 3. Optimisation via electrospraying, physical-chemical characterisation and in-vitro efficacy of imatinib-loaded PLGA NPs

Part of the following chapter has been published:

Tsilova, S. L., Schreiber, B. E., Lever, R., & Parhizkar, M. (2024). Polymeric nanoparticles produced by electrohydrodynamic atomisation for the passive delivery of imatinib. *European Journal of Pharmaceutics and Biopharmaceutics*, *202*, 114412. https://doi.org/10.1016/J.EJPB.2024.114412

3.1. Introduction

Imatinib, a tyrosine kinase inhibitor, has shown tremendous potential for the treatment of PAH; however, its safety profile, low solubility in aqueous solution, and short half-life when administered orally led to a drug concentration that is toxic to normal cells but marginally effective in treating cancer cells or ultimately PAH cells [207]. Therefore, an alternative delivery system was considered a target for optimal bioavailability and efficacy. Several studies investigating drug delivery systems have looked at poly(lactic-co-glycolic acid) (PLGA), an FDA-approved biodegradable polymer, to create polymeric nanoparticles (NPs) as they show improved storage stability and a more sustained and controlled delivery of their compounds [5]. Imatinib has already been investigated in PLGA-based NPs; however, these studies used time-consuming multi-step processes to produce the NPs that can lead to increased risk of errors, unwanted interaction with the drug, and large particles. Electrohydrodynamic atomisation or electrospray (ES) is a simple and inexpensive one-step technique to fabricate micro and nanoparticles [12]. The technique is known for its high level of control over the final particle characteristics, which is achieved by changing the interdependent parameters of the method.

This chapter aimed to create, optimise, and evaluate polymeric NPs produced through electrospray technology to achieve a more precise and efficient delivery of imatinib and improve dosing effectiveness. The work in this chapter focused on answering several questions regarding manufacturing the imatinib-loaded NPs through electrospraying. It will first establish which key parameters were crucial in optimising the ES to yield NPs for desired characteristics such as size, shape, composition, and morphology for optimal delivery. After forming the NPs, work was undertaken to ensure processing PLGA into NPs through electrospraying did not alter the chemical structure of the polymer. Additionally, as the NPs are intended to be tested on cells, efforts were made to ensure the encapsulation of imatinib did not cause modifications significant enough to prevent its use in vitro. The effect of introducing the drug was investigated to determine the dosage carried by the NPs and the dosage being released and, therefore, administered over time. Assessing the NPs' cytotoxicity alone

was required before introducing drug-alone and drug-loaded NPs. Considering imatinib has been indicated for many cancer types, the goal was to explore the drug's effectiveness on a cancerous line and to ensure the effect seen by the free drug was maintained after being encapsulated. Finally, it was of interest to determine the end location of the NPs after treating the cells and assess whether the effects seen were due to the internalisation of the NPs.

3.2. Methodology

3.2.1. Imatinib-loaded nanoparticles and rhodamine-B loaded nanoparticles (RhD-B NPs) production and characterisation

3.2.1.1. Production of NPs

The electrospray solutions were prepared by dissolving the polymer and drug, if applicable, in organic solvents (alone or a mixture of organic solvents). All polymer solutions were prepared with 2wt% PLGA. First, we investigated the effect of solvents on the generated blank particles, as the choice of solvent was crucial to the particles' characteristics. Acetone, dimethylacetamide, dichloromethane and tetrahydrofuran were tested and generated under the same conditions to maintain similar temperatures and humidity. The rest of the parameters were kept the same: polymer type (PLGA 50:50) and concentration (2% wt.), flow rate (5µl/min) and voltage (8kV) for consistency and to investigate the effect of solvents effectively.

Formulations F1, F2, F3, F4 dissolved the PLGA using a co-solvent system of acetone and DMAc, with a ratio of 1:1 and formulations F5, F6, F7, F8 dissolved PLGA using DMAc alone. Imatinib (0.2wt%) was added to F2, F4, F6, and F8 to produce drug-loaded nanoparticles. F1, F3, F5, and F7 were prepared without the drug as blanks, and RhD-B (0.2wt%) was added to F9 to produce rhodamine-loaded NPs (RhD-B NPs). Formulations F1, F2, F5, F6 and F9 were made using PLGA 50:50 and F3, F4, F7 and F8 were made using PLGA 75:25. Droplets of polymer solutions were ejected out of a needle under a constant flow rate of 5µL/min and at a voltage of 12kV for F1, F2, F3, and F4 and 2µL/min and 14kV for F5, F6, F7, F8, F9. A voltage power supply applies an electrical field to the needle to break the droplet's surface tension and create smaller droplets. While the droplets migrate towards the collector, which is 20cm from the needle, they separate into smaller droplets, and the solvent evaporates, generating small dry particles on the collection plate [290]. Electrospraying occurred at room temperature (20-25ºC) and 35-55% relative humidity. A summary of all the parameters is displayed in Table 3.1. Nanoparticles (NPs) production parameters.

	Polymer Solution properties						Electrospraying processing parameters	
Formulations	PLGA concentration	PLGA ratio	Drug used and concentration			Solvents	Voltage	Flow rate
F1	2wt%	50:50	Blank	Imatinib	0	Acetone and DMAc (1:1)	12kv	5µL/min
F2			Encapsulated		0.2wt%			
F3		75:25	Blank		0			
F4			Encapsulated		0.2wt%			
F5		50:50	Blank		0	DMAc	14kv	2µL/min
F6			Encapsulated		0.2wt%			
F7		75:25	Blank		0			
F8			Encapsulated		0.2wt%			
F9		50:50	Encapsulated	Rhodamine-B	0.2wt%			

Table 3.1. Nanoparticles (NPs) production parameters.

3.2.1.2. Characterisation of NPs

The morphology and porosity of the NPs were studied using scanning electron microscopy. The electrosprayed particles were collected on a microscope slide, then cut and attached to aluminium SEM stubs using a double-sided carbon sticker (TAAB Laboratories, UK). The stubs were then processed as mentioned in methodology section 2.2.2.1. Formulations F1-F8 were each electrosprayed on three separate occasions to demonstrate the reproducibility of the technique. The Zeta potential of the imatinib-loaded and blank particles and pure imatinib were also measured, and results were statistically compared using one-way ANOVA.

3.2.1.3. Fourier transform infrared spectroscopy.

Fourier transform infrared (FTIR) spectroscopy (PerkinElmer Spectrum 100 FT-IR) was conducted with spectra recorded in the wavelength region of 4000 to 650cm^{-1}. Pure, blank, and imatinib-loaded particles from different PLGA ratios were tested as described in 2.2.2.3.

3.2.1.4. Encapsulation efficiency (EE%)

A calibration curve was generated for imatinib encapsulation efficiency by dissolving a range of concentrations of imatinib (20, 40, 80, 160, 320, and 640µg/ml) in a co-solvent mixture of Acetone and DMAc (9:1) and measuring their absorbance at a wavelength of 332nm using a UV-Vis Spectrophotometer (Cary Series UV-Vis Spectrophotometer, Agilent Technology). Encapsulation efficiency was determined by using the calibration curve and measuring the absorbance of the dissolved imatinib-loaded particles at the same wavelength of 332nm using a UV-Vis Spectrophotometer, as described in 2.2.2.4.

Imatinib concentration in the particles was found using the calibration curve, which led to the calculated mass of imatinib. The encapsulation efficiency (EE %) was calculated using the ratio of theoretical drug loading to the actual drug loading, as shown in Equation 3.1. Theoretical (TDL %) and actual (ADL%) drug loading can be described below in Equation 3.2 and Equation 3.3 respectively:

$$EE\ (\%) = \frac{ADL\ (\%)}{TDL\ (\%)} \times 100$$

Equation 3.1. Encapsulation Efficiency equation.

$$TDL(\%) = \frac{mass\ of\ drug\ added\ (mg)}{mass\ of\ drug\ and\ polymer\ added\ (mg)} \times 100$$

Equation 3.2. Theoretical Drug Loading equation.

$$ADL\ (\%) = \frac{\boldsymbol{Measured\ drug\ mass\ (mg)}}{Mass\ of\ particles\ dissolved\ (\mathrm{mg})} \times 100$$

Equation 3.3. Actual Drug Loading equation. Measured drug mass was determined by measuring the absorbance of dissolved particles at λ_{max} and obtaining the concentration through the calibration curve.

3.2.1.5. In-vitro drug release profile

A release study measured the percentage of imatinib released in PBS over 7 days. PBS has been a UPS standard physiological buffer for replicating the human body's pH, osmolarity, and ion concentration to simulate the conditions in-vivo [291], but also due to its studied effect on drug release from PLGA microparticles [292]. 8mg of Imatinib-loaded particles (representing theoretically 0.72mg of imatinib) and 1mg of pure Imatinib were suspended and dissolved respectively in dialysis bags filled with 1.5mL PBS which were placed in vials of 20mL of PBS. Aliquots were withdrawn at specific time points, every 2 hours during the first day and every 24 hours after that until day 7. The aliquots were passed through a 0.22μm filter. UV absorbance of the resulting filtrates was then measured at 261nm. The imatinib concentration of each aliquot was determined using the release study calibration curve, generated by dissolving a range of concentrations of imatinib (6.25, 12.5, 25, 50, 100 and 200μg/ml) in a co-solvent mixture of PBS and methanol (4:1) and measuring their absorbance at a wavelength of 261nm.

3.2.2. Cell studies

3.2.2.1. Materials

A549 cells were purchased from PromoCell and grown in Dulbecco's Modified Eagle Medium (DMEM), supplemented with 10% fetal bovine serum and 1% penicillin-streptomycin. Media, supplements and phosphate-buffered saline (PBS) were purchased from ThermoFisher. CellTiter 96 ® Non-Radioactive Cell Proliferation Assay (MTT) was purchased from Promega and LIVE/DEAD™ Cell Imaging Kit (488/570) from ThermoFisher.

3.2.2.2. Cell viability and live/dead assay

The methods for growth and maintenance of the cells are highlighted in section 2.2.3.1. Imatinib-loaded NPs were assessed following F6 and F8 (PLGA 50:50 and 75:25, DMAc, 2µL/min), on A549 cell lines, due to their size and release profile, with their respective blanks. Cell viability was measured using a colorimetric MTT assay as described in section 2.2.3.3. The live/dead assay was also performed as described in section 0. 96-well plates were seeded with 2000 cells in each well and treated the next day with medium alone (untreated), F5 NPs or F6 NPs (both at 1mg/ml) and a range of imatinib concentrations of 50µM, 100µM, and 150µM. MTT assay was conducted 72 hours after the cells were treated. 72 hours after treating the cells, they were washed and stained with the live/dead assay dye. Qualitative images were taken using an EVOS fluorescence microscope 30 minutes after adding the dyes. The fluorescence signal was measured on a SpectraMax absorbance plate reader at their respective emission and excitation wavelengths at 488 and 515nm respectively.

3.2.2.3. Uptake study

A 24-well plate was seeded with A549 cells at a density of 95,000 cells in each well. The uptake study treated cells with medium (untreated), F5 NPs, free RhD-B at 50µg/mL (equivalent to 100µM free imatinib), and F9 NPs (blank PLGA 50:50 and rhodamine-B PLGA 50:50) at 1mg/mL. One row was left unseeded to serve as an additional negative control to ensure that measurements reflected the interaction of the NPs with the cells rather than the plate. The following day, the wells were rinsed three times with PBS to remove any NPs or RhD-B that were not internalised. Rhodamine-B fluorescence was measured on a SpectraMax plate reader with an excitation peak at 550 nm and an emission peak at 570 nm, and images were obtained using the Invitrogen EVOS Digital Inverted Fluorescence Microscope, as described in 2.2.3.2.

3.3. Results and discussion

3.3.1. Impact of choice of solvent on the generated particles

The choice of solvent is a significant factor in governing the size and shape of the NPs through the evaporation rate, electrical conductivity, viscosity, and surface tension of a polymeric solution [293]. To investigate how different solvents can affect the generated particles, four solvents, acetone, dimethylacetamide, dichloromethane and tetrahydrofuran, were investigated due to their availability and varied characteristics: evaporation rate, electrical conductivity, viscosity and surface charge which are shown in Table 1.7 and obtained from their respective safety data sheets. The solvents were used to electrospray PLGA particles while maintaining the same condition for the remaining parameters (Voltage at 8kV, flow rate of 5µL/min, and polymer concentration of 2%wt with PLGA 50:50) to exclusively observe the effect of the solvent.

3.3.1.1. Polymer concentration affects solution viscosity

Various particle morphology and size were possible to achieve through the tailoring of the polymer solution and processing parameters, where each parameter has an interdependent influence on the particles' characteristics. A polymer concentration of 2wt% was selected and kept consistent when testing the effect of each solvent since the polymer concentration parameter has a significant effect on the particles' size and shape. The polymer's molecular weight and concentration can significantly impact the polymer solution characteristics, such as its viscosity [294]. A low polymer concentration was chosen for all the tests to ensure the formation of spherical particles, as a higher polymer concentration could generate more elongated particles or non-uniform particles [295]. This can be explained by the rise in viscosity and polymer chain entanglement as the polymer concentration is increased [296]. The increase in polymer chain entanglement has been shown to inhibit the fission process of the particles [297], leading to larger particles since promoting the fission of the particles is responsible for generating small particles [298]. A study on electrospray polycaprolactone NPs encapsulating bosentan monohydrate found that smaller particles were formed as the

polymer concentration was reduced [299]. Park & Lee (2009) found that the conductivity and surface tension of the polymer solutions were almost independent of concentration [300].

Figure 3.1. shows the SEM images of the generated PLGA particles and their respective size distribution. The SEM images show that the particle structure changes with the choice of solvent. ACE and DCM have created irregular and porous particles. Both solvents have a high evaporation rate (DCM=27.5 and ACE=11.6, Table 1.7). As mentioned in section 1.5.2, a volatile solvent evaporates before Coulomb's fission happens, which means the droplets solidify too early and may create larger, irregular, and porous particles [232]. DCM particles generated the largest particles with the most extensive distribution (3.3± 0.96µm). Trotta et al. (2010) investigated the effect of different solvents on the production of electrosprayed solid lipid-based particles [301]. They found that using the solvent with a high boiling point, therefore a low evaporation rate, made the particles' structure more robust and their morphology less irregular [301]. The same observation was made by Park & Lee (2009), where an increase in the solvent's boiling point correlated with a decrease in the particle size [300]. Indeed, when using a low-evaporation solvent such as DMAc (0.17), the particle size decreased to 1.8µm compared to when DCM (3.3µm) was used as the solvent choice.

3.3.1.2. Surface tension

ACE particles generated the smallest and most irregular particles with the most minor distribution (1.27± 0.26µm). Their irregularity is due to their high evaporation rate. However, their small size is due to their higher conductivity (20µS/m) and low surface tension (24 Dyn/cm) [302]. When the surface tension of a solution increases, a larger voltage is required to overcome the surface tension to break the solution into droplets; a lower surface tension, such as acetone, will, therefore, not require a high voltage compared to DMAc, which has a higher surface tension (32.43 Dyn/cm) [232]. High solvent conductivity and high surface tension can also alter the morphology or shape of particles by elongating the particles, as seen in a few particles made with DMAc. DMAc usually requires a higher voltage to produce smaller particles, as presented in

the study by Parhizkar et al. (2016), where at the same concentration of PLGA (2wt%), 16 kV was used to achieve a small average particle size of 550nm [227].

3.3.1.3. Conductivity

Despite its high evaporation rate, THF generated smaller particles (2.03± 0.35µm) than DCM particles (3.3± 0.96µm), as shown in Figure 3.1. This difference could be due to the very low electrical conductivity of THF ($1.5x10^{-16}$S/m), as a low conductivity means there is less charge carried by the jet, making it more stable to produce more monodisperse particles [252]. High electrical conductivity can lead to smaller particles as higher charges mean higher Coulombic repulsion forces. This facilitates breaking the initial droplets into smaller droplets, leading to smaller particles. However, such an increase in the charge can also lead to more disparity in the size distribution [232,252]. This explains how DMAc can generate small particles (1.84± 0.4µm) with a slightly higher distribution with high conductivity (0.5 S/m) despite having a much lower evaporation rate than the other solvents. Although the conductivity and surface tension are not concentration-dependent, these two parameters highly influence the critical voltage [300]. In a study by Xie et al. (2006), 5 wt.% PLGA in acetonitrile was electrosprayed, and by adding organic salts to the polymer, conductivity increased and led to a decrease in particle size from 1.2µm to 355 nm [303].

Based on these observations, DMAc and acetone were taken further and optimised in the next part of the study. Acetone generated the smallest particles with the lowest size disparity, and DMAc generated the smoothest and most spherical and second smallest particles. Moreover, their contrasting evaporation rate, surface tension, and viscosity allow for further tailoring of these parameters by adjusting the ratio of acetone and DMAc. DMAc was also favoured due to its high conductivity supporting the generation of smaller particles.

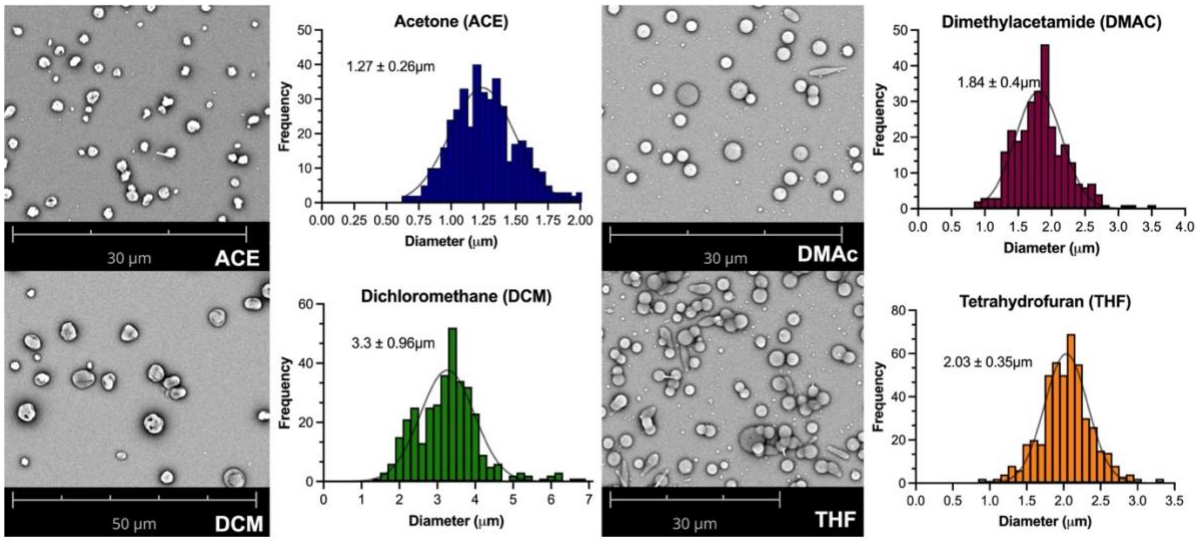

Figure 3.1. Scanning electron microscopy (SEM) images of electrosprayed particles with their respective size distribution using four solvents: acetone, dimethylacetamide, dichloromethane, and tetrahydrofuran. Data are expressed as the mean +/- s.e. mean of 3 independent experiments carried out in triplicates.

3.3.2. Imatinib-loaded particles characterisation

3.3.2.1. Size and morphology

The electrohydrodynamic atomisation of the polymer solutions generated individual, smooth, and spherical particles using all formulations in Figure 3.2, along with each formulation's respective size distribution, mean size and PDI. All formulations showed a low polydispersity index (all below 0.3) as well as a decreasing mean size in F5 (430±160nm; PDI 0.14), F6 (483±133nm; PDI 0.07), F7 (489±189nm; PDI 0.14), and F8 (473±175nm; PDI 0.15) compared to F1 (902±274nm; PDI 0.09), F2 (694±159nm; PDI 0.05), F3 (561±221nm; PDI 0.16) and F4 (815±251nm; PDI 0.10).

The solvents chosen for this study were acetone and DMAc, with the latter having a higher electrical conductivity, viscosity, and surface tension [227] than acetone, whilst acetone has a higher evaporation rate [5,304]. The binary solvent system of acetone and DMAc for F1, F2, F3 and F4 allowed a higher flow rate of 5µL/min. A binary solvent system would allow for a balanced solvent evaporation rate, allowing droplets to further atomise before reaching the collection plate and ensuring dense, smooth, and thoroughly dried particles are collected. In our study, F5, F6, F7, and F8 produced smaller particles than F1, F2, F3, and F4 by further decreasing the evaporation rate of the solvent by removing acetone [305].

Processing parameters such as flow rate and voltage were then adjusted to match the polymer solution characteristics. For instance, the flow rate was also adjusted to the less volatile solvent, DMAc, and reduced from 5 to 2µL/min. The lower flow rate also produces smaller particles by decreasing the dispensed droplet size, ultimately decreasing the size of the separating droplets. Yao et al. (2008) electrosprayed two solutions of PLGA using acetonitrile and dichloromethane at two different concentrations. They showed an increase in the particle size from 0.5µm to 25µm by increasing the flow rate from 2 to 4 mL/hr in both solutions [306]. The voltage had to be then adjusted to match the new solution and processing parameters, which was increased from 12 to 14kV as a higher electrical charge can overcome the cohesive forces of the particles and break the droplet into smaller droplets but can also lead to samples with a low polydispersity index [290,307]. When looking at the effect of solvent

on the electrospraying technique, Park & Lee (2009) found that particle size would decrease as the flow rate decreased and voltage increased when electrospraying a 7wt% polystyrene solution in DMF [300]. Meng et al. (2009) looked at the variables in the electrospraying of four different molecular weights of PLGA and the effect of the applied potential. They showed a decline in particle diameter when the applied voltage increased [308]. This study, along with the ones mentioned, showed the potential of electrospraying in producing particles of various sizes and morphologies but mainly demonstrated a high level of control over the particles' characteristics, making the electrospraying technique highly reproducible, versatile, and flexible.

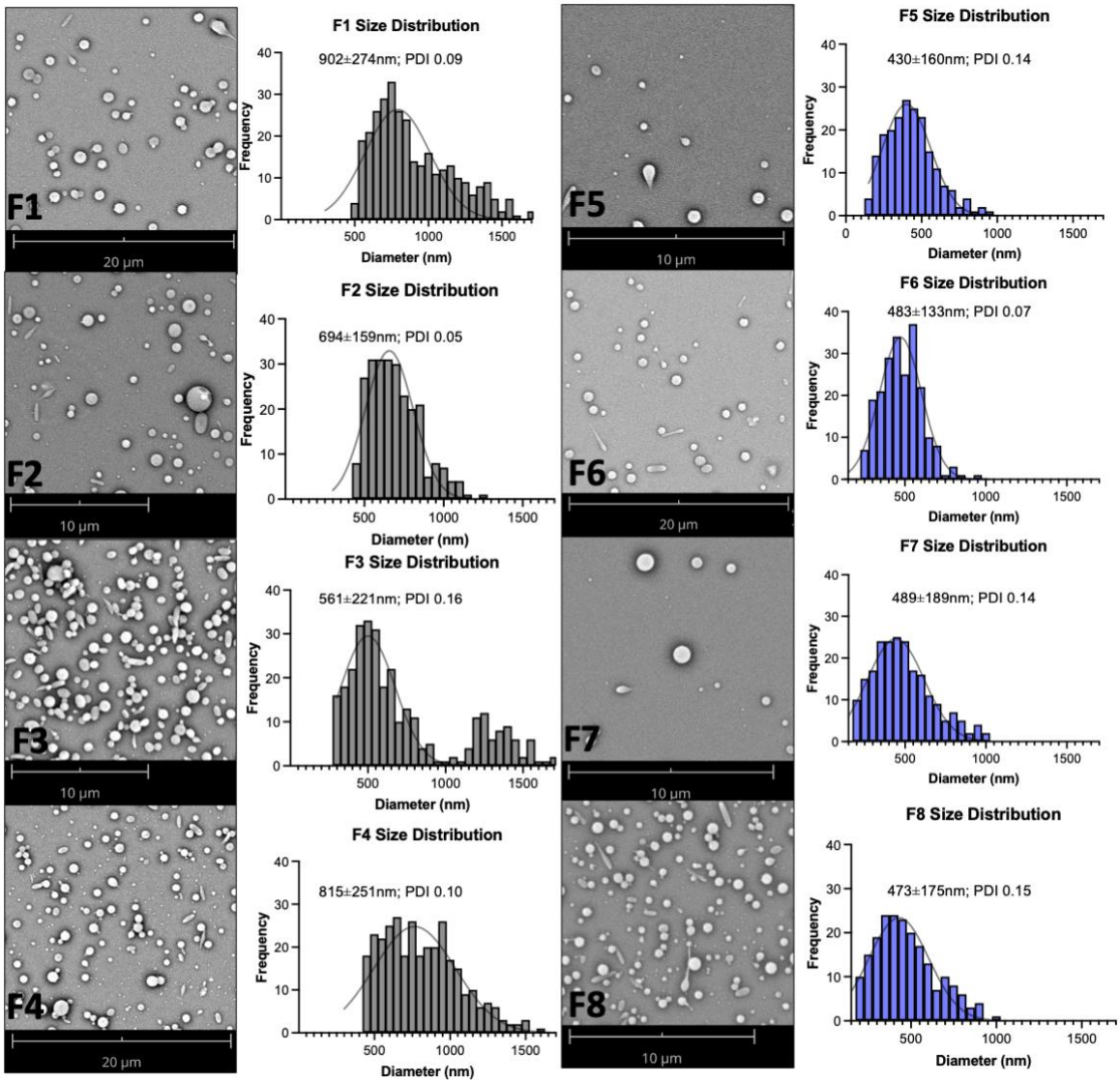

Figure 3.2. Scanning electron microscopy (SEM) images of all formulations of NPs with their respective size distribution and PDI. Data are expressed as the mean +/- s.e. mean of 3 independent experiments carried out in triplicates.

3.3.2.2. Zeta-potential and FTIR

The surface charge of the particles was measured as it was reported that the charge influenced the particles' effect on cytotoxicity and their cellular uptake [309].

Figure 3.3A displays the surface charge of the blank and imatinib-loaded PLGA 50:50 and 75:25 NPs and the charge of imatinib alone. The charge increase in the encapsulated particles indicates that adding imatinib significantly affects the charge of the particles. Indeed, the mean charge of pure imatinib at -9 ± 2mV is higher than the blank NPs at -21 ± 4mV (PLGA 50:50) or -17 ± 7mV (PLGA 75:25) and it is shown that the encapsulation of imatinib in PLGA NPs increases the zeta potential to -13 ± 7mV (PLGA 50:50) or -15 ± 4mV (PLGA 75:25). The addition of the drug appeared to influence the surface charge of the particles.

FTIR has been chosen to identify the incorporation of the drug within the polymeric particles.

Figure 3.3B displays the FTIR spectrum of the pure PLGA 50:50 and 75:25, which yielded the same spectrum as their respective blank PLGA, encapsulated PLGA particles and pure imatinib. The C=O stretch of imatinib can be observed in the encapsulated-PLGA particle spectra in the 1600 cm^{-1}, indicated by the red circles in both Imatinib-PLGA 50:50 and Imatinib-PLGA 75:25.

This study has also shown that adding imatinib increased the zeta potential of the particles, indicating that imatinib was found partially on the surface of the particles. When the particles are formed through electrospraying, the high voltage applied breaks the initial droplets dispensed by the needle into smaller droplets, which form the particles [223,236]; and as the solvent evaporates, the dry particles travel to the collection plate [237]. During that process, the separation of these droplets can cause some of the drugs to precipitate on the surface of the particles instead of being incorporated in the PLGA matrix, especially in NPs with a high encapsulation efficiency likely due to the polymer reaching saturation with the encapsulated drug; this could explain the increased zeta potential seen in imatinib-loaded particles [310].

Imatinib incorporation within the PLGA particles has been shown through the FTIR spectrum of Imatinib-loaded NPs. Indeed, Imatinib's FTIR spectrum obtained corresponds to the ones found in the literature by Veverka et al. (2012), and Bhattacharya (2020) [210,311] and PLGA spectrum by Fu et al. (1999) [312]. The FTIR spectrum for both types of pure PLGA has a strong peak at 1086 cm^{-1} and 1750 cm^{-1} indicating a C-O-C and C=O stretching respectively [312].

Imatinib's characteristic peaks can be found at around 3279 cm^{-1} and 2798 cm^{-1} indicating the presence of N-H and carboxylic acid C=O and O-H stretch respectively [313]. The sharp stretches at around 1500 cm^{-1} signify the presence of a C=O stretch and finally, the ones between 1500 to 650 cm^{-1} display the presence of an aromatic group. The addition of imatinib found in the 1600 cm^{-1} indicates its aromatic group however this characteristic peak was significantly reduced in the encapsulated-PLGA spectra [311].

Imatinib is a BCS class II small molecule [314] and was found to be amphiphilic as its chemical structure contains both polar (nitrogen and hydrogen groups) and nonpolar groups (benzene rings and methyl groups), creating a small molecule with hydrophobic and hydrophilic properties [315,316]. The reduction of intensity could be due to hydrophobic interaction between the long carbon chain of PLGA and imatinib's benzene ring, as observed by Liu et al. (2021) on their FTIR spectrum of electrospray imatinib and paclitaxel-loaded core-shell microparticles [215]. According to a study by Kumar et al. (2021) that investigated the in-silico interaction between imatinib and PLGA, the configuration pattern showed that the hydrogen on imatinib's benzene ring forms a hydrogen bond with PLGA's ester and imatinib's methyl group (CH_3) also forms a hydrogen bond with the ketonic group of PLGA (R−C(=O)−R') [317].

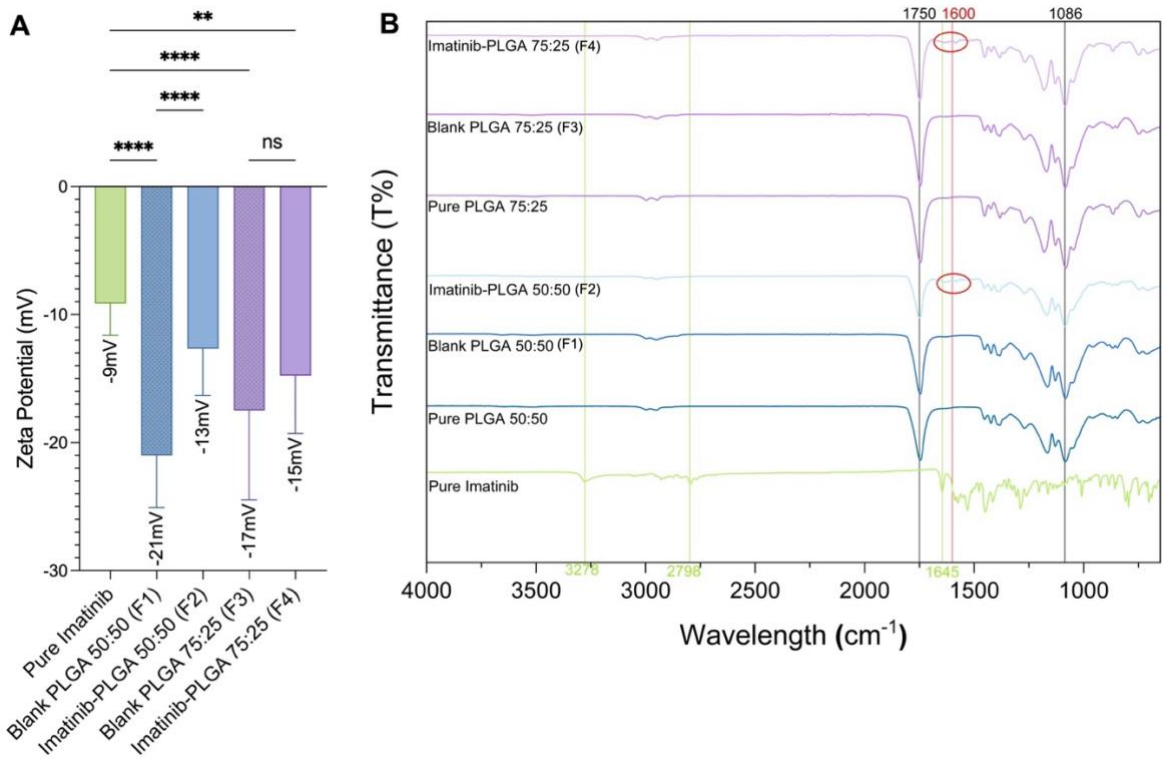

Figure 3.3. A. Zeta potential of pure imatinib, blank (F1 and F3) and imatinib-loaded PLGA NPs with PLGA ratio 50:50 (F2) and 75:25 (F4). Data are expressed as the mean +/- s.e. mean of 3 independent experiments, each carried out in triplicates (*P < 0.05, **P < 0.01, ***P < 0.001; data analysed by one-way ANOVA followed by Tukey's post hoc test.) and B. Corresponding FTIR spectrum with pure PLGA spectrum (50:50 and 75:25). Red circles showing the Imatinib specific amine group in the drug encapsulated PLGA nanoparticles.

3.3.2.3. Encapsulation efficiency and release profile of imatinib-loaded NPs

The encapsulation and release of imatinib in the four different drug-loaded formulations (F2, F4, F6 and F8) were studied and compared to observe the effect of the type of polymer and the effect of solvent on the encapsulation efficiency and release of imatinib. When comparing the effect of the different types of PLGA polymer, the mean encapsulation efficiency for F2 was found to be around 89 ± 4% and 98 ± 13% for F6 in PLGA 50:50, and a slight decrease in the mean encapsulation efficiency in F4 with 79 ± 5% and F8 with 93 ± 9% using PLGA 75:25, however not significantly different as shown in Figure 3.4A.

Our study has demonstrated a high encapsulation of imatinib with a slightly lower encapsulation efficiency when using PLGA 75:25. The electrospraying method allows for a high encapsulation of both hydrophobic and hydrophilic drugs, regardless of the hydrophobicity of the polymer. Valo et al. (2009) electrosprayed beclomethasone dipropionate, a hydrophobic drug, and salbutamol sulphate, a hydrophilic drug, and showed that the hydrophobicity and hydrophilicity of the drugs did not affect their encapsulation efficiency when electrosprayed [318]. The solvents used for F2 and F4 were DMAc and acetone, and DMAc was only used for F6 and F8. The evaporation rate of acetone is higher than that of DMAc, which can lead to irregular and porous particles when electrosprayed [232]. This could explain the slightly lower encapsulation efficiency in F2 and F4.

All release profiles in Figure 3.4B showed an initial burst release of imatinib in the first 12 hours. The burst release in the particles generated from F6 was more significant than in F8, F2 and F4. F6 (483±133nm) have indeed shown subsequently to release much faster than F8 (473±175nm), F2 (694 ± 159nm) and F4 (815 ± 521nm). Pure Imatinib's release is much slower than all the other release profiles and only reaches a release of 16% after seven days.

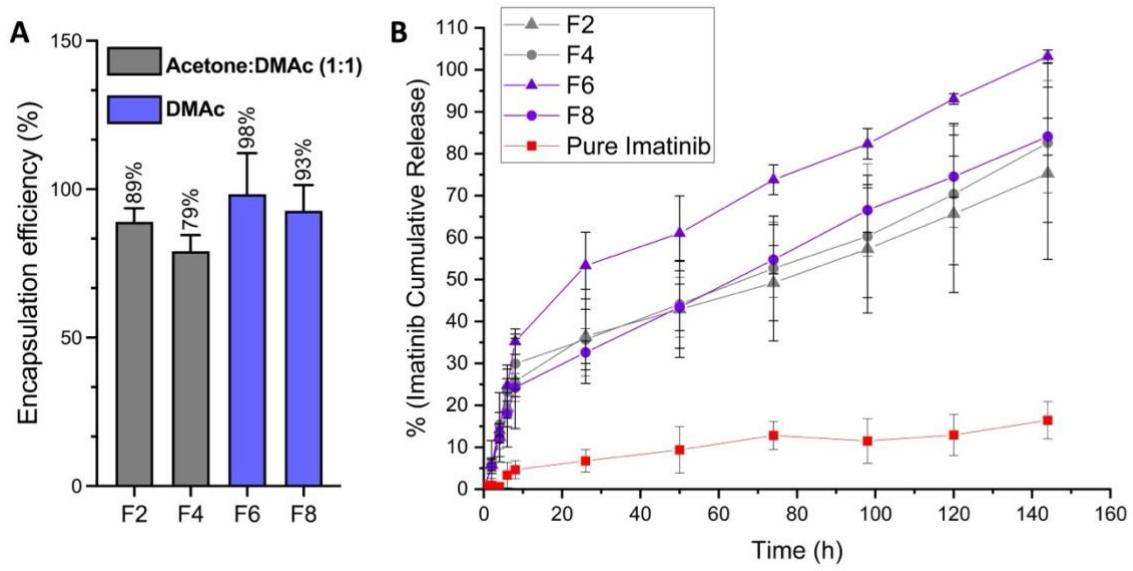

Figure 3.4. A. Respective encapsulation efficiency of imatinib in F2, F4, F6, F8 IMA-NPs. B. Imatinib cumulative percentage release from F2, F4, F6 and F8 IMA-NPs and pure imatinib after being suspended in PBS over seven days. Data are expressed as the mean +/- s.e. mean of 3 independent experiments (*P < 0.05, **P < 0.01, ***P < 0.001; encapsulation efficiency data analysed by Kruskal-Wallis test).

Mathematical models have been investigated to predict polymeric particles' drug release and diffusion behaviour, and the obtained release data were fitted to four common models: zero-order, first-order, Higuchi and Korsmeyer Peppas models. Table 3.2 displays the relevant model equations, with f being the amount of drug released over time t, and R^2 the correlation coefficient, with the latter indicating which model is appropriate for the drug release. Our drug release profiles better fit the Korsmeyer Peppas model with an R^2 of 0.99, 0.98, 0.97 and 0.99 for F2, F4, F6 and F8, respectively.

The drug release profiles from the particles presented in this study follow a biphasic profile, with the first phase being the initial burst release and the second phase being a slow-release phase compared to the slower release of pure imatinib. The drug release from nanoparticles displayed a greater burst release and faster release from F6 (483nm). This initial burst release could be due to the heterogeneous distribution of the drug in the polymer matrix during the formation of the particles through electrospraying, as previously mentioned by the increased zeta potential (

Figure 3.3A) [310,319]. The initial burst release of imatinib can also be attributed to the surface degradation of the particles following the start of PLGA hydrolysis [147]. Drug diffusion, swelling and polymer degradation are the other mechanisms involved in drug release from PLGA drug delivery systems [320,321]. Indeed, following the diffusion of imatinib out of the particles, water invades the particles causing it to swell and the PLGA matrix erodes, making the polymer fragments become water-soluble and then fully degrade homogenously [148].

Various common mathematical models were investigated to fit the drug release, such as zero-order, first-order, Higuchi, and Korsmeyer-Peppas. The Korsmeyer-Peppas model was determined to be the best fit and is expressed as:

$$f = \frac{M_t}{M_\infty} = Kt^n$$

Equation 3.4. The Korsmeyer-Peppas model

The amount of drug release f over time t, with K being the kinetic constant incorporating nanoparticles' structures and n the exponent characterising the release mechanism [322].

The drug release mechanism suggests a Fickian diffusion as the calculated exponent n for all formulations was <0.5 [323]. The Korsemeyer Peppas model has been previously used to evaluate the release of actives from PLGA NPs. For instance, Esmaili et al. (2018) encapsulated PLGA NPs for the controlled release of curcumin, and the Korsemeyer Peppas model has also been found to fit the release of the active (R^2=0.90) and to follow Fickian diffusion (n= 0.282) [324]. In the study by Chatterjee et al. (2020), the electrosprayed PLGA NPs carrying the anti-cancer treatment methotrexate was also found to fit the Korsemeyer Peppas model (R^2=0.99) and to follow Fickian diffusion (n= 0.49) in their release of the drug [229].

Kinetic models	***Kinetic parameters***	***F2***	***F4***	***F6***	***F8***
Zero-order *Eq 1.* $f = K_0 t$ [325]	K_0	0.693	6.434	1.497	6.752
	R^2	0.922	0.914	0.894	0.943
First-order *Eq 2.* $ln(1-f) = K_1 t$ [326]	K_1	0.011	6.434	1.497	6.752
	R^2	0.949	0.938	0.919	0.960
Higuchi *Eq 3.* $f = K_H \sqrt{t}$ [325]	K_H	6.093	6.434	9.372	6.752
	R^2	0.981	0.973	0.967	0.988
Korsemeyer Peppas *Eq 4.* $f = \frac{M_t}{M_\infty} = Kt^n$ [327]	K	8.784	10.226	9.962	6.877
	n	0.409	0.384	0.481	0.493
	R^2	0.987	0.982	0.968	0.988

Table 3.2. Release kinetics models of imatinib-loaded NPs.

Studies have shown that size and porosity significantly affect the drug release from PLGA-based particles as they affect polymer erosion and drug diffusion [321]. Previous work has shown that smaller particles were associated with faster release. Berkland et al. (2002) demonstrated that the rate of release decreased with the increase in particle size when they looked at rhodamine-B and piroxicam-loaded PLGA microspheres [328]. This is also consistent with the increase in surface area to volume ratio in smaller particles [328], allowing more water to encounter the NPs, contributing to swelling and leading to higher hydrolysing of the polymer, faster diffusion and ultimately a faster release [9,147].

It was also noted that although F6 have a similar size to F8 (473nm), F6 showed a faster release. This is due to F6 being produced using PLGA 50:50, which has a lower lactic acid to glycolic acid ratio and is the least hydrophobic polymer, which increases the rate of water absorption and hydrolysis, leading to a faster drug release [147] as seen here compared to F8 and as reported in previous studies [329]. Both Benny et al. (2009) and Karal-Yalmaz et al. (2016) investigated PLGA 50:50, 75:25 and 85:15 for the release of imatinib mesylate and found that PLGA 50:50 released the drug faster than 75:25. Benny et al. (2009) attributed the difference to the higher hydrophobicity of PLGA 75:25 [6] and Karal-Yalmaz et al. (2016) to the difference in size where smaller size led to a faster release [9].

Although the literature suggests that larger particles release the drug at a slower rate, the larger particles prepared in this work using F2 (902 nm) and F4 (674nm) had a similar imatinib release rate to F8 (473nm). This can be explained as adding acetone in F2 and F4 can lead to more porous NPs and impact its release. Porous PLGA-based microparticles release their content much faster than non-porous PLGA-based microparticles [330] by facilitating the water erosion of the polymer by the broader surface area and increasing the mobility of the drug molecules [331].

The slower release of free imatinib may be due to the low solubility of the free base imatinib [332]. Because of imatinib's low solubility, we do not expect the same release profile experienced by NPs. Imatinib's solubility was significantly enhanced by its encapsulation into particles via electrospraying. Indeed, due to the fast solidification

of the particles during electrospraying, molecules do not have enough time to arrange in their crystalline form leading to imatinib being entrapped with the polymer in a matrix system in the amorphous state and thereby improving its solubility [333,334].

Additionally, the encapsulation enabled a controlled release rate of imatinib, which does not rely on imatinib's solubility; its release may also be controlled by changing the NP characteristics, in this case, the size and porosity of the NPs [335]. Overall, imatinib was released faster in this work than in other studies such as Karal-Yilmaz et al. (2016; 35 days) or Benny et al. (2009; 30 days). It has been shown that a faster release has been associated with higher drug content. A study by Zhang et al. (2018) achieved close to 100% release of progesterone from electrosprayed PLGA particles in approximately one week with an encapsulation efficiency of 83% [230].

3.3.3. Effect of the imatinib-loaded NPs (F6 and F8) and RhD-B NPs (F9) on A549 cells.

3.3.3.1. Cytotoxicity of F5, F6, and F8 NPs on A549 cells

Formulations F5, F6, and F8 NPs were chosen for the in-vitro cell studies due to their small size, as their delivery relies on the EPR effect in the 100-400nm range. The resulting NPs range from 400-500nm in size. Imatinib IC_{50} was found to be approximately 120μM, which is within the range of the concentrations found in the literature for this cell line of 61 and 150μM [336,337]. The drug release results obtained from F6, and F8 NPs allowed for calculating the dose of NPs that would encapsulate enough imatinib needed to achieve inhibition of proliferation. It was found that a concentration of 1mg/ml of NPs can release between 120 to 180μM of imatinib within 72 hours.

Both assays used in these experiments measure cell viability, either by measuring mitochondrial or cellular enzymatic activities, and both approaches exhibit a reduction in these parameters when cells are treated with the imatinib-loaded NPs and a range of imatinib concentrations alone, when compared with the untreated cells (control). Indeed, cell viability has been shown to decrease to 48 ± 11% and the percentage of live cells to 38 ± 20% when cells were treated with F6 and decrease to 57 ± 13% in cell viability and 25 ± 9% in the percentage of live cells when treated with F8.

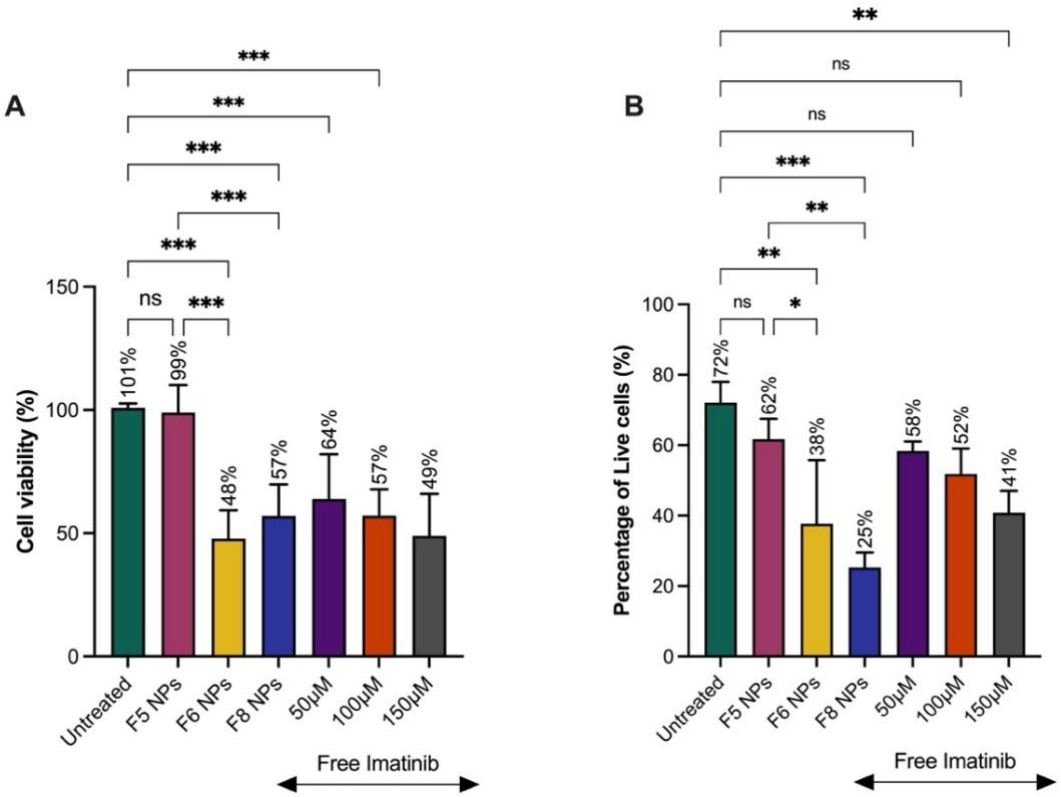

Figure 3.5. A. MTT assay results and B. Live/Dead cells ratio, both conducted 72 hours after treatment with imatinib-loaded NPs and free imatinib. Data are expressed as the mean +/- s.e. mean of 3 independent experiments (*P < 0.05, **P < 0.01, ***P < 0.001; data analysed by one-way ANOVA followed by Tukey's post hoc test).

These quantitative results are reflected qualitatively in the data shown in Figure 3.5. Since it was shown that the type of PLGA did not affect cell viability, only F5 and F6 were tested for the qualitative aspect of the live/dead assay. Figure 3.6 displays the qualitative results of the live/dead assay, following treatment of the cells with imatinib-loaded and blank-loaded NPs (F5 and F6) and a range of imatinib concentrations (50, 100, 150μM), respectively. No visual changes in the green-labelled cells were seen between the untreated cells and F5, indicating no changes in the proportion of live cells when cells are treated with blank PLGA. A concentration-dependent reduction in live cells can be observed when cells were treated with increasing imatinib concentrations. The imatinib-loaded nanoparticles have been shown to have efficacy in assays measuring A549 cell viability regardless of the type of PLGA used to encapsulate imatinib: their in-vitro cell viability results show decreased cell viability and live-cell ratio following treatment with free imatinib and with imatinib-loaded NPs (F6 and F8).

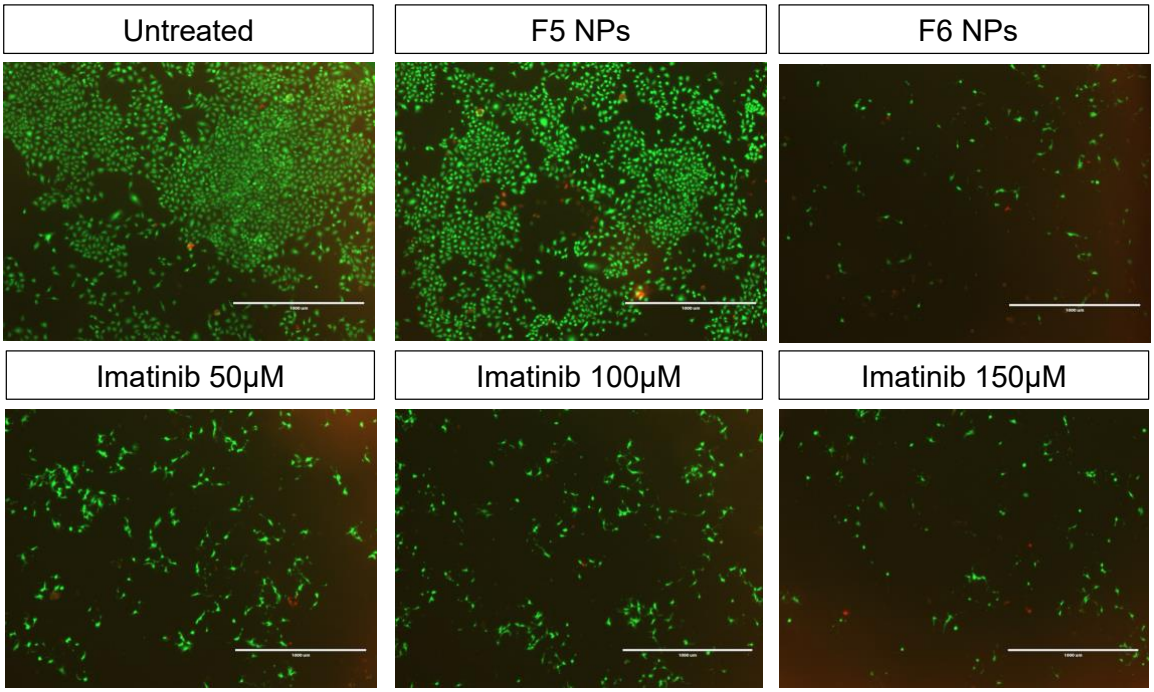

Figure 3.6. Live/Dead Assay on A549 cells 72 hours after treatment with medium (untreated), F5 NPs (blank), and F6 NPs (imatinib-loaded), both at 1mg/ml and a range of imatinib concentrations (50, 100, 150μM). Live cells were stained green with Calcein AM, and dead cells were stained red with BOBO™-3 Iodide.

These results are consistent with the previous studies where imatinib and its derivatives were tested on A549 cells [336,337] and with studies in other cells and tissues [338]. A study by Khan et al. (2016) investigated the effect of imatinib-loaded nanoparticles in various glioma and glioblastoma cell lines, and they found a decrease by more than half in imatinib's IC_{50} when cells were treated with imatinib-loaded NPs [209]. The study by Benny et al. (2009) also measured the effect of their imatinib-loaded PLGA microspheres on glioma and glioblastoma cells and found that cell viability was decreased by 57% to 65% in response to imatinib released from PLGA microspheres over twelve days. As established earlier, imatinib is released much more slowly from these NPs because of their size and fabrication method. This reduction in live cells was also reflected here in our study when the cells were treated with imatinib-loaded NPs, both using PLGA 50:50 or PLGA 75:25 (F6 and F8), showing that the lactic/glycolic ratio in PLGA did not significantly affect the release and effect of imatinib on A549 cells. This lack of difference was also found in the study by Karal-Yilmaz et al. (2016), looking at imatinib-loaded microspheres for craniopharyngioma where PLGA 75:25 and 50:50 exhibited the same effect for up to 10 days [9]. Blank PLGA-treated cells led to no changes in the population of live cells, as expected due to PLGA being a biodegradable and non-toxic polymer [145].

3.3.3.2. *Cellular uptake of F9 NPs into A549 cells*

Here, the facilitation of imatinib's internalisation by the cells was investigated. The fluorescent dye rhodamine-B was used to examine the uptake of the NPs into the cells. The fluorescence was measured in untreated cells and in cells treated with blank NPs (F5), which showed little to no fluorescence (Figure 3.7). The F9 NPs were added to both cell-seeded and non-seeded wells to ensure that relevant fluorescence measurements reflected the interaction of NPs with the cells and not the tissue culture plate. F9 NPs in non-seeded wells showed no significant difference from those untreated, indicating that NPs not taken up by cells can be successfully rinsed out of the wells. Only the F9 NP-treated wells showed significant fluorescence readings, also higher than free RhD-B, indicating the uptake of rhodamine-loaded NPs into the cells within 24 hours. Imatinib may exert its anti-proliferative effect by targeting intracellular tyrosine kinase proteins [256].

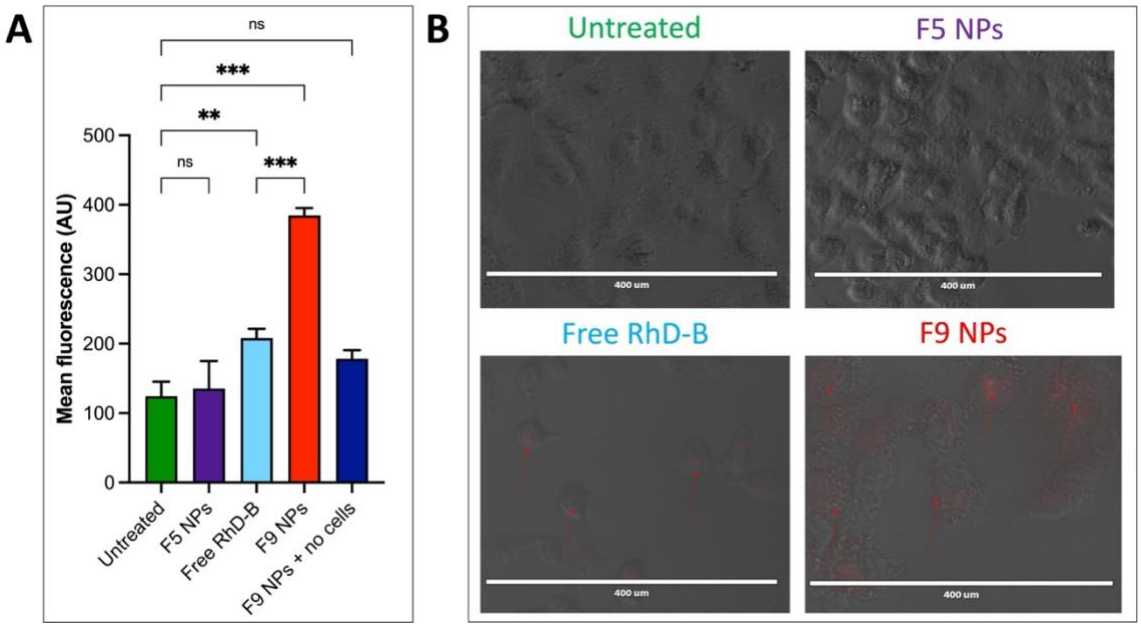

Figure 3.7. A. The uptake assay result was obtained 24 hours after treating A549 cells with rhodamine-B-loaded NPs. Data are expressed as the mean +/- s.e. mean of 3 independent experiments, each carried out in duplicate (*P < 0.05, **P < 0.01, ***P < 0.001; data analysed by one-way ANOVA followed by Tukey's post hoc test.) B. Corresponding EVOS fluorescence images demonstrating the uptake of RhD-B pointed out by red arrows.

The present data suggest that the PLGA NPs obtained in this study are able to deliver imatinib into the cells via endocytosis. Indeed, many studies have hypothesised that PLGA NPs' uptake occurs via endocytosis or receptor-mediated endocytosis [339–341]. For instance, Yin & Feng (2005) established that the endocytosis of PLGA NPs was size-dependent, with the highest uptake seen for NPs between 100 and 500nm, suggesting that the NPs produced in this study (400-500nm) would also be taken up via endocytosis [342]. Panyam & Labhasetwar (2002) and Yin & Feng (2005) both demonstrated that the uptake was also time-dependent with an increase in intracellular NPs as early as within 1 min post-treatment in smooth muscle cells and 30 min in colon epithelial cells (Caco-2 cells) and kept increasing in the presence of NPs in the media [339,342].

Rhodamine-B has been used previously as a model drug to investigate the cellular uptake of PLGA NPs in epithelial cells to deliver RNAi material and it was shown that the rate of uptake of rhodamine-B-loaded NPs into cells is cell-dependent, varying from 6 to 24hrs [343]. A study of docetaxel-loaded PLGA NPs investigated the NP uptake in A549 cells and found that high cellular uptake was achieved by 6 hours. The overexpression of caveolin-1, a cell surface protein, in A549 cell line and another lung cancerous line, BEAS-2B has also been found to cause an increase in NP uptake, which supports the caveolin-mediated endocytosis of the PLGA NPs in A549 cells [341,344].

The fast and suggested protein-mediated cellular uptake displayed in these studies aligns with the NPs and the payload being delivered intracellularly within the 24-hour incubation time set in the present study. Khan et al. (2016), comparing imatinib's relative IC50 in imatinib-loaded NPs to free imatinib, attributed the decrease in IC50 by imatinib-loaded NPs to the improved cellular uptake of the NPs and, therefore, better uptake of imatinib when it has been encapsulated in PLGA, showing consistency with the results presented here [345].

Imatinib resistance has been reported in the treatment of chronic myeloid leukaemia (CML), and an uptake study using radiolabelled imatinib has shown that this resistance could be due to the dysfunction of cell transporters responsible for the influx and efflux

of imatinib into cells [105]. This further indicates the need for an intracellular carrier to safely deliver imatinib into the cells and exert its antiproliferative effects. The present results indicate that the PLGA NPs obtained in this study may achieve this without reliance on cell transporters.

3.4. Conclusion

The present study has shown its high control over the production of polymeric particles by first changing the solvent to generate particles of various morphology and size. The versatility of electrospraying and its ability to produce a wide range of imatinib-loaded NPs was also demonstrated, and the effective control over the load's release by changing the technique's parameters. Electrospraying, therefore, shows high potential for encapsulating a wide range of actives and gaining control over their physical-chemical characteristics and release profiles while yielding uniform and spherical NPs. The change in formulations has indeed demonstrated the ability to control the size of the nanoparticles while maintaining their uniformity, and imatinib was shown to be incorporated in the NPs using FTIR spectroscopy.

The tunability in producing these NPs, generated by a single-step electrospraying technique for the first time, enabled the high encapsulation of imatinib and its controlled release. The resulting imatinib-loaded NPs have been shown to possess efficacy in an in vitro cell-based assay, with a comparable capacity to inhibit A549 cell proliferation as free imatinib. It was also demonstrated that the effect of imatinib on A549 cells was maintained when it was encapsulated in either PLGA 50:50 or 75:25 NPs. The uptake of the NPs by A549 cell cultures was also successfully demonstrated using rhodamine B-loaded NPs.

In conclusion, this work has shown excellent prospects for the passive delivery of imatinib in managing proliferative conditions, whereby its encapsulation and controlled release from NPs may enhance its efficacy and safety. The work also opens the potential for the surface functionalisation of the NPs for more active drug delivery. Owing to the over-proliferation of vascular cells in PAH, the cell viability results after the treatment with imatinib-loaded NPs on the rapidly proliferating A549 cell line are particularly promising. This prompted the evaluation of the drug-loaded NPs on vascular cells: the focus of the next chapter.

Chapter 4. The Effect of the electrosprayed NPs on vascular cells

4.1. Introduction

Pulmonary hypertension has been characterised by the dysfunction of the pulmonary arterial cells, particularly endothelial and smooth muscle cells [36]. The condition's multifactorial mechanism has been deemed comparable to the complex pathways that underpin cancer, which has ignited the search for anti-cancer agents, such as imatinib.

Imatinib has well-established inhibitory effects on smooth muscle cell function [72,111]. It has been investigated here, and in other studies, for the treatment of pulmonary hypertension mainly due to its inhibitory effect on pulmonary arterial smooth muscle cell (PASMC) over-proliferation [72], by targeting the platelet-derived growth factor (PDGF) signalling pathways in these cells [16,346].

Imatinib has been shown to maintain an antiproliferative effect, especially when the cells are stimulated by the growth factor PDGF [10,72,346]. On the other hand, Imatinib has been shown to be non-toxic to human umbilical vein endothelial cells (HUVEC) by not affecting cell viability and it has been found that PDGF signalling is relatively insignificant in HUVEC proliferation [111,347]. Another study found that, even when stimulated with VEGF, imatinib did not inhibit proliferation or induce apoptosis in endothelial cells [348]. All these studies suggest that imatinib should not affect HUVECs in preventing their growth, survival, or migration ability.

The effect of free imatinib was tested on HUVECs to ensure our findings were comparable to those reported in the literature and to ensure that the imatinib-loaded NPs would not have any unwanted antiproliferative effect on healthy endothelial cells. The encapsulation of imatinib in PLGA nanoparticles has been studied for various applications; however, the use of imatinib-loaded NPs for PAH was only investigated in a single study by Akagi et al. (2015), which encapsulated the salt version of imatinib (imatinib mesylate) using the emulsion solvent diffusion method.

The present study investigates the effect of imatinib-loaded NPs, on the cell viability of endothelial cells (HUVECs) and pulmonary arterial smooth muscle cells (HPASMCs). The latter cell type was further tested with stimulation in the presence of the growth factor PDGF, with respect to the effect of the imatinib-loaded NPs.

4.2. Methodology

The general methods for cell growth and maintenance are highlighted in section 2.2.3.1. Cell viability was measured by the MTT assay outlined in 2.2.3.3 for both cell types investigated. All the PLGA NPs tested in this chapter were electrosprayed following F5 for blanks and F6 for imatinib-loaded NPs (PLGA 50:50, DMAc, 2μL/min), as described in Chapter 3.

4.2.1. Measurement of HUVEC viability

HUVECs were seeded in 96-well plates at a seeding density of 2000 cells per well. The cells were treated 24 hours later with medium alone (untreated), blank NPs (F5 NPs) or imatinib-loaded NPs (F6 NPs), both at 1mg/mL, or with a range of imatinib concentrations of 50μM, 100μM, and 150μM. These were similar to the treatment conditions used in Chapter 3 to measure A549 cell behaviour. MTT assay was conducted 72 hours after the cells were treated. In other experiments, 96-well plates were seeded with HUVECs with the same seeding density, and 24 hours later the cells were treated with a wider range of imatinib concentrations: 4,10, 16, 20, 30, 40, and 60μM. The MTT Assay was conducted 72 hours after treatment in the same way. Finally, in some experiments, following preparation of 96-well plates was with the same seeding density, cell monolayers were allowed to reach 100% confluence. Plates were again treated with medium alone (untreated), blank NPs (F5 NPs) and imatinib-loaded NPs (F6 NPs), both at 1mg/mL, and a lower range of imatinib concentrations of 20μM, 30μM, and 40μM. Similarly, the MTT assay was conducted 72 hours after treatment. The optimised methods are summarised in Figure 4.1.

4.2.2. Measurement of HPASMC viability

4.2.2.1. Effect of confluence and imatinib concentration

HPASMCs were seeded in 96-well plates at a seeding density of 2500 cells per well. The conditions and treatments applied investigated the effects of confluence level and imatinib concentration on the cell viability of the HPASMCs. Cells were either allowed to reach 100% confluence before treatment or were treated at a confluence of 60%.

For each level of cell confluence, the cells were treated with a high (50, 100, 150μM) and low (10, 20, 40μM) range of imatinib concentrations. MTT assay was conducted 72 hours after the cells were treated.

4.2.2.2. HPASMC viability time course

HPASMCs were seeded in four 96-well plates at the same seeding density of 2500 cells per well. The wells were treated once the cells had reached 60% confluence with medium alone (untreated) and a higher range of imatinib concentrations of 100μM, 150μM, and 200μM. The MTT assay was conducted 4, 8, and 12 hours after treatment for plate 1, 24 hours for plate 2, 48 hours for plate 3, and 72 hours for plate 4. The NPs were then introduced in a new time course experiment, in which the cells were seeded in three 96-well plates for 8, 24 and 48-hour time points at a reduced seeding density of 2000 cells per well. The timepoint wells were again treated at 60% confluence with medium alone (untreated), blank NPs (F5 NPs) and imatinib-loaded NPs (F6 NPs), both at 1mg/mL, and with a reduced range of imatinib concentrations of 50, 100, and 150μM. The MTT assay was conducted 8 hours after treatment for plate 1, 24 hours for plate 2, and 48 hours for plate 3. The optimised methods are summarised in Figure 4.2.

4.2.3. Measurement of mitogen-stimulated HPASMC viability

HPASMCs were seeded in two 96-well plates at the same reduced seeding density of 2000 cells per well. Once the cells had reached 60% confluence, three out of six well columns were treated with medium alone (untreated), imatinib-loaded NPs (F6 NPs), or imatinib at a single concentration of 150μM, and the rest were treated the same way in the presence of 10ng/mL of the mitogen PDGF. The MTT assay was conducted after 24 hours for plate 1 and after 48 hours for plate 2.

The same experiment was subsequently repeated with blank NPs added, and an increased imatinib concentration of 176μM, which represents the highest concentration attainable within the drug solubility. The following experiment seeded, treated and stimulated the cells on the same day and the imatinib concentration was decreased to 20μM. The final experiment seeded the cells using the standard smooth

muscle cell medium at a doubled seeding density of 4000 cells per well for two plates. The cells were treated 16 hours later, and the medium was replaced with a low-serum medium: Dulbecco's Modified Eagle Medium (DMEM), supplemented with 1% fetal bovine serum and 1% penicillin-streptomycin. The MTT assay was conducted 24 hours later for plate 1 and 48 hours for plate 2. The optimised methods are summarised in Figure 4.3.

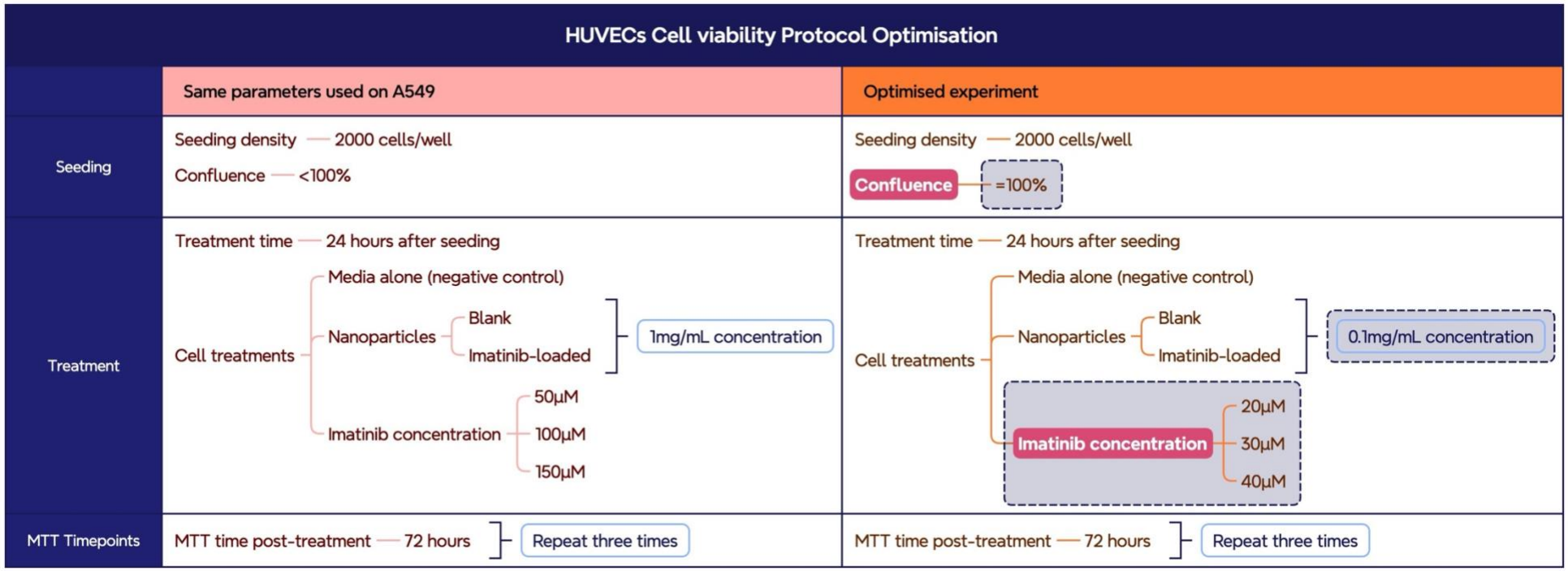

Figure 4.1. Summary of the methods used to test cell viability of HUVECs. The dotted squares mark each optimisation; important changes are highlighted in red.

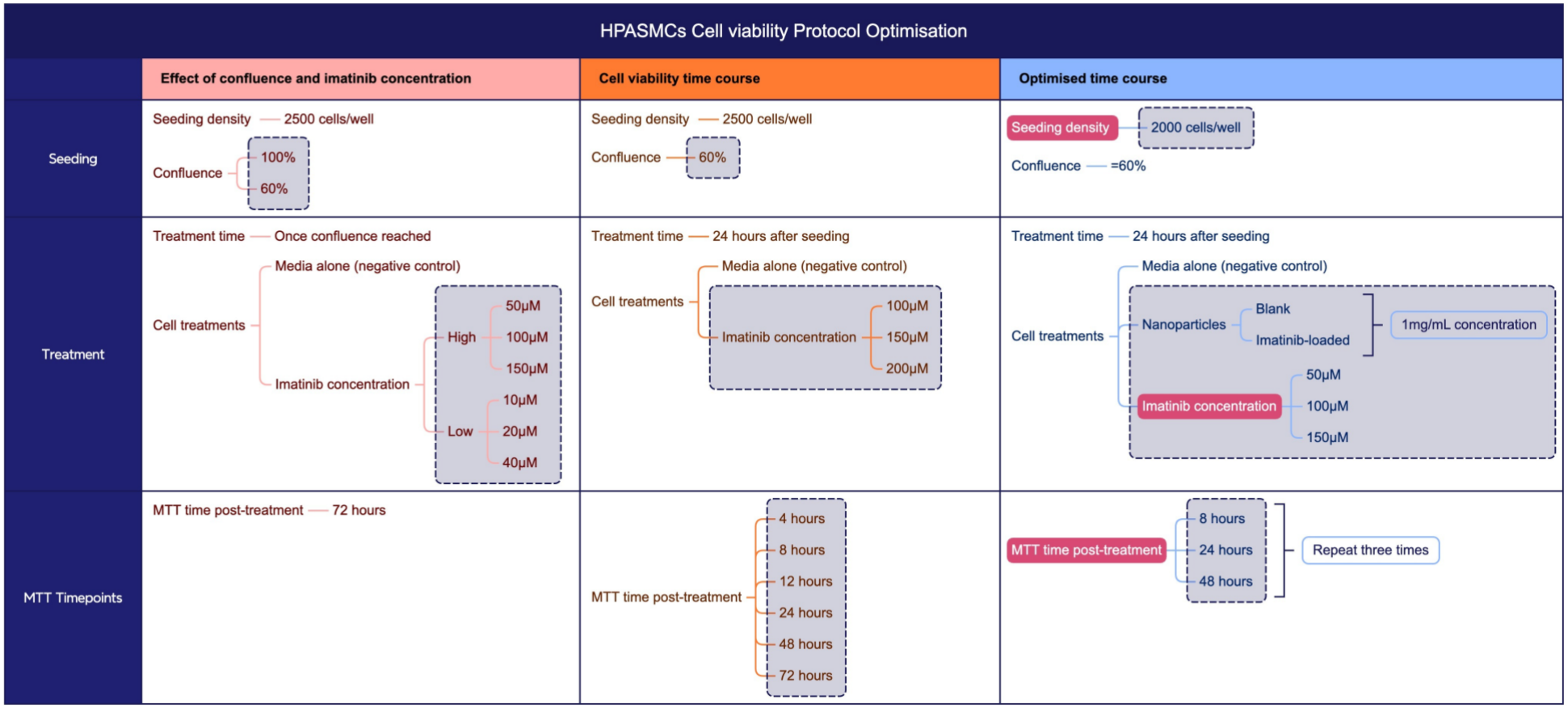

Figure 4.2. Summary of the methods used to test cell viability of HPASMCs. The dotted squares mark each optimisation; important changes are highlighted in red.

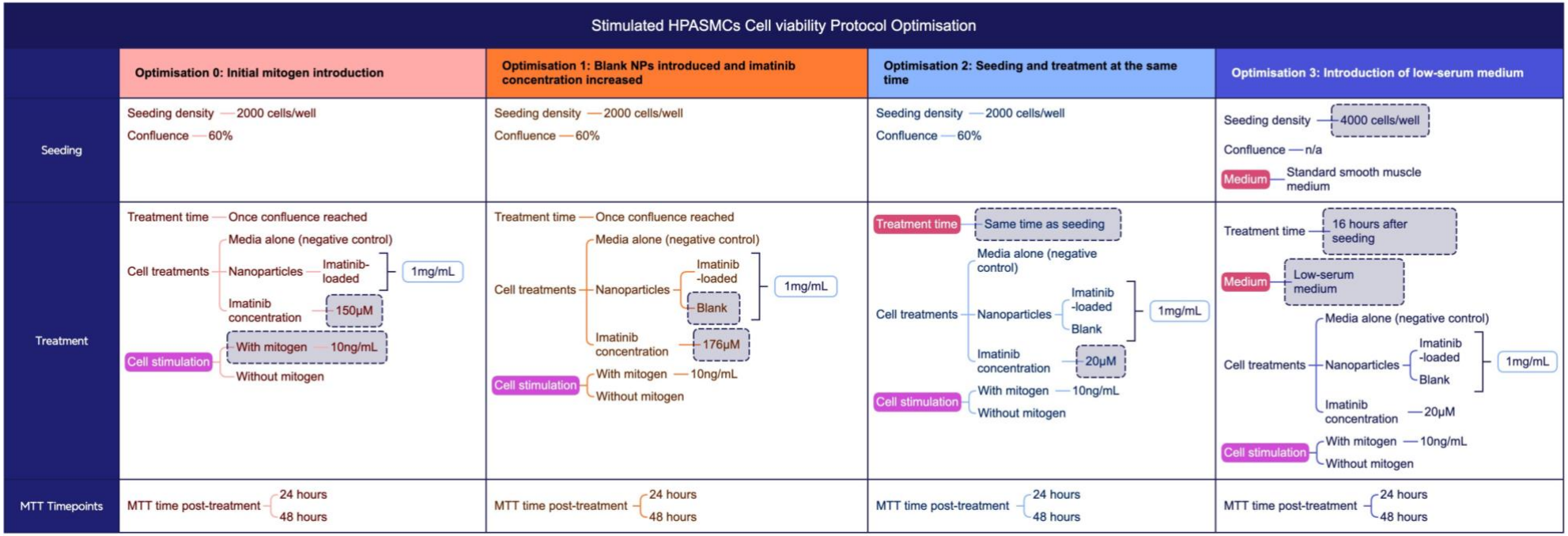

Figure 4.3. Summary of the methods used to test cell viability of PDGF-stimulated HPASMCs. The dotted squares mark each optimisation; important changes are highlighted in red.

4.3. Results and Discussion

4.3.1. Effect of imatinib-loaded NPs on human umbilical vein endothelial cells (HUVECs)

Imatinib's impact on endothelial cells was investigated, as the vascular endothelium is the first protective barrier that NPs encounter from blood when intravenously administered [349]. This study started with the same imatinib concentrations (50μM, 100μM, and 150μM) and imatinib-loaded NPs used in Chapter 3, which led to decreased cell viability, as shown in Figure 4.4A.

Gopal et al. (2018) studied the endothelial toxicity of various tyrosine kinase inhibitors (TKIs) (dasatinib, ponatinib, nilotinib and imatinib). Unlike the other TKIs, imatinib, at 4μM, was non-toxic to HUVECs by not affecting leukocyte adhesion, wound healing, or cell viability in HUVECs after 20 hours of treatment [347]. Gover-Proaktor et al. (2017) reported similar effects, where imatinib, at 5.3μM, had no significant impact on HUVEC cell viability, tube formation, and gene expression after 48 hours of exposure [350]. Aoyama et al. (2021) have reported similar findings, even with increased exposure time of 72 hours. Another study by Venalis et al. (2008) found that, even when cells were stimulated with VEGF, imatinib did not inhibit proliferation, induce migration, or apoptosis in endothelial cells. Thus, Venalis et al. (2008) suggest the drug has no inhibitory effect on endothelial cells [348]. Masuda et al. (2011) investigated imatinib-loaded PLGA NPs eluting from a stent for acute coronary syndrome and their effect on vascular smooth muscle and endothelial cells. They found an inhibitory effect on smooth muscle cells but no negative impact on the endothelial cells (HUVECs) [351]. All these studies show that imatinib, loaded in NPs or not, did not prevent HUVEC growth, survival, or migration ability.

In the experiments described in this chapter, a reduction in HUVEC viability was seen when concentrations of imatinib were used in the 50 – 150μM range (Figure 4.4A). Gover-Proaktor et al. (2017) compared the effect of imatinib to that of ponatinib, another TKI, on HUVECs in another study and found that beyond a given concentration, imatinib did affect HUVEC cell viability; at 8μM, imatinib did not have an impact, but at 20μM, imatinib decreased cell viability. Oertel et al. (2006) studied

the combined effects of imatinib and radiation on human carcinoma (A431) and glioblastoma (U87) cells. They also tested imatinib and radiation combined and individually on HUVECs to test their antiangiogenic effects and found that HUVEC cell viability was reduced by 2μM imatinib alone, without radiation, and IC50 was reached at around 7μM [352]. Haguet et al. (2020) showed that 5μM imatinib did not induce HUVEC apoptosis but had an influence as early as 24 hours after treatment and inhibited proliferation after 72 hours [353]. This was reported as an increase in lactate dehydrogenase (LDH) release, which indicates cell damage [353,354]. Since PDGF is known to be responsible for cell repair in damaged cells, its inhibition can augment cell damage, possibly explaining the decrease in cell viability in our study and others [352]. Vallières et al. (2009) investigated the effect of imatinib mesylate on endothelial cells using HUVECs [355]. They showed that at a concentration up to 3.7μM, the drug did not affect proliferation. From 11.1μM, they saw a decrease and finally showed a complete reduction to nearly 0% cell viability using 33.3μM, which they attributed to toxicity. They also speculated that the lack of effect in endothelial cells could be potentially due to the additional inhibition of inhibitory tyrosine kinases in the cells [355].

The imatinib-loaded NPs led to a slight reduction in cell viability, which was not as significant as the free imatinib (Figure 4.4A). Free imatinib is administered to the cells in one immediate dose rather than being released cumulatively over time by the NPs. The NPs dosage is chosen based on the drug cumulative release and therefore the amount cumulatively released will sit within the free imatinib range of concentrations given in Figure 4.4A. However, the amount of imatinib released from the NPs over time do not reach a toxic concentration to the cells due to its controlled release.

The observations from the literature supported the conclusion that the imatinib concentrations used in Figure 4.4A led to cell damage and, in the higher concentration may have, led to direct cell toxicity rather than an inhibition of proliferation It is important to note that the cell viability measurements in these experiments reflect the number of cells present in comparison to untreated wells and therefore show the net effects of both cell proliferation and cell death in the respective well.

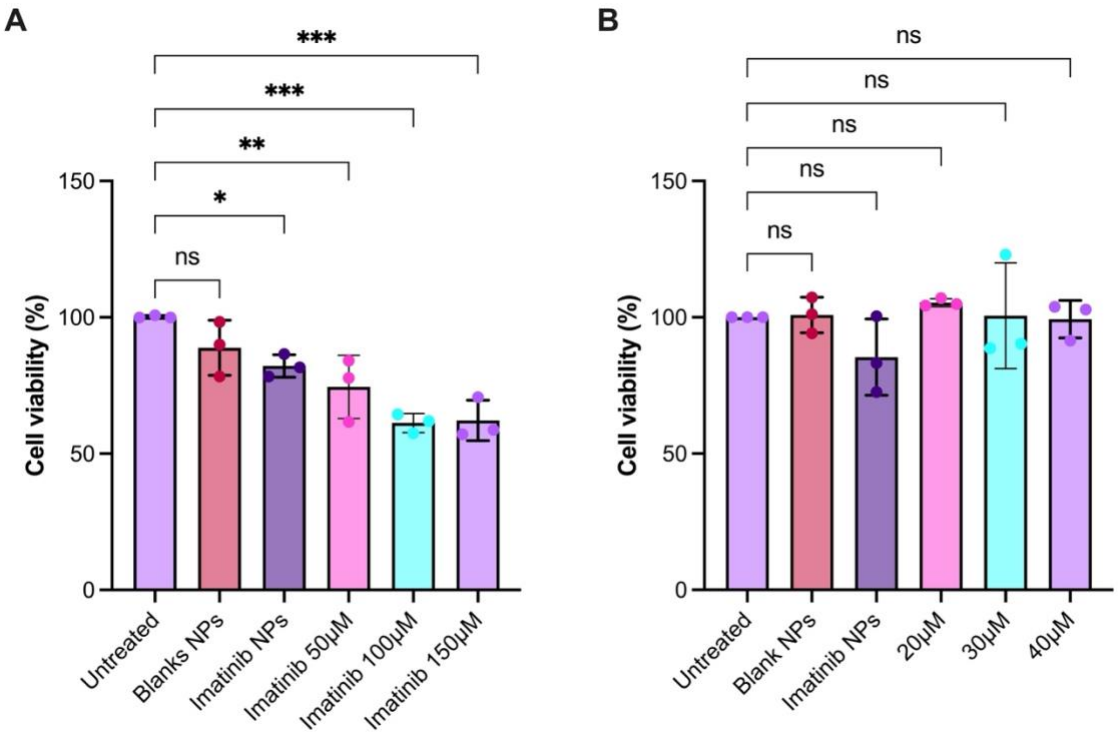

Figure 4.4. HUVEC viability, as a percentage of untreated control, was investigated via MTT assay 72 hours after treatment with blank and 1mg/mL imatinib-loaded NPs and free imatinib A. with less than 100% confluence B. with 100% cell confluence. Data are expressed as the mean +/- s.e. mean of 3 independent experiments, carried out in duplicates (*P < 0.05, **P < 0.01, ***P < 0.001; data analysed by one-way ANOVA followed by Dunnett's post hoc test).

Therefore, the concentrations were decreased to 20μM, 30μM, 40μM for imatinib, in alignment with the results of the dose-finding experiment (data not shown), and 0.1mg/ml for NPs in the subsequent experiment. The confluence was also increased to 100% to create a complete monolayer of endothelial cells, allowing the formation of tight junctions between the cells, and mimicking the in-vivo endothelium more closely [356]. Also, because proliferation of HUVECs should be minimal once cultures are confluent it is easier to detect any directly toxic effects of drug treatments on the cells.

Figure 4.4B shows that by allowing formation of a complete monolayer and decreasing the drug concentration, imatinib did not affect HUVEC cell viability, as expected from the literature. In PAH, the endothelial dysfunction creates an abnormally hyperpermeable barrier preceding development of pulmonary hypertension [357]. Sugita et al. (1983) showed that endothelial permeability increased within the first week following monocrotaline treatment in rats, two weeks before right ventricular hypertrophy developed [116]. Inflammatory stimulation of the endothelial monolayer

increases its permeability, and imatinib has also been shown to prevent this effect through the suppression of the Abl kinases [117]. We have not studied these effects here but such changes in disease models support the approach of using complete monolayers of endothelial cells to study the effects of potential treatments for PAH.

The present findings suggest that imatinib, free or encapsulated, does not affect endothelial cells at lower concentrations and when the endothelial cells form a complete monolayer.

4.3.2. Effect of imatinib-loaded NPs on pulmonary artery smooth muscle cells (HPASMCs)

4.3.2.1. Effect of confluence and imatinib concentration on HPASMC cell viability

Following on from the HUVEC experiments, the effect of imatinib's concentration and confluence were tested on HPASMCs 72 hours after treatment. Cell-to-cell contact controls the proliferative response via contact inhibition, where cell growth stops when cells reach confluence [358]. The effect of cell confluence on the response of PASMC was studied when a high and low concentration of imatinib was introduced. When treated with low imatinib concentration, as shown in Figure 4.5A, and the blank NPs, the 60% confluence led to more variable measurements of cell viability. When the cells reached 100% confluence, as shown in Figure 4.5B, the cells maintained comparable viability throughout the treatments.

Cell confluence is a valuable parameter to determine the cellular growth phase [359]; therefore, testing the cell viability at a confluence of 60% allows for the cells to be in a logarithmic state of growth when treated, which provides a good indication of the effect of treatment on growing cells. Still, the concentration was not high enough to show any reduction in cell viability 72 hours after treatment, and it is likely that the cells would have grown and "recovered" from any effect of PDGFR inhibition over this timeframe. However, when the confluence reached 100%, and a low concentration of imatinib was applied, as shown in Figure 4.5B, the cells were less likely to be proliferating. The low concentrations of imatinib did not impact on cell viability in either of the confluence conditions. The imatinib-loaded NPs did however reduce cell viability, which may be due to the sustained release of imatinib from the NPs maintaining a proliferation inhibition. The blank NPs showed no effect.

On the other hand, the high imatinib concentrations caused a decrease in cell viability of 100% confluent cells, using 100 and 150μM, which can indicate cytotoxicity as opposed to the inhibition of proliferation or promotion of apoptosis. For instance, Sancho-Martínez et al. (2011) observed that beyond "pronecrotic" drug concentrations, cisplatin, another chemotherapy agent, would activate other signalling pathways and cause additional cell injury, resulting in cell death without going through

any apoptosis programme or mitochondrial injury [360]. This decrease could also be attributed to the high cell density. Indeed, the cells might already experience cell injury due to the high drug concentration, and the high cell density further exacerbates the injury by insufficient nutrient supply to the cells and metabolic by-product accumulation, ultimately contributing to their necrosis [361]. Due to the rapid proliferation of PASMCs, a time course was necessary to assess their proliferation at certain time points and when treated with high imatinib concentration, to optimise the conditions for measurement of the effects of imatinib-loaded NPs..

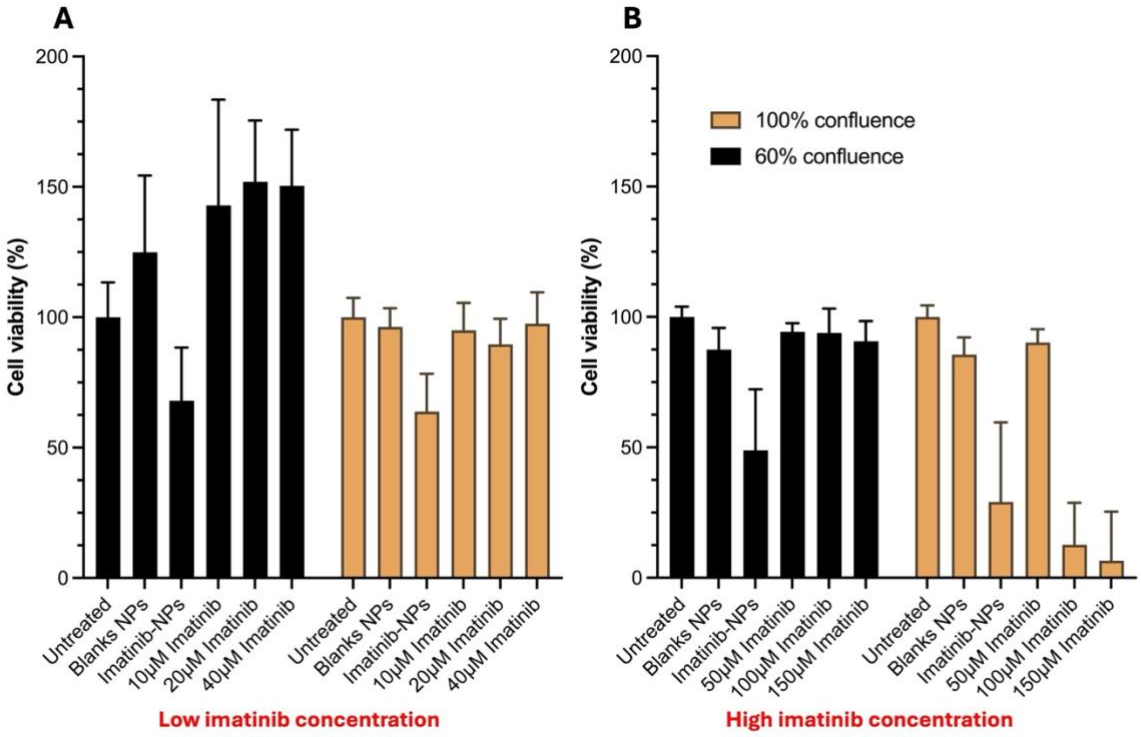

Figure 4.5. Effect of A. low and B. high imatinib concentration and cell confluency on HPASMC viability 72hrs after treatment. Data are expressed as the mean of a single experiment +/- s.d. of 8 measurements.

4.3.2.2. HPASMC viability time course after imatinib treatment

Figure 4.6 shows the result of the time course experiment, in which cell viability was tested 4, 8, 12, 24, 48, and 72 hours after PASMCs were treated with an increasing concentration of imatinib. Imatinib started to affect cell viability 8 hours after treatment and maintained the inhibition until 24 hours after treatment when cell growth recovered from the inhibition. After 72 hours, the highest concentration of imatinib reduced cell viability, likely indicating cell toxicity rather than inhibition of proliferation.

Cell viability also seemed to be more variable after 24 hours, which suggests that the cells were in a logarithmic state of growth. From this experiment, it was decided to discard the 72-hour timepoint as the cell density would be too high. The imatinib concentrations were lowered as well to avoid drug toxicity since no changes were observed at the 4-hour timepoint, and the effects were first seen at the 8-hour timepoint and maintained at the 12-hour timepoint; the next time course tested the NPs, both blank and loaded, at 8, 24 and 48 hours after treatment. Additionally, imatinib-loaded NPs led to a decrease in cell viability 72 hours post-treatment in Figure 4.5. However, this measure of cell viability was performed 72 hours post-treatment, and it would be interesting to see if the drug-loaded NPs could still inhibit cell proliferation during the cells' logarithmic phase of growth.

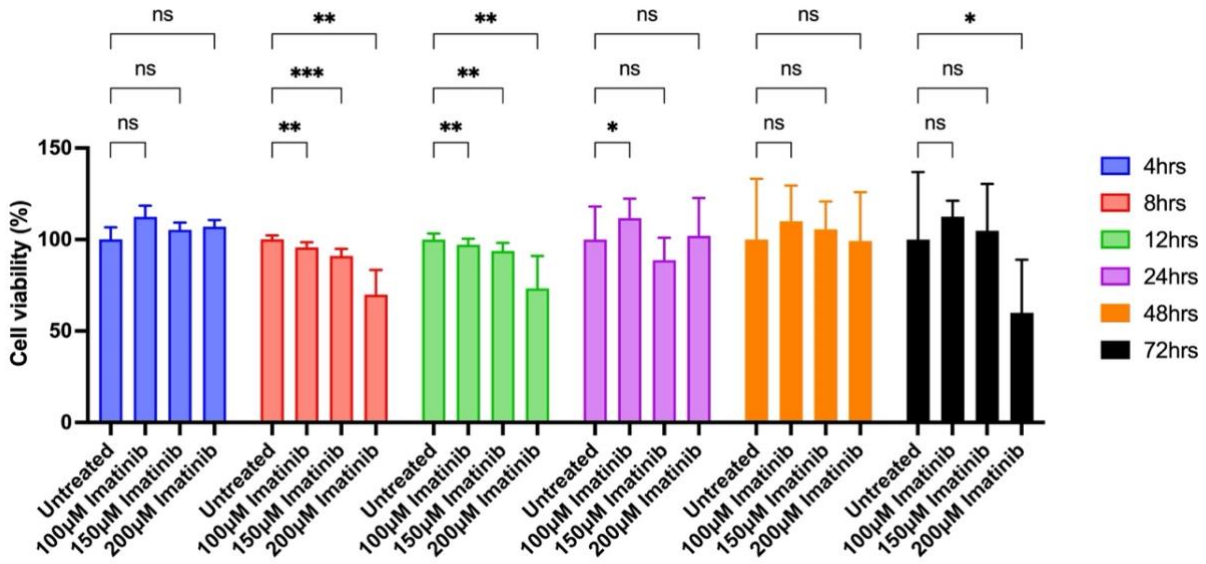

Figure 4.6. Time course of HPASMC viability, as a percentage of untreated control, when treated with a range of imatinib concentrations. Data are expressed as the mean of a single experiment +/- s.d. of 8 measurements (*P < 0.05, **P < 0.01, ***P < 0.001; data analysed by two-way ANOVA followed by Dunett's post hoc test).

Figure 4.7 shows HPASMC viability 8, 24 and 48 hours after introducing blank and imatinib-loaded NPs and a lower range of imatinib concentrations. Free imatinib concentrations did not affect cell viability until 48 hours after treatment, with the highest concentration (150μM) only reducing the cell viability to 70% of control. As expected, the blank NPs showed similar cell viability to the untreated cells, while the imatinib-loaded NPs gradually decreased cell viability 24 hours after treatment onwards.

Various studies have shown imatinib's ability to inhibit smooth muscle cell proliferation. Vallières et al. (2009), mentioned earlier for finding no effect on HUVECs, also investigated imatinib mesylate's capacity to inhibit smooth muscle cell proliferation to address restenosis following surgical intervention. They reported the same inhibition on vascular and aortic smooth muscle cells as the concentration of imatinib increases with a reduction to less than 20% cell viability with 33.3μM, which they confirmed as being due to necrosis [355]. Rocha et al. (2007) also demonstrated that HUVECs were not affected by imatinib but showed that the drug reduced smooth muscle cell viability by downregulating the expression of the PDGF-α receptors and inducing apoptosis,

which in turn prevents cell proliferation, survival and migration [111]. This study indicates the sustained release of imatinib from the NPs, enabling consistent cell viability reduction over time.

In contrast, the cells treated with free drug recovered from the inhibition faster than the drug-loaded NPs. Indeed, Marslin et al. (2015) encapsulated imatinib in PLGA NPs and tested their effect on breast cancer cell viability, finding that the drug-loaded NPs led to a higher cytotoxicity than the free drug [8]. Akagi et al. (2015) also tested imatinib-loaded PLGA NPs and their effect on HPASMCs for treating PAH. They specifically measured differences in proliferation as opposed to cell viability, following the addition of the mitogen PDGF. The study did not test the drug-loaded NPs on non-stimulated HPASMCs; however, even when stimulated, a reduction in cell proliferation is shown when treating the cells with the drug-loaded NPs [10]. This latter study prompted the following part of this work, where the NPs were tested on HPASMCs stimulated by the PDGF mitogen.

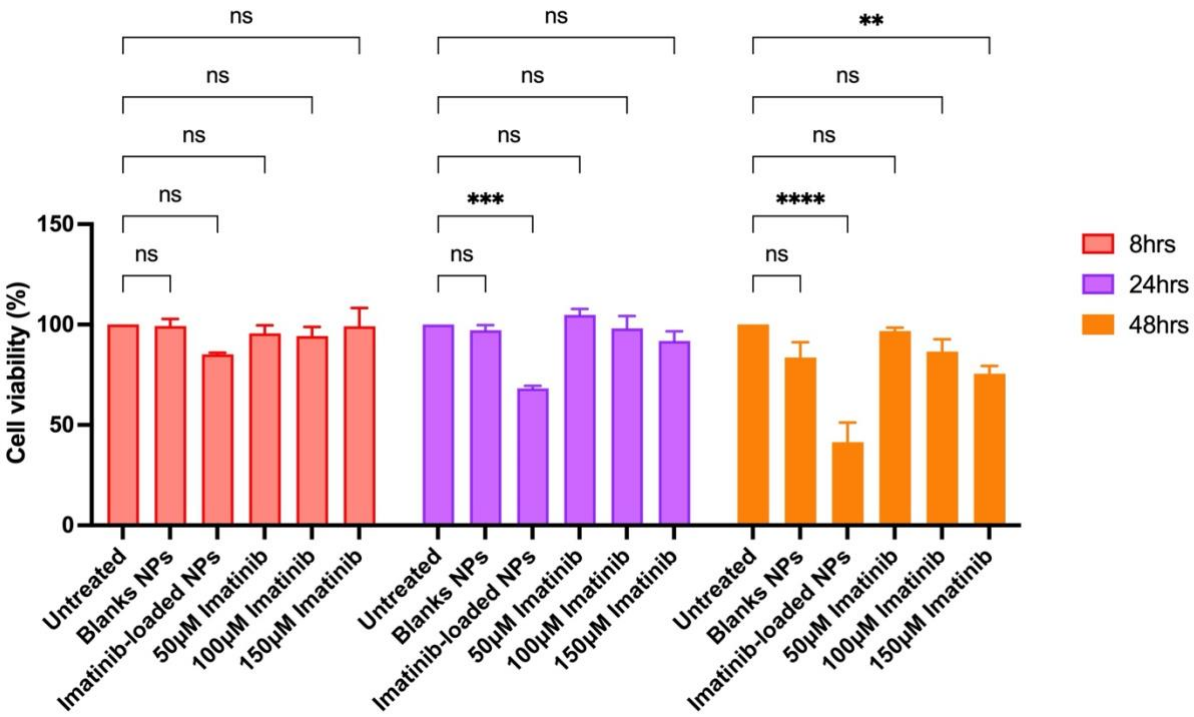

Figure 4.7. Time course of HPASMC viability as a percentage of untreated control, when treated with blank and imatinib-loaded NPs and free imatinib. Data are expressed as the mean +/- s.e. mean of 4 independent experiments (*P < 0.05, **P < 0.01, ***P < 0.001; data analysed by two-way ANOVA followed by Dunett's post hoc test).

4.3.3. Effect of imatinib-loaded NPs on pulmonary artery smooth muscle cells (HPASMCs) following stimulation via mitogen (PDGF-BB)

This study investigated two main aspects in parallel: it first worked towards establishing a baseline for the stimulation of the untreated cells. It also addressed the effect of the NPs (loaded and blank) and the impact of the free imatinib on the cells, with and without stimulation.

The first introduction of the mitogen, optimisation 0, did not yield a significant difference in cell viability compared with the untreated cells, as shown in Figure 4.8 A and B for 24 and 48 hours. The first optimisation aimed to adjust the imatinib concentration and reintroduce the blank NPs; therefore, this optimisation had no impact on the untreated cells, and the cell viability remained the same with or without stimulation at both time points. This could indicate that within 24 hours, the non-stimulated cells proliferated rapidly enough to converge with the stimulated cells in terms of the number of viable cells present at the time of MTT assay.

In an attempt to see the effect of the mitogen on the untreated cells in their logarithmic growth phase, optimisation 2 investigated the effect of the cells being seeded, treated and stimulated simultaneously. The hypothesis was that PDGF would encourage further proliferation over the non-stimulated cells during their initial growth. The mean cell viability of the stimulated cells at 24 hours was not significantly higher than that of the non-stimulated cells (Figure 4.8A) and no further changes in cell viability were observed at the 48-hour time point in Figure 4.8B.

The complete medium used in this study already included two other growth factors: epidermal growth factor (EGF) and fibroblast growth factor (FGF). The latter growth factors and PDGF all stimulate vascular smooth muscle cell proliferation [362]. Adding the mitogen led to little to no further effect on the cell viability, indicating that the other growth factors were likely sufficient to induce proliferation, and the other two growth factors could therefore have masked PDGF's known effect. Nilsson et al. (1985) have shown that arterial smooth muscle cells produce PDGF and could maintain growth without external growth factors [363], which suggests that the non-stimulated cells may

already have been producing PDGF. Since receptors for PDGF can saturate beyond a particular concentration, additional PDGF might not affect the proliferation further [364].

The subsequent optimisation was to introduce a low-serum medium at the time of the treatment and stimulation. This optimisation was made after considering the complete media composition. The complete medium was replaced with a low-serum medium, supplemented with 10-times less serum than a standard complete medium. The study by Akagi et al. (2015) and Li et al. (2006) also switched to low-serum media, 1% and 0.5%, respectively, before treating vascular SMCs with PDGF and imatinib [10,346]. Rocha et al. (2007) also showed that PDGF stimulates human aortic smooth muscle cell proliferation when using a serum-free medium [111]. This optimisation 3, shown in Figure 4.8A, led to a significantly increased cell viability at the 24-hour timepoint compared to non-stimulated. The increase in cell viability when stimulated is the expected effect of the mitogen PDGF, which has been reported by other studies stimulating vascular smooth muscle cells using PDGF [10,72,346]. This increased cell growth is no longer demonstrated at the 48-hour time point, which could indicate that the stimulated cells were confluent enough to be contact-inhibited, and the non-stimulated cells had proliferated sufficiently to converge in number with the stimulated cells.

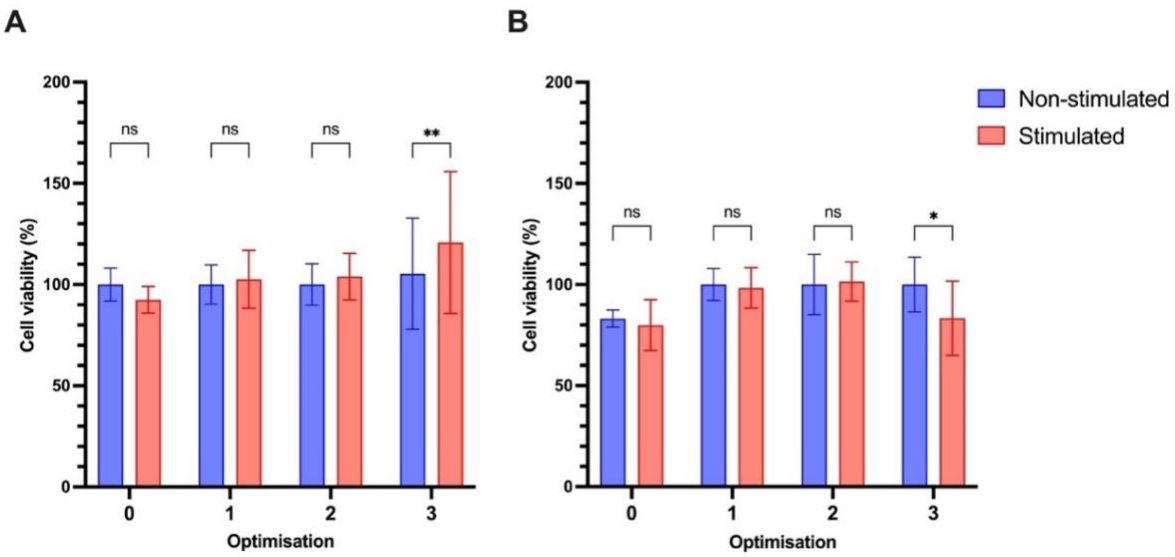

Figure 4.8. Untreated HPASMC viability, as a percentage of untreated control, was measured via MTT assay A. 24 hours and B. 48 hours following stimulation using the mitogen PDGF. Optimisation 0 and 1 marked the introduction of the mitogen, the same way for the untreated cells; Optimisation 2 seeded the cells and treated/stimulated them simultaneously, and Optimisation 3 used a low serum medium during the stimulation/treatment stage. Data are expressed as the mean of a single experiment +/- s.d. of 8 measurements (*P < 0.05, **P < 0.01, ***P < 0.001; data analysed by two-way ANOVA followed by Sidak's post hoc test).

The optimisations were used to observe the effects of the stimulation and various treatments on the HPASMC cell viability, as shown in Figure 4.9 to Figure 4.12. Blank NPs , resulted in similar cell viability to untreated cells, stimulated and not stimulated, in all optimisations except when using low-serum media, where cell viability decreased slightly to an average of 65% of control (non-significant) at the 48-hour time point, as shown in Figure 4.12B.

Free imatinib treatment only seems to affect the cell viability when HPASMC are stimulated. A possible explanation would be that stimulation by PDGF was mainly responsible for the proliferation of the cells, which imatinib significantly inhibited in Figure 4.9. The non-stimulated cells treated with imatinib could have proliferated due to other growth factors that did not rely on the PDGF pathway and, therefore, were not impacted by its inhibition. However, no studies posited competition between the growth factors or any indication that PDGF could dominate the proliferation of vascular smooth muscle cells. However, Hwang et al. (1992) showed that PDGF caused an 8-fold increased proliferation compared to the 6-fold increase that EGF as the growth factor caused in porcine aortic smooth muscle cells in culture [365]. Consistent results were demonstrated in cultured human gliomas in a study by Westphal et al. (1988), where PDGF led to a higher number of cells per culture than EGF and FGF [366]. Interestingly, Rocha et al. (2007) and Nakamura et al. (2012) also showed that imatinib decreased cell viability to the same level regardless of the stimulation [72,111].

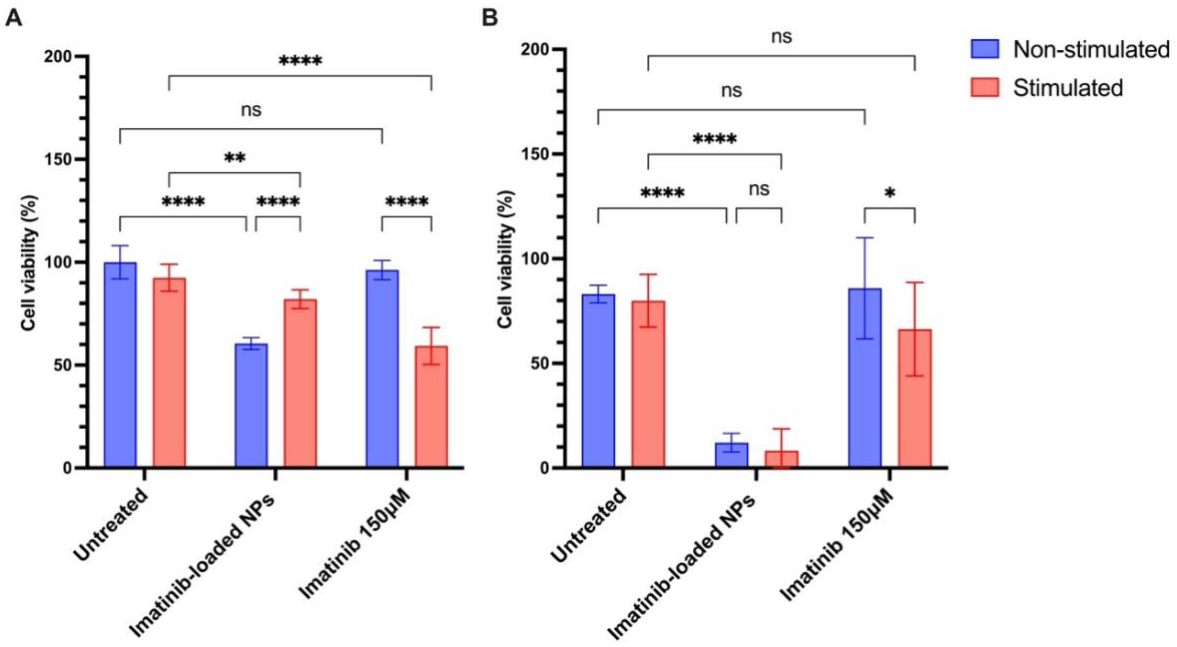

Figure 4.9. HPASMC viability, as a percentage of untreated control, was measured after treatment with imatinib-loaded NPs and free 150μM imatinib, with and without PDGF stimulation, via MTT assay A. 24 hours and B. 48 hours after treatment. Data are expressed as the mean of a single experiment +/- s.d. of 8 measurements (*P < 0.05, **P < 0.01, ***P < 0.001; data analysed by two-way ANOVA followed by Sidak's post hoc test).

Nevertheless, cell viability was further lowered following imatinib treatment when cells were stimulated with PDGF in both studies, consistent with the results in Figure 4.9 and Figure 4.10. When the cells were seeded and treated simultaneously, at the 24-hour time point in Figure 4.11A, the effect of the stimulation was seen on the imatinib-treated cells, suggesting that the lower concentration of imatinib used could have been insufficient to impact cell behaviour. The effect of the mitogen was not however sustained at the 48-hour timepoint. In all optimisations, treatment with free imatinib had a low effect on cell viability and was inconsistent when cells were stimulated.

This inconsistency was observed also when using the highest imatinib concentration attainable within the drug solubility in optimisation 2 (Figure 4.10). Indeed, the free base imatinib is used in our study, which limits its solubility and imatinib mesylate is mainly used in other studies as the salt version increases its solubility [367]. The free base imatinib was encapsulated in part to address its mentioned low solubility and to allow a higher concentration to be sustainably released over time. As noted, imatinib

mesylate is used in most studies; these studies show the same reduction in cell viability or proliferation when cells are treated with imatinib-loaded NPs or imatinib alone. However, when encapsulated, Imatinib mesylate impacts the drug release and its encapsulation as the drug becomes more soluble in water, as shown in Ramazani et al. (2015) [11]. They showed that encapsulating imatinib mesylate reduces the microparticle loading efficiency compared to free base imatinib, due to the drug's improved water solubility [11]. The present study shows that by using a salt-free version of imatinib, the encapsulation of imatinib is possible, bypassing the solubility issue and maintaining a higher efficacy in cell-based assays than the free drug.

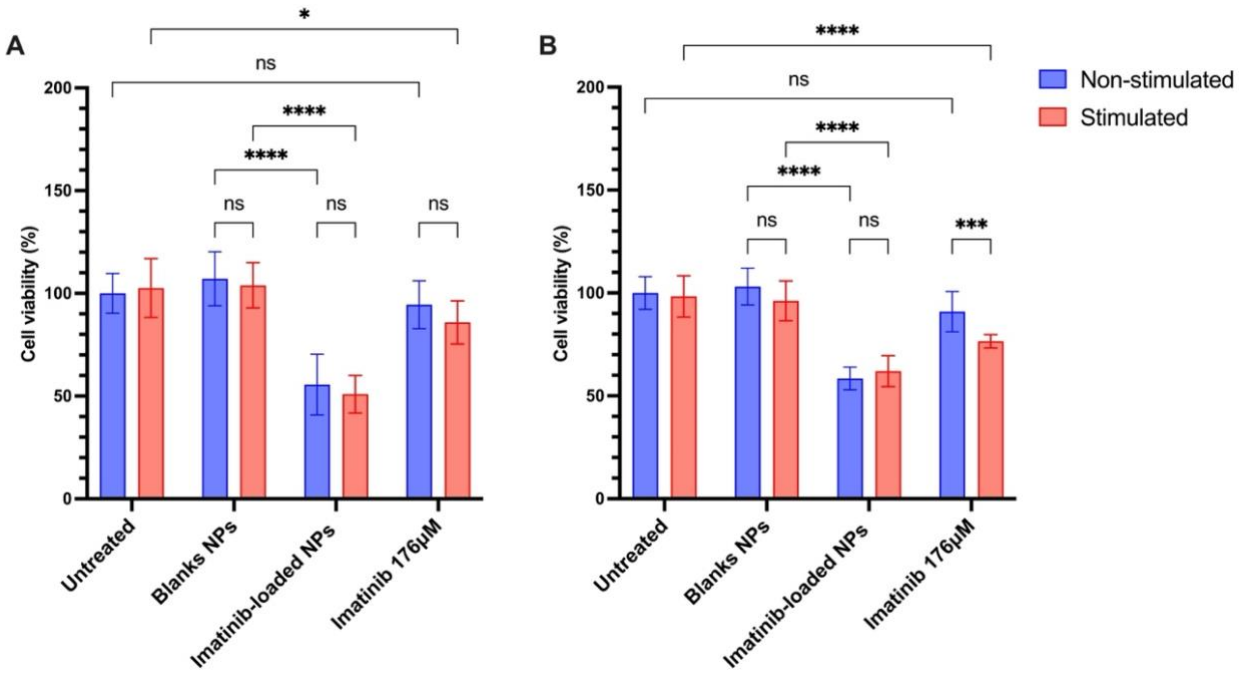

Figure 4.10. HPASMC viability, as a percentage of untreated control, was measured after treatment with blank, imatinib-loaded NPs and free 176μM imatinib, with and without PDGF stimulation, via MTT assay A. 24 hours and B. 48 hours after treatment. Data are expressed as the mean of a single experiment +/- s.d. of 8 measurements (*P < 0.05, **P < 0.01, ***P < 0.001; data analysed by two-way ANOVA followed by Sidak's post hoc test).

At optimisation 0, imatinib-loaded NPs at 24 hours led to a higher decrease in cell viability in the non-stimulated cells than the stimulated ones, as shown in Figure 4.9. This indicates that the amount of imatinib released at 24 hours was not enough to reduce cell viability when stimulated. This explanation is consistent with the cell viability seen at 24 hours in optimisation 2, when the cells were seeded and treated simultaneously (Figure 4.11). Within 24 hours, the amount of imatinib, on average 86μM, expected to be released through the burst release was not effective enough to affect the cells in their logarithmic growth phase, while the antiproliferative effect was seen once the amount of imatinib cumulatively released at 150μM had been cumulatively released in 48 hours, as shown in Figure 4.11B.

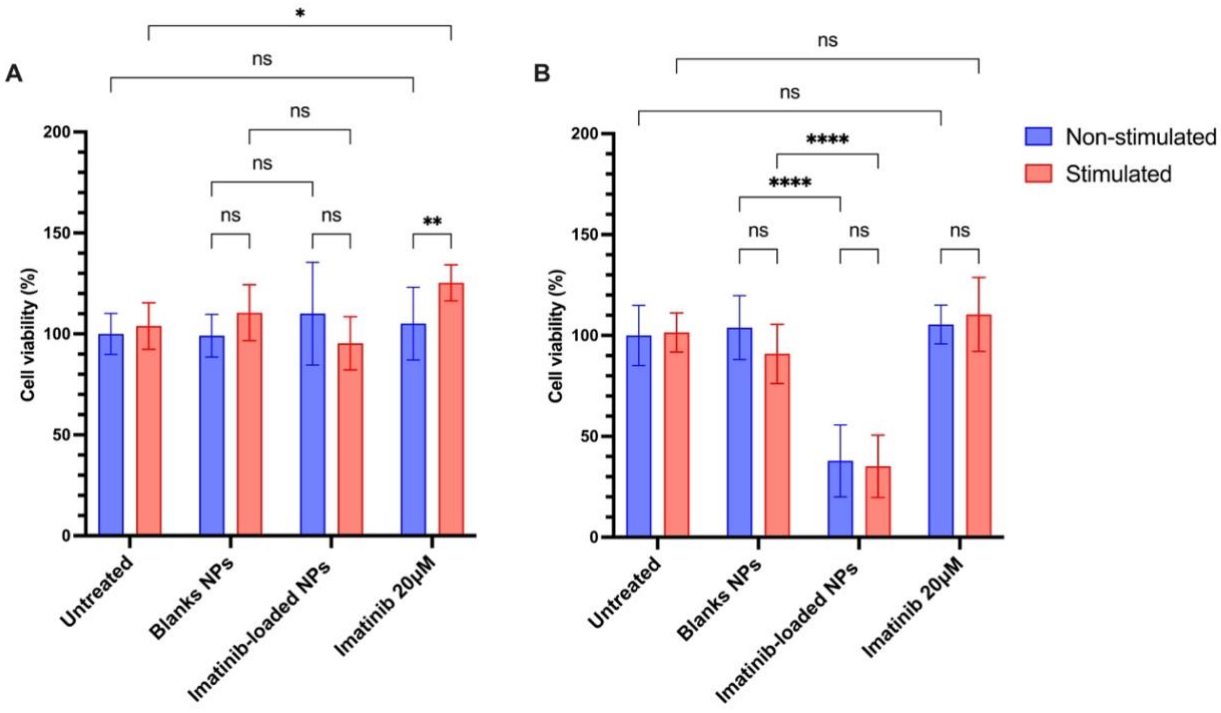

Figure 4.11. HPASMC viability, as a percentage of untreated control, was measured after seeding and treatment at the same time with blank, imatinib-loaded NPs and free 20μM imatinib, with and without PDGF stimulation, via MTT assay A. 24 hours and B. 48 hours after treatment. Data are expressed as the mean of a single experiment +/- s.d. of 8 measurements (*P < 0.05, **P < 0.01, ***P < 0.001; data analysed by one-way ANOVA followed by Sidak's post hoc test).

Similarly, in optimisation 3, when using a low-serum medium, the imatinib-loaded NPs led to lower cell viability; however, the results remained very variable, as shown in Figure 4.12A, resulting in no significant difference to the blank NPs, possibly due to the low-serum conditions causing inconsistent cell growth. At 48 hours, the concentration of imatinib released was high enough, as described above (150μM), to reduce cell viability significantly in both stimulation conditions, as shown in Figure 4.12B.

The drug-loaded NPs have shown a consistently high effect on HPASMC cell viability with or without stimulation in all optimisation conditions, especially at the 48-hour time point. This consistent effect can be attributed to the sustained release of imatinib, since the blank NPs did not affect the cell viability. Similar effects of imatinib-loaded NPs have been reported in the Akagi et al. (2015) study, which compared the inhibitory effect of imatinib-loaded PLGA NPs and free imatinib on PASMCs from PAH patients and showed that they were comparable. When the free drug or NPs were removed, cell proliferation was restored in the free-drug-treated cells; however, the inhibitory effect was maintained in the NP-treated cells.

Although the present results are promising in establishing a stimulated baseline, further optimisation is required to establish a reproducible effect of the mitogen on the untreated cells. This can include optimising the cell density and the mitogen concentration, but mostly the timing of the experiments. Indeed, earlier time points, before 24 hours, and additional time points between 24 and 48 hours, could be tested to obtain a more precise time-course of the effects of the mitogen and imatinib on the cells, which have been shown to replicate rapidly even in the low-serum medium. The timing of the stimulation with the natural growth of the cells, along with the release of the drug from the NPs, has been demonstrated to be a challenge to accommodate in terms of optimising an experimental model for NP validation and remains a study that needs to be further optimised.

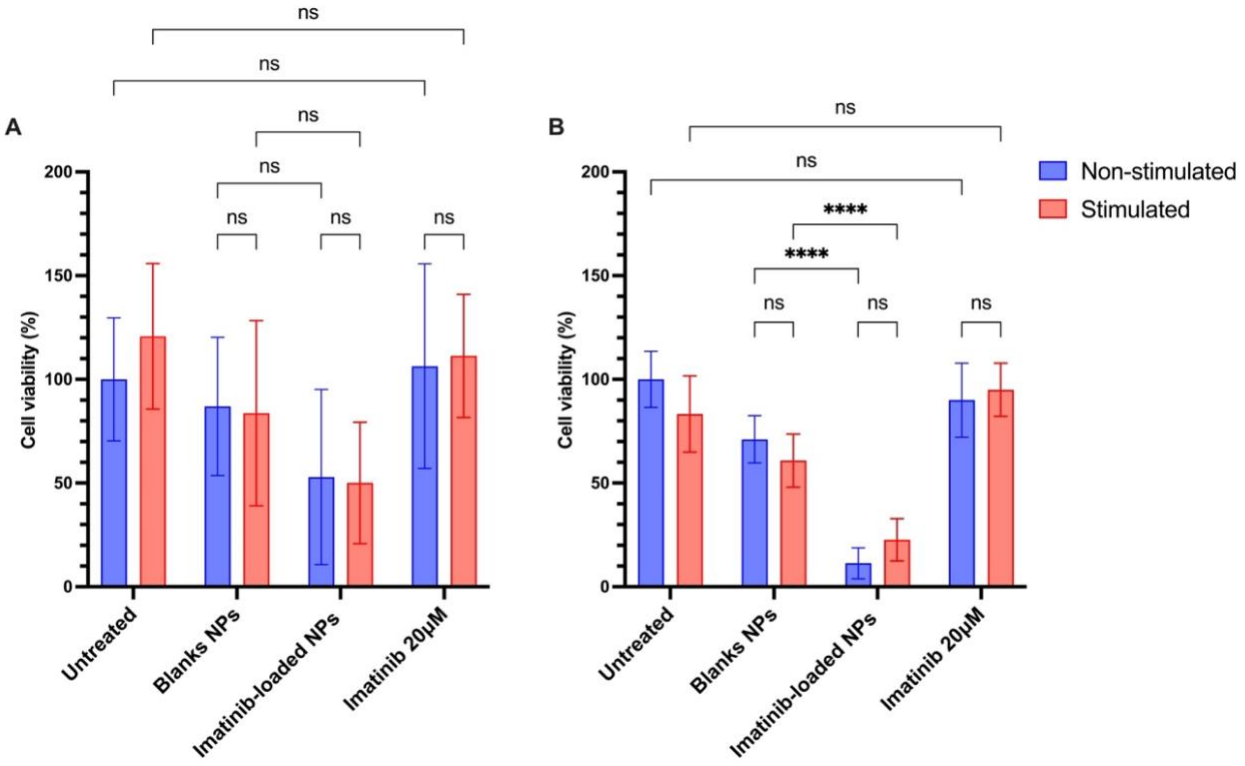

Figure 4.12. HPASMC viability, as a percentage of untreated control, was measured after treatment in low-serum media with blank, imatinib-loaded NPs and free 20μM imatinib, with and without PDGF stimulation, via MTT assay A. 24 hours and B. 48 hours after treatment. Data are expressed as the mean of a single experiment +/- s.d. of 8 measurements (*P < 0.05, **P < 0.01, ***P < 0.001; data analysed by two-way ANOVA followed by Sidak's post hoc test).

It is particularly important to note that the measured end-point in this study was cell viability, which was measured indirectly via mitochondrial activity in the MTT assay. This method only indirectly provides information about cell proliferation, although it does also allow inferences to be made regarding direct cytotoxicity of treatments. A more direct method to display the effect of the NPs on cell proliferation would be to use assays investigating DNA incorporation to quantify DNA synthesis. Another limitation of the study is the artificial aspect of studying individual cell populations in culture. In-vivo testing, on the other hand, can provide a continuous and more accurate representation of clinical results.

The Akagi et al. (2015) study also demonstrated the halt of PAH progression using imatinib-loaded NPs in an MCT model in vivo. The imatinib-loaded NPs led to a significant decrease in right ventricular systolic pressure and hypertrophy. The NPs also reduced the percentage of fully muscularised small pulmonary arteries by nearly half compared to the control [10]. Since it has been established that the imatinib released from the NPs produced in our study led to a decrease in cell viability, which is not seen in the blank NPs, the results are promising for the potential production of NPs for suppressing the development of PAH.

4.4. Conclusion

This study has demonstrated the effect of imatinib-loaded NPs on vascular cells, which includes endothelial cells and stimulated and non-stimulated pulmonary arterial smooth muscle cells. Imatinib and imatinib-loaded NPs have been shown to have concentration and confluence-dependent effects on both cell types. Indeed, imatinib and, hence, imatinib-loaded NPs were not expected to impact upon endothelial cell viability. In this study, it was found that imatinib had no effect on cell viability when the cells formed a complete monolayer and were treated with the drug below a toxic concentration. The literature supported these findings, where the drug was reportedly toxic to endothelial cells beyond a specific concentration.

Imatinib-loaded NPs showed the expected effect on pulmonary arterial smooth muscle cells, where cell viability was consistently decreased. The rapid growth rate of the HPASMCs required a few optimisations in the experiments designed to test the effects of free-imatinib and the imatinib-loaded NPs. This was particularly important when looking at the cell viability following stimulation by PDGF and how the NPs would affect it. Throughout the optimisation performed to obtain a stimulation baseline, the imatinib-loaded NPs led to a consistent reduction in cell viability and showed how the NPs also helped bypass the poor solubility of the drug being encapsulated.

Chapter 5. Quantifying antibody conjugation to PLGA nanoparticles via carbodiimide conjugation

5.1. Introduction

PLGA-based drug delivery systems (DDS) have shown their potential to offer a more localised delivery of their load, improved solubility and bioavailability, reduced side effects, and controlled sustained drug release [5]. To achieve a localised impact, the delivery of the load cannot rely on the EPR effect and requires its active delivery to the relevant cells [15]. Indeed, active targeting is more relevant in dictating the intracellular trafficking and the intracellular destination of the NPs to affect the overall therapeutic outcome [17].

The targeted delivery of treatments to the lungs has been widely examined for various lung disorders, such as lung cancer or cystic fibrosis, however, actively targeting the pulmonary vasculature for the treatment has remained relatively understudied[368]. Nonetheless, a couple of studies have investigated pulmonary vasculature-expressed or overexpressed molecules in PAH and targeted them to actively deliver PAH treatments in nanosystems. For instance, Song et al. (2016) have shown that the expression of E-selectin, a membrane protein, was upregulated by hypoxia in pulmonary arterial endothelial cells (PAECs) obtained from calf lungs [369]. Li et al. (2024) then conjugated sialic acid, a natural ligand, on their chitosan-based micelle to target E-selectin and deliver ambrisentan to human PAECs and was tested in hypoxic rats [370]. The peptide CARSKNKDC (CAR) has been shown to accumulate in PAH animal models in all layers of the remodelled pulmonary arteries, including the endothelial and smooth muscle cells [371]. This prompted Gupta et al. (2015) to conjugate this peptide to liposomes to deliver superoxide dismutase and fasudil for PAH [372].

Since conjugating PAH-specific agents has not been extensively studied, and not at all for their conjugation to PLGA NPs, the alternative was to investigate agents targeting the lungs or blood vessels more generally. Danilov et al. (2001) performed a biodistribution study investigating the antibody uptake capability in organs using radiolabelled antibodies. It was found that monoclonal antibodies targeting the antigen angiotensin-converting enzyme (ACE) and the intracellular adhesion molecule 1 (ICAM-1) had the highest uptake and selectivity in the lungs with anti-ACE retaining the most even after systemic injection [373]. Shenoy et al. (2011) have studied

angiotensin converting enzyme 2 (ACE2) as a therapeutic target for PAH and have reported its expression on vascular endothelium and smooth muscle cells [374]. Integrin α9, a heterodimeric transmembrane receptor, has also emerged as a potential target found to be overexpressed on vascular smooth muscle cells [375].

Targeting vascular endothelial growth factors (VEGF) using antibodies was also investigated, as they are overexpressed in severe PH [376]. Bevacizumab, an anti-VEGF-A monoclonal antibody, is currently used to treat several cancers, including cervical, metastatic colorectal, glioblastoma, and ovarian, by blocking the interaction between the growth factor and its receptors. Indeed, activating VEGF receptors activates a downstream signalling pathway of survival, leading to endothelial cell proliferation and angiogenesis [377]. Its expression also increases significantly during ischemia, hypoxia, and inflammation, which induces the formation of dysfunctional blood vessels. This makes the antibody relevant as a targeting and therapeutic agent [165,378].

Interestingly, studies have reported that the administration of bevacizumab is associated with the development of hypoxia-induced PH, establishing the concept of the angiogenesis paradox [379–381]. However, bevacizumab was used in the present study as a model antibody that is readily available and well-characterised, as any selected ligand with an amine group, such as bevacizumab, can be conjugated using the method described.

Indeed, the chemical structure of PLGA, specifically its carboxyl end groups, allows the NP's surfaces to be functionalised to improve its targeting. The EDC/NHS crosslinkers facilitate the covalent binding by first activating PLGA on its carboxylic group by attaching NHS. An amide bond is created between the reactive ester of the PLGA (NHS-PLGA NPs) and the antibody amine group on its variable region, as shown in Figure 5.1.

This study aimed to produce anti-VEGF antibody bevacizumab-conjugated PLGA nanoparticles. They were produced using the one-step electrospraying technique and conjugated via carbodiimide. A study on the conjugation's methods of quantification was subsequently established. The NPs were produced via electrospraying following F1, as its higher flow rate leads to a higher yield. This chapter will discuss the

optimisation of the protocol. It will also investigate methods used to confirm the first step of the conjugation protocol, which is the activation. The resulting activated and conjugated NPs were characterised by measuring their surface charge and obtaining their FTIR spectrum. Consequently, the activation of the PLGA NPs (NHS-PLGA NPs) was confirmed.

This chapter will finally consider the various methods used to verify the success of conjugation. This will provide critical insight into the methods reported by the literature and the results expected from a successful conjugation, such as recognising the amide bond-specific peaks in the ^{1}H-NMR and FTIR spectrum. A secondary antibody was also used to confirm conjugation indirectly. Finally, protein concentration assays were tested to quantify bevacizumab concentration on the surface of the NPs, to more conclusively establish the conjugation of bevacizumab to PLGA NPs.

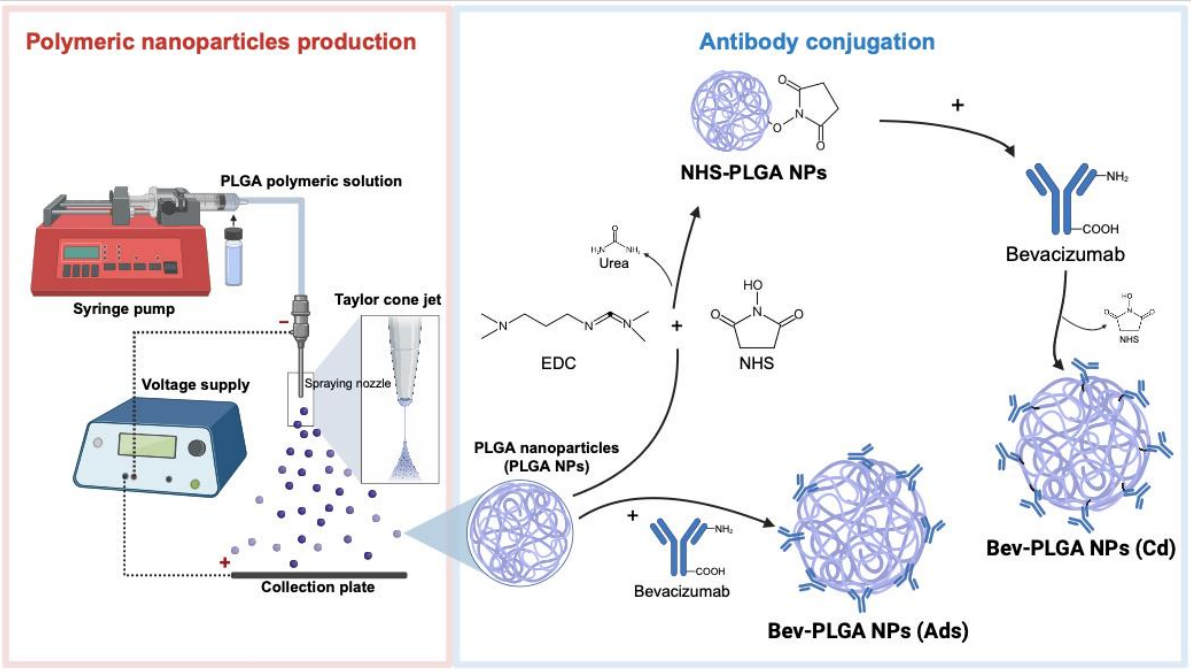

Figure 5.1. Nanoparticle production via electrospraying and antibody conjugation through carbodiimide chemistry to PLGA NPs (Bev-PLGA NPs (Cd)) and through antibody adsorption to PLGA NPs (Bev-PLGA NPs (Ads)). Image created using ChirysDraw and Biorender and adapted from [162].

5.2. Methodology

5.2.1. Carbodiimide conjugation of bevacizumab to PLGA NPs

The PLGA NPs used in this study were manufactured through electrospraying, as described in section 2.2.4.1, using the parameters established for F1 and an acid-terminated PLGA. The carbodiimide protocol was optimised. The final optimised protocol suspends 5mg of PLGA NPs in 5mL 0.5M MES (pH 5.4) with 20mg of EDC and 2mg of NHS, and the NPs were shaken and incubated at room temperature (RT) for 90 minutes. The suspension was then washed thrice with MES to remove the unreacted reagents via centrifugation (Sigma Centrifuge 3-16KL) at 4ºC, 10000rpm for 20 minutes each cycle. The NPs were resuspended in deionised water (pH 8.8), and 4µL (equivalent to 0.1mg of antibody) bevacizumab was added to the suspension for a final antibody concentration of 20µg/mL. The same volume of deionised water was added to another set of samples to serve as a control: the activated NPs. The samples were then incubated at 4ºC overnight, washed thrice to remove unbound antibodies via centrifugation at 4ºC, 10000rpm for 15 minutes each cycle, and resuspended in deionised water (pH 8.8). This procedure was performed in duplicate for both activated (NHS-PLGA NPs) and conjugated NPs (Bev-PLGA NPs), and unreacted NPs (PLGA NPs) were also tested.

The adsorption method was also tested and only quantified using ELISA to compare the adsorption method (Bev-PLGA NPs (Ads)) to the carbodiimide method (Bev-PLGA NPs (Cd)). To generate adsorbed NPs, 5mg of unreacted PLGA NPs were suspended in 5mL of deionised water (pH 8.8) and directly incubated overnight at 4ºC with 4µL of bevacizumab alongside the Bev-PLGA (Cd) NPs conjugated. This procedure was performed in triplicates for both activated (NHS-PLGA NPs), conjugated NPs (Bev-PLGA (Cd) NPs), adsorbed NPs (Bev-PLGA NPs (Ads)), and unreacted NPs (PLGA NPs) were also tested. A summary of the reagent used to prepare each sample can be found in Table 5.1.

Reagents	**Unreacted NPs** (PLGA NPs)	**Activated NPs** (NHS-PLGA NPs)	**Conjugated NPs** (Bev-PLGA (Cd) NPs)	**Adsorbed NPs** (Bev-PLGA (Ads) NPs)	**Moles (mmoles)**
PLGA NPs (17 kg/mol)	5mg	5mg	5mg	5mg	0.0014
EDC (191.7 g/mol)	-	20mg	20mg	-	0.104
NHS (115.05 g/mol)	-	2mg	2mg	-	0.017
Antibody (149 kg/mol)	-	-	4µL (equivalent to 0.1mg)	4µL (equivalent to 0.1mg)	6.71×10^{-4}

Table 5.1. Reagents used to prepare each sample with their respective moles. PLGA NPs moles were calculated based on the PLGA mass found in 5mg of NPs. (PLGA concentration was 2%wt, 5mg of NPs was produced using approximately 1.2mL polymeric solution which is equivalent to 24mg of PLGA).

5.2.1. Bicinchoninic acid assay (BCA) reliability test

The resulting Bev-PLGA NPs and the control NHS-PLGA NPs were tested using the BCA assay, as described in the BCA assay section 2.2.4.2 and each conjugation reagent, EDC and NHS, was tested for interference with the BCA assay. In addition, to check the dependence of BCA assay on the concentration of the compounds (PLGA, NHS and EDC), various concentrations of PLGA NPs ranging from 1 to 5mg were tested. This was followed by increasing the concentrations of NHS and EDC, ranging from 0.2 to 2mg/ml and 6.7 to 67mg/ml, respectively. The mixture was left to incubate for 30 minutes at 37ºC for the reaction. After the Cu^{+}+BCA Complex or purple complex was formed, the generated optical density (OD) was read on a SpectraMax absorbance plate reader at the wavelength of 562nm [286]. The corresponding protein concentration was then found using a calibration curve created by using albumin standards.

5.2.2. Further methods to quantify antibody conjugation

5.2.2.1. Zeta-potential

Various other methods were investigated to confirm conjugation and attempt to quantify it. The zeta potential (mV) of samples (PLGA NPs, NHS-PLGA NPs, and Bev-PLGA NPs) were measured using a Nano Zetasizer (Malvern Panalytical), and each sample already resuspended in deionised water (pH 8.8) was run in triplicate.

5.2.2.2. Fourier transform infrared (FTIR) spectroscopy.

Fourier transform infrared (FTIR) spectroscopy (PerkinElmer Spectrum 100 FT-IR) was also performed to confirm conjugation. The background scan and the sample scan consisted of 8 scan times. A range of antibody concentrations (1µL, 2µL, 4µL) was tested and added before incubation overnight. For this approach, the samples were lyophilised using the Buchi Lyovapor L-300, then dispersed on the crystal light path and compressed to obtain respective spectra in the wavelength region of 4000 to 650cm^{-1}.

5.2.2.3. *Proton Nuclear magnetic resonance (^{1}H-NMR) spectrometry*

The lyophilised samples were also analysed using ^{1}H-NMR through Bruker Avance Neo 400 MHz NMR spectrometer, as described in 2.2.4.2, using $CDCl_3$ as the deuterated solvent.

5.2.2.4. *Secondary antibody – Alexa Fluor 488*

Following the conjugation protocol, PLGA NPs, NHS-PLGA NPs and Bev-PLGA NPs were incubated with 2µL of AlexaFluor488 for 2 hours at 4ºC. the samples were washed twice at 15,000 rpm for 15 minutes to remove any excess secondary antibodies and redispersed in deionised water (pH 8.8). The NPs were then analysed using flow cytometry described in 2.2.4.2 to detect the secondary antibody-generated fluorescence. The fluorescence intensity was displayed as a histogram. As a control, activated NPs were also analysed, and an overlap histogram was generated, as depicted in Figure 5.2.

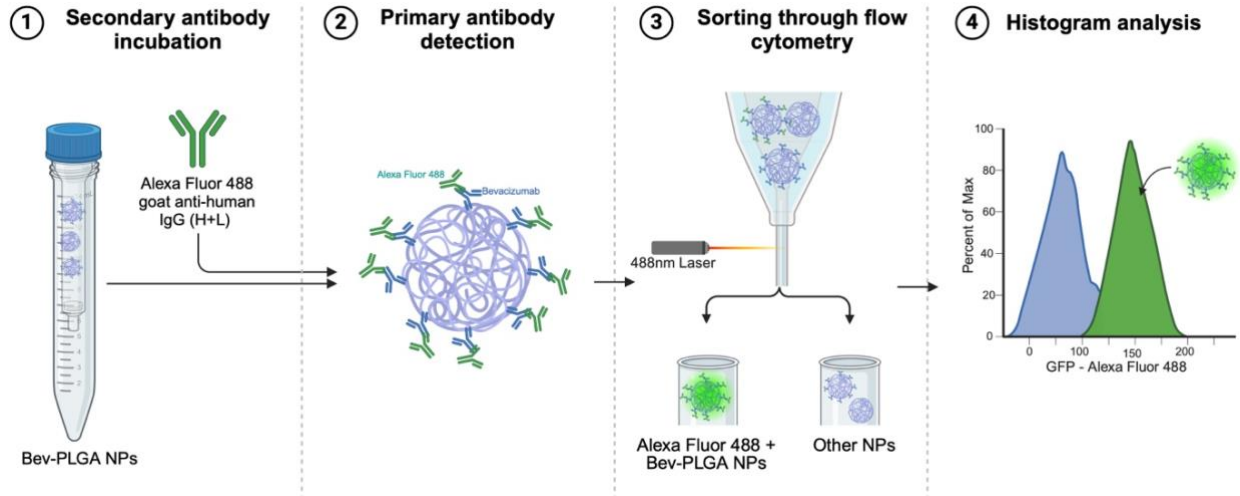

Figure 5.2. Schematic of the secondary antibody experiment.

5.2.3. Bevacizumab Sandwich ELISA Kit

The bevacizumab concentration from the adsorbed NPs Bev-PLGA NPs (Ads) and Bev-PLGA (Cd) NPs was measured using the ELISA kit, as described in 2.2.4. The bevacizumab concentration in samples was determined from a calibration curve created using bevacizumab standards.

5.2.3.1. ELISA calibration curve

The ELISA kit analysed known antibody concentrations (0-25,000ng/mL), used as standards for determining the bevacizumab concentration. The measured absorbance fitted a four-parameter logistic (4PL) regression curve shown in Figure 5.3 to obtain the 4PL model Equation 5.1 below.

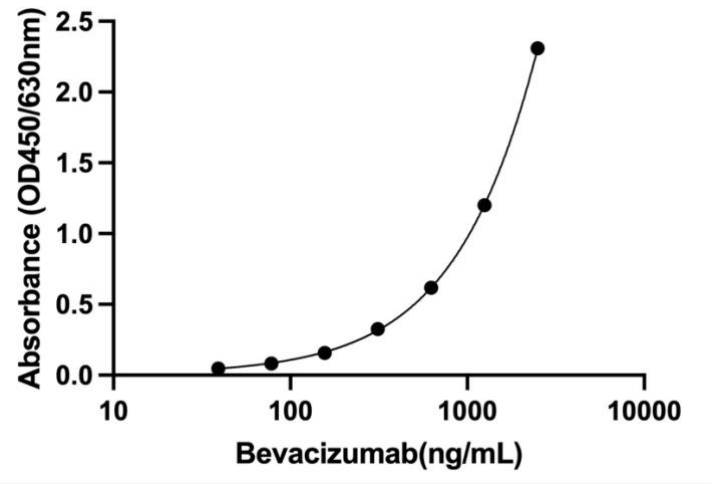

Figure 5.3. Bevacizumab standards in a four-parameter logistic (4PL) regression curve.

$$OD = \frac{a - d}{\left[1 + \left(\frac{Conc}{c}\right)^{b}\right]} + d$$

Equation 5.1. Four parameter (4PL) logistic regression model, where OD = optical density, Conc = antibody concentration, a = minimum value, b = Hill's curve slope, c = concentration at an inflexion point, and d = maximum value.

5.3. Results and Discussion

5.3.1. Optimisation of the conjugation protocol

The protocol optimisation was performed through a literature search of research articles mentioning the carbodiimide conjugation method for PLGA or other carboxylic-based polymers. The research expanded to antibody conjugates and specifically the cross-linkers EDC/NHS. The optimisation steps are summarised in Table 5.2.

The first protocol introduced by Liu et al. (2019) conjugated bevacizumab to PLGA and served as the starting point of the protocol optimisation [165]. In the subsequent optimisation, the reagents were halved to reduce the amount of PLGA NPs needed. The temperature of the washing of the particles was maintained at 4ºC. Xia et al. (2013) found that an increase in temperature decreases the activation efficiency of EDC and NHS [382].

In the third optimisation, the activation media was moved from HCl to MES, increasing the pH from 3 to 5, and this activation media was kept to wash the NPs following the incubation of the reagents. Increasing the pH ensured that PLGA would hydrolyse slower as a low pH increases the hydrolysis speed of PLGA [5]. MES also replaced HCl as its zwitterionic nature can stabilise pH-sensitive reactions by accepting or donating protons [269]. The usage of MES was confirmed by a study by Sehgal et al. (1994), stating that PBS is incompatible with the stability of the EDC acylurea intermediate [383]. Another study by Cammarata et al. (2015) compared the effect of four different buffers on the EDC cross-linking reaction with gelatine and found that MES was the most favourable [384].

Sehgal et al. (1994) also showed that a ratio of 5:1 of EDC to NHS leads to a high coupling efficiency with no significant changes beyond this ratio. This led to an increase in EDC in optimisation 4, making a molar ratio of 6:1 (EDC:NHS). The acid-terminated form of PLGA was also introduced in this optimisation since the EDC/NHS requires the carboxylic group for its activation, and using a carboxylic-rich type of PLGA would increase the reaction efficiency. Moura et al. (2014) have reported using acid-terminated PLGA to conjugate anti-CD64 antibodies to PLGA NPs [167].

The pH for the antibody incubation was also changed to deionised water at pH 8.76, which was seen in a study by Banstola et al. (2020) conjugating panitumumab to PLGA NPs, whereby a pH of 8.5 was used to suspend their antibodies and PLGA NPs. East et al. (2011) looked at quantum dots-antibody conjugates and the variables involved in the carbodiimide coupling and observed that the best conjugation occurred at pH 10.8 [385].

The incubation time for the activation was also reduced to 1.5 hours since a higher temperature speeds reaction time, and the reaction temperature was at room temperature [382]. This observation was confirmed by Srinivasan et al. (2014), who used a 30-minute reaction time for their PLGA activation at room temperature [177]. Finally, centrifugal concentrators with the antibody molecular weight were introduced to ensure the same amount of NPs were retrieved after each wash and to ensure unbound antibodies were not left in the suspension. The antibody concentration was reduced after optimisation 2 to conserve material while establishing a reliable method to confirm the conjugation.

Optimisation	1 [165]	2 [165,382]	3 [173,383]	4 [163,167,382]	5 [164,177,382]	6
PLGA quantity	10mg	5mg	5mg	5mg	5mg	5mg
Type of PLGA	PLGA	PLGA	PLGA	PLGA-A	PLGA-A	PLGA-A
EDC quantity	20mg	10mg	10mg	20mg	20mg	20mg
NHS quantity	5mg	2.5mg	2.5mg	2mg	2mg	2mg
Type and pH of buffer	HCl	HCl	MES	MES	MES	MES
Buffer pH	3	3	5	6	6	6
Incubation time	4 hours				1hrs 30min	
Temperature of incubation	RT					
Washing temperature and speed	RT– 15 minutes	4ºC – 15 minutes				
Activation Washing buffer	PBS	PBS	MES	MES	MES	MES
Washing speed	10 000rpm					
MWCO Filter used	n/a	n/a	n/a	n/a	30kDa	300kDa
Type of buffer	PBS	PBS	MES	dH2O	dH2O	dH2O

Conjugation washing buffer	PBS	PBS	MES	dH2O	dH2O	dH2O
Buffer pH	7.4	7.4	6	7.4	8.76	8.76
Antibody concentration	5mg/mL	0.1mg/mL				0.05, 0.1, 0.2mg/mL
Antibody quantity	24µL	2µL				1µL, 2µL, 4µL
Antibody incubation time	Overnight					
Antibody incubation temperature	4ºC					
Washing temperature and speed	RT – 20 minutes	4ºC – 20 minutes				
Washing speed	10 000rpm					

Table 5.2. Carbodiimide conjugation protocol optimisation.

5.3.2. Physicochemical characterisation

5.3.2.1. Confirmation of activation of PLGA NPs (NHS-PLGA NPs)

As previously stated, physical-chemical characterisation, such as using zeta potential, can be used to investigate how changes on the surface of the NPs can affect the NP's surface electric charge. The decoration of the NPs, whether by NHS through activation or bevacizumab by conjugation, leads to structural changes to the surface of the NPs.

These changes can be observed in the change in zeta potential. Figure 5.4A displays how the surface charge changes from the unreacted stage (PLGA NPs) to the activated stage (NHS-PLGA NPs) and the conjugated stage (Bev-PLGA NPs). PLGA NPs show a zeta potential of -18.35 ± 0.12mV, which increases to -13.93 ± 0.61mV following its activation by the attachment of NHS to the NPs. The acid-terminated PLGA frequently used for PLGA functionalisation is rich in carboxylic groups, which explains the negative surface charge of the unreacted NPs [386]. The conjugation of bevacizumab to the NHS-PLGA NPs also increased the zeta potential to -15.86 ± 0.70mV from the unreacted PLGA NPs.

The increase in zeta potential in both NHS-PLGA NPs and Bev-PLGA NPs is consistent with the reports from the literature. Moura et al. (2014) characterised the conjugation of anti-CD64 to PLGA NPs [167]. They found that the zeta potential increased following conjugation and credited it to the depletion and shielding of the negatively charged carboxylic group of the PLGA during the binding of the antibody [167]. These findings confirmed those of another study by Manoochehri et al. (2013), that observed the same increase in zeta potential following the conjugation of human serum albumin to PLGA NPs due to the involvement of the negatively charged carboxylic group in the conjugation [170].

In another study by Zumaya et al. (2022), the zeta potential was measured and compared between PLGA and PEG-conjugated PLGA NPs [169]. They attributed the slight increase in the conjugated NP zeta potential to the functional group present on the surface, which was the presence of amine groups in the PEGylated PLGA [169]. Therefore, the changes in the zeta potential confirmed the modification of the PLGA terminal group by activating the NPs with the EDC/NHS crosslinkers and suggested

the successful conjugation of bevacizumab. Measurement of the zeta potential has not been widely used in studies to verify conjugation, as the parameter is primarily used to predict particle stability, establishing it as a supplementary method rather than a primary source for confirmation of antibody conjugation [387].

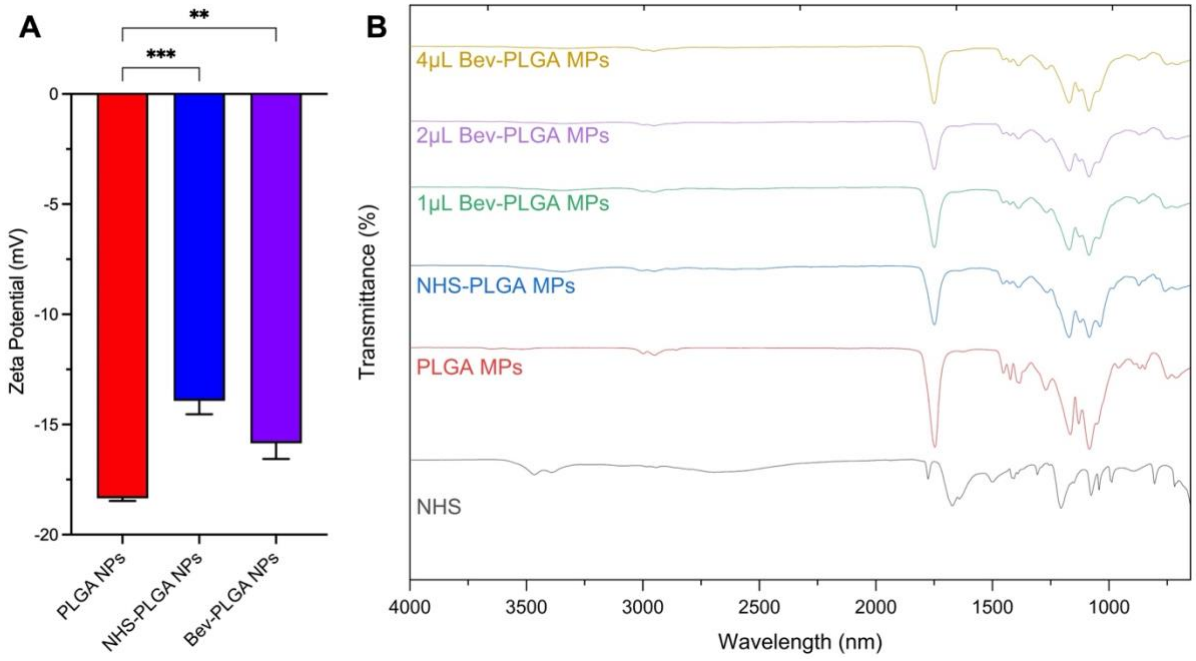

Figure 5.4. A. Zeta potential of unreacted NPs (PLGA NPs) activated NPs (NHS-PLGA NPs) and conjugated NPs (Bev-PLGA NPs). Data are expressed as mean +/- s.e. mean of 3 independent experiments (*P < 0.05, **P < 0.01, ***P < 0.001; data analysed by one-way ANOVA followed by Tukey post hoc test). B. FTIR spectrum confirming the activation of the PLGA NPs and showing conjugation spectra as antibody concentration increases.

FTIR was investigated to obtain information about the samples' chemical fingerprints, such as functional groups, which would confirm the surface modification of the NPs by the EDC/NHS crosslinkers [276]. Indeed, FTIR detects molecular vibrational energy after exposing the sample to infrared light. The sample absorbs the light and jumps to an excited vibrational state. The vibration frequencies of the bonds between the atoms create absorption peaks identifying the various functional groups.

Figure 5.4B compares the FTIR spectra from PLGA NPs, NHS and NHS-PLGA NPs, the activated form of PLGA. The strong peaks at 1086 cm^{-1} and 1750 cm^{-1} in the PLGA NPs spectrum indicate a C-O-C and C=O stretching, respectively [312]. NHS characteristics peaks consist of the 3464 cm^{-1} representing the N-OH stretching

vibration, two peaks at 1774 cm^{-1} and 1672 cm^{-1} representing the stretching vibration of the dicarbonyl C=O and the peak at 1204 cm^{-1} showing the stretching vibration of C-N [388]. The activation was confirmed as the NHS characteristic peak of the N-H stretching vibration is seen in NHS-PLGA NPs at 3341cm^{-1}.

A study by Khan et al. (2016) showed consistent results in creating PEG-PLGA conjugates using the EDC and NHS crosslinkers to improve the anticancer drug bendamustine delivery stability [153]. They showed the activation of PLGA into NHS-PLGA via FTIR and showed the same presence of N-H at 3446cm^{-1}. Another similar study by Tuyen Dao et al. (2014) used PLGA-PEG to deliver the antioxidant curcumin to prolong circulation time. It showed the same N-H peak at 3457cm^{-1} [154].

Confirming the activation of the PLGA NPs is the first step in functionalising various agents on the NPs via carbodiimide. The secondary amide group (O=C-N-H) created by the antibody conjugation to PLGA is expected to generate a peak at around 3300 to 3400cm^{-1}, representing the N-H group characteristic peak from the amide group [181]. The FTIR results in Figure 5.4.B do not show this characteristic peak even with the increase in antibody concentration and, therefore, could not confirm conjugation. Khan et al. (2016) conjugated PEG to improve the stability of the drug delivery from PLGA NPs and the same characteristic peak of N-H at 3446.2cm^{-1}. They attributed the N-H peak to the amide group (O=C-N-H), showing successful conjugation, rather than the N-H from the NHS group from the activation of the NPs [153]. However, this same N-H characteristic peak can also be observed in NHS-PLGA NPs generated by the NHS molecule, as demonstrated in our study.

Therefore, this characteristic peak cannot conclusively demonstrate successful conjugation, as the peak could originate from either the NHS molecule from the activated NPs or the amide group from the conjugated NPs. Amide compounds were also reported to absorb at 1660 cm^{-1} with a strong intensity [389]. Khan et al. (2019) conjugated the chemotherapy drug doxorubicin to PLGA to improve its PLGA entrapment using carbodiimide [178]. They reported that the amide bond created between PLGA and doxorubicin by the conjugation was seen at 1641.33 cm^{-1} [178]. Nevertheless, studies from Manoochehri et al. (2013) and Jahan & Haddadi (2015) presented a successful conjugation through the range of absorption peaks at 1600 to

1650cm^{-1}, whilst they attributed their peak to different functional groups. Indeed, characteristic peaks around this region have been reported to possibly be from the C=O stretching or the N-H bending [390]. The study by Manoochehri et al. (2013) attributed the 1650cm^{-1} peak to the amide bond stretch N-H [170]. On the other hand, Jahan & Haddadi (2015) attributed the 1610cm^{-1} peak to C=O stretching vibration from amide-I vibration [175]. The expected strong peak around that region was not seen in Figure 5.4.B., whether it arose from the C=O stretching or the N-H bending.

However, this does not conclusively confirm the conjugation was unsuccessful as the quantity of antibody bound and, thus, the proportion of amide bond in the sample could be marginal for a signal to be observed. However, the inconsistency in the absorbance peaks confirming antibody conjugation in the literature confirms FTIR can be only used as a supplementary method to confirm configuration but cannot be relied on as a primary method to prove the conjugation of antibodies on the surface of NPs. FTIR can still be used to demonstrate the presence of the N-H stretching vibration, which can confirm activation, as seen in our results from the activated NPs with NHS.

5.3.2.2. Proton nuclear magnetic resonance (^{1}H-NMR) spectrometry

^{1}H-NMR was investigated as a means to confirm conjugation by showing the amide bond formation, similar to the rationale behind using FTIR. Since ^{1}H-NMR detects how protons react to an applied magnetic field, essential information about the protons in the molecules can provide information about functional groups present in the sample and could confirm conjugation.

The ^{1}H-NMR spectrum of pure PLGA, pure PLGA acid-terminated and electrosprayed PLGA were obtained and compared to the literature. Figure 5.5A shows the spectrum and the PLGA characteristic peaks with the protons from the methyl group (CH_3) at 1.6ppm, the methylene group (CH_2) at 4.8ppm and the methine group (CH) at 5.2ppm. The same peaks are shown in each spectrum, demonstrating that the processing of the PLGA into NPs does not affect the PLGA chemical structure obtained by ^{1}H-NMR. This result is consistent with the FTIR results shown in Chapter 3, where the pure PLGA and PLGA NPs FTIR spectra did not differ. The peaks found are consistent with the spectrum found in the literature, such as Sun et al. (2021), who showed how the intensity of the peak changed as the ratio of glycolic to lactic acid in PLGA was altered [391]. Chen et al. (2017) showed the same characteristics peak in DMSO instead of $CDCl_3$. Figure 5.5B displays how the addition of NHS or the activation of PLGA affects the ^{1}H-NMR spectrum.

The present results show two peaks between 2.75 and 3.05ppm, also seen in the conjugated spectrum in Figure 5.6. These results are consistent with studies that used NHS in their coupling reactions, as they have reported finding the NHS ester bond at around 2.5 to 3.5ppm. Song et al. (2014) double-coated their iron oxide NPs using a silica coating layered with a polymer coating [392]. The polymer coating, composed of two polymers, PEG and PLA, was synthesised using DCC/NHS crosslinkers, and the successful synthesis was verified using ^{1}H-NMR and reported the NHS peak being between 2.5 and 3ppm [392]. Bai et al. (2018) also produced chitosan-based electrosprayed MPs carrying iron oxide NPs and doxorubicin for hepatic carcinoma [393]. They conjugated hydrophobic palmitoyl groups to chitosan through EDC/NHS crosslinkers to coat and protect the MPs from pH changes due to cancer metabolites. They confirmed the conjugation through ^{1}H-NMR, reporting a chemical shift of 2.7ppm

from NHS in formic acid (as opposed to $CDCl_3$) [393]. Another study by Prainito et al. (2022) used carbodiimide chemistry to create a colorimetric biosensor to detect the COVID-19 spike protein by conjugating the anti-spike antibody to the diacetylene-based paper biosensor [394]. They reported the NHS ester bond at 2.8ppm on the ^{1}H-NMR spectrum [394].

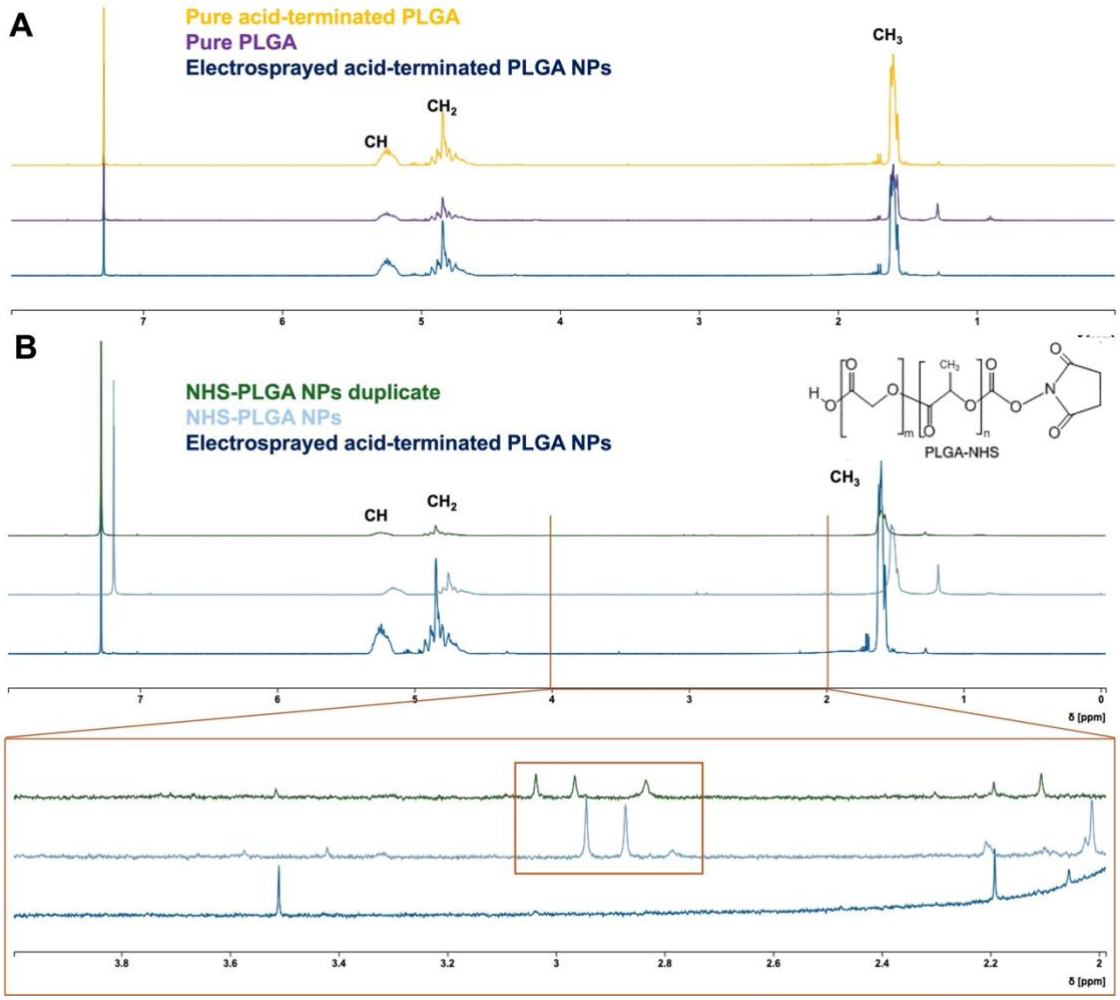

Figure 5.5. ^{1}H-NMR spectra of pure PLGA, acid-terminated PLGA and the electrosprayed acid-terminated PLGA NPs (PLGA NPs) in $CDCl_3$, B. ^{1}H-NMR spectra of lyophilised NHS-PLGA NPs in duplicates with electrosprayed acid-terminated PLGA NPs as a negative control for activation in $CDCl_3$.

A secondary amine is created when the amide bond is made through the NHS displacement. The hydrogen attached to the nitrogen of the secondary amine (R−C(=O)−NHR, where R indicates the rest of the molecule) can be detected by ^{1}H-NMR at a chemical shift between 5 to 9ppm along with a singlet since only one hydrogen is in the environment [180,182].

This has been reported by Khan et al. (2019). They confirmed the success of the conjugation via ^{1}H-NMR. They found two peaks at 7.54 and 7.70 ppm for the anthracene ring of doxorubicin but, most importantly, the evidence of an amide bond formation in a singlet at 8.24 ppm [178]. The peak within that range indicating the amide bond formation could not be found in our spectrum in Figure 5.6, even with varying antibody concentrations. While using deuterated chloroform, the hydrogen-deuterium exchange occurs, which means protons from heteroatom (non-carbon atoms) exchange with deuterium [395]. Therefore, the amide from the conjugation exchanges its proton for deuterium and can make the resonances disappear on the ^{1}H-NMR spectrum [396].

This demonstrates the need to optimise the ^{1}H-NMR method further to confirm the creation of the amide bond. For instance, the ^{1}H-NMR method can be optimised to confirm the creation of the amide bond. Other NMR methods can be explored, such as heteronuclear single quantum coherence (HSQC), also known as 2D NMR, which records ^{1}H and ^{13}C chemical shifts [397]. Heteronuclear multiple bond correlation (HMBC) can also be used, as complementary to HSQC, to further analyse the product's structure by determining proton-carbon single bond correlations or correlations separated by more than one bond [397]. Zumaya et al. (2021) used carbodiimide chemistry to create PEGylated PLGA NPs [398]. They used HMQC with both ^{1}H and ^{13}C to further confirm the amide bond formation in addition to the traditional ^{1}H-NMR spectrum [398]. These findings highlight the challenges in detecting amide bond formation using ^{1}H-NMR and the importance of exploring advanced NMR techniques such as HMBC and HMQC to confirm the bond formation.

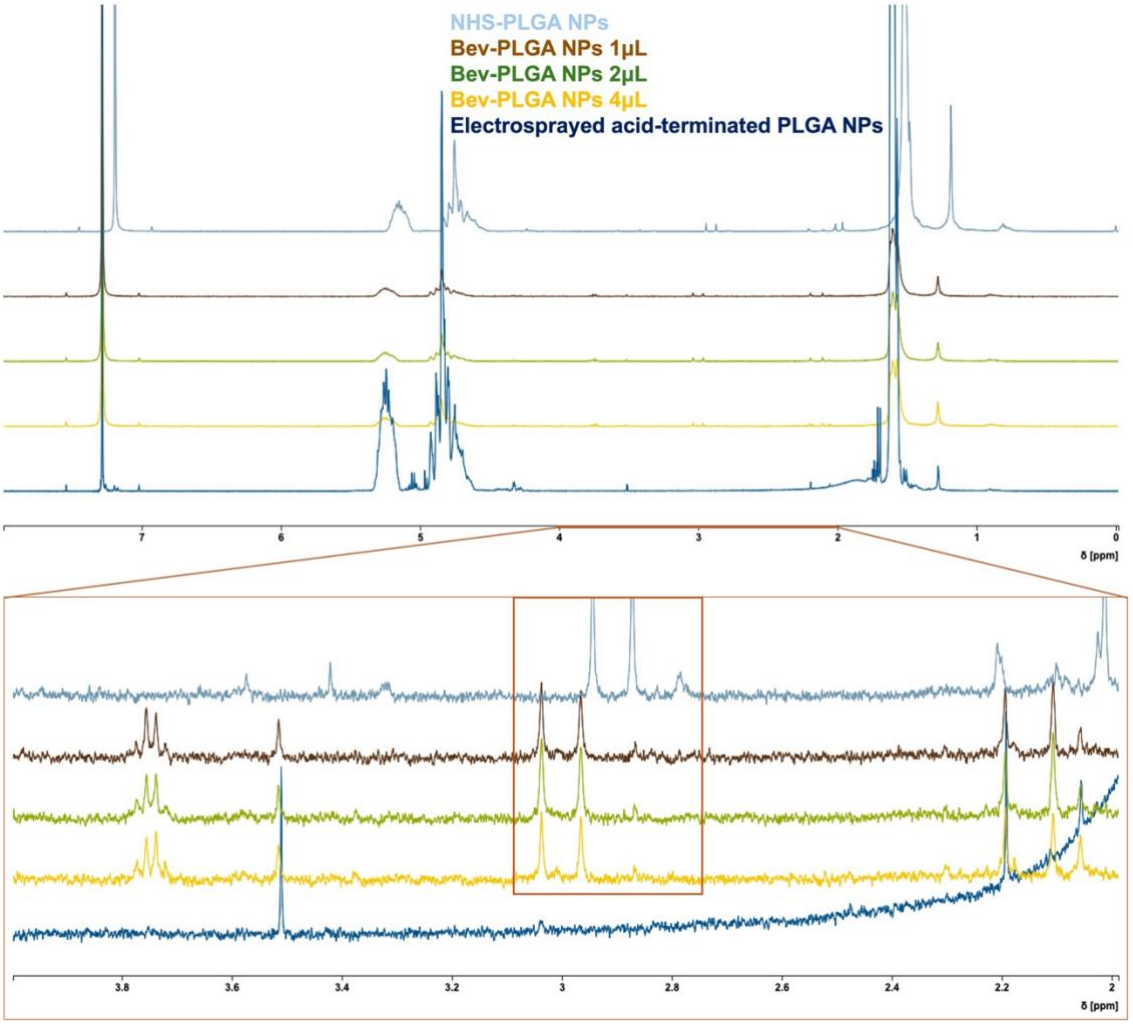

Figure 5.6. ^{1}H-NMR spectra of lyophilised Bev-PLGA NPs with a range of antibody concentrations (1µL, 2µL, 4µL) in $CDCl_3$, along with lyophilised NHS-PLGA NPs and electrosprayed acid-terminated PLGA NPs as negative controls for conjugation in $CDCl_3$.

5.3.2.3. Secondary antibody – AlexaFluor488

Fluorescence techniques such as flow cytometry and secondary antibody binding were used to indirectly prove the successful conjugation [183]. The secondary antibody's variable region binds to the primary antibody's constant region [184] and emits fluorescence when excited, which can be measured. Flow cytometry was used to sort and count individual particles when excited with a 488 nm laser to emit the fluorescence from the secondary antibody [184].

Figure 5.7 shows the flow cytometry results in a histogram form. A shift in the histogram peak towards the right indicates more fluorescence and is expected to confirm conjugation. Kocbek et al. (2007) prepared monoclonal antibodies against soluble proteins of breast cancer cells and attached a secondary antibody to them. This complex was then covalently attached to PLGA NPs, and the particles were analysed through flow cytometry. Their results showed a shift of their histogram to the right, compared to the non-coated NPs, which stayed on the left, similar to the activated NPs in Figure 5.7.A. [174]. Similar results were reported by Chen et al. (2008) when they conjugated anti-HER2 monoclonal antibody to PLGA NPs. They confirmed conjugation by labelling the antibody with fluorescein isothiocyanate (FITC), a fluorescent probe, and analysed the NPs using flow cytometry. The same shift to the right of the fluorescence histogram was reported [163].

Although a complete shift of the histogram to the right cannot be seen in this study in Figure 5.7.B. compared to the studies mentioned, a gated comparison of the right-hand side of the histogram shows that 7.5% of the signal was found to emit fluorescence in the conjugated NPs compared to a 5.3% in the activated NPs. These results show that although not all particles have emitted fluorescence, a small population of particles still emitted fluorescence, which is promising regarding optimising the experimental parameters.

For instance, the ratio between primary and secondary antibodies and the order, temperature and length of incubation can be investigated. In this study, the secondary antibody was added after the conjugation. In the other studies, the primary antibody was initially incubated with the secondary before conjugating to PLGA NPs, such as in Kocbek et al. (2007) [174]. Additionally, a study by Zhong et al. (2020) conjugated

trastuzumab (Herceptin) to PLGA NPs to deliver paclitaxel in the treatment of breast cancer. The secondary antibody and flow cytometry method were used to calculate the binding efficiency of the antibody following carbodiimide conjugation, which can also be investigated [171].

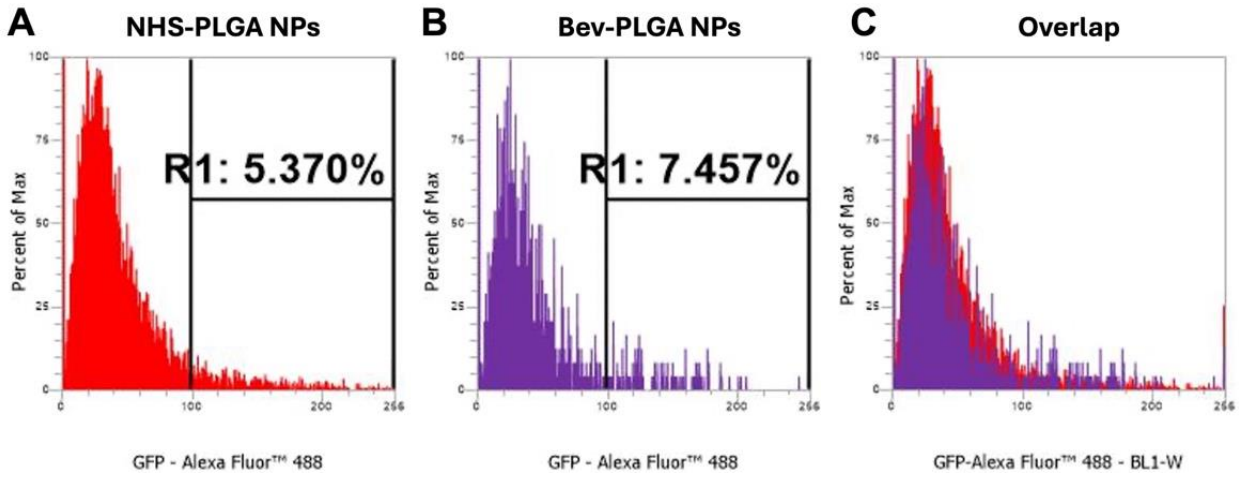

Figure 5.7. Flow cytometry analysis of A. Activated PLGA NPs (NHS-PLGA NPs),B. conjugated PLGA NPs (Bev-PLGA NPs) and C. their overlap following incubation with secondary antibody Alex Fluor 488.

5.3.3. Quantifying antibody conjugation

5.3.3.1. Bicinchoninic acid assay (BCA)

Studies have determined the success of carbodiimide conjugation to PLGA particles in various ways. To quantify the antibody conjugation to our PLGA particles in this study, the colorimetric protein detection bicinchoninic acid assay (BCA) was initially used, which relies on a chemical reaction dependent on the amino acid composition of the measured proteins.

As part of the protocol, a baseline for PLGA NPs was obtained by measuring the optical density of newly electrosprayed blank PLGA NPs. Expected optical density was recorded from the blank NPs, which translated to recording protein content in blank NPs. These results prompted the analysis of the different reagents used in the conjugation protocol using the BCA assay for possible interference.

Figure 5.8 shows plots of optical intensity versus the concentration of compounds and reagents tested. Here, we aimed to identify the interference of 3 compounds, PLGA, EDC and NHS, with the BCA quantification methods. The plots show that the optical density intensifies as the concentration of the reagents used (EDC (R^2=0.99), NHS (R^2=0.98), and PLGA NPs (R^2=0.99)) is increased, establishing a linearity between the concentration and the optical density inferring protein content.

Wiechelman et al. (1988) investigated the various functional groups in the amino acids responsible for colour formation in the BCA assay. They reported that the amino acids containing thiol and amino groups could cause the biuret reaction [399]. Since NHS also have amino groups, NHS could, therefore, cause the biuret reaction. This NHS interference was also shown in a study by Vashist & Dixit (2011) and again in another study by Smith et al. (2018), where they found that NHS interfered with the BCA assay when measuring gelatine conjugation to PLGA particles [400,401].

The challenges posed by this finding arise when studies look at quantifying antibody conjugation through the amount of unbound antibody. For instance, Liu et al. (2019) used the BCA assay to measure antibody content in the supernatant following their washes to determine the amount of unbound antibody and, from that information, indirectly determined the amount of bound antibody [165]. Indeed, when the antibody is

introduced to the activated NPs (NHS-PLGA NPs), the NHS group attached to the PLGA NPs is displaced by the antibody, as seen in Figure 5.1. When this displacement occurs, NHS is released back into the medium, allowing the antibody to create the amide bond with PLGA's carboxylic group [162]. When the NPs solution is filtered to remove any unbound antibody, the displaced NHS is also filtered out with the unbound antibody. The final supernatant, therefore, contains both unbound antibody and NHS.

Since it was established that they could both cause the biuret reaction, the BCA assay would measure the total "protein" content in the sample, including both NHS and unbound antibody, without being able to discriminate one from the other. Therefore, the method posited by Liu et al. can lead to a higher optical density emitting from both compounds, leading to a higher unreliable reading, culminating in an unreliable antibody conjugation quantification. Additionally, using this indirect method assumes that the amount of antibody in the filtrate is all successfully bound to the PLGA NPs, which relies on the washing process to be accurate.

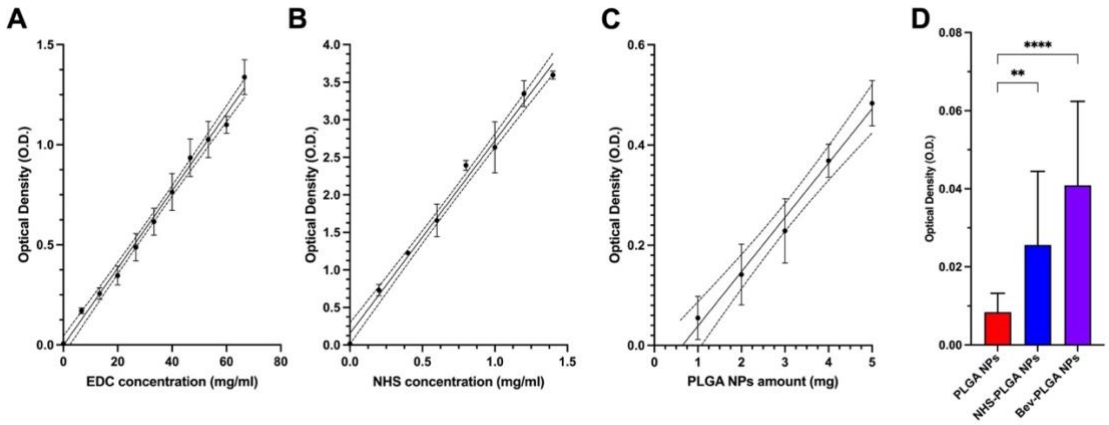

Figure 5.8. Optical density (O.D.) results from the BCA assay of the increasing concentration of A. EDC (R^2=0.99), B. NHS (R^2=0.98), C. PLGA NPs (R^2=0.99), D. the resulting conjugated PLGA NPs (Bev-PLGA NPs), the activated (NHS-PLGA NPs) and unreacted NPs (PLGA NPs). Data expressed as mean +/- s.e. mean of 3 independent (*P < 0.05, **P < 0.01, ***P < 0.001, ****P < 0.0001 ; data analysed by one-way ANOVA followed by Dunnett post hoc test), dotted lines represent the 95% confidence interval bands.

Figure 5.8C demonstrates further interference as the optical density increases with the concentration of PLGA NPs. Although the results clearly show that PLGA affects the optical density, further investigation is needed to confirm this and explain how PLGA causes interference. A possible explanation that could be explored would be that PLGA's carboxylic group becomes deprotonated from being introduced to an alkaline sodium potassium tartrate solution [402]. This could lead to a lone pair of electrons on the oxygen atoms, ultimately reducing the number of cupric ions to cuprous ions.

The study by McCarron et al. (2008) conjugating Anti-Fas, targeting Fas, a membrane protein displayed on various cancer cells, to PLGA NPs to deliver an anti-cancer agent, tested the effect of changing the PLGA composition and measured how it affected the antibody conjugation using the BCA assay [172]. They reported a higher antibody content when using a PLGA with a higher carboxylic content, which was attributed to more antibody covalently binding to more carboxylic groups [172]. However, they quantified the conjugation using the BCA assay, and the present study shows a linearity between the PLGA concentration and the optical density of the BCA assay, indicating the interference of PLGA. Therefore, the higher amount of antibody reported from the McCarron et al. (2008) study could be from the increased carboxylic group content in PLGA, which could have led to more deprotonation, increasing the BCA reading, and not a higher amount of antibody binding.

The same observation was made by Choi et al. (2018), where PLGA NPs with more carboxylic groups led to a higher binding efficiency following carbodiimide conjugation when measured using BCA assay [403]. Although these studies showed that a higher availability of carboxylic groups led to higher antibody binding, the BCA assay cannot be used as a direct method to measure binding efficiency due to interference with PLGA, as shown from the results obtained in the present work.

In Figure 5.8D, NHS-PLGA NPs displayed a higher optical density than unreacted PLGA NPs, and Bev-PLGA NPs showed even higher optical density. The previously described observation in this chapter indicates that the higher level of amino groups in these samples increase the optical density of the sample. As expected, NHS-PLGA NPs show a higher optical density than PLGA NPs due to the additional amino group that NHS carries. Bev-PLGA NPs demonstrate a significantly higher optical density

than NHS-PLGA NPs, possibly indicating the successful conjugation of bevacizumab to the PLGA NPs.

Chen et al. (2008) also used the BCA assay to quantify the conjugation of anti-HER2 to PLGA NPs, encapsulating a protein toxin to actively target this agent to cancer cells [163]. The study highlights the inability of the protein assay to distinguish between bound antibodies and the encapsulated protein in the conjugated drug-loaded PLGA. Therefore, unconjugated drug-loaded NPs served as a control to normalise the reading [163]. However, the protein is reported to be encapsulated; therefore, unless the drug is released at the time of the reading, the protein should not be capable of causing the biuret reaction. This method has to account for the drug release to obtain an accurate reading for normalisation, making it prone to additional inaccuracies. Moreover, normalising the conjugated reading with the PLGA signal to mitigate interference would still result in inaccuracies, as the PLGA signal is concentration-dependent. This introduces variability and reduces reproducibility, given the difficulty in ensuring consistent PLGA concentration across conjugation solutions.

Banstola et al. (2020) reported a conjugation efficiency (CE%) of 65.5% when using the BCA assay coupled with FTIR to confirm and quantify panitumumab conjugation to PLGA NPs. Their supporting information displays the effect of increasing antibody concentration on the CE% [164]. However, the data does not include a baseline when no antibody is added. A study by Domínguez et al. (2019) examined conjugating the anti-HER2 monoclonal antibody, trastuzumab, to cisplatin-loaded NPs. They also reported that due to the number of interferences, the determination of antibody conjugation using the BCA assay could not be accurate [151]. Many other studies reported interferences in the BCA assay from a variety of substances [404], including methylated proteins [405], lipids [406], and sugars [407]. Additionally, the accuracy of the assay has also been scrutinised due to its sensitivity to pH, protein concentration and incubation time [408].

The interferences and the inconsistencies exhibited in the literature and in the present study strongly advise against using the BCA assay as a reliable direct method to accurately confirm and quantify the antibody conjugation to PLGA NPs.

5.3.3.2. Enzyme-linked Immunosorbent Assay (ELISA)

ELISA is an immunoassay that uses enzyme catalytic properties to detect and measure immunologic reactions. This assay employs a plate coated with bevacizumab anti-idiotypic monoclonal antibody, which presents a mirror image of the original antibody, allowing it to bind to bevacizumab specifically [409].

Whilst BCA assay has been widely used due to its low cost and ease of use, its downfall is in its simplicity as it measures the total amount of protein in a sample and, therefore, lacks the specificity seen in ELISA [410]. Conjugation studies have used the BCA assay to confirm the conjugation and performed additional experimental work, such as cell or animal work, to further demonstrate the additional characteristics of the conjugated NPs.

For instance, Chen et al. (2008), as well as using the BCA assay, also performed flow cytometry and FTIR analysis to confirm conjugation further [163]. They then performed in-vitro studies investigating antibody recognition, binding and uptake to breast cancer cells, and finally, in-vivo studies where they showed a significantly higher reduction in tumour volume in mice using the conjugated drug-loaded NPs, compared to solely drug-loaded NPs [163]. McCarron et al. (2008) and Banstola et al. (2020) used the BCA assay to confirm conjugation as established above, and both tested the conjugated NP uptake using fluorescence microscopy and eventually tested the conjugated NPs' effectiveness in cells [164,172]. The conjugated drug-loaded NPs ultimately led to a higher reduction in tumour activity than drug-loaded NPs either measured by cytotoxicity assay, apoptosis assay or reactive oxygen species (ROS) assay [164,172]. These studies yielded valid results despite their initial assessment of the conjugation using the BCA assay.

However, a robust and reliable method to quantify antibody conjugation is essential to avoid investing time and resources into experiments that may not perform as expected due to the limitations of the BCA assay. Indeed, cell-based studies can be costly in terms of cells, media and other resources. The work is also time and effort-intensive and can be energy-consuming due to storage requirements. Animal-based studies are even more unfavourable, including higher and more complex waste generation, greater human resources requirements due to additional experiments and higher

energy demand to maintain the animals. Therefore, finding an alternative to animal studies for this end-point is crucial to follow the replace method from the 3R framework: replace, reduce and refine [411]. Thus, a more robust and precise method of quantifying antibody conjugation is required, and ELISA is considered for this study as it has been designed specifically to recognise bevacizumab immunologically [288].

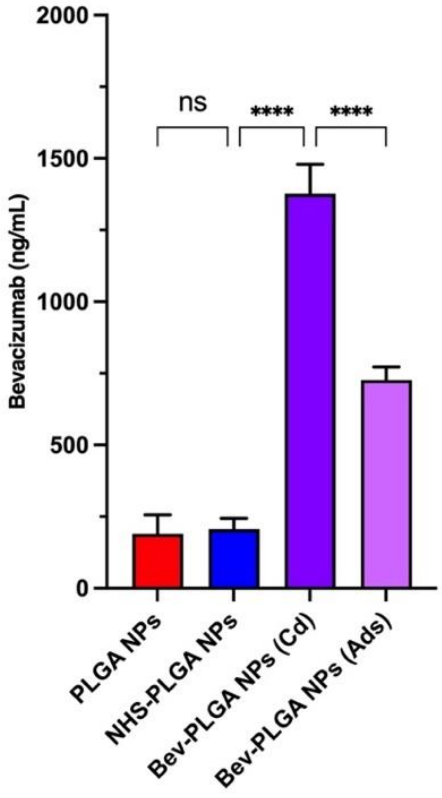

Figure 5.9. Measured bevacizumab concentration of activated (NHS-PLGA NPs). conjugated NPs (Bev-PLGA NPs (Cd) and adsorbed (Ads)) following carbodiimide conjugation and adsorption, respectively. Data expressed as mean +/- s.e. mean of 3 independent experiments (*P < 0.05, **P < 0.01, ***P < 0.001, ****P < 0.0001; data analysed by one-way ANOVA followed by Tukey post hoc test),

Figure 5.9 displays the ELISA results in the measured bevacizumab concentration of 1377 ± 102 ng/ml for Bev-PLGA NPs compared to the PLGA NPs and NHS-PLGA NPs, 190 ± 67 ng/ml and 207 ± 37 ng/ml, respectively. Antibody conjugation is confirmed by the highly significant increase in bevacizumab concentration in Bev-PLGA NPs compared to the unreacted and activated NPs.

Zhong et al. (2020) produced PLGA nanobubbles carrying the chemotherapy drug paclitaxel and functionalised it with trastuzumab (herceptin) to target breast cancer

cells [171]. The ELISA method was used to assess the antibody activity, and it was found that the activity increased as its concentration increased. The ELISA test showed that the antibody activity was preserved at 74.43% even as they increased antibody concentration, which could indicate saturation [171]. This demonstrates the superiority of ELISA to provide a comprehensive set of information about antibody conjugation.

Indeed, the ELISA enabled the quantification of antibody conjugation and the quantification of antibody activity since bevacizumab was able to bind to the anti-idiopathic antibody to provide a signal. Greene et al. (2017) compared conventional conjugation chemistry, such as carbodiimide and maleimide chemistry, to their modified click method [187]. ELISA was used to determine the targeting specificity of the conjugated PLGA NPs throughout the study until cellular studies, which further emphasised the method's reliability [187].

ELISA has also been used in a study by Vashist (2012) comparing carbodiimide-based strategies to conjugate antibodies to the amine-functionalised platform. However, instead of crosslinking the antibody's amine and the polymer's carboxylic acid, the carboxylic group from the antibody's constant region was crosslinked to a functionalised platform with amine groups through EDC. The study then compares the addition of NHS, sulfo-NHS, water or no activating reagent and how they impact the crosslinking between the antibodies and the platform. ELISA was used to compare crosslinking efficiency, and the amount of antibody immobilised on the platform [188]. This comparison study was repeated for different antibodies with their associated ELISA method, making the technique reliable for quantifying antibodies following carbodiimide conjugation.

It is noteworthy that BCA assay was also used in this study to measure antibody binding as a supplementary method to quantify the antibody binding but was not discussed extensively as ELISA and an optical technique, surface plasmon resonance, were the main methods employed [188]. As a comparison, our study also tested the adsorption method to assess the robustness of the ELISA test. The antibody was attached to the NPs using hydrogen bonding, electrostatic and hydrophobic, and Van der Waal's attractive forces, which are shown to have weak interactions [18].

Figure 5.9 shows the bevacizumab concentration in adsorbed NPs to bevacizumab, 727 ± 45 ng/ml, is nearly twice as low as the PLGA NPs conjugated using carbodiimide chemistry.

Kocbek et al. (2007) reported a higher fluorescence intensity from adsorbed NPs, representing a higher binding of the NPs to the cells [174]. They attributed this to the NPs creating hydrophobic interaction with the antibody's constant region, which frees the variable region to bind to the relevant antigen instead of covalently bound antibodies, which have only one free variable region [174]. The study shows confocal images of the adsorbed NPs bound to a secondary antibody but does not show conjugated NPs bound to a secondary antibody for comparison. The fluorescence intensity from the binding of the NPs to antigens in breast cancer cells (MCF-7 cell line) was compared using both methods. A higher fluorescence intensity is reported from the adsorbed NPs, and the conjugated NPs led to the lowest fluorescence intensity, which was even lower than its control. The Kocbek et al. (2007) study reported incubating the cells with the NPs for 2 hours [174]. The antibody used in this study is not specified but is established to recognise soluble membrane proteins of human invasive ductal breast carcinoma (MCF-7).

Another study by Chatterjee et al. (2020) reported that antibody-conjugated PLGA NPs, using a modified carbodiimide method, showed significant NP uptake in the same cell line, MCF-7, within 2 hours [229]. Choi et al. (2018) conjugated trastuzumab (Herceptin) on the surface of carboxylic-rich modified-PLGA NPs and compared the carbodiimide, adsorption, and charged adsorption methods [403]. They found that the NPs conjugated using carbodiimide have the highest level of binding (94.0 ± 0.9%), almost four times higher than the adsorption method using BCA assay. Additionally, the study also reported similar results to Chatterjee et al. (2020), where the Herceptin-conjugated NPs led to a cellular uptake nearly 2-fold higher than the absorbed NPs within 2 hours [403]. This could indicate that the low fluorescence intensity seen in Kocbek et al. (2007) could be due to the faster internalisation of the conjugated NPs.

Additionally, Gao et al. (2022) and Juan et al. (2020) posited that although adsorbed antibodies can maintain a higher biological activity than covalently bound antibodies, they lack stability and control over their orientation, which could impact their

internalisation [18,412]. The lack of orientation could also explain the much lower binding efficiency in the present study using adsorbed PLGA NPs, as bevacizumab could have adsorbed on the PLGA NPs through their variable region, not enabling their binding to the ELISA platform.

The adsorption method indicates the absence of the EDC and NHS crosslinkers, which have been established to cause interference in the BCA assay. However, the BCA assay remains unreliable even without their presence as it would not discriminate bevacizumab from PLGA in the total concentration measured. The present study has shown that the bevacizumab ELISA accurately measures bevacizumab concentration. This constitutes a more reliable method for confirming and quantifying carbodiimide conjugation of antibodies to NPs.

5.4. Conclusion

This study offers a critical analysis of the methods used to confirm and quantify antibody conjugation via carbodiimide conjugation. This study demonstrates the conjugation of anti-VEGF, bevacizumab, to electrosprayed PLGA NPs using the carbodiimide chemistry for a more targeted delivery. The NPs were initially shown to be activated by the EDC/NHS crosslinkers, as illustrated by the changes in the zeta potential results and the FTIR spectrum, which demonstrated successful activation of the NPs.

The methods, however, have shown to be limited in conclusively confirming conjugation. A further two methods (BCA and ELISA) were used to confirm the conjugation. The commonly used protein assay, BCA assay, has been shown to significantly interfere with the reagents used in the conjugation, including the NPs, making it unreliable for quantifying the conjugation. This also established that the ELISA method is more reliable in quantifying the bevacizumab concentration to the PLGA NPs.

As our study established that ELISA method is the most suitable and reliable technique to quantify antibody conjugation, we compared the physical adsorption method to the carbodiimide method and demonstrated that the carbodiimide chemistry was more effective in conjugating more antibodies on the surface of electrosprayed PLGA NPs. The reliability of this method opens the possibility to test and compare other conjugation methods and to test the stability of the conjugated NPs over time and in different conditions.

Chapter 6. Conclusions and Future work

6.1. Conclusion

Pulmonary hypertension has remained a subject of investigation since its discovery in 1891 [413]. Still, to this day, no curative treatment has been approved for this progressive condition, and the prognosis for patients remains poor. The currently approved treatments address the condition symptomatically by inhibiting vascular constriction or stimulating vasodilation [414]. The search for an effective cure is still ongoing, and many studies have explored various pathways to target PAH, which has been found to be a multifactorial condition similar in many respects to cancer [415].

One small molecule stands out for having reached phase III in clinical trials for the treatment of PAH: Imatinib was initially approved for CML and was then repurposed for PAH due to its effect on the PDGF signalling pathway, which was found to play a significant role in PAH pathogenesis. The drug, however, was found to be unsafe when taken orally due to its systemic delivery. Drug delivery systems such as polymeric nanoparticles have been examined for various APIs to address the safety, bioavailability and solubility issues.

Imatinib was encapsulated for additional application, but the methods of nanoparticle fabrication were limited in their multi-step protocol, which involved high temperature, toxic surfactants, and high waste. The electrospray method used in this work addressed these issues. It offers a continuous one-step method, which does not involve temperature or additional surfactant and leads to a high encapsulation and monodisperse distribution of particles. The technique also allows tight control of the produced nanoparticle characteristics. This includes a high level of control over the drug release, which is very relevant for further in-vitro and in-vivo work.

Now, focusing on the in-vivo aspect, as demonstrated in Chapter 4, the NPs have inhibited proliferation in vitro in the relevant cells. However, mammalian cell culture remains stationary and non-dynamic. However, when NPs are administered in-vivo, many studies have reported that the NPs rely on the EPR effect to be delivered, which lacks targeting. Binding a relevant antibody onto the surface of the NPs could enhance its delivery and actively target it to the appropriate antigen-presenting cells.

The one-step electrospraying (ES) technique allowed the production of PLGA NPs of various sizes and hydrophobicity by varying parameters of the methodology. Indeed, by reducing the flow rate, the solvent evaporation rate, and increasing the voltage, the ES produced NPs nearly half the size of the first set of NPs. All NPs showed a high encapsulation efficiency, and the incorporation of the drug was confirmed through changes in its surface charge and chemical fingerprints.

By increasing the ratio of lactic acid to glycolic acid in PLGA, the hydrophobicity of the polymer was altered, which allowed for control of the drug release from the NPs. The release profile of the NPs underpinned the choice of formulation taken forward for cell studies. The imatinib-loaded NPs showed an antiproliferative effect on the A549 cell line, which was comparable in magnitude to that of the free drug. The lack of effect of the blank NPs showed that the polymer and ES process method had no toxic effect on the cells. Experiments using dye-loaded NPs demonstrated cellular uptake of the NPs in these cells within 24 hours.

Since a baseline for the effect of the NPs in cells was established, the effects of the imatinib-loaded PLGA NPs on endothelial (HUVECs) and pulmonary arterial smooth muscle cells (HPASMCs) were investigated. Varying imatinib concentration and cell confluence demonstrated the expected effects of imatinib on endothelial cells, in accordance with the published literature. These parameters were also shown to affect HPASMC cell viability. Due to the proliferative nature of the HPASMCs, a time course of the cell viability when treated with a range of imatinib concentrations was examined. The time points of 8, 24 and 48 hours were chosen from this for subsequent studies, and the free imatinib concentration was adjusted.

The imatinib-loaded NPs were shown to be more effective than the free drug in reducing cell viability compared with control cultures, while the blank NP-treated cells maintained a similar level of cell viability to the untreated controls. The HPASMCs were then stimulated with the mitogen PDGF, and a series of optimisations were performed to establish a baseline to show the effect of the mitogen on cell growth in the absence and presence of the free drug. The drug-loaded NPs showed a consistent inhibitory effect on cell growth, reflecting the drug release because the blank NPs were without effect in the same experiments.

The antibody conjugation to the NPs was then studied, which first started with the optimisations behind the successful carbodiimide conjugation of bevacizumab to the electrosprayed PLGA NPs. Various methods of confirming and quantifying the antibody conjugation were explored and compared.

The NPs were shown to be activated first by the EDC/NHS crosslinkers, by the changes shown in the surface charge and its chemical fingerprints via FTIR and ^{1}H-NMR. A secondary antibody was also introduced to the conjugated NPs to attempt to confirm the antibody conjugation by using flow cytometry.

Although the results were not conclusive, they were promising. These methods were still unable to confirm conjugation conclusively. Therefore, two other methods were used to verify the conjugation. The commonly used protein assay, BCA assay, was shown to significantly interfere with the reagents used in the conjugation, including the NPs. The ELISA method was established as more reliable in quantifying the binding efficiency of bevacizumab to the PLGA NPs. Since ELISA was shown to be reliable, it was possible to compare the physical adsorption method to the carbodiimide method and conclude that the carbodiimide chemistry was more effective in conjugating antibody to PLGA NPs.

Overall, the versatility of the electrospray technique was shown by precisely controlling nanoparticle size and characteristics through adjusting production parameters. It enabled the production of PLGA nanoparticles (NPs) to encapsulate imatinib, offering controlled drug release and high encapsulation efficiency. The technique can be utilised for a wide range of applications due to the variety of materials that NPs can be made from and the diverse payloads they can carry while maintaining product consistency. The imatinib-loaded NPs demonstrated effects on a lung cancer cell line and vascular cells relevant to PAH that were similar to or superior to those of free imatinib. Moreover, successful antibody conjugation using carbodiimide chemistry was confirmed through specific ELISA testing, paving the way for future enhanced NP targeting. This approach presents a promising platform for safer, more effective PAH treatment, with potential applications in other diseases.

6.2. Future work

Future work can take different paths from the work presented in this thesis; outlined below are potential future directions based on the work undertaken and presented in this thesis, with potential areas for broader future work examined.

6.2.1. Project-specific future work

It would be relevant to test the effect of the drug-loaded NPs on patient cells, both endothelial and smooth muscle cells. Indeed, before testing the NPs in preclinical animal models, it is relevant to ensure they maintain their efficacy on patient cells, translating to a lower proliferation rate from the PAH cells. However, obtaining patient cells can be challenging due to limited access, on account of PAH's prevalence of 1% globally [21]. Moreover, PAH cells and tissues are typically obtained during lung transplantation, representing the end-stage of the disease. At this advanced stage, the condition may no longer progress, potentially limiting the effects of the nanoparticles in terms of understanding their potential benefits earlier in the disease process [416]. Additionally, it is impossible to obtain true control samples from lung tissues due to the uniqueness of each individual [416].

Cell studies can also be performed to examine the enhanced uptake of the antibody-conjugated NPs. Relevant cells, such as PASMCs or PAECs, can be stimulated to present the corresponding antigen to a PAH-relevant antibody, such as anti-ACE2 or integrin α9. The antibody-conjugated NPs would be expected to be taken up by the cells faster than unconjugated NPs through the time course experiment. Nevertheless, as mentioned, mammalian cell culture remains stationary which can sometimes lead to misleading or overly optimistic results as it does not replicate the dynamic in vivo environment.

Animal studies can therefore be more beneficial in gaining a greater understanding of NP biodistribution and the efficacy of the targeted imatinib-loaded NPs in PAH animal models.

Following the success of the ELISA approach in confirming and quantifying antibody NP conjugation opens the possibility of performing biodistribution studies which can

demonstrate the effective delivery of the conjugated NPs to the relevant cells. In Chapter 5, blank NPs were conjugated to bevacizumab; the next step would be to conjugate imatinib-loaded NPs and to ensure their antiproliferative effect and enhanced delivery to pulmonary vasculature cells.

Biodistribution studies can be performed to monitor the trajectory of NPs and ensure they are delivered to the correct target site by creating multifunctional NPs, conjugating antibodies and imaging modalities such as radioisotopes or fluorophores on the surface of the NPs. The use of the EDC/NHS crosslinkers can also be used to radiolabel PLGA NPs by radionucleotide conjugation[417]. Creating multifunctional NPs with an imaging modality could ensure the course of the NPs is maintained with the help of labelled radioisotopes and conjugated antibodies in vivo.

The study of the NPs in vivo would be mostly relevant in PAH animal models to investigate the effect of the produced NPs in a biological system mimicking PAH. The monocrotaline (MCT) animal model of PAH is a common choice as it is relatively inexpensive, reproducible, well-characterised and easy to perform. Another common and reversible animal model for PAH is the combination of Sugen5416, a VEGF receptor antagonist, and hypoxia exposure for 3 weeks. This combination leads to the progressive formation of plexiform lesions over the following months [418]. The condition also develops due to germline autosomal dominant mutations in the BMPR2 gene [419]. *Bmpr2* transgenic mice were developed to show increased proliferation of smooth muscle cells, thrombosis, and an increase in apoptotic cells and inflammatory cells to make a PAH animal model [420]. These three animal models are the common types used for the study of pulmonary hypertension group 1 or PAH and can potentially be used to study the effect of NPs in-vivo.

Demonstrating the efficacy of the conjugated NPs on the affected tissues while maintaining the safety of the surrounding tissues would be the primary end-point of the preclinical animal studies.

6.2.1. Broad future work

6.2.1.1. Scaling up and multi-layered NPs

Although the ES technique can be showcased for versatility and control over the produced NPs, it still has limitations for various applications. Its yield, for instance, relies on the flow rate, which needs to be low to generate small particles, making manufacturing challenging to upscale. Studies have examined manufacturing a multi-needles ES setup to increase yield by allowing multiple streams of polymeric solution to be electrosprayed [421].

Electrospraying also enables the creation of multiple-layered nanoparticles using a coaxial needle [422]. Two independent electrospray solutions feed the coaxial needle at two flow rates through two syringe pumps. An electrical field is applied to the coaxial needle, similar to the single needle used in this thesis, creating nanoparticles with multiple layers [423]. The independent solutions can be composed of different materials and drugs.

Since pulmonary hypertension is a multifactorial condition, a potential upgrade in the particles made in this study would be to encapsulate another type of treatment, targeting another pathway, in a separate layer. For instance, two treatments from Table 1.2 could be delivered simultaneously for a synergistic effect. Since inflammation appears to be one of the major contributors to PAH pathogenesis, NPs composed of imatinib, and an anti-inflammatory agent could potentially be beneficial in two aspects of the condition [86]. One can decide which layer each treatment would reside in depending on how fast each treatment would need to be administered. Indeed, the outer layer would release its treatment first as hydrolysis would start there. Considering this, treatments alleviating symptoms, such as the currently approved treatments displayed in Table 1.1 could be released first to improve symptoms before releasing imatinib. The relief the patients would experience from those treatments would potentially be prolonged due to the mode of delivery using NPs, with underlying disease control maintained through imatinib's antiproliferative nature.

6.2.1.2. Cell culture considerations

Another aspect of future work is to investigate vascular cell-based work further before going into in-vivo work.

The study performed on vascular cells in this thesis has provided valuable insight into how the imatinib-loaded NPs impact cell viability. However, the studies were performed in the cells separately, denying the impact one type of cell has on the other in-vivo. Indeed, pulmonary artery endothelial cells (PAECs) have been established to release pro-inflammatory cytokines, growth factors and vasoactive mediators, impacting PASMC proliferation and function in PAH, most pertinently the mitogen PDGF [424]. Therefore, co-culturing PAECs and PASMCs together using Transwell plates could demonstrate how treating the cells with free imatinib and imatinib-loaded NPs can affect both PAEC and PASMC cell viability, but also how the drug, free and encapsulated, affect the way the cells communicate with each other. This information can provide insight into how their communication influences the growth and function of blood vessels [425,426].

Another indirect method would be to use a conditioned medium from the culture of HUVECs or PAECs after being treated with NPs and apply it to the smooth muscle cells. However, this method remains indirect, and co-culturing can provide information about the movement of the NPs between the pulmonary arterial endothelial cells and smooth muscle, which cannot be obtained using the conditioned medium method.

It was discussed earlier in the thesis that the assay used to show the NPs effect on cells measured cell viability as a function of mitochondrial activity and therefore provided indirect information about cell proliferation. Therefore, another method, such as the ^{3}H-thymidine incorporation assay or another nucleoside-analogue incorporation assay, the bromodeoxyuridine method, would give information on DNA synthesis and proliferation [427]. These methods would be more relevant and accurate in providing input about the effect of treatment on the proliferation of the cells as they quantify newly synthesised DNA [427]. Indeed, as demonstrated, in some cases, necrosis was assumed when cell viability was dramatically decreased. An apoptosis assay such as the terminal deoxynucleotidyl transferase-mediated dUTP nick end labelling (TUNEL)

assay can be performed to confirm apoptosis by labelling the DNA fragmentation following apoptosis in its late stage [428].

6.2.1.3. Antibody conjugation optimisation

Additional experiments could be conducted to further examine the success of the antibody conjugation, confirm its activity, demonstrate its ability to enhance NP delivery and test the stability of the conjugated NPs over time and in different conditions, such as the temperature or pH of the suspension.

Since the carbodiimide conjugation method binds PLGA NPs to the antibody variable region, it raises questions about whether the other variable region can be free to bind to the antigen-presenting cells or could potentially bind to other PLGA NPs. This remains a limitation of this method, so other conjugation methods, such as maleimide or click chemistry, should also be investigated and compared.

6.2.1.4. Animal studies considerations

Additional consideration needs to be taken when administering the NPs in vivo, such as the method of administration. Functionalising the NPs does not guarantee their correct delivery. Indeed, if the NPs are administered intravenously, the shear stress of blood flow and different magnitudes and patterns can impact their structural integrity and hence delivery and uptake [429]. NPs have been shown to interact with proteins upon entering biological systems, resulting in the coating of the nanoparticles. This coating can alter the protein's shape, expose new areas, or affect its function due to structural changes or high local concentrations [430]. The coating of proteins on the NPs can affect their distribution and influence blood flow. Specifically, it can increase the nanoparticle size, leading to higher blood flow resistance, which is problematic in conditions already characterised by narrow blood vessels [431]. The coating can also alter the NP surface charge and shield the antibody that is intended to ensure the active delivery of the NPs, affecting its active delivery [431,432].

It was also found that less than 1% of NPs traverse the endothelial barrier and that the extravasation of the barrier in tumour tissues is insufficient to let NPs through [433]. It was found that the basement membrane surrounding the endothelial cells was responsible for pooling of the NPs at this site[434]. Moreover, an increase in the thickness

of the basement layer was observed in the PAH pulmonary vessel[435]. Therefore, more in-vivo work should be performed to investigate the various challenges that may hinder the correct delivery of the NPs to their intended site of action. For instance, a study by Wang et al. (2023) used local hyperthermia therapy to attract platelets to the pooling site, which then recruits neutrophils to break and release the NPs from the basement membrane [434]. Alternatively, the coaxial electrospraying technique can also be used to carry both imatinib and anti-fibrotic agents, such as pirfenidone, to potentially facilitate NP penetration of the basement membrane [436].

References

1. Zamanian, R. T. *et al.* Current Clinical Management of Pulmonary Arterial Hypertension. *Circ Res.* 115, 131–147 (2014).

2. Iqbal, N. & Iqbal, N. Imatinib: A Breakthrough of Targeted Therapy in Cancer. *Chemother Res Pract* 2014, 1–9 (2014).

3. Okur, N. Ü., Siafaka, P. I. & Gökçe, E. H. Challenges in Oral Drug Delivery and Applications of Lipid Nanoparticles as Potent Oral Drug Carriers for Managing Cardiovascular Risk Factors. *Curr Pharm Biotechnol* 22, 892–905 (2020).

4. Wei, Y. & Zhao, L. Passive lung-targeted drug delivery systems via intravenous administration. *Pharm Dev Technol* 19, 129–136 (2014).

5. Makadia, H. & Siegel, S. Poly Lactic-co-Glycolic Acid (PLGA) as Biodegradable Controlled Drug Delivery Carrier. *Polymers (Basel)* 3, 1377–1397 (2011).

6. Benny, O. *et al.* Local Delivery of Poly Lactic-co-glycolic Acid Microspheres Containing Imatinib Mesylate Inhibits Intracranial Xenograft Glioma Growth. *Clinical Cancer Research* 15, 1222–1231 (2009).

7. Esfandyari-Manesh, M. *et al.* S2P peptide-conjugated PLGA-Maleimide-PEG nanoparticles containing Imatinib for targeting drug delivery to atherosclerotic plaques. *DARU Journal of Pharmaceutical Sciences* 28, 131–138 (2020).

8. Marslin, G. *et al.* Delivery as nanoparticles reduces imatinib mesylate-induced cardiotoxicity and improves anticancer activity. *Int J Nanomedicine* 10, 3163–3170 (2015).

9. Karal-Yilmaz, O. *et al.* Controlled release of imatinib mesylate from PLGA microspheres inhibit craniopharyngioma mediated angiogenesis. *J Mater Sci Mater Med* 24, 147–153 (2013).

10. Akagi, S. *et al.* Delivery of Imatinib-Incorporated Nanoparticles into Lungs Suppresses the Development of Monocrotaline-Induced Pulmonary Arterial Hypertension. *Int Heart J* 56, 354–359 (2015).

11. Ramazani, F. *et al.* Formulation and characterization of microspheres loaded with imatinib for sustained delivery. *Int J Pharm* 482, 123–130 (2015).

12. Almería, B., Deng, W., Fahmy, T. M. & Gomez, A. Controlling the morphology of electrospray-generated PLGA microparticles for drug delivery. *J Colloid Interface Sci* 343, 125–133 (2010).

13. Chen, C., Liu, W., Jiang, P. & Hong, T. Coaxial electrohydrodynamic atomization for the production of drug-loaded micro/nanoparticles. *Micromachines* vol. 10 Preprint at https://doi.org/10.3390/mi10020125 (2019).

14. Gutiérrez, T. J. Polymers for food applications: News. *Polymers for Food Applications* 1–4 (2018) doi:10.1007/978-3-319-94625-2_1/COVER.

15. Sequeira, J. A. D., Pereira, I., Ribeiro, A. J., Veiga, F. & Santos, A. C. Surface functionalization of PLGA nanoparticles for drug delivery. in *Handbook of Functionalized Nanomaterials for Industrial Applications* 185–203 (Elsevier, 2020). doi:10.1016/B978-0-12-816787-8.00008-9.

16. Schermuly, R. T. *et al.* Reversal of experimental pulmonary hypertension by PDGF inhibition. *J Clin Invest* 115, 2811–2821 (2005).

17. Clemons, T. D. *et al.* Distinction between Active and Passive Targeting of Nanoparticles Dictate Their Overall Therapeutic Efficacy. *Langmuir* 34, 15343–15349 (2018).

18. Juan, A. *et al.* An Overview of Antibody Conjugated Polymeric Nanoparticles for Breast Cancer Therapy. *Pharmaceutics 2020, Vol. 12, Page 802* 12, 802 (2020).

19. Segura-Ibarra, V. *et al.* Nanotherapeutics for Treatment of Pulmonary Arterial Hypertension. *Front Physiol* 9, 890 (2018).

20. Dorfmüller, P. Pathology of pulmonary arterial hypertension. *Pulmonary Vascular Disorders* 41, 14–22 (2012).

21. Hoeper, M. M. *et al.* Pulmonary hypertension. *Dtsch Arztebl Int* 114, 73–84 (2017).

22. George, M. G., Schieb, L. J., Ayala, C., Talwalkar, A. & Levant, S. Pulmonary hypertension surveillance: United States, 2001 to 2010. *Chest* 146, 476–495 (2014).

23. Goldberg, A. B., Mazur, W. & Kalra, D. K. Pulmonary hypertension: Diagnosis, imaging techniques, and novel therapies. *Cardiovasc Diagn Ther* 7, 405–417 (2017).

24. McGoon, M. D. & Kane, G. C. Pulmonary hypertension: Diagnosis and management. in *Mayo Clinic Proceedings* vol. 84 191–207 (Elsevier Ltd, 2009).

25. Farber, H. W. & Loscalzo, J. Pulmonary arterial hypertension. *N Engl J Med* 351, 1655–1665 (2004).

26. Rabinovitch, M. Pathology of pulmonary hypertension. *Prog Pediatr Cardiol* 12, 223–247 (2001).

27. Galiè, N. *et al.* 2015 ESC/ERS Guidelines for the diagnosis and treatment of pulmonary hypertension. in *European Respiratory Journal* vol. 46 903–975 (European Respiratory Society, 2015).

28. Stamm, J. A., Risbano, M. G. & Mathier, M. A. Overview of current therapeutic approaches for pulmonary hypertension. *Pulm Circ* 1, 138–159 (2011).

29. Albouaini, K., Egred, M., Alahmar, A. & Wright, D. J. Cardiopulmonary exercise testing and its application. *Postgrad Med J* 83, 675 (2007).

30. Crapo, R. O. *et al.* Guidelines for the Six-Minute Walk Test. *Am J Respir Crit Care Med* 166, 111–117 (2012).

31. Barst, R. J. *et al.* Diagnosis and Differential Assessment of Pulmonary Arterial Hypertension. *J Am Coll Cardiol* 43, 40S-47S (2004).

32. Frost, A. *et al.* Diagnosis of pulmonary hypertension. *Eur Respir J* 53, (2019).

33. Mani, B. C. & Chaudhari, S. S. Right Heart Cardiac Catheterization. *StatPearls* 1–9 (2021).

34. Nagaya, N. *et al.* Serum uric acid levels correlate with the severity and the mortality of primary pulmonary hypertension. *Am J Respir Crit Care Med* 160, 487–492 (1999).

35. Townsley, M. I. Structure and composition of pulmonary arteries, capillaries and veins. *Compr Physiol* 2, 675 (2012).

36. Schermuly, R. T., Ghofrani, H. A., Wilkins, M. R. & Grimminger, F. Mechanisms of disease: pulmonary arterial hypertension. *Nature Reviews Cardiology 2011 8:8* 8, 443–455 (2011).

37. Savai, R. *et al.* Immune and inflammatory cell involvement in the pathology of idiopathic pulmonary arterial hypertension. *Am J Respir Crit Care Med* 186, 897–908 (2012).

38. Tuder, R. M. Pathology of pulmonary arterial hypertension. *Semin Respir Crit Care Med* 30, 376–385 (2009).

39. Bazan, I. S. & Fares, W. H. Pulmonary hypertension : diagnostic and therapeutic challenges. *Ther Clin Risk Manag* 11, 1221–1233 (2015).

40. van de Veerdonk, M. C. *et al.* Progressive Right Ventricular Dysfunction in Patients With Pulmonary Arterial Hypertension Responding to Therapy. *J Am Coll Cardiol* 58, 2511–2519 (2011).

41. Kuhr, F. K., Smith, K. A., Song, M. Y., Levitan, I. & Yuan, J. X. J. New mechanisms of pulmonary arterial hypertension: role of Ca2+ signaling. *Am J Physiol Heart Circ Physiol* 302, (2012).

42. Medarov, B. I. & Judson, M. A. The role of calcium channel blockers for the treatment of pulmonary arterial hypertension: How much do we actually know and how could they be positioned today? *Respir Med* 109, 557–564 (2015).

43. Humbert, M., Sitbon, O. & Simonneau, G. Treatment of pulmonary arterial hypertension. *N Engl J Med* 351, 1425–1436 (2004).

44. Patel, R. *et al.* Treatment of pulmonary hypertension. *Med Sci Monit* 18, (2012).

45. Tuder, R. M. *et al.* Prostacyclin synthase expression is decreased in lungs from patients with severe pulmonary hypertension. *Am J Respir Crit Care Med* 159, 1925–1932 (1999).

46. Christman, B. W. *et al.* An Imbalance between the Excretion of Thromboxane and Prostacyclin Metabolites in Pulmonary Hypertension. *New England Journal of Medicine* 327, 70–75 (1992).

47. Shao, D., Park, J. E. S. & Wort, S. J. The role of endothelin-1 in the pathogenesis of pulmonary arterial hypertension. *Pharmacol Res* 63, 504–511 (2011).

48. Giaid, A. *et al.* Expression of Endothelin-1 in the Lungs of Patients with Pulmonary Hypertension. *New England Journal of Medicine* 328, 1732–1739 (1993).

49. Bevacqua, R. J., Bortman, G. & Perrone, S. V. Endothelin receptor antagonists for pulmonary arterial hypertension. *Insuficiencia Cardiaca* 8, 77–94 (2013).

50. Hoeper, M. M. Liver toxicity: the Achilles' heel of endothelin receptor antagonist therapy? *European Respiratory Journal* 34, 529–530 (2009).

51. Zhang, R. *et al.* Profiling nitric oxide metabolites in patients with idiopathic pulmonary arterial hypertension. *European Respiratory Journal* 48, 1386–1395 (2016).

52. Tonelli, A. R., Haserodt, S., Aytekin, M. & Dweik, R. A. Nitric oxide deficiency in pulmonary hypertension: Pathobiology and implications for therapy. *Pulm Circ* 3, 20 (2013).

53. Tettey, A., Jiang, Y., Li, X. & Li, Y. Therapy for Pulmonary Arterial Hypertension: Glance on Nitric Oxide Pathway. *Front Pharmacol* 12, 767002 (2021).

54. Galiè, N. *et al.* Risk stratification and medical therapy of pulmonary arterial hypertension. *European Respiratory Journal* 53, (2019).

55. del Pozo, R., Hernandez Gonzalez, I. & Escribano-Subias, P. The prostacyclin pathway in pulmonary arterial hypertension: a clinical review. *Expert Rev Respir Med* 11, 491–503 (2017).

56. Sitbon, O. & Gaine, S. Beyond a single pathway: combination therapy in pulmonary arterial hypertension. *European Respiratory Review* 25, 408–417 (2016).

57. Galiè, N., Negro, L. & Simonneau, G. The use of combination therapy in pulmonary arterial hypertension: new developments. *European Respiratory Review* 18, 148–153 (2009).

58. National Health Service (NHS). *National Audit of Pulmonary Hypertension, 12th Annual Report*. https://files.digital.nhs.uk/75/83A559/NAPH%2012AR%20-%20Main%20Report%20v1.1.pdf (2022).

59. Skoro-Sajer, N., Lang, I. & Naeije, R. Treprostinil for pulmonary hypertension. *Vascular Health and Risk Management* vol. 4 507–513 Preprint at https://doi.org/10.2147/vhrm.s2477 (2008).

60. Badesch, D. B. *et al.* Prostanoid therapy for pulmonary arterial hypertension. in *Journal of the American College of Cardiology* vol. 43 S56–S61 (Elsevier USA, 2004).

61. Simonneau, G. *et al.* Selexipag: An oral, selective prostacyclin receptor agonist for the treatment of pulmonary arterial hypertension. *European Respiratory Journal* 40, 874–880 (2012).

62. Ghofrani, H.-A. *et al.* Riociguat for the Treatment of Pulmonary Arterial Hypertension. *New England Journal of Medicine* 369, 330–340 (2013).

63. Klinger, J. R., Chakinala, M. M., Langleben, D., Rosenkranz, S. & Sitbon, O. Riociguat: Clinical research and evolving role in therapy. *Br J Clin Pharmacol* 87, 2645–2662 (2021).

64. Roux, S. & Rubin, L. J. Bosentan: a dual endothelin receptor antagonist. *Expert Opin Investig Drugs* 11, 991–1002 (2005).

65. Rubin, L. J. *et al.* Bosentan Therapy for Pulmonary Arterial Hypertension. *New England Journal of Medicine* 346, 896–903 (2002).

66. Khadka, A., Brashier, D. B. S., Tejus, A. & Sharma, A. K. Macitentan: An important addition to the treatment of pulmonary arterial hypertension. *J Pharmacol Pharmacother* 6, 53 (2015).

67. Galié, N. *et al.* Ambrisentan therapy for pulmonary arterial hypertension. *J Am Coll Cardiol* 46, 529–535 (2005).

68. Sastry, B. K. S., Narasimhan, C., Reddy, N. K. & Raju, B. S. Clinical efficacy of sildenafil in primary pulmonary hypertension: A randomized, placebo-controlled, double-blind, crossover study. *J Am Coll Cardiol* 43, 1149–1153 (2004).

69. Galiè, N. *et al.* Tadalafil Therapy for Pulmonary Arterial Hypertension. *Circulation* 119, 2894–2903 (2009).

70. Nakamura, K. *et al.* Current Treatment Strategies and Nanoparticle-Mediated Drug Delivery Systems for Pulmonary Arterial Hypertension. *Int J Mol Sci* 20, 5885 (2019).

71. Xu, W. & Erzurum, S. C. Endothelial Cell Energy Metabolism, Proliferation, and Apoptosis in Pulmonary Hypertension. in *Comprehensive Physiology* vol. 1 357 (John Wiley & Sons, Inc., 2010).

72. Nakamura, K. *et al.* Pro-apoptotic effects of imatinib on PDGF-stimulated pulmonary artery smooth muscle cells from patients with idiopathic pulmonary arterial hypertension. *Int J Cardiol* 159, 100–106 (2012).

73. Gomberg-Maitland, M. *et al.* A Dosing/Cross-Development Study of the Multikinase Inhibitor Sorafenib in Patients With Pulmonary Arterial Hypertension. *Clin Pharmacol Ther* 87, 303 (2010).

74. Zhang, X. *et al.* Effects of Fasudil on Patients with Pulmonary Hypertension Associated with Left Ventricular Heart Failure with Preserved Ejection Fraction: A Prospective Intervention Study. *Can Respir J* 2018, 1–7 (2018).

75. Zhang, Y. & Wu, S. Effects of fasudil on pulmonary hypertension in clinical practice. *Pulmonary Pharmacology and Therapeutics* vol. 46 54–63 Preprint at https://doi.org/10.1016/j.pupt.2017.08.002 (2017).

76. Nakamura, K. *et al.* Crucial role of RAGE in inappropriate increase of smooth muscle cells from patients with pulmonary arterial hypertension. *PLoS One* 13, (2018).

77. Prasad, K. AGE–RAGE Stress in the Pathophysiology of Pulmonary Hypertension and its Treatment. *Int J Angiol* 28, 71 (2019).

78. Meloche, J. *et al.* Critical Role for the Advanced Glycation End-Products Receptor in Pulmonary Arterial Hypertension Etiology. *Journal of the American Heart Association: Cardiovascular and Cerebrovascular Disease* 2, (2013).

79. Keefe, A. D., Pai, S. & Ellington, A. Aptamers as therapeutics. *Nature Reviews Drug Discovery 2010 9:7* 9, 537–550 (2010).

80. Laval University. Olaparib for PAH: a Pilot Study - Full Text View - ClinicalTrials.gov. *ClinicalTrials.gov* https://clinicaltrials.gov/ct2/show/NCT03251872 (2020).

81. Harbaum, L. *et al.* Complete resolution of idiopathic pulmonary arterial hypertension following chemotherapy. *European Respiratory Journal* vol. 43 1513–1515 Preprint at https://doi.org/10.1183/09031936.00185713 (2014).

82. Boucherat, O. *et al.* HDAC6: A Novel Histone Deacetylase Implicated in Pulmonary Arterial Hypertension. *Sci Rep* 7, 1–14 (2017).

83. Spiekerkoetter, E., Kawut, S. M., De, V. A. & Perez, J. New and Emerging Therapies for Pulmonary Arterial Hypertension. *Annu. Rev. Med. 2019* 70, 45–59 (2019).

84. Zhou, G., Chen, T. & Usha Raj, J. MicroRNAs in pulmonary arterial hypertension. *Am J Respir Cell Mol Biol* 52, 139–151 (2015).

85. Courboulin, A. *et al.* Role for miR-204 in human pulmonary arterial hypertension. *Journal of Experimental Medicine* 208, 535–548 (2011).

86. Dorfmüller, P., Perros, F., Balabanian, K. & Humbert, M. Inflammation in pulmonary arterial hypertension. *Eur Respir J* 22, 358–363 (2003).

87. Reata Pharmaceuticals, Inc. Bardoxolone Methyl Evaluation in Patients With Pulmonary Hypertension (PH) - LARIAT - Full Text View - ClinicalTrials.gov. *ClinicalTrials.gov* https://clinicaltrials.gov/ct2/show/NCT02036970 (2021).

88. Arita, Y. *et al.* The efficacy of tocilizumab in a patient with pulmonary arterial hypertension associated with Castleman's disease. *Heart Vessels* 25, 444–447 (2010).

89. Liparulo, A. *et al.* Formulation and Characterization of Solid Lipid Nanoparticles Loading RF22-c, a Potent and Selective 5-LO Inhibitor, in a Monocrotaline-Induced Model of Pulmonary Hypertension. *Front Pharmacol* 11, 1 (2020).

90. Piao, L. *et al.* The inhibition of pyruvate dehydrogenase kinase improves impaired cardiac function and electrical remodeling in two models of right ventricular hypertrophy: Resuscitating the hibernating right ventricle. *J Mol Med* 88, 47–60 (2010).

91. Spiekerkoetter, E. *et al.* FK506 activates BMPR2, rescues endothelial dysfunction, and reverses pulmonary hypertension. *Journal of Clinical Investigation* 123, 3600–3613 (2013).

92. Toshner, M. *et al.* Transform-UK: A Phase 2 Trial of Tocilizumab in Pulmonary Arterial Hypertension. *Am J Respir Crit Care Med* 197, (2018).

93. Tataranni, T. & Piccoli, C. Dichloroacetate (DCA) and Cancer: An Overview towards Clinical Applications. *Oxidative Medicine and Cellular Longevity* vol. 2019 Preprint at https://doi.org/10.1155/2019/8201079 (2019).

94. Michelakis, E. D. *et al.* Inhibition of pyruvate dehydrogenase kinase improves pulmonary arterial hypertension in genetically susceptible patients. *Sci Transl Med* 9, (2017).

95. University of Alberta. Dichloroacetate (DCA) for the Treatment of Pulmonary Arterial Hypertension - Full Text View - ClinicalTrials.gov. *ClinicalTrials.gov* https://clinicaltrials.gov/ct2/show/NCT01083524 (2014).

96. Guignabert, C. *et al.* Transgenic mice overexpressing the 5-hydroxytryptamine transporter gene in smooth muscle develop pulmonary hypertension. *Circ Res* 98, 1323–1330 (2006).

97. Aiello, R. J. *et al.* Tryptophan hydroxylase 1 inhibition impacts pulmonary vascular remodeling in two rat models of pulmonary hypertension. *Journal of Pharmacology and Experimental Therapeutics* 360, 267–279 (2017).

98. Boehringer Ingelheim. Safety and Efficacy of Terbogrel in Patients With Primary Pulmonary Hypertension - Full Text View - ClinicalTrials.gov. *ClinicalTrials.gov* https://clinicaltrials.gov/ct2/show/NCT02223481 (2014).

99. Langleben, D. *et al.* Effects of the thromboxane synthetase inhibitor and receptor antagonist terbogrel in patients with primary pulmonary hypertension. *Am Heart J* 143, 4A-10A (2002).

100. Harada-Shiba, M. *et al.* Intratracheal gene transfer of adrenomedullin using polyplex nanomicelles attenuates monocrotaline-induced pulmonary hypertension in rats. *Molecular Therapy* 17, 1180–1186 (2009).

101. Kim, J. Apelin-APJ Signaling: a Potential Therapeutic Target for Pulmonary Arterial Hypertension. *Mol. Cells* 37, 196–201 (2014).

102. Chen, L. *et al.* Nanoparticle-mediated delivery of pitavastatin into lungs ameliorates the development and induces regression of monocrotaline-induced pulmonary artery hypertension. *Hypertension* 57, 343–350 (2011).

103. Bhullar, K. S. *et al.* Kinase-targeted cancer therapies: progress, challenges and future directions. *Molecular Cancer 2018 17:1* 17, 1–20 (2018).

104. Jones, R. L. & Judson, I. R. The development and application of imatinib. *Expert Opin Drug Saf* 4, 183–191 (2005).

105. Thomas, J., Wang, L., Clark, R. E. & Pirmohamed, M. Active transport of imatinib into and out of cells: implications for drug resistance. *Blood* 104, 3739–3745 (2004).

106. Nies, A. T. *et al.* Cellular uptake of imatinib into leukemic cells is independent of human organic cation transporter 1 (OCT1). *Clin Cancer Res* 20, 985–94 (2014).

107. Dohse, M. *et al.* Comparison of ATP-binding cassette transporter interactions with the tyrosine kinase inhibitors imatinib, nilotinib, and dasatinib. *Drug Metab Dispos* 38, 1371–80 (2010).

108. Ammar, M. *et al.* Overexpression of P-glycoprotein and resistance to Imatinib in chronic myeloid leukemia patients. *J Clin Lab Anal* 34, (2020).

109. Jones, R. L. & Judson, I. R. The development and application of imatinib. *Expert Opin Drug Saf* 4, 183–191 (2005).

110. Perros, F. *et al.* Platelet-derived Growth Factor Expression and Function in Idiopathic Pulmonary Arterial Hypertension. *Am J Respir Crit Care Med* 178, 81–88 (2008).

111. Rocha, A., Azevedo, I. & Soares, R. Anti-angiogenic effects of imatinib target smooth muscle cells but not endothelial cells. *Angiogenesis* 10, 279–286 (2007).

112. Chhina, M. K., Nargues, W., Grant, G. M. & Nathant, S. D. Evaluation of imatinib mesylate in the treatment of pulmonary arterial hypertension. *Future Cardiol* 6, 19–35 (2010).

113. Gao, Y., Chen, T. & Raj, J. U. Endothelial and smooth muscle cell interactions in the pathobiology of pulmonary hypertension. *Am J Respir Cell Mol Biol* 54, 451–460 (2016).

114. Ciuclan, L. *et al.* Imatinib Attenuates Hypoxia-induced Pulmonary Arterial Hypertension Pathology via Reduction in 5-Hydroxytryptamine through Inhibition of Tryptophan Hydroxylase 1 Expression. *https://doi.org/10.1164/rccm.201206-1028OC* 187, 78–89 (2013).

115. Kurakula, K. *et al.* Endothelial Dysfunction in Pulmonary Hypertension: Cause or Consequence? *Biomedicines 2021, Vol. 9, Page 57* 9, 57 (2021).

116. Sugita, T. *et al.* Lung vessel leak precedes right ventricular hypertrophy in monocrotaline-treated rats. *J Appl Physiol Respir Environ Exerc Physiol* 54, 371–374 (1983).

117. Koning, N. J. *et al.* Reduction of vascular leakage by imatinib is associated with preserved microcirculatory perfusion and reduced renal injury markers in a rat model of cardiopulmonary bypass. *Br J Anaesth* 120, 1165–1175 (2018).

118. Wu, K. *et al.* Endothelial platelet-derived growth factor-mediated activation of smooth muscle platelet-derived growth factor receptors in pulmonary arterial hypertension. *Pulm Circ* 10, 1–15 (2020).

119. Rizzo, A. N. *et al.* Imatinib attenuates inflammation and vascular leak in a clinically relevant two-hit model of acute lung injury. *Am J Physiol Lung Cell Mol Physiol* 309, L1294–L1304 (2015).

120. Aman, J., Peters, M. J. L., Weenink, C., Van Nieuw Amerongen, G. P. & Noordegraaf, A. V. Reversal of vascular leak with imatinib. *Am J Respir Crit Care Med* 188, 1171–1173 (2013).

121. Freyhaus, H. Ten *et al.* Imatinib mesylate for the treatment of pulmonary arterial hypertension. *Expert Opinion on Investigational Drugs* 21, 119–134 (2011).

122. Ghofrani, H. A., Seeger, W. & Grimminger, F. Imatinib for the Treatment of Pulmonary Arterial Hypertension. *New England Journal of Medicine* 353, 1412–1413 (2005).

123. Ghofrani, H. A. *et al.* Imatinib in Pulmonary Arterial Hypertension Patients with Inadequate Response to Established Therapy. *Am J Respir Crit Care Med* 182, 1171–1177 (2010).

124. Hoeper, M. M. *et al.* Imatinib mesylate as add-on therapy for pulmonary arterial hypertension: Results of the randomized IMPRES study. *Circulation* 127, 1128–1138 (2013).

125. Novartis Pharmaceuticals. Imatinib (QTI571) in Pulmonary Arterial Hypertension. *ClinicalTrials.gov* Preprint at https://clinicaltrials.gov/ct2/show/study/NCT00902174 (2011).

126. Frost, A. E. *et al.* Long-term safety and efficacy of imatinib in pulmonary arterial hypertension. *J Heart Lung Transplant* 34, 1366–1375 (2015).

127. Novartis Pharmaceuticals. *Extension to CQTI571A2102 to Evaluate Long-Term Safety, Tolerability and Efficacy of Imatinib in Severe Pulmonary Arterial Hypertension (PAH) . ClinicalTrials.gov* https://clinicaltrials.gov/study/NCT01392495 (2015).

128. Torchilin, V. P. Drug targeting. *European Journal of Pharmaceutical Sciences* 11, 81–91 (2000).

129. Hardenia, A. *et al.* Scientific Rationale for Designing Controlled Drug Delivery Systems. in *Basic Fundamentals of Drug Delivery* 1–28 (Academic Press, 2019). doi:10.1016/B978-0-12-817909-3.00001-7.

130. Kohane, D. S. Microparticles and Nanoparticles for Drug Delivery. *Biotechnol Bioeng* 96, 203–209 (2007).

131. Nakamura, K. *et al.* Nanoparticle-Mediated Drug Delivery System for Pulmonary Arterial Hypertension. *J Clin Med* 6, 48 (2017).

132. Brenner, J. S., Greineder, C., Shuvaev, V. & Muzykantov, V. Endothelial nanomedicine for the treatment of pulmonary disease. *Expert Opin Drug Deliv* 12, 239–261 (2014).

133. García, M. C. Stimuli-responsive nanogels as promising carriers for controlled delivery of anticancer therapeutics. *Stimuli-Responsive Nanocarriers* 429–450 (2022) doi:10.1016/B978-0-12-824456-2.00005-9.

134. Greish, K. Enhanced permeability and retention (EPR) effect for anticancer nanomedicine drug targeting. *Methods Mol Biol* 624, 25–37 (2010).

135. Iyer, A. K., Khaled, G., Fang, J. & Maeda, H. Exploiting the enhanced permeability and retention effect for tumor targeting. *Drug Discov Today* 11, 812–818 (2006).

136. Nichols, J. W. & Bae, Y. H. EPR: Evidence and fallacy. *Journal of Controlled Release* 190, 451–464 (2014).

137. Swider, E. *et al.* Customizing poly(lactic-co-glycolic acid) particles for biomedical applications. *Acta Biomater* 73, 38–51 (2018).

138. Laskinc, D. L. & Patrick J. Sinkoa Hilliard L. Kutschera Piyun Chaoa, M. D. Y. S. P. H. L. B. J. D. C. R. S. S. Threshold size for optimal passive pulmonary targeting and retention of rigid microparticles in rats. *Journal of Controlled Release* 143, 31–37 (2010).

139. Holmannova, D., Borsky, P., Svadlakova, T., Borska, L. & Fiala, Z. Carbon Nanoparticles and Their Biomedical Applications. *Applied Sciences 2022, Vol. 12, Page 7865* 12, 7865 (2022).

140. Joudeh, N. & Linke, D. Nanoparticle classification, physicochemical properties, characterization, and applications: a comprehensive review for biologists. *Journal of Nanobiotechnology 2022 20:1* 20, 1–29 (2022).

141. Ealias, A. M. & Saravanakumar, M. P. A review on the classification, characterisation, synthesis of nanoparticles and their application. *IOP Conf Ser Mater Sci Eng* 263, 032019 (2017).

142. Lu, H., Zhang, S., Wang, J. & Chen, Q. A Review on Polymer and Lipid-Based Nanocarriers and Its Application to Nano-Pharmaceutical and Food-Based Systems. *Front Nutr* 8, 783831 (2021).

143. Mitchell, M. J. *et al.* Engineering precision nanoparticles for drug delivery. *Nat Rev Drug Discov* 20, 101–124 (2021).

144. Begines, B. *et al.* Polymeric Nanoparticles for Drug Delivery: Recent Developments and Future Prospects. *Nanomaterials* 10, 1403 (2020).

145. Kapoor, D. N. *et al.* PLGA: A unique polymer for drug delivery. *Therapeutic Delivery* vol. 6 41–58 Preprint at https://doi.org/10.4155/tde.14.91 (2015).

146. Chung, T. W., Tsai, Y. L., Hsieh, J. H. & Tsai, W. J. Different ratios of lactide and glycolide in PLGA affect the surface property and protein delivery characteristics of the PLGA microspheres with hydrophobic additives. *J Microencapsul* 23, 15–27 (2008).

147. Fredenberg, S., Wahlgren, M., Reslow, M. & Axelsson, A. The mechanisms of drug release in poly(lactic-co-glycolic acid)-based drug delivery systems—A review. *Int J Pharm* 415, 34–52 (2011).

148. Husmann, M., Schenderlein, S., Lück, M., Lindner, H. & Kleinebudde, P. Polymer erosion in PLGA microparticles produced by phase separation method. *Int J Pharm* 242, 277–280 (2002).

149. Fredenberg, S., Wahlgren, M., Reslow, M. & Axelsson, A. The mechanisms of drug release in poly(lactic-co-glycolic acid)-based drug delivery systems - A review. *Int J Pharm* 415, 34–52 (2011).

150. Clemons, T. D. *et al.* Distinction between Active and Passive Targeting of Nanoparticles Dictate Their Overall Therapeutic Efficacy. *Langmuir* 34, 15343–15349 (2018).

151. Domínguez-Ríos, R. *et al.* Cisplatin-loaded PLGA nanoparticles for HER2 targeted ovarian cancer therapy. *Colloids Surf B Biointerfaces* 178, 199–207 (2019).

152. Patel, J. *et al.* Targeted delivery of monoclonal antibody conjugated docetaxel loaded PLGA nanoparticles into EGFR overexpressed lung tumour cells. *J Microencapsul* 35, 204–217 (2018).

153. Khan, I. *et al.* Biodegradable nano-architectural PEGylated approach for the improved stability and anticancer efficacy of bendamustine. *Int J Biol Macromol* 92, 1242–1251 (2016).

154. Tuyen Dao, T. P. *et al.* A new formulation of curcumin using poly (lactic-co-glycolic acid)—polyethylene glycol diblock copolymer as carrier material. *Advances in Natural Sciences: Nanoscience and Nanotechnology* 5, 035013 (2014).

155. Gu, F., Langer, R. & Farokhzad, O. C. Formulation/preparation of functionalized nanoparticles for in vivo targeted drug delivery. *Methods Mol Biol* 544, 589–598 (2009).

156. Patil, M. A. *et al.* Targeted delivery of YSA-functionalized and non-functionalized polymeric nanoparticles to injured pulmonary vasculature. *Artif Cells Nanomed Biotechnol* 46, 1059–1066 (2018).

157. Juan, A. *et al.* An Overview of Antibody Conjugated Polymeric Nanoparticles for Breast Cancer Therapy. *Pharmaceutics 2020, Vol. 12, Page 802* 12, 802 (2020).

158. Beck, A., Goetsch, L., Dumontet, C. & Corvaïa, N. Strategies and challenges for the next generation of antibody–drug conjugates. *Nature Reviews Drug Discovery 2017 16:5* 16, 315–337 (2017).

159. Meldal, M. & Tomøe, C. W. Cu-catalyzed azide-alkyne cycloaddition. *Chem Rev* 108, 2952–3015 (2008).

160. Pickens, C. J., Johnson, S. N., Pressnall, M. M., Leon, M. A. & Berkland, C. J. Practical Considerations, Challenges, and Limitations of Bioconjugation via Azide-Alkyne Cycloaddition. *Bioconjug Chem* 29, 686 (2018).

161. Marques, A. C., Costa, P. J., Velho, S. & Amaral, M. H. Functionalizing nanoparticles with cancer-targeting antibodies: A comparison of strategies. *Journal of Controlled Release* 320, 180–200 (2020).

162. Hermanson, G. T. 2 - The Chemistry of Reactive Groups. in *Bioconjugate Techniques* 137–166 (Academic Press, 1996). doi:10.1016/B978-012342335-1/50003-8.

163. Chen, H. *et al.* Preparation and characterization of PE38KDEL-loaded anti-HER2 nanoparticles for targeted cancer therapy. *Journal of Controlled Release* 128, 209–216 (2008).

164. Banstola, A., Duwa, R., Emami, F., Jeong, J. H. & Yook, S. Enhanced caspase-mediated abrogation of autophagy by temozolomide-loaded and panitumumab-conjugated poly(lactic- co-glycolic acid) nanoparticles in epidermal growth factor receptor overexpressing glioblastoma cells. *Mol Pharm* 17, 4386–4400 (2020).

165. Liu, J. *et al.* Anti-Angiogenic Activity Of Bevacizumab-Bearing Dexamethasone-Loaded PLGA Nanoparticles For Potential Intravitreal Applications. *Int J Nanomedicine* 14, 8819–8834 (2019).

166. Zhou, Y. *et al.* Anti-CD206 antibody-conjugated Fe3O4-based PLGA nanoparticles selectively promote tumor-associated macrophages to polarize to the pro-inflammatory subtype. *Oncol Lett* 20, 1–1 (2020).

167. Moura, C. C., Segundo, M. A., das Neves, J., Reis, S. & Sarmento, B. Co-association of methotrexate and SPIONs into anti-CD64 antibody-conjugated PLGA nanoparticles for theranostic application. *Int J Nanomedicine* 9, 4911–4922 (2014).

168. Hu, H. *et al.* Hyaluronic acid-coated and Olaparib-loaded PEI − PLGA nanoparticles for the targeted therapy of triple negative breast cancer. *Journal of Microencapsulation* 39, 25–36 (2021).

169. Zumaya, A. L. V. ; *et al.* Antibody Conjugated PLGA Nanocarriers and Superparmagnetic Nanoparticles for Targeted Delivery of Oxaliplatin to Cells from Colorectal Carcinoma. *Int J Mol Sci* 12, (2022).

170. Manoochehri, S. *et al.* Surface modification of PLGA nanoparticles via human serum albumin conjugation for controlled delivery of docetaxel. *DARU Journal of Pharmaceutical Sciences* 21, 58 (2013).

171. Zhong, S. *et al.* Herceptin-decorated paclitaxel-loaded poly(lactide-co-glycolide) nanobubbles: ultrasound-facilitated release and targeted accumulation in breast cancers. *Pharm Dev Technol* 25, 454–463 (2020).

172. McCarron, P. A. *et al.* Antibody targeting of camptothecin-loaded PLGA nanoparticles to tumor cells. *Bioconjug Chem* 19, 1561–1569 (2008).

173. Zhang, N., Chittasupho, C., Duangrat, C., Siahaan, T. J. & Berkland, C. PLGA nanoparticle-peptide conjugate effectively targets intercellular cell-adhesion molecule-1. *Bioconjug Chem* 19, 145–152 (2008).

174. Kocbek, P., Obermajer, N., Cegnar, M., Kos, J. & Kristl, J. Targeting cancer cells using PLGA nanoparticles surface modified with monoclonal antibody. *Journal of Controlled Release* 120, 18–26 (2007).

175. Jahan, S. T. & Haddadi, A. Investigation and optimization of formulation parameters on preparation of targeted anti-CD205 tailored PLGA nanoparticles. *Int J Nanomedicine* 10, 7371 (2015).

176. Mo, Y. & Lim, L. Y. Preparation and in vitro anticancer activity of wheat germ agglutinin (WGA)-conjugated PLGA nanoparticles loaded with paclitaxel and isopropyl myristate. *Journal of Controlled Release* 107, 30–42 (2005).

177. Srinivasan, S. *et al.* Targeted nanoparticles for simultaneous delivery of chemotherapeutic and hyperthermia agents – An in vitro study. *J Photochem Photobiol B* 136, 81–90 (2014).

178. Khan, I. *et al.* Nano-Co-Delivery of Berberine and Anticancer Drug Using PLGA Nanoparticles: Exploration of Better Anticancer Activity and In Vivo Kinetics. *Pharm Res* 36, 1–17 (2019).

179. Smith, P. K. *et al.* Measurement of protein using bicinchoninic acid. *Anal Biochem* 150, 76–85 (1985).

180. Clayden, J., Greeves, N. & Warren, S. 3 Determining organic structures. in *Organic Chemistry* 52–63 (Oxford University Press, 2012).

181. Smith, C. B. Organic Nitrogen Compounds, VII: Amides—The Rest of the Story. *Spectroscopy* 35, 10–15 (2020).

182. Soderberg, T. Structure determination, part II: Nuclear magnetic resonance spectroscopy. in *Organic Chemistry with a Biological Emphasis Volume I* vol. 1 (Chemistry Publications, 2019).

183. Herzenberg, L. A., De Rosa, S. C. & Herzenberg, L. A. Monoclonal antibodies and the FACS: Complementary tools for immunobiology and medicine. *Immunol Today* 21, 383–390 (2000).

184. Joshi, S. & Yu, D. Immunofluorescence. *Basic Science Methods for Clinical Researchers* 135–150 (2017) doi:10.1016/B978-0-12-803077-6.00008-4.

185. Cerda-Kipper, A. S., Montiel, B. E. & Hosseini, S. Immunoassays | Radioimmunoassays and Enzyme-Linked Immunosorbent Assay. *Encyclopedia of Analytical Science* 55–75 (2019) doi:10.1016/B978-0-12-409547-2.14510-X.

186. Sakamoto, S. *et al.* Enzyme-linked immunosorbent assay for the quantitative/qualitative analysis of plant secondary metabolites. *J Nat Med* 72, 32 (2017).

187. Greene, M. K. *et al.* Forming next-generation antibody–nanoparticle conjugates through the oriented installation of non-engineered antibody fragments. *Chem Sci* 9, 79–87 (2017).

188. Vashist, S. K. Comparison of 1-Ethyl-3-(3-Dimethylaminopropyl) Carbodiimide Based Strategies to Crosslink Antibodies on Amine-Functionalized Platforms for Immunodiagnostic Applications. *Diagnostics* 2, 23 (2012).

189. Gupta, V. *et al.* Inhaled PLGA Particles of Prostaglandin E1 Ameliorate Symptoms and Progression of Pulmonary Hypertension at a Reduced Dosing Frequency. *Mol Pharm* 10, 1655 (2013).

190. Hanna, L. A., Basalious, E. B. & ELGazayerly, O. N. Respirable controlled release polymeric colloid (RCRPC) of bosentan for the management of pulmonary hypertension: *in vitro* aerosolization, histological examination and *in vivo* pulmonary absorption. *Drug Deliv* 24, 188–198 (2017).

191. Shahin, H. *et al.* Formulation and optimization of sildenafil citrate-loaded PLGA large porous microparticles using spray freeze-drying technique: A factorial design and in-vivo pharmacokinetic study. *Int J Pharm* 597, 120320 (2021).

192. Rashid, J. *et al.* Inhaled sildenafil as an alternative to oral sildenafil in the treatment of pulmonary arterial hypertension (PAH). *J Control Release* 250, 96–106 (2017).

193. Almutairi, M. *et al.* Formulation and evaluation of inhaled Sildenafil-loaded PLGA microparticles for treatment of pulmonary arterial hypertension (PAH): A novel high drug loaded formulation and scalable process via hot melt extrusion technology (Part Ⅰ). *Int J Pharm* 655, 124044 (2024).

194. Zhang, H. *et al.* Microfluidic fabrication of inhalable large porous microspheres loaded with H2S-releasing aspirin derivative for pulmonary arterial hypertension therapy. *Journal of Controlled Release* 329, 286–298 (2021).

195. Varshosaz, J., Taymouri, S., Hamishehkar, H., Vatankhah, R. & Yaghubi, S. Development of dry powder inhaler containing tadalafil-loaded PLGA nanoparticles. *Res Pharm Sci* 12, 222 (2017).

196. Devadasu, V. R., Wadsworth, R. M. & Ravi Kumar, M. N. V. Tissue localization of nanoparticles is altered due to hypoxia resulting in poor efficacy of curcumin nanoparticles in pulmonary hypertension. *European Journal of Pharmaceutics and Biopharmaceutics* 80, 578–584 (2012).

197. Zheng, Y. *et al.* Fatty Oil of Descurainia Sophia Nanoparticles Improve Monocrotaline-Induced Pulmonary Hypertension in Rats Through PLC/IP3R/Ca2+ Signaling Pathway. *Int J Nanomedicine* 18, 7483–7503 (2023).

198. Acharya, A. P. *et al.* Simultaneous Pharmacologic Inhibition of Yes-Associated Protein 1 and Glutaminase 1 via Inhaled Poly(Lactic-co-Glycolic) Acid–Encapsulated Microparticles Improves Pulmonary Hypertension. *Journal of the American Heart Association: Cardiovascular and Cerebrovascular Disease* 10, 19091 (2021).

199. Rashid, J., Nozik-Grayck, E., Mcmurtry, I. F., Stenmark, K. R. & Ahsan, F. Inhaled combination of sildenafil and rosiglitazone improves pulmonary hemodynamics, cardiac function, and arterial remodeling. *Am J Physiol Lung Cell Mol Physiol* 316, L119–L130 (2019).

200. Labiris, N. R. & Dolovich, M. B. Pulmonary drug delivery. Part I: Physiological factors affecting therapeutic effectiveness of aerosolized medications. *Br J Clin Pharmacol* 56, 588–599 (2003).

201. Shah, A. J., Beckmann, T., Vorla, M. & Kalra, D. K. New Drugs and Therapies in Pulmonary Arterial Hypertension. *International Journal of Molecular Sciences 2023, Vol. 24, Page 5850* 24, 5850 (2023).

202. Obata, H. *et al.* Single injection of a sustained-release prostacyclin analog improves pulmonary hypertension in rats. *Am J Respir Crit Care Med* 177, 195–201 (2008).

203. Akagi, S. *et al.* Intratracheal administration of prostacyclin analogue-incorporated nanoparticles ameliorates the development of monocrotaline and sugen-hypoxia-induced pulmonary arterial hypertension. *J Cardiovasc Pharmacol* 67, 290–298 (2016).

204. Rashid, J. *et al.* Repurposing rosiglitazone, a PPAR-γ agonist and oral antidiabetic, as an inhaled formulation, for the treatment of PAH. *J Control Release* 280, 113–123 (2018).

205. Varshosaz, J., Taymouri, S., Hamishehkar, H., Vatankhah, R. & Yaghubi, S. Development of dry powder inhaler containing tadalafil-loaded PLGA nanoparticles. *Res Pharm Sci* 12, 222 (2017).

206. Liu, B. *et al.* Endothelial PHD2 deficiency induces nitrative stress via suppression of caveolin-1 in pulmonary hypertension. *European Respiratory Journal* 60, (2022).

207. Gupta, B. *et al.* Effects of Formulation Variables on the Particle Size and Drug Encapsulation of Imatinib-Loaded Solid Lipid Nanoparticles. *AAPS PharmSciTech* 17, 652–662 (2016).

208. Molaahmadi, M. R., Varshosaz, J., Taymouri, S. & Akbari, V. Lipid Nanocapsules for Imatinib Delivery: Design, Optimization and Evaluation of Anticancer Activity Against Melanoma Cell Line. *Iranian Journal of Pharmaceutical Research* 18, 1676–1693 (2019).

209. Khan, A. M., Ahmad, F. J., Panda, A. K. & Talegaonkar, S. Investigation of imatinib loaded surface decorated biodegradable nanocarriers against glioblastoma cell lines: Intracellular uptake and cytotoxicity studies. *Int J Pharm* 507, 61–71 (2016).

210. Bhattacharya, S. Fabrication and characterization of chitosan-based polymeric nanoparticles of Imatinib for colorectal cancer targeting application. *Int J Biol Macromol* 151, 104–115 (2020).

211. Saka, R., Chella, N. & Khan, W. Development of Imatinib Mesylate-Loaded Liposomes for Nose to Brain Delivery: In Vitro and In Vivo Evaluation. *AAPS PharmSciTech* 22, (2021).

212. Sadat Shandiz, S. A. *et al.* Novel imatinib-loaded silver nanoparticles for enhanced apoptosis of human breast cancer MCF-7 cells. *http://dx.doi.org/10.1080/21691401.2016.1202257* 45, 1082–1091 (2016).

213. Hasandoost, L., Akbarzadeh, A., Attar, H. & Heydarinasab, A. In vitro effect of imatinib mesylate loaded on polybutylcyanoacrylate nanoparticles on leukemia cell line K562. *http://dx.doi.org/10.1080/21691401.2016.1175444* 45, 665–669 (2016).

214. Bhattacharya, S. Double w/o/w self-nano emulsifying drug delivery system of imatinib mesylate for colon cancer treatment. *J Mol Liq* 341, 117368 (2021).

215. Liu, Z. *et al.* Sequential release of paclitaxel and imatinib from core–shell microparticles prepared by coaxial electrospray for vaginal therapy of cervical cancer. *Int J Mol Sci* 22, (2021).

216. Sobierajska, P., Serwotka-Suszczak, A., Szymanski, D., Marycz, K. & Wiglusz, R. J. Nanohydroxyapatite-Mediated Imatinib Delivery for Specific Anticancer Applications. *Molecules 2020, Vol. 25, Page 4602* 25, 4602 (2020).

217. Li, Y., Yang, B. & Zhang, X. Oral delivery of imatinib through galactosylated polymeric nanoparticles to explore the contribution of a saccharide ligand to absorption. *Int J Pharm* 568, 118508 (2019).

218. Sridhar, R. & Ramakrishna, S. Electrosprayed nanoparticles for drug delivery and pharmaceutical applications. *Biomatter* vol. 3 Preprint at https://doi.org/10.4161/biom.24281 (2013).

219. MODAN, E. M. & PLĂIAȘU, A. G. Advantages and Disadvantages of Chemical Methods in the Elaboration of Nanomaterials. *The Annals of "Dunarea de Jos" University of Galati. Fascicle IX, Metallurgy and Materials Science* 43, 53–60 (2020).

220. Fonte, P. *et al.* Effect of cryoprotectants on the porosity and stability of insulin-loaded PLGA nanoparticles after freeze-drying. *Biomatter* 2, 329 (2012).

221. Zhao, S. *et al.* Application advance of electrosprayed micro/nanoparticles based on natural or synthetic polymers for drug delivery system. *Mater Des* 220, 110850 (2022).

222. Nguyen, D. N., Clasen, C. & van den Mooter, G. Pharmaceutical Applications of Electrospraying. *Journal of Pharmaceutical Sciences* vol. 105 2601–2620 Preprint at https://doi.org/10.1016/j.xphs.2016.04.024 (2016).

223. Wang, J., Jansen, J. A. & Yang, F. Electrospraying: Possibilities and challenges of engineering carriers for biomedical applications - a mini review. *Frontiers in Chemistry* vol. 7 258 Preprint at https://doi.org/10.3389/fchem.2019.00258 (2019).

224. Luoh, R. & Hahn, H. T. Electrospun nanocomposite fiber mats as gas sensors. *Compos Sci Technol* 66, 2436–2441 (2006).

225. Dey, A. Semiconductor metal oxide gas sensors: A review. *Materials Science and Engineering B: Solid-State Materials for Advanced Technology* vol. 229 206–217 Preprint at https://doi.org/10.1016/j.mseb.2017.12.036 (2018).

226. Prabhakaran, M. P., Zamani, M., Felice, B. & Ramakrishna, S. Electrospraying technique for the fabrication of metronidazole contained PLGA particles and their release profile. *Materials Science and Engineering: C* 56, 66–73 (2015).

227. Parhizkar, M. *et al.* Electrohydrodynamic encapsulation of cisplatin in poly (lactic-co-glycolic acid) nanoparticles for controlled drug delivery. *Nanomedicine* 12, 1919–1929 (2016).

228. Xie, J., Marijnissen, J. C. M. & Wang, C. H. Microparticles developed by electrohydrodynamic atomization for the local delivery of anticancer drug to treat C6 glioma in vitro. *Biomaterials* 27, 3321–3332 (2006).

229. Chatterjee, M. *et al.* Electrospray-based synthesis of fluorescent poly(d , l -lactide- co -glycolide) nanoparticles for the efficient delivery of an anticancer drug and self-monitoring its effect in drug-resistant breast cancer cells. *Mater Adv* 1, 3033–3048 (2020).

230. Zhang, Y., Shams, T., Harker, A. H., Parhizkar, M. & Edirisinghe, M. Effect of copolymer composition on particle morphology and release behavior in vitro using progesterone. *Mater Des* 159, 57–67 (2018).

231. Kibler, E. *et al.* Electrosprayed poly(lactic-co-glycolic acid) particles as a promising drug delivery system for the novel JNK inhibitor IQ-1. *Eur Polym J* 127, 109598 (2020).

232. Boda, S. K., Li, X. & Xie, J. Electrospraying an enabling technology for pharmaceutical and biomedical applications: A review. *J Aerosol Sci* 125, 164–181 (2018).

233. The Editors of Encyclopaedia Britannica. Cohesion. *Encyclopaedia Britannica* https://www.britannica.com/science/cohesion.

234. von Fraunhofer, J. A. Adhesion and Cohesion. *Int J Dent* 2012, (2012).

235. Lord Rayleigh F.R.S. XX. On the equilibrium of liquid conducting masses charged with electricity. *The London, Edinburgh, and Dublin Philosophical Magazine and Journal of Science* 14, 184–186 (1882).

236. Xu, Y. & Hanna, M. A. Electrospray encapsulation of water-soluble protein with polylactide: Effects of formulations on morphology, encapsulation efficiency and release profile of particles. *Int J Pharm* 320, 30–36 (2006).

237. WANG. *Introduction to Electrospinning*. *Electrospinning for tissue regeneration* / (Woodhead Pub, Oxford ; Cambridge :, 2011). doi:10.1533/9780857092915.1.3.

238. Pelofsky, A. H. Surface Tension-Viscosity Relation for Liquids. *J Chem Eng Data* 11, 394–397 (1966).

239. Hsu, M. Y., Feng, C. H., Liu, Y. W. & Liu, S. J. An Orthogonal Model to Study the Effect of Electrospraying Parameters on the Morphology of poly (d,l)-lactide-co-glycolide (PLGA) Particles. *Applied Sciences 2019, Vol. 9, Page 1077* 9, 1077 (2019).

240. Liu, X. *et al.* Electrospinnability of Poly Lactic-co-glycolic Acid (PLGA): the Role of Solvent Type and Solvent Composition. *Pharm Res* 34, 738–749 (2017).

241. Xu, J. *et al.* Studies on preparation and formation mechanism of poly(lactide-co-glycolide) microrods via one-step electrospray and an application for drug delivery system. *Eur Polym J* 148, 110372 (2021).

242. Nguyen, T. T. & Jeong, J. H. Development of a single-jet electrospray method for producing quercetin-loaded poly (lactic-co-glycolic acid) microspheres with prolonged-release patterns. *J Drug Deliv Sci Technol* 47, 268–274 (2018).

243. Parhizkar, M. *et al.* Performance of novel high throughput multi electrospray systems for forming of polymeric micro/nanoparticles. *Mater Des* 126, 73–84 (2017).

244. Reardon, P. *et al.* Electrohydrodynamic Fabrication of Core-Shell PLGA Nanoparticles with Controlled Release of Cisplatin for Enhanced Cancer Treatment. *Int J Nanomedicine* 12–3913 (2017) doi:10.2147/IJN.S134833.

245. Kadivar, N., Tavanai, H. & Allafchian, A. Fabrication of cellulose nanoparticles through electrospraying. *IET Nanobiotechnol* 12, 807 (2018).

246. Sigma-Aldrich. DICHLOROMETHANE SAFETY DATA SHEET . *Sigma-Aldrich* (2023).

247. ThermoFisher Scientific. N,N-Dimethylacetamide Safety Data Sheet. *ThermoFisher Scientific* 1–8 https://www.fishersci.com/store/msds?partNumber=D1601&productDescription=N%2CN-DIMETHYLACETAMIDE+GC+HS+1L&vendorId=VN00033897&countryCode=US&language=en (2023).

248. Sigma-Aldrich. TETRAHYDROFURAN SAFETY DATA SHEET. *Sigma-Aldrich* 1–24 (2024).

249. Sigma-Aldrich. ACETONE SAFETY DATA SHEET. *Sigma-Aldrich* 1–24 (2024).

250. Smeets, A., Clasen, C. & Van den Mooter, G. Electrospraying of polymer solutions: Study of formulation and process parameters. *European Journal of Pharmaceutics and Biopharmaceutics* 119, 114–124 (2017).

251. Bock, N., Woodruff, M. A., Hutmacher, D. W. & Dargaville, T. R. Electrospraying, a reproducible method for production of polymeric microspheres for biomedical applications. *Polymers (Basel)* 3, 131–149 (2011).

252. Bock, N., Dargaville, T. R. & Woodruff, M. A. Electrospraying of polymers with therapeutic molecules: State of the art. *Prog Polym Sci* 37, 1510–1551 (2012).

253. Wang, F. *et al.* Machine learning to empower electrohydrodynamic processing. *Materials Science and Engineering* 132, 112553 (2022).

254. Corbion. Bioresorbable polymer portfolio . *Corbion* https://www.corbion.com/Products/Biomedical-products/purasorb.

255. MedChem Express. Imatinib. *MedChem Express* https://www.bioscience.co.uk/product~922107.

256. Iqbal, N. & Iqbal, N. Imatinib: A Breakthrough of Targeted Therapy in Cancer. *Chemother Res Pract* 2014, 1–9 (2014).

257. Al-Hadiya, B. M. H., Bakheit, A. H. H. & Abd-Elgalil, A. A. Imatinib Mesylate. in *Profiles of Drug Substances, Excipients and Related Methodology* vol. 39 265–297 (Academic Press, 2014).

258. Sigma-Aldrich. Rhodamine B. *Sigma-Aldrich* https://www.sigmaaldrich.com/GB/en/product/sigma/83689#.

259. Giard, D. J. *et al.* In Vitro Cultivation of Human Tumors: Establishment of Cell Lines Derived From a Series of Solid Tumors. *JNCI: Journal of the National Cancer Institute* 51, 1417–1423 (1973).

260. Fearnley, G. W. *et al.* Vascular endothelial growth factor a-stimulated signaling from endosomes in primary endothelial cells. *Methods Enzymol* 535, 265–292 (2014).

261. Nesterova, A. P. *et al.* Diseases of the circulatory system. *Disease Pathways* 327–390 (2020) doi:10.1016/B978-0-12-817086-1.00008-7.

262. Solinc, J. *et al.* The Platelet-Derived Growth Factor Pathway in Pulmonary Arterial Hypertension: Still an Interesting Target? *Life* 12, (2022).

263. Bogdanovich, S. *et al.* Human IgG1 antibodies suppress angiogenesis in a target-independent manner. *Signal Transduct Target Ther* 1, 15001 (2016).

264. Thermo Fisher Scientific. EDC (1-ethyl-3-(3-dimethylaminopropyl)carbodiimide hydrochloride). *Thermo Fisher Scientific* https://www.thermofisher.com/order/catalog/product/22980 (2017).

265. Grabarek, Z. & Gergely, J. Zero-length crosslinking procedure with the use of active esters. *Anal Biochem* 185, 131–135 (1990).

266. Thermo Fisher Scientific. NHS (N-hydroxysuccinimide). *Thermo Fisher Scientific* https://www.thermofisher.com/order/catalog/product/24500 (2020).

267. Staros, J. V., Wright, R. W. & Swingle, D. M. Enhancement by N-hydroxysulfosuccinimide of water-soluble carbodiimide-mediated coupling reactions. *Anal Biochem* 156, 220–222 (1986).

268. Zwitterionic buffer. *Oxford Dictionary of Biochemistry and Molecular Biology* (2006) doi:10.1093/ACREF/9780198529170.001.0001.

269. Santa Cruz Biotechnology. MES . *Santa Cruz Biotechnology* https://www.scbt.com/p/mes-4432-31-9.

270. Bio X Cell. Antibody Structure. https://bioxcell.com/educational-articles/antibody-structure/ (2024).

271. Antonis, N. What is SEM? Scanning Electron Microscopy Explained. *ThermoFisher Scientific* https://www.thermofisher.com/blog/materials/what-is-sem-scanning-electron-microscopy-explained/ (2019).

272. Scanning Electron Microscopy (SEM). *Electron Microscopy of Polymers* 87–120 (2008) doi:10.1007/978-3-540-36352-1_5.

273. Joy, D. C. , Ford, B. J. , & Bradbury, S. Scanning electron microscope (SEM) . *Encyclopedia Britannica* https://www.britannica.com/technology/scanning-electron-microscope (2024).

274. Kaszuba, M., Corbett, J., Watson, F. M. N. & Jones, A. High-concentration zeta potential measurements using light-scattering techniques. *Philosophical Transactions of the Royal Society A: Mathematical, Physical and Engineering Sciences* 368, 4439–4451 (2010).

275. Dutta, A. Fourier Transform Infrared Spectroscopy. *Spectroscopic Methods for Nanomaterials Characterization* 2, 73–93 (2017).

276. Thermo Nicolet Corporation. *Introduction to Fourier Transform Infrared Spectrometry*. (2001).

277. Picollo, M., Aceto, M. & Vitorino, T. UV-Vis spectroscopy. *Physical Sciences Reviews* 4, (2019).

278. Yadav, L. D. S. Ultraviolet (UV) and Visible Spectroscopy. in *Organic Spectroscopy* 7–51 (Springer, Dordrecht, 2005). doi:10.1007/978-1-4020-2575-4_2.

279. Patil, R., Kale, A., Mane, D. & Patil, D. Isolation, culture and characterization of primary cell lines of human buccal mucosal fibroblasts: A combination of explant enzamytic technique. *Journal of Oral and Maxillofacial Pathology* 24, 68–75 (2020).

280. Lichtman, J. W. & Conchello, J.-A. Fluorescence microscopy. (2005) doi:10.1038/NMETH817.

281. Ghasemi, M., Turnbull, T., Sebastian, S. & Kempson, I. The mtt assay: Utility, limitations, pitfalls, and interpretation in bulk and single-cell analysis. *Int J Mol Sci* 22, (2021).

282. Supino, R. MTT assays. *Methods Mol Biol* 43, 137–149 (1995).

283. Uggeri, J. *et al.* Calcein-AM is a detector of intracellular oxidative activity. *Histochem Cell Biol* 122, 499–505 (2004).

284. Thermo Fisher Scientific. Bioconjugation and crosslinking technical handbook. *Thermo Fisher Scientific* (2018).

285. Shen, C.-H. Quantification and analysis of proteins. in *Diagnostic Molecular Biology* 231–257 (Academic Press, 2023). doi:10.1016/B978-0-323-91788-9.00002-8.

286. Thermo Fisher Scientific. PierceTM BCA Protein Assay Kit. *Thermo Fisher Scientific Inc* https://www.thermofisher.com/bcafaqs (2020).

287. Bothwell, J. H. F. & Griffin, J. L. An introduction to biological nuclear magnetic resonance spectroscopy. *Biological Reviews* 86, 493–510 (2011).

288. Alhajj M & Farhana A. Enzyme Linked Immunosorbent Assay - StatPearls - NCBI Bookshelf. *StatPearls* (2022).

289. McKinnon, K. M. Flow Cytometry: An Overview. *Curr Protoc Immunol* 120, 5.1.1-5.1.11 (2018).

290. Morais, A. Í. S. *et al.* Fabrication of polymeric microparticles by electrospray: The impact of experimental parameters. *J Funct Biomater* 11, (2020).

291. Burgess, D. J., Hussain, A. S., Ingallinera, T. S. & Chen, M. L. Assuring quality and performance of sustained and controlled release parenterals: AAPS workshop report, co-sponsored by FDA and USP. *Pharm Res* 19, 1761–1768 (2002).

292. Faisant, N., Akiki, J., Siepmann, F., Benoit, J. P. & Siepmann, J. Effects of the type of release medium on drug release from PLGA-based microparticles: Experiment and theory. *Int J Pharm* 314, 189–197 (2006).

293. Jaworek, A. & Sobczyk, A. T. Electrospraying route to nanotechnology: An overview. *J Electrostat* 66, 197–219 (2008).

294. Castro Coelho, S., Nogueiro Estevinho, B. & Rocha, F. Encapsulation in food industry with emerging electrohydrodynamic techniques: Electrospinning and electrospraying – A review. *Food Chem* 339, 127850 (2021).

295. Anu Bhushani, J. & Anandharamakrishnan, C. Electrospinning and electrospraying techniques: Potential food based applications. *Trends in Food Science and Technology* vol. 38 21–33 Preprint at https://doi.org/10.1016/j.tifs.2014.03.004 (2014).

296. Shenoy, S. L., Bates, W. D., Frisch, H. L. & Wnek, G. E. Role of chain entanglements on fiber formation during electrospinning of polymer solutions: good solvent, non-specific polymer–polymer interaction limit. *Polymer (Guildf)* 46, 3372–3384 (2005).

297. Festag, R. *et al.* Effects of molecular entanglements during electrospray of high molecular weight polymers. *J Am Soc Mass Spectrom* 9, 299–304 (1998).

298. Rodríguez-Tobías, H., Morales, G. & Grande, D. Comprehensive review on electrospinning techniques as versatile approaches toward antimicrobial biopolymeric composite fibers. *Materials Science and Engineering: C* 101, 306–322 (2019).

299. Giménez, V. M. *et al.* Preparation and characterization of bosentan monohydrate/ε-polycaprolactone nanoparticles obtained by electrospraying. *Biotechnol Prog* 35, e2748 (2019).

300. Park, C. H. & Lee, J. Electrosprayed polymer particles: Effect of the solvent properties. *J Appl Polym Sci* 114, 430–437 (2009).

301. Trotta, M., Cavalli, R., Trotta, C., Bussano, R. & Costa, L. Electrospray technique for solid lipid-based particle production. *Drug Dev Ind Pharm* 36, 431–438 (2010).

302. Castro Coelho, S., Nogueiro Estevinho, B. & Rocha, F. Encapsulation in food industry with emerging electrohydrodynamic techniques: Electrospinning and electrospraying – A review. *Food Chem* 339, 127850 (2021).

303. Xie, J., Lim, L. K., Phua, Y., Hua, J. & Wang, C. H. Electrohydrodynamic atomization for biodegradable polymeric particle production. *J Colloid Interface Sci* 302, 103–112 (2006).

304. Ito, F. *et al.* Study of types and mixture ratio of organic solvent used to dissolve polymers for preparation of drug-containing PLGA microspheres. *Eur Polym J* 45, 658–667 (2009).

305. Horibe, H. *et al.* Quantification of the solvent evaporation rate during the production of three PVDF crystalline structure types by solvent casting. *Polym J* 46, 104–110 (2014).

306. Yao, J., Kuang Lim, L., Xie, J., Hua, J. & Wang, C. H. Characterization of electrospraying process for polymeric particle fabrication. *J Aerosol Sci* 39, 987–1002 (2008).

307. Tapia-Hernández, J. A., Rodríguez-Félix, F. & Katouzian, I. Nanocapsule formation by electrospraying. *Nanoencapsulation Technologies for the Food and Nutraceutical Industries* 320–345 (2017) doi:10.1016/B978-0-12-809436-5.00009-4.

308. Meng, F., Jiang, Y., Sun, Z., Yin, Y. & Li, Y. Electrohydrodynamic liquid atomization of biodegradable polymer microparticles: Effect of electrohydrodynamic liquid atomization variables on microparticles. *J Appl Polym Sci* 113, 526–534 (2009).

309. Platel, A. *et al.* Influence of the surface charge of PLGA nanoparticles on their in vitro genotoxicity, cytotoxicity, ROS production and endocytosis. *J Appl Toxicol* 36, 434–444 (2016).

310. Cao, Y., Wang, B., Wang, Y. & Lou, D. Polymer-controlled core–shell nanoparticles: a novel strategy for sequential drug release. *RSC Adv* 4, 30430–30439 (2014).

311. Veverka, M., Šimon, P., Lokaj, J. & Veverková, E. Crystal habit modifications of imatinib mesylate under various precipitation conditions. *Monatsh Chem* 143, 65–71 (2012).

312. Fu, K., Griebenow, K., Hsieh, L., Klibanov, A. M. & Langer, R. FTIR characterization of the secondary structure of proteins encapsulated within PLGA microspheres. *Journal of Controlled Release* 58, 357–366 (1999).

313. Bhattacharya, S. Fabrication and characterization of chitosan-based polymeric nanoparticles of Imatinib for colorectal cancer targeting application. *Int J Biol Macromol* 151, 104–115 (2020).

314. Bhattacharya, S. Fabrication and characterization of chitosan-based polymeric nanoparticles of Imatinib for colorectal cancer targeting application. *Int J Biol Macromol* 151, 104–115 (2020).

315. Roos, N. J., Mancuso, R. V., Sanvee, G. M., Bouitbir, J. & Krähenbühl, S. Imatinib disturbs lysosomal function and morphology and impairs the activity of mTORC1 in human hepatocyte cell lines. *Food Chem Toxicol* 162, (2022).

316. Ramazani, F. *et al.* Strategies for encapsulation of small hydrophilic and amphiphilic drugs in PLGA microspheres: State-of-the-art and challenges. *Int J Pharm* 499, 358–367 (2016).

317. Senthil Kumar, V., Irfan, N., Kumar, T. V. A. & Parthasarathy, V. Assessing the Molecular Interaction between Poly Lactic-co-glycolic Acid (PLGA) 50:50 and Poly Ethylene Glycol in Presence of Diethyl Phthalate Using in silico Study-A Novel Approach of Pre-Formulation Study. *J Pharm Res Int* 33, 144–150 (2021).

318. Valo, H. *et al.* Electrospray Encapsulation of Hydrophilic and Hydrophobic Drugs in Poly(L-lactic acid) Nanoparticles. *Small* 5, 1791–1798 (2009).

319. Huang, X. & Brazel, C. S. On the importance and mechanisms of burst release in matrix-controlled drug delivery systems. *Journal of Controlled Release* 73, 121–136 (2001).

320. Kamaly, N., Yameen, B., Wu, J. & Farokhzad, O. C. Degradable controlled-release polymers and polymeric nanoparticles: Mechanisms of controlling drug release. *Chem Rev* 116, 2602–2663 (2016).

321. Okada, H. & Toguchi, H. Biodegradable Microspheres in Drug Delivery. *Critical Reviews™ in Therapeutic Drug Carrier Systems* 12, 1–99 (1995).

322. Ahmed, L. *et al.* Study the Using of Nanoparticles as Drug Delivery System Based on Mathematical Models for Controlled Release. *International Journal of Latest Technology in Engineering* VIII, (2019).

323. Korsmeyer, R. W., Gurny, R., Doelker, E., Buri, P. & Peppas, N. A. Mechanisms of solute release from porous hydrophilic polymers. *Int J Pharm* 15, 25–35 (1983).

324. Esmaili, Z. *et al.* Development and characterization of electrosprayed nanoparticles for encapsulation of Curcumin. *J Biomed Mater Res A* 106, 285–292 (2018).

325. Marcos Luciano Bruschi. Mathematical models of drug release. in *Strategies to Modify the Drug Release from Pharmaceutical Systems* (ed. Marcos Luciano Bruschi) 63–86 (Elsevier, 2015). doi:10.1016/B978-0-08-100092-2.00005-9.

326. Azadi, S., Ashrafi, H. & Azadi, A. Mathematical modeling of drug release from swellable polymeric nanoparticles. *J Appl Pharm Sci* 7, 125–133 (2017).

327. SUVAKANTA DASH;, ADALA NARASIMHA MURTHY;, LILAKANTA NATH; & PRASANTA CHOWDHURY. KINETIC MODELING ON DRUG RELEASE FROM CONTROLLED DRUG DELIVERY SYSTEMS. *Acta Poloniae Pharmaceutica - Drug Research* 67, 217–223 (2010).

328. Berkland, C., King, M., Cox, A., Kim, K. & Pack, D. W. Precise control of PLG microsphere size provides enhanced control of drug release rate. *J Control Release* 82, 137–147 (2002).

329. Chung, T.-W., Tsai, Y.-L., Hsieh, J.-H., Tsai, W.-J. & Chung, W. Different ratios of lactide and glycolide in PLGA affect the surface property and protein delivery characteristics of the PLGA microspheres with hydrophobic additives. *Journal of Microencapsulation Micro and Nano Carriers* 23, 15–27 (2008).

330. Fan, L. & Singh, S. K. Controlled Release. *Controlled Release* (1989) doi:10.1007/978-3-642-74507-2.

331. Lagreca, E. *et al.* Recent advances in the formulation of PLGA microparticles for controlled drug delivery. *Progress in Biomaterials 2020 9:4* 9, 153–174 (2020).

332. Manley, P. W. *et al.* Imatinib: a selective tyrosine kinase inhibitor. *Eur J Cancer* 38, S19–S27 (2002).

333. Nyström, M., Murtomaa, M. & Salonen, J. Fabrication of amorphous pharmaceutical materials by electrospraying into reduced pressure. *J Electrostat* 69, 351–356 (2011).

334. Tanhaei, A., Mohammadi, M., Hamishehkar, H. & Hamblin, M. R. Electrospraying as a novel method of particle engineering for drug delivery vehicles. *Journal of Controlled Release* 330, 851–865 (2021).

335. Zhou, J., Zhang, Y. & Wang, R. Controllable loading and release of nanodrugs in polymeric vesicles. *Giant* 12, 100126 (2022).

336. Chen, S., He, L., Wang, X., Gong, X. & Zhang, H. Synthesis and Cytotoxic Activity of Imatinib Derivatives. *Chinese Journal of Organic Chemistry* 35, 2377 (2015).

337. Oliveira, A. *et al.* New Imatinib Derivatives with Antiproliferative Activity against A549 and K562 Cancer Cells. *Molecules 2022, Vol. 27, Page 750* 27, 750 (2022).

338. Samei, L., Yaling, P., Lihua, Y., Yan, Z. & Shuyan, J. Effects and Mechanism of Imatinib in Inhibiting Colon Cancer Cell Proliferation. *Med Sci Monit* 22, 4126 (2016).

339. Panyam, J. & Labhasetwar, V. Dynamics of endocytosis and exocytosis of poly(D,L-lactide-co-glycolide) nanoparticles in vascular smooth muscle cells. *Pharm Res* 20, 212–220 (2003).

340. Qaddoumi, M. G. *et al.* The characteristics and mechanisms of uptake of PLGA nanoparticles in rabbit conjunctival epithelial cell layers. *Pharm Res* 21, 641–648 (2004).

341. Gupta, P. *et al.* The Anti-Tumor and Immunomodulatory Effects of PLGA-Based Docetaxel Nanoparticles in Lung Cancer: The Potential Involvement of Necroptotic Cell Death through Reactive Oxygen Species and Calcium Build-Up. *Vaccines (Basel)* 10, (2022).

342. Yin Win, K. & Feng, S. S. Effects of particle size and surface coating on cellular uptake of polymeric nanoparticles for oral delivery of anticancer drugs. *Biomaterials* 26, 2713–2722 (2005).

343. Cartiera, M. S., Johnson, K. M., Rajendran, V., Caplan, M. J. & Saltzman, W. M. The uptake and intracellular fate of PLGA nanoparticles in epithelial cells. *Biomaterials* 30, 2790–2798 (2009).

344. Simón, L., Campos, A., Leyton, L. & Quest, A. F. G. Caveolin-1 function at the plasma membrane and in intracellular compartments in cancer. *Cancer Metastasis Rev* 39, 435 (2020).

345. Khan, A. M., Ahmad, F. J., Panda, A. K. & Talegaonkar, S. Investigation of imatinib loaded surface decorated biodegradable nanocarriers against glioblastoma cell lines: Intracellular uptake and cytotoxicity studies. *Int J Pharm* 507, 61–71 (2016).

346. Li, L., Blumenthal, D. K., Masaki, T., Terry, C. M. & Cheung, A. K. Differential effects of imatinib on PDGF-induced proliferation and PDGF receptor signaling

in human arterial and venous smooth muscle cells. *J Cell Biochem* 99, 1553–1563 (2006).

347. Gopal, S. *et al.* A phosphoproteomic signature in endothelial cells predicts vascular toxicity of tyrosine kinase inhibitors used in CML. *Blood Adv* 2, 1680–1684 (2018).

348. Venalis, P. *et al.* Effect of imatinib mesylate (IM) on endothelial cells (EC) functions. *Joint Bone Spine* 75, 248 (2008).

349. Kazakoff, P. W., Mcguire, T. R., Hoie, E. B., Cano, M. & Iversen, P. L. *AN IN VITRO MODEL FOR ENDOTHELIAL PERMEABILITY: ASSESSMENT OF MONOLAYER INTEGRITY*. *In Vitro Ceil. Dev. Biol. Animal* vol. 31 (1995).

350. Gover-Proaktor, A. *et al.* Bosutinib, dasatinib, imatinib, nilotinib, and ponatinib differentially affect the vascular molecular pathways and functionality of human endothelial cells Bosutinib, dasatinib, imatinib, nilotinib, and ponatinib differentially affect the vascular molecular pathways and functionality of human endothelial cells. *Leukemia & Lymphoma* 60, 189–199 (2017).

351. Masuda, S. *et al.* Imatinib Mesylate-Incorporated Nanoparticle-Eluting Stent Attenuates In-Stent Neointimal Formation in Porcine Coronary Arteries. *J Atheroscler Thromb* 18, 1043–1053 (2011).

352. Oertel, S. *et al.* Human glioblastoma and carcinoma xenograft tumors treated by combined radiation and imatinib (Gleevec®). *Strahlentherapie und Onkologie* 182, 400–407 (2006).

353. Haguet, H. *et al.* The Risk of Arterial Thrombosis in Patients With Chronic Myeloid Leukemia Treated With Second and Third Generation BCR-ABL Tyrosine Kinase Inhibitors May Be Explained by Their Impact on Endothelial Cells: An In-Vitro Study. *Front Pharmacol* 11, (2020).

354. Kumar, P., Nagarajan, A. & Uchil, P. D. Analysis of Cell Viability by the Lactate Dehydrogenase Assay. *Cold Spring Harb Protoc* 2018, 465–468 (2018).

355. Vallières, K., Petitclerc, É. & Laroche, G. On the ability of imatinib mesylate to inhibit smooth muscle cell proliferation without delaying endothelialization: An in vitro study. *Vascul Pharmacol* 51, 50–56 (2009).

356. Nooteboom, A., Hendriks, T., Ottehöller, I. & Van Der Linden, C. J. Permeability characteristics of human endothelial monolayers seeded on different extracellular matrix proteins. *Mediators Inflamm* 9, 235 (2000).

357. Zhou, C., Townsley, M. I., Alexeyev, M., Voelkel, N. F. & Stevens, T. Ion Channels and Transporters in Lung Function and Disease: Endothelial hyperpermeability in severe pulmonary arterial hypertension: role of store-operated calcium entry. *Am J Physiol Lung Cell Mol Physiol* 311, L560 (2016).

358. Nelson, P. J. & Daniel, T. O. Emerging targets: Molecular mechanisms of cell contact-mediated growth control. *Kidney Int* 61, S99–S105 (2002).

359. Assanga, I. & Luján, L. Cell growth curves for different cell lines and their relationship with biological activities. 4, 60–70 (2013).

360. Sancho-Martínez, S. M., Piedrafita, F. J., Cannata-Andía, J. B., López-Novoa, J. M. & López-Hernández, F. J. Necrotic Concentrations of Cisplatin Activate the Apoptotic Machinery but Inhibit Effector Caspases and Interfere with the Execution of Apoptosis. *Toxicological Sciences* 122, 73–85 (2011).

361. Patil, A. A., Bhor, S. A. & Rhee, W. J. Cell death in culture: Molecular mechanisms, detections, and inhibition strategies. *Journal of Industrial and Engineering Chemistry* 91, 37–53 (2020).

362. Wang, D. *et al.* Vascular smooth muscle cell proliferation as a therapeutic target. Part 1: molecular targets and pathways. *Biotechnol Adv* 36, 1586–1607 (2018).

363. Nilsson, J., Sjolund, M., Palmberg, L., Thyberg, J. & Heldin, C. H. Arterial smooth muscle cells in primary culture produce a platelet-derived growth factor-like protein. *Proc Natl Acad Sci U S A* 82, 4418 (1985).

364. Heldin, C.-H., Westermarkt, B. & Wasteson, A. Specific receptors for platelet-derived growth factor on cells derived from connective tissue and glia (cultured

cells/iodine-labeled tracer/binding assay/high affinity). *Cell Biology* 78, 3664–3668 (1981).

365. Hwang, D. L., Latus, L. J. & Lev-Ran, A. Effects of platelet-contained growth factors (PDGF, EGF, IGF-I, and TGF-β) on DNA synthesis in porcine aortic smooth muscle cells in culture. *Exp Cell Res* 200, 358–360 (1992).

366. Westphal, M., Brunken, M., Rohde, E. & Herrmann, H. D. Growth factors in cultured human glioma cells: Differential effects of FGF, EGF and PDGF. *Cancer Lett* 38, 283–296 (1988).

367. Gupta, D., Bhatia, D., Dave, V., Sutariya, V. & Gupta, S. V. Salts of Therapeutic Agents: Chemical, Physicochemical, and Biological Considerations. *Molecules : A Journal of Synthetic Chemistry and Natural Product Chemistry* 23, 1719 (2018).

368. Vaidya, B. & Gupta, V. Novel therapeutic approaches for pulmonary arterial hypertension: Unique molecular targets to site-specific drug delivery. *Journal of Controlled Release* 211, 118–133 (2015).

369. Song, S. *et al.* Hypoxia inhibits pulmonary artery endothelial cell apoptosis via the e-selectin/biliverdin reductase pathway. *Microvasc Res* 106, 44–56 (2016).

370. Li, M. *et al.* Active Anchoring Stimuli-Responsive Nano-Craft to Relieve Pulmonary Vasoconstriction by Targeting Smooth Muscle Cell for Hypoxic Pulmonary Hypertension Treatment. *Adv Healthc Mater* 13, 2400113 (2024).

371. Urakami, T. *et al.* Peptide-Directed Highly Selective Targeting of Pulmonary Arterial Hypertension. *Am J Pathol* 178, 2489–2495 (2011).

372. Gupta, N., Al-Saikhan, F. I., Patel, B., Rashid, J. & Ahsan, F. Fasudil and SOD packaged in peptide-studded-liposomes: Properties, pharmacokinetics and ex-vivo targeting to isolated perfused rat lungs. *Int J Pharm* 488, 33–43 (2015).

373. Danilov, S. M. *et al.* Lung uptake of antibodies to endothelial antigens: Key determinants of vascular immunotargeting. *Am J Physiol Lung Cell Mol Physiol* 280, (2001).

374. Shenoy, V., Qi, Y., Katovich, M. J. & Raizada, M. K. ACE2, a promising therapeutic target for pulmonary hypertension. *Curr Opin Pharmacol* 11, 150 (2011).

375. Jain, M. *et al.* Integrin α9 regulates smooth muscle cell phenotype switching and vascular remodeling. *JCI Insight* 6, e147134 (2021).

376. Tuder, R. M. *et al.* Expression of angiogenesis-related molecules in plexiform lesions in severe pulmonary hypertension: evidence for a process of disordered angiogenesis. *J Pathol* 195, 367–374 (2001).

377. Gerriets, V. & Kasi, A. Bevacizumab. *StatPearls* (2023).

378. Hsu, J. Y. & Wakelee, H. A. Monoclonal antibodies targeting vascular endothelial growth factor: Current status and future challenges in cancer therapy. *BioDrugs* 23, 289–304 (2009).

379. Voelkel, N. F. & Gomez-Arroyo, J. The role of vascular endothelial growth factor in pulmonary arterial hypertension: The angiogenesis paradox. *Am J Respir Cell Mol Biol* 51, 474–484 (2014).

380. Le Cras, T. D., Markham, N. E., Tuder, R. M., Voelkel, N. F. & Abman, S. H. Treatment of newborn rats with a VEGF receptor inhibitor causes pulmonary hypertension and abnormal lung structure. *Am J Physiol Lung Cell Mol Physiol* 283, (2002).

381. Demir, C. *et al.* Effects of bevacizumab administration on the hypoxia - induced pulmonary hypertension rat model. *Turk J Med Sci* 51, 2752 (2021).

382. Xia, N. *et al.* Probing of EDC/NHSS-Mediated Covalent Coupling Reaction by the Immobilization of Electrochemically Active Biomolecules. *Int J Electrochem Sci* 8, 2459–2467 (2013).

383. Sehgal, D. & Vijay, I. K. A method for the high efficiency of water-soluble carbodiimide-mediated amidation. *Anal Biochem* 218, 87–91 (1994).

384. Cammarata, C. R., Hughes, M. E. & Ofner, C. M. Carbodiimide induced cross-linking, ligand addition, and degradation in gelatin. *Mol Pharm* 12, 783–793 (2015).

385. East, D. A., Mulvihill, D. P., Todd, M. & Bruce, I. J. QD-antibody conjugates via carbodiimide-mediated coupling: A detailed study of the variables involved and a possible new mechanism for the coupling reaction under basic aqueous conditions. *Langmuir* 27, 13888–13896 (2011).

386. Sousa, F. *et al.* A new paradigm for antiangiogenic therapy through controlled release of bevacizumab from PLGA nanoparticles. *Scientific Reports 2017 7:1* 7, 1–13 (2017).

387. Bhattacharjee, S. DLS and zeta potential – What they are and what they are not? *Journal of Controlled Release* 235, 337–351 (2016).

388. Zhuang, C., Tao, F. & Cui, Y. Properties of gelatin films cross–linked by N-hydroxysuccinimide–activated furandicarboxylic acid (NHS-FDCA). *Polymer Bulletin* 73, 1565–1580 (2016).

389. McMurry, J. Structure Determination: Mass Spectrometry and Infrared Spectroscopy. in *Organic chemistry* 434–441 (Brooks/Cole Cengage Learning, 2011).

390. Barth, A. Infrared spectroscopy of proteins. *Biochimica et Biophysica Acta (BBA) - Bioenergetics* 1767, 1073–1101 (2007).

391. Sun, J., Walker, J., Moritz Beck-Broichsitter, ·, Steven, · & Schwendeman, P. Characterization of commercial PLGAs by NMR spectroscopy. *Drug Deliv Transl Res* 12, 720–729 (2021).

392. Song, L., Sun, M., Zhao, Y. & Wang, Z. Tailored dual coating of magnetic nanoparticles for enhanced drug loading. *RSC Adv* 4, 4893–4896 (2014).

393. Bai, M. Y., Tang, S. L., Chuang, M. H., Wang, T. Y. & Hong, P. Da. Evaluation of chitosan derivative microparticles encapsulating superparamagnetic iron

oxide and doxorubicin as a pH-Sensitive delivery carrier in hepatic carcinoma treatment: An in vitro comparison study. *Front Pharmacol* 9, 408947 (2018).

394. Prainito, C. D. *et al.* Colorimetric Detection of the SARS-CoV-2 Virus (COVID-19) in Artificial Saliva Using Polydiacetylene Paper Strips. *Biosensors (Basel)* 12, 804 (2022).

395. Koukos, P. I. & Bonvin, A. M. J. J. Integrative Modelling of Biomolecular Complexes. *J Mol Biol* 432, 2861–2881 (2020).

396. Klotz, I. M. & Frank, B. H. Deuterium-Hydrogen Exchange in Amide N-H Groups. *J Am Chem Soc* 87, 2721–2728 (1965).

397. McKenzie, J. S., Donarski, J. A., Wilson, J. C. & Charlton, A. J. Analysis of complex mixtures using high-resolution nuclear magnetic resonance spectroscopy and chemometrics. *Prog Nucl Magn Reson Spectrosc* 59, 336–359 (2011).

398. Zumaya, A. L. V. *et al.* Comparison between two multicomponent drug delivery systems based on PEGylated-poly (l-lactide-co-glycolide) and superparamagnetic nanoparticles: Nanoparticulate versus nanocluster systems. *J Drug Deliv Sci Technol* 64, 102643 (2021).

399. Wiechelman, K. J., Braun, R. D. & Fitzpatrick, J. D. Investigation of the bicinchoninic acid protein assay: Identification of the groups responsible for color formation. *Anal Biochem* 175, 231–237 (1988).

400. Smith, D. L., Lemieux, E. N. & Barua, S. Correction in Bicinchoninic Acid (BCA) Absorbance Assay to Analyze Protein Concentration. *Nano Life* 08, 1850005 (2018).

401. Vashist, S. K. & Dixit, C. K. Interference of N-hydroxysuccinimide with bicinchoninic acid protein assay. *Biochem Biophys Res Commun* 411, 455–457 (2011).

402. Rapier, C. E., Shea, K. J. & Lee, A. P. Investigating PLGA microparticle swelling behavior reveals an interplay of expansive intermolecular forces. *Sci Rep* 11, 14512 (2021).

403. Choi, J. S., Jang, W. S. & Park, J. S. Comparison of adsorption and conjugation of Herceptin on poly(lactic-co-glycolic acid) nanoparticles – Effect on cell internalization in breast cancer cells. *Materials Science and Engineering: C* 92, 496–507 (2018).

404. Brown, R. E., Jarvis, K. L. & Hyland, K. J. Protein measurement using bicinchoninic acid: elimination of interfering substances. *Anal Biochem* 180, 136–139 (1989).

405. Brady, P. N. & Macnaughtan, M. A. Evaluation of Colorimetric Assays for Analyzing Reductively Methylated Proteins: Biases and Mechanistic Insights. *Anal Biochem* 491, 43 (2015).

406. Kessler, R. J. & Fanestil, D. D. Interference by lipids in the determination of protein using bicinchoninic acid. *Anal Biochem* 159, 138–142 (1986).

407. Milton, J. D. & Mullen, P. J. The effect of reducing and non-reducing sugars on the bicinchoninic acid reaction for protein determination. *Clinica Chimica Acta* 208, 141–143 (1992).

408. Rogatsky, E. Pandora box of BCA assay. Investigation of the accuracy and linearity of the microplate bicinchoninic protein assay: Analytical challenges and method modifications to minimize systematic errors. *Anal Biochem* 631, 114321 (2021).

409. Gómez, R. E. & Ardigo, M. L. Anti-idiotype antibodies in cancer treatment: the pharmaceutical industry perspective. *Front Oncol* 2, 147 (2012).

410. Hueso, D., Fontecha, J. & Gómez-Cortés, P. Comparative study of the most commonly used methods for total protein determination in milk of different species and their ultrafiltration products. *Front Nutr* 9, 925565 (2022).

411. Prescott, M. J. & Lidster, K. Improving quality of science through better animal welfare: the NC3Rs strategy. *Lab Animal 2017 46:4* 46, 152–156 (2017).

412. Gao, S., Guisán, J. M. & Rocha-Martin, J. Oriented immobilization of antibodies onto sensing platforms - A critical review. *Anal Chim Acta* 1189, 338907 (2022).

413. Barst, R. Pulmonary hypertension: Past, present and future. *Ann Thorac Med* 3, 1 (2008).

414. McLaughlin, V. V. *et al.* Treatment goals of pulmonary hypertension. in *Journal of the American College of Cardiology* vol. 62 (2013).

415. Boucherat, O. *et al.* The cancer theory of pulmonary arterial hypertension. *Pulm Circ* 7, 285–299 (2017).

416. Bonnet, S. *et al.* Translating research into improved patient care in pulmonary arterial hypertension. *Am J Respir Crit Care Med* 195, 583–595 (2017).

417. Ratzinger, G. *et al.* Surface modification of PLGA nanospheres with Gd-DTPA and Gd-DOTA for high-relaxivity MRI contrast agents. *Biomaterials* 31, 8716–8723 (2010).

418. Vitali, S. H. *et al.* The Sugen 5416/hypoxia mouse model of pulmonary hypertension revisited: long-term follow-up. *Pulm Circ* 4, 619–629 (2014).

419. Hautefort, A. *et al.* Bmpr2 Mutant Rats Develop Pulmonary and Cardiac Characteristics of Pulmonary Arterial Hypertension. *Circulation* 139, 932–948 (2019).

420. Majka, S. *et al.* Physiologic and molecular consequences of endothelial Bmpr2 mutation. *Respir Res* 12, 1–12 (2011).

421. Parhizkar, M. *et al.* Performance of novel high throughput multi electrospray systems for forming of polymeric micro/nanoparticles. *Mater Des* 126, 73–84 (2017).

422. Liu, Y., Craig, D. Q. M. & Parhizkar, M. Controlled release of doxorubicin from Poly-(D,L-lactide-co-glycolide) (PLGA) nanoparticles prepared by coaxial electrospraying. *Int J Pharm* 666, 124724 (2024).

423. Zhang, L., Huang, J., Si, T. & Xu, R. X. Coaxial electrospray of microparticles and nanoparticles for biomedical applications. *Expert Rev Med Devices* 9, 595 (2012).

424. Humbert, M. *et al.* Endothelial cell dysfunction and cross talk between endothelium and smooth muscle cells in pulmonary arterial hypertension. *Vascul Pharmacol* 49, 113–118 (2008).

425. Heydarkhan-Hagvall, S. *et al.* Co-culture of endothelial cells and smooth muscle cells affects gene expression of angiogenic factors. *J Cell Biochem* 89, 1250–1259 (2003).

426. Truskey, G. A. Endothelial vascular smooth muscle cell coculture assay for high throughput screening assays to identify antiangiogenic and other therapeutic molecules. *Int J High Throughput Screen* 2010, 171 (2010).

427. Romar, G. A., Kupper, T. S. & Divito, S. J. Research Techniques Made Simple: Techniques to Assess Cell Proliferation. *Journal of Investigative Dermatology* 136, e1–e7 (2016).

428. Kyrylkova, K., Kyryachenko, S., Leid, M. & Kioussi, C. Detection of apoptosis by TUNEL assay. *Methods Mol Biol* 887, 41–47 (2012).

429. Zhang, H. *et al.* Shear stress regulation of nanoparticle uptake in vascular endothelial cells. *Regen Biomater* 10, rbad047 (2023).

430. Cedervall, T. *et al.* Understanding the nanoparticle-protein corona using methods to quantify exchange rates and affinities of proteins for nanoparticles. *Proc Natl Acad Sci U S A* 104, 2050–2055 (2007).

431. Xu, M. *et al.* Size-Dependent In Vivo Transport of Nanoparticles: Implications for Delivery, Targeting, and Clearance. *ACS Nano* 17, 20825–20849 (2023).

432. Alexis, F., Pridgen, E., Molnar, L. K. & Farokhzad, O. C. Factors Affecting the Clearance and Biodistribution of Polymeric Nanoparticles. *Mol Pharm* 5, 505 (2008).

433. Wilhelm, S. *et al.* Analysis of nanoparticle delivery to tumours. *Nature Reviews Materials 2016 1:5* 1, 1–12 (2016).

434. Wang, Q. *et al.* Breaking through the basement membrane barrier to improve nanotherapeutic delivery to tumours. *Nature Nanotechnology 2023 19:1* 19, 95–105 (2023).

435. Jandl, K. *et al.* Basement Membrane Remodeling Controls Endothelial Function in Idiopathic Pulmonary Arterial Hypertension. *Am J Respir Cell Mol Biol* 63, 104–117 (2020).

436. Luo, G. F., Chen, W. H. & Zhang, X. Z. Nanomedicine Disrupts Stromal Barriers to Augment Drug Penetration for Improved Cancer Therapy†. *Chin J Chem* 42, 1175–1189 (2024).